Department of Civil Engineering,
Middle East Technical University,
Ankara - TURKEY

27 February, 1981

The Librarian,
Department of Civil Engineering,
Imperial College,
LONDON SW7
ENGLAND

Dear Sir,

On p.12 of my Ph.D. thesis entitled 'Short Term Stability of Slopes in Ankara Clay', (completed in 1976 as an external student of the University of London), the reader is advised to check the pocket inside the back cover of the thesis for any corrigenda or addenda sheets.

I enclose a copy of the first of such sheets which contains some minor omissions and typing errors as well as a logical error which has come to my attention while writing up a report on the laboratory wedge shear test, a modified version of the in situ test, I describe in my thesis (see my Discussion on p.153, Vol.4 of the 7th European Conf. on Soil Mech. and Fdn. Engng, Brighton, 1979). None of these affect the essence of the thesis.

I should be much obliged if you could place the attached sheets inside the pocket at the back of the copy of my thesis which I had presented to your Departmental Library in October 1976.

Your faithfully,

Türker MİRATA, M.Sc(Eng),PhD,DIC,
Assoc.Prof.of Civil Eng.

SHORT-TERM STABILITY OF SLOPES IN ANKARA CLAY

a thesis submitted to the
Faculty of Engineering of the
University of London

for the degree of

Doctor of Philosophy

as an external student

by

Türker Mirata, M.Sc. (Eng.), D.I.C., M.I.C.E.,
Associate Professor of Civil Engineering

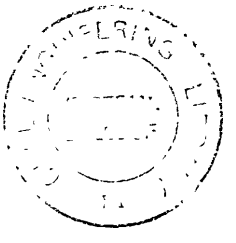

Middle East Technical University
Ankara

August, 1976

ABSTRACT

A review of the available literature on the relevant properties of the partly saturated, stiff, fissured Ankara Clay, and a comparative review of recent research and the methods of treatment adopted in the thesis are presented.

A new testing technique is described whereby a wedge of the in situ soil is sheared by means of a single hydraulic jack and some simple devices. By altering the inclination of the failure plane to the direction of loading, the ratio of shear strength to normal stress on the failure plane can be varied for an unsaturated soil, and a shear strength envelope in terms of total stresses obtained over about the same range of normal stresses as in a critical slope of the soil being tested.

The undrained shear strength parameters measured in such tests are used in a total stress type of stability analysis for the calculation of the factor of safety of three failed slopes in the Ankara Clay. The stability of the three slips plus a fourth slip is then analysed in terms of effective stresses using the shear strength parameters measured in triaxial tests, keeping the axial stress constant and decreasing the cell pressure, and the pore pressures estimated through triaxial tests and in situ pore pressure measurements. The stability analyses are finally repeated using the shear strength parameters measured in 'slow' shear box tests.

It is concluded that the developed in situ test is by far the most reliable means of assessing the short-term stability of slopes in the Ankara Clay. Triaxial tests, although giving a reasonable estimate of the factor of safety involved, are found to be less reliable, and the shear box tests are the least reliable in this respect.

TO MY WIFE, DAUGHTER, AND SON

CONTENTS

CHAPTER 1

INTRODUCTION

Ankara, the capital of Turkey since the foundation of the Turkish Republic in 1923, has since grown from a small, historic town of some 30,000 inhabitants into a modern city of nearly 2 million inhabitants. Single-and double-storeyed houses in the residential quarters are being replaced by 4-to 5 - storeyed blocks of flats, and even such blocks near the commercial centre of the city are being pulled down to leave their place to 20-to 25 - storeyed buildings.

These structures are founded almost invariably on the Ankara Clay, an inland deposit of the Upper Pliocene. This is a partly saturated, stiff, fissured clay of high plasticity, and has a property liberally mined by the local contractors in carrying out excavations in this clay : more often than not, the vertical sides of excavations taken to depths as much as 10 metres (Günece, 1968) in this clay can stand unsupported long enough for the construction to reach the ground surface. But occasionally, a sudden failure results in considerable material loss if not also in loss of life.

Summarized in the next chapter, the survey of the available literature on the relevant properties of the Ankara Clay reveals the lack of a comprehensive study of the short - term stability of slopes in this deposit.

This study has been aimed at establishing a satisfactory

method of assessing the propensity to short - term slope instability of the Ankara Clay. In doing this, it was desired to add to the existing methods of treatment and to improve on these. Other methods of treatment that have become possible on the basis of the literature published since this research was started are reviewed in Chapter 3.

A new testing technique has been developed for the in situ measurement of the undrained shear strength, particularly of unsaturated soils. This test is described in Chapter 4. Parameters determined by such tests have been used in a total stress type of stability analysis for the calculation of the factor of safety of three failed slopes in the Ankara Clay (Chapter 5).

In Chapter 6, these slips plus a fourth slip are analysed in terms of effective stresses using parameters measured in triaxial tests, keeping the axial stress constant and decreasing the cell pressure. The pore pressures estimated through measurements on laboratory specimens have been verified by in situ pore pressure measurements. A number of minor improvements that have been made to the procedure and the interpretation of the triaxial test, and the results of stability analyses using the shear strength parameters measured in slow shear box tests are also presented.

No consideration has been given to the effect of earthquakes, as Ankara falls outside the significant earthquake regions of Turkey.

Symbols have generally been defined once, where they first appear in the text, and an index is provided for rapid location of the pages on which such definitions as well as the equations, tables and figures appear. Abbreviations, mostly appearing in tables, are explained before this index. The reader is advised to check the pocket, inside the back cover, for any corrigenda or addenda sheets.

This study was initiated in late 1968. Part of the work presented here has been written up in different forms previously (Mirata, 1970, 1972, 1973(a)), and some has been published (Mirata, 1973(b), 1974, 1975(a) to (d)). The distribution of the hours of effort, spent on different items of work, over the years is presented at the end of the thesis.

CHAPTER 2

REVIEW OF LITERATURE ON RELEVANT PROPERTIES OF ANKARA CLAY

2.1 Geological history

Fig. 2.1 shows a contour map of the city of Ankara and its immediate environment. A geological map of the same region, together with two geological sections are shown in Fig. 2.2. Unless otherwise stated, the remarks in this sub-section have been summarized from an unpublished note by Erol (1962).

The sediments constituting the Ankara Plain (Fig. 2.2) have been deposited during the Upper Pliocene under shallow water by rivers originating from the mountains surrounding a geological depression. Thus the material encountered nearer the periphery of the basin have a higher percentage of coarse particles, while the sediments towards the central parts of the basin have a higher clay fraction.

The material constituting the upper sediments in the central parts of the Ankara basin is known as the Ankara Clay amongst civil engineers. It usually exhibits a brownish red colour, but also frequently occurs in a light brown colour. Occasional lenses of sand and gravel are encountered in this clay, particularly towards the outer parts of the basin.

Geomorphological studies have indicated that the initial elevation of the sedimentary deposits must have ranged between

1050 m (above mean sea level) in the outer parts of the basin and 1000 m in the central regions (Figs 2.2(b) and(c)). This implies that in the central part of the Ankara plain where the existing elevation is of the order of 850 m , some 150 m of overburden has been removed by erosion. The corresponding figure for the gradually rising outer parts of the plain lies between 50 and 150 m.

Recent studies on the preconsolidation pressure of the Ankara Clay (Arda, 1966; Kocabayoğlu, 1971; Tümerdem, 1973; Ağaoğlu, 1974; Ildız, 1974), by applying Schmertmann's (1955) method to oedometer test results, have confirmed the geologists' view regarding the maximum elevation of the sedimentary deposits, although no more than the submerged unit weight of the overburden appears to have ever become effective.

Erol (1974) believes that the climatic conditions at the time of deposition of the Ankara Clay were semi - arid, but slightly warmer than the present climate. So occasional desiccation of the sediments deposited under shallow water might have well occurred, and this probably accounts for the partly saturated nature of the Ankara Clay.

2.2 Regional variation of index properties

Figs 2.3 and 2.4 show the variation of the index properties of the Ankara Clay along two broken sections (shown by chain-dotted lines in Fig. 2.1 and by dashed lines in Fig. 2.2), one running in a SW - NE direction, the other in

a NW - SE direction. The depth and the description, mostly by visual inspection by the different investigators, are given in Figs 2.3(b) and 2.4(b). Although missing from these descriptions, it has been established (Ordemir et al., 1965) that the Ankara Clay is fissured, and that this property of the clay together with the frequently encountered coarse particles that it contains make it a difficult material to sample.

Figs 2.3 and 2.4 indicate that the liquid limit w_L, the plastic limit w_P, and the clay fraction C generally lie between the approximate limits of 50 % to 90 %, 20 % to 40 %, and 20 to 60 % respectively. The proximity of the natural water content w_N to w_P is another indication of the preconsolidated nature of the clay.

Fig. 2.5 shows the values of plasticity index I_P for the samples presented in Figs 2.3 and 2.4 plotted against the corresponding w_L on the Casagrande plasticity chart. This shows that the Ankara Clay can generally be classified as an inorganic clay of high plasticity.

The limited number of determinations of the degree of saturation S_r by the authors quoted in Fig. 2.3 indicate that S_r for the Ankara Clay generally lies between 85 % and 95 %.

The fact that some of the sites (e.g. Sites 7, 8, 9, 12), where the soil properties are typical of the Ankara Clay, fall outside the regions marked on the geological map (Fig. 2.2) as Ankara Clay, shows that this map requires refinement. A step

in this direction has recently been taken by Lohnes (1974), who has, however, misinterpreted the age of deposition of the Ankara Clay as Pleistocene.

2.3 Undisturbed shear strength

Values of the unconfined shear strength of the Ankara Clay ranging between about 0.5 kg/cm^2 and 2.4 kg/cm^2 have been reported (Ordemir and Alyanak, 1964-65; Dinç, 1965; Uçkan, 1966; Günece, 1968; Tuncer, 1972; Baykam, 1974). These results, as those of the laboratory and field vane tests (yielding on the average, about 2.3 times the undrained strength measured in unconfined compression tests) by Çolpan (1960) clearly give only a rough idea about the strength of this partly saturated deposit.

Uçkan (1966) reports the results of unconsolidated undrained triaxial tests mostly in terms of total stresses. Shear strength parameters in terms of efefctive stresses, obtained through unconsolidated-undrained triaxial tests on undisturbed specimens at Site 4 (Fig. 2.3) by İnal (1967) and at Sites 11 and 12 (Fig. 2.4) by Günece (1968) range from 0.4 kg/cm^2 to 1.4 kg/cm^2 for c' and from 26° to 16° for ϕ'. Corresponding values reported in terms of total stresses range from 0.6 kg/cm^2 to 1.8 kg/cm^2 and from 16° to 7°. The accuracy of these determinations is limited by the facts that the available compression machine did not permit rates of testing slower than at least 10 times the rate required for 95 % equalization of pore pressures; the cell pressure and pore pressure gauges gave readings differing from

each other by as much as 8 % under a pressure of about 50 lb/in^2, with no attempt made to establish their correct calibration; no temperature control was possible in the available laboratory; volume changes of the specimen were not measured and these, as well as the corrections for rubber membrane and filter paper side drains, were neglected in the calculations.

The results of shear box tests on the Ankara Clay have been reported by Uçkan (1966), Inal (1967), Günece (1968), Topkara (1974), and Ekmekçioğlu (1975). The last two investigators have also endeavoured to measure the residual strength parameters through multiple reversal tests, although the accuracy of their determinations is somewhat limited, as only three tests under different normal stresses have been used to define each strength envelope. The average of the peak strength parameters reported range between about 0.35 kg/cm^2 and 0.85 kg/cm^2 for the cohesion and 23^o to 34^o for the angle of shearing resistance. The corresponding values for the residual strength range between 0.25 kg/cm^2 and 0.45 kg/cm^2, and 18^o to 24^o. The limitations of the shear box, in the study of the shear strength of the partly saturated Ankara Clay, is pointed out in Section 6.3.

The values quoted in this sub-section are mainly for samples whose natural moisture contents lie at or slightly below the plastic limit.

2.4 Coefficient of consolidation

For deciding on the rate of testing in triaxial tests, a

knowledge of the coefficient of consolidation c_v is required. The values of c_v so far reported (Ordemir and Alyanak, 1964-65; Kaya, 1965; Gürkök, 1970; Tümerdem, 1973; Ağaoğlu, 1974), ranging between 0.0001 cm^2/s and 0.0180 cm^2/s have been obtained from oedometer test results on specimens allowed to soak prior to testing. This soaking, however, fails to produce full saturation in the specimen, and, as the c_v values are calculated using the initial part of the square-root of time vs. compression curve, when the air in the voids is rapidly compressed or goes into solution, the quoted values of c_v result in a large over-estimate of the true rate at which pore pressures can dissipate in the Ankara Clay.

2.5 Pore pressure studies

There has so far been no significant studies of pore pressures on laboratory specimens of the Ankara Clay.

The only in situ measurements of pore pressure have been done by Elias (1967), using tensiometers. This device, used by agronomists, consists of a porous ceramic cup at the lower end of a water-filled pipe, the upper end of which is connected to a Bourdon gauge. It registers negative pressures up to -0.85 kg/cm^2, but under-estimates the negative pore pressures in the soil because a finite amount of water has to be sucked by the soil to actuate the Bourdon gauge. Elias recorded the pore pressures beneath asphalted road pavements at two sites where a perched water table existed at about 3.9 m below the road surface. He found that up to a height of about 1.9 m

above the water table, the measured negative pore pressures coincided with the pore pressure estimated by extending the hydrostatic pressure distribution line above the water table. Above this level, the measured negative pore pressures were higher than those obtained by the extension of the hydrostatic pressure distribution line, the maximum difference recorded being 0.09 kg/cm^2 at a height of 3.0 m above the water table.

2.6 Analyses of short-term stability of slopes

Günece (1968) has studied,in an approximate way,the stability of two stable vertical cuts, about 8.5 m in height. The factor of safety calculated for these cuts, using different test results and different methods of analysis, ranged between about 2.5 and 4.5.

There has so far been no studies of short-term slope failures in the Ankara Clay.

2.7 Concluding remarks

Available literature, particularly on the shear strength of the Ankara Clay, although providing valuable preliminary information on the properties of this deposit, lack in accuracy and in evidence of reliability in predicting the short-term stability of slopes. The material being partly saturated, stiff, fissured, frequently containing coarse particles, and exhibiting a definite angle of friction even when sheared under undrained conditions are the main characteristics that have urged the seeking of means of studying its shear strength in situ and over a larger area than in conventional laboratory tests.

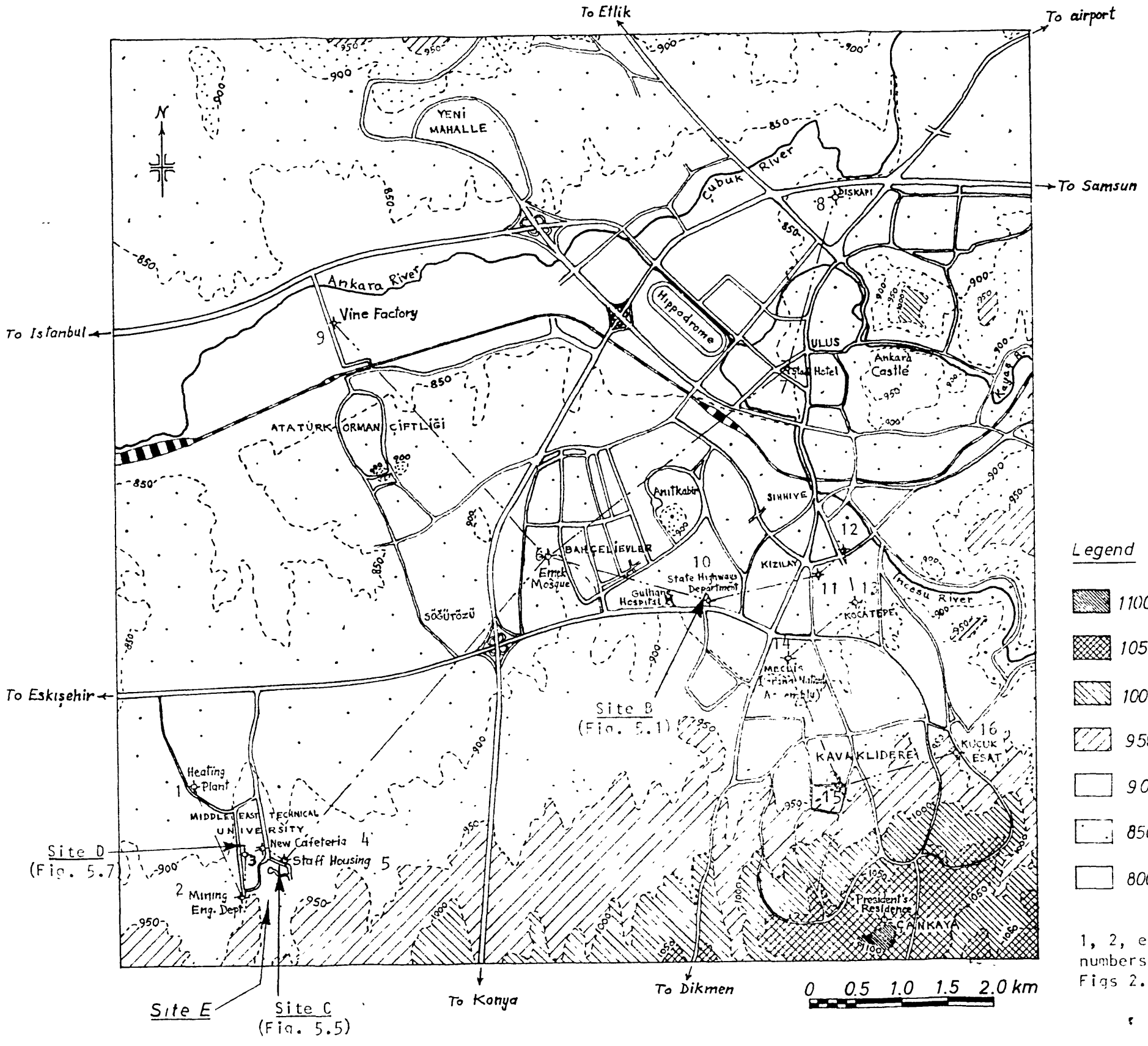

Fig. 2.1. Contour map of Ankara (selectively traced from a map supplied by the Water Authority of Ankara Municipality)

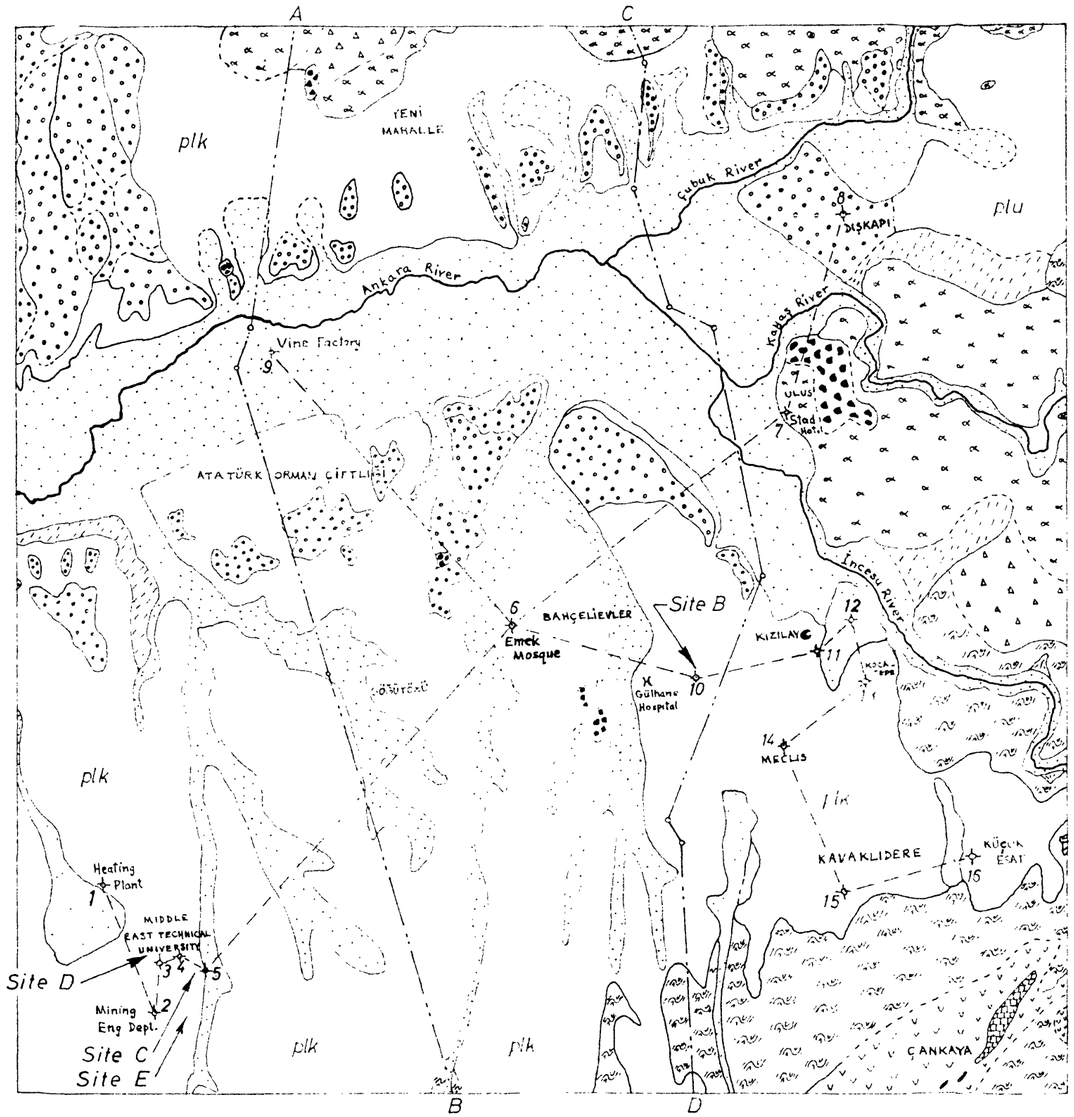

(a) Geological map of Ankara (Scale : 1/50000)

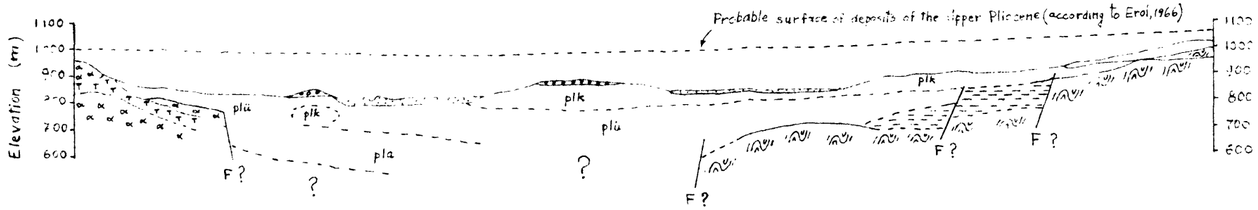

(b) Geological section A - B

Scale for geological sections

Horizontal 1 / 50 000

Vertical : 1 / 20 000

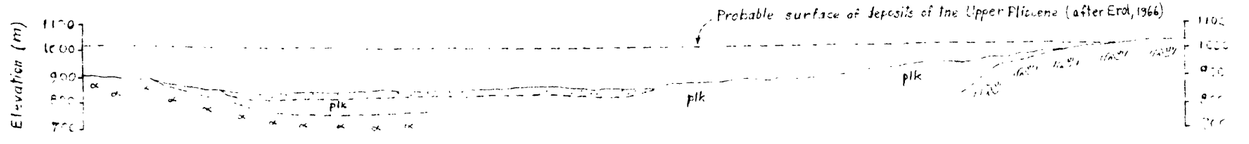

(c) Geological section C - D

Legend

- Recent alluvial deposits
- Old alluvial deposits
- Quaternary deposits other than alluvions
- plk - Red clay of the Upper Pliocene
- plu - Brown clay of the Upper Pliocene
- pla - Deposits of the Lower Pliocene
- Lake deposits (generally Miocene)
- Agglomerate
- Andesite
- Tuff
- Tectonic rocks of mixed facies (Lower Mesozoic - Upper Palaeozoic)
- Massive limestone (Upper Palaeozoic, probably partly Mesozoic)
- Schist - greywacke formations (pre - Carboniferous)
- F? Probable fault
- ? Uncertainty
- o Borehole
- Alluvial fan
- Rubble (artificial deposits)

Fig 2 2. Geological map and sections of Ankara (reduced, by pantograph, to half scale from Erol, 1964)

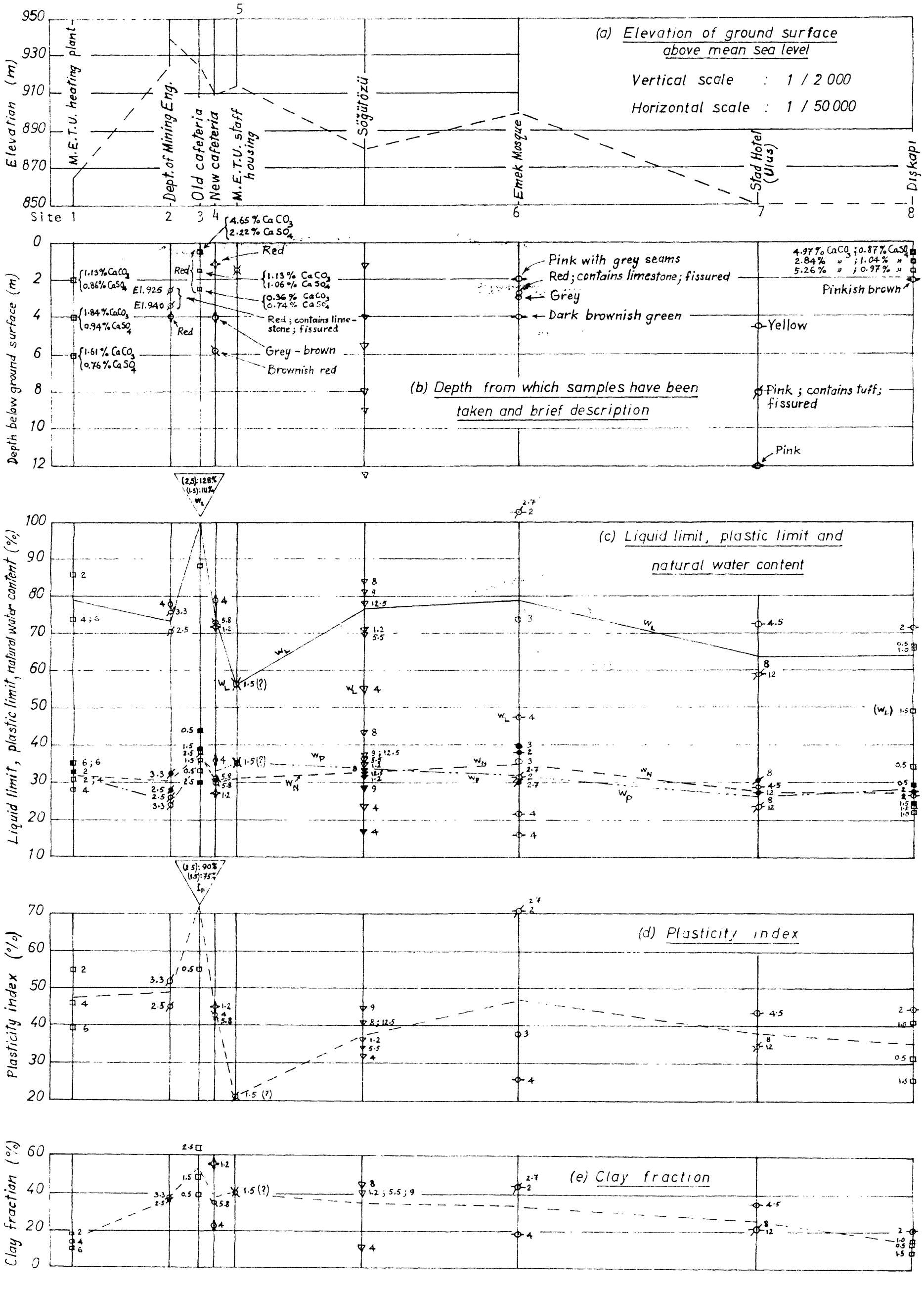

Legend

□ Birand (1963) ◇ Oral (1964) ▽ Dinç (1965) ○ Özkan (1965) ◈ Tosun (1966)

ø Arda (1966) ⊸ Şener (1966) ⌑ Inal (1967) ✧ Elias (1967) ✦ Doruk (1968)

△ Gunece (1968) ◁ Ordemir & Alyanak (1964 - 65)

Notes : (1) Numbers next to plotted points indicate depth in metres from which samples have been taken.
(2) Solid points indicate natural water content.
(3) (?) indicates uncertain values.

Fig. 2.3. Variation of index properties of Ankara Clay along a S.W. - N.E. section

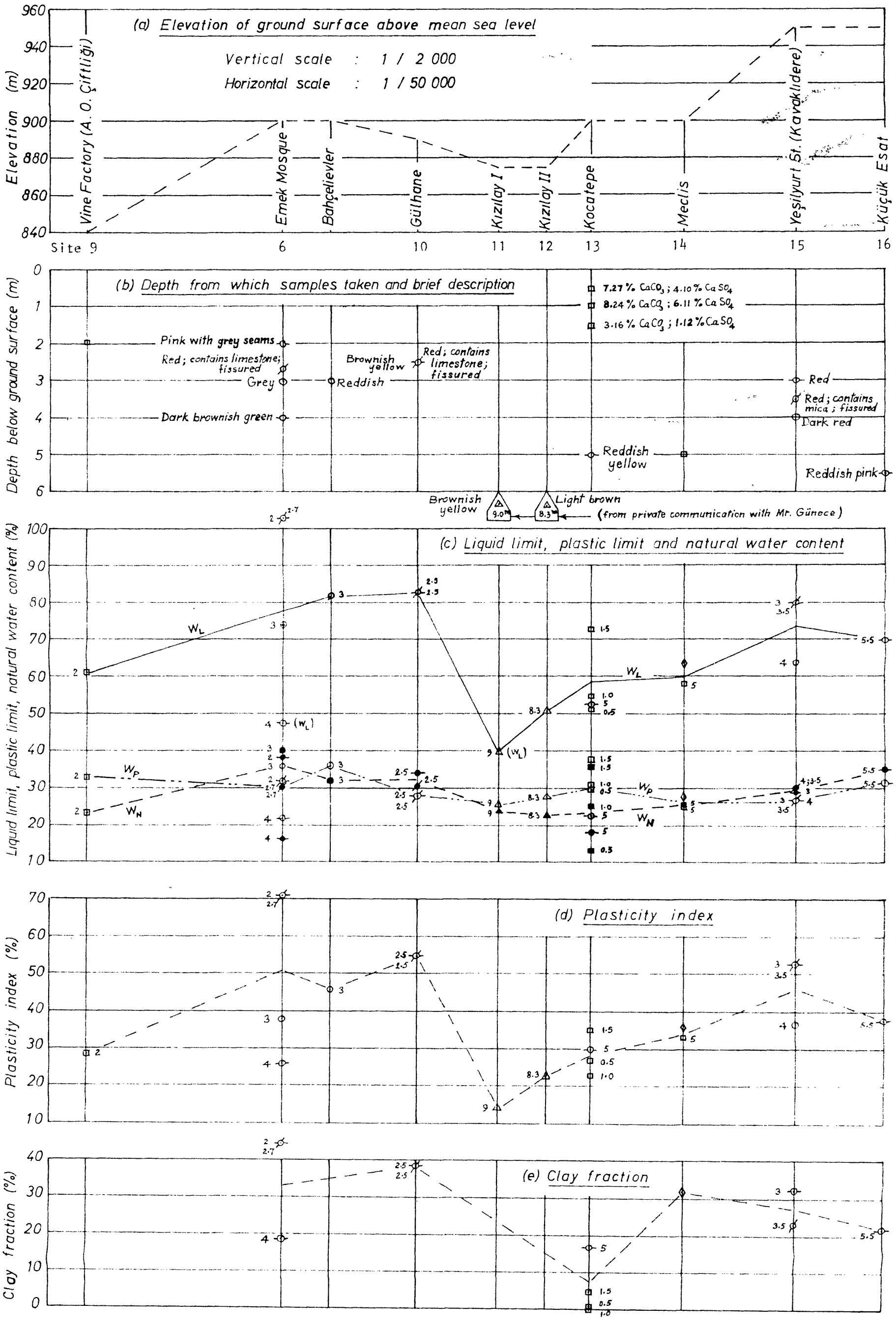

Legend : see Fig.

Notes : (1) Numbers next to plotted points indicate depth, in metres, of sampling.
(2) Solid points indicate natural water content.

Fig. 2.4. Variation of index properties of Ankara Clay along a N.W. - S.E. section

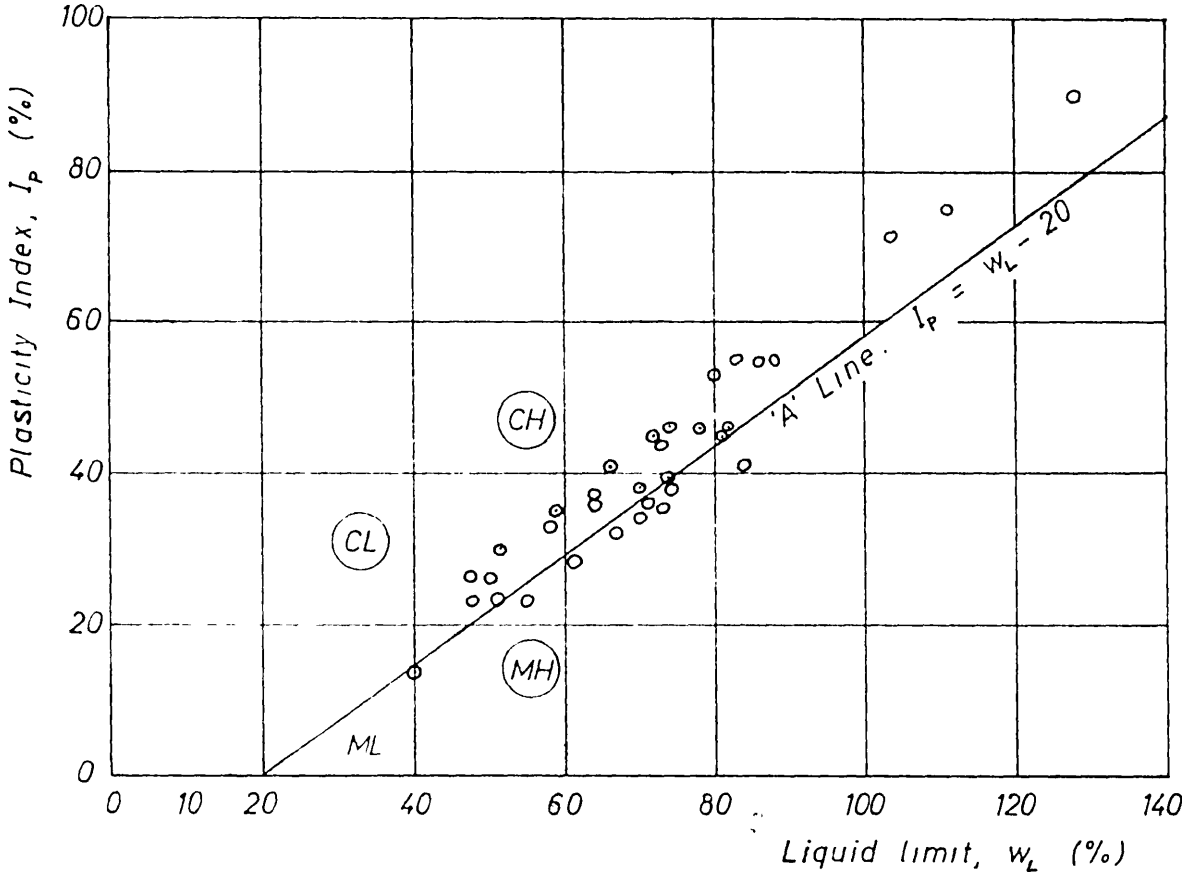

Fig 2 5. Atterberg limits of Ankara Clay plotted on the Casagrande plasticity chart

CHAPTER 3

A COMPARATIVE REVIEW OF RECENT RESEARCH AND THE CHOSEN METHODS OF TREATMENT

3.1 Introduction

The purpose of the present review is to compare the methods of treatment, that could be adopted on the basis of the more recent research, with the methods adopted in this thesis, and hence to point out the possible sources of error in the latter, and possible topics for further research. The references quoted are examples supporting the different statements.

3.2 Progressive failure analysis

In most of the recent comparisons between the shear strength measured in laboratory or field tests and the average shear strength that was mobilized along the shear surface in an actual slip, part of the difference between the compared quantities has been attributed to progressive failure (Skempton, 1964; Skempton and LaRochelle, 1965; Bjerrum, 1967). When used in the sense of a complete drop in the shear strength parameters to their residual values, due probably to non - homogeneous swelling (James, 1971), progressive failure is clearly a factor concerning the long-term stability of slopes. However, when used, as will be done here, in the sense that the peak strength will not be mobilized simultaneously along the complete shear surface at the time of the failure (Terzaghi and Peck, 1948; Bishop, 1966), progressive failure

can be effective in short-term stability problems as well (Skempton and LaRochelle, 1965; Bjerrum, 1967; Bishop, 1971), provided a drop in the soil strength occurs after the peak strength is reached.

Bishop (1971) reports the existence of some empirical evidence to suggest that where the brittleness index I_B (defined as the difference, between the peak and residual strengths, expressed as a percentage of the former) is less than 30 %, a stability analysis based on the peak strength will overestimate the factor of safety by only a small amount (about 5 %), but that where I_B is more than 70 %, the average stress along the slip surface may lie closer to the residual than to the peak strength value. For the short-term progressive failure of cut slopes, the relevant value of I_B has to be defined in terms of the undrained strength, and this can best be determined by quick tests in the ring shear device (Bishop et al., 1971).

Slow shear box tests were performed on 32 cm^2 specimens from near the shear surface of three of the slips studied in this thesis. Measurements in triaxial tests indicated that the pore pressures in the shear box specimens tested under normal stresses, of the order of the average normal stress acting along the corresponding slip surface, must have been negative. As the shear box tests were performed without flooding the specimens with water, such negative pore pressures could not dissipate; so the tests under the lower normal stresses can be considered as undrained. Based on a

residual strength measured at an average shear displacement about 7 times that at peak strength, the I_B values calculated from such tests are 74 %, 72 % and 32 % for the Slips 1 and 2 at Site B and the slip at Site C (Figs 2.1 and 2.2) respectively. Based on these values of I_B, one would conclude that a certain degree of progressive failure must have been effective in the slips studied.

However, undrained in situ direct shear tests on 900 cm^2 wedge samples by a new technique described in Chapter 4, have indicated much lower I_B values for all three of the sites investigated; assuming the residual strength is measured nearly correctly in these tests, the I_B values corresponding to the average normal stress along the shear surface of Slip 1 at Site B and the slips at Sites C and D were respectively 21 %, 21 % and 49 %. There is some reason to believe that at least the first of these values is an underestimate, but these values indicate that progressive failure might not have been as influential in the slips studied as thought on the basis of slow shear box tests on small specimens. This view is substantiated by the fact that the values of factor of safety calculated on the basis of the peak strength measured in the in situ tests were quite close to unity for the slips studied. If Taylor's (1948) view that a certain degree of progressive failure takes place in all types of test in which non-uniform stress and strain conditions occur, particularly in direct shear tests, is correct, this may explain the success of the peak strength measured in the in situ tests in

predicting the short-term stability of the slips studied.

Accordingly no progressive failure analysis has been done here. If such an analysis is seen as necessary by future investigators, this can best be done on the lines demonstrated by Lo and Lee (1973). The in situ stresses required for such an analysis could be measured by a developed version of the self-boring pressuremeter described by Wroth and Hughes (1973) or Amar et al. (1975), if the drilling mud used in these devices can be prevented from increasing the moisture content of this partly saturated deposit. More accurate information on the pre-peak and post-peak stress-strain behaviour of the soil could be obtained through the laboratory testing techniques mentioned in the next sub-section.

3.3 Developments in laboratory testing equipment

Apart from the corrections for the rubber membrane and filter paper side drains, and minor developments to the setting up and interpretation of the tests, Bishop and Henkel's (1962) work has been used as a hand-book for the triaxial tests performed in this study. Several developments, not made use of here, are reveiwed below.

A number of investigators have studied the effect of end friction on the triaxial test results (Blight, 1963(a); Rowe and Barden, 1964; Bishop and Green, 1965; Khera and Krizek, 1967; Kirkpatrick and Belshaw, 1968; Kirkpatrick et al., 1974). Blight (1963 (a)) quotes evidence indicating that except perhaps in the case of normally consolidated clays and

sensitive clays, end friction causes higher pore pressures to be set up at the ends than at the centre of the specimen. If the test is run at slow enough a rate for 95 % equalization of pore pressures, for overconsolidation ratios up to 20, the underestimate in the effective minor principal stress is considered unlikely to be more than 5 %, which, for example, leads to a 30 % overestimate in the measured cohesion, and a 3 % underestimate in the angle of shearing resistance for a soil whose actual shear strength parameters in terms of effective stresses are $c' = 0.14$ kg/cm^2 and $\phi' = 25^\circ$ (Blight, 1963(a)). Both Barden (1963) and Blight (1963(b)) assert that a reduced rate of testing without free ends will give accurate values of c' and ϕ' but the pore pressure coefficient A_f (Skempton, 1954) will be in error. All the quoted investigators have observed that the use of free ends results in a much more uniform distribution of strains and stresses throughout the specimen. Thus it is seen that for more accurate studies of pore pressure and the stress-strain behaviour of the soil, the use of free ends is advisable, although difficulties may arise in measuring suctions in partly saturated soils when free ends are used (Khera and Krizek, 1967).

Two similar transducers are described by Holubec and Finn (1969) and El-Ruwayih (1976) for the direct measurement of lateral deformations of the specimen in the triaxial test. In the absence of such devices, a semi-direct method of measuring these deformations, using a lateral strain indicator of the type described by Bishop and Henkel (1962), and

calibrating it by means of the changes in area caused by axial strain in the same specimen, has been employed here.

Alongside with the developments in the conventional triaxial test, developments in plane strain and true triaxial equipment have taken place (Bishop, 1966; Ko and Scott, 1967; Hambly and Roscoe, 1969; Hambly, 1969; Pearce, 1971; Mitchell, 1973), although most of these equipment have been used for more accurate studies of the stress-strain behaviour of the soil. Comparative tests by Lee and Shubeck (1971) on compacted clay, saturated by a back-pressure, have indicated that the pore pressure coefficient A_f and the shear strength parameters (in terms of both total and effective stresses) of samples tested in plane strain were the same as those tested in the conventional triaxial apparatus under the same consolidation conditions. The stress-strain curves were somewhat different. For the overconsolidated Ankara Clay a similar agreement between triaxial and plane strain strengths and pore pressure coefficients may be expected. It should be of interest to verify this point in future studies.

3.4 Failure criterion

The Mohr-Coulomb failure criterion, being the most widely used practical criterion of failure (Bishop, 1971; Lee and Ingles, 1972), has been used throughout this thesis. Also, as the use of the stress circles corresponding to maximum principal effective stress ratio for undisturbed clays has been questioned (Crawford, 1963), the stress circles corresponding

to maximum deviator stress have been used here, in the evaluation of the triaxial test results, except where the contrary is stated.

3.5 Calculation of stress changes in cut slopes

The stress changes in cut slopes, necessary for the calculation of the changes in pore pressure, can be determined fairly accurately by means of the finite element method (Dunlop et al., 1968). Owing to the low response of the Ankara Clay to changes in stress, such an analysis has not been undertaken here. Instead, the calculations based on simplifying assumptions were checked by in situ measurements of pore pressure in a slope before and after the excavation.

3.6 Developments in the study of shear strength of unsaturated soils

The developments up to 1961 in the study of the shear strength of partly saturated soils have been summarized by Bishop and Henkel (1962). The more recent techniques for the separate measurement of pore water pressure u_w and pore air pressure u_a, are described by Gibbs and Coffey (1969). Blight (1967) presents a method for evaluating the parameter χ in the equation

$$\sigma' = \sigma - u_a + \chi (u_a - u_w) \quad \ldots\ldots\ldots \quad (3.1)$$

where σ' and σ are the effective and total normal stresses respectively, without having to assume that the shear strength

parameters c' and $\emptyset'$ are independent of water content.

In part of the work presented here, the need to use equation 3.1 has been eliminated by the use of undrained shear strength parameters, determined by means of the developed in situ test, in a total stress type of stability analysis. In the study of stability in terms of effective stresses using parameters measured in the triaxial test, use has been made of the observation by Bishop and Henkel (1962) that where the degree of saturation is above 90 %, the shear strength will be controlled primarily by ($\sigma - u_w$). Data presented by Bishop and Blight (1963) show that any errors due to this assumption lead to an underestimate of c' and an overestimate of $\emptyset'$. The quantitative evaluation of these errors for the Ankara Clay remains to be investigated.

3.7 Importance of large-scale in situ tests for fissured clays

The importance of subjecting as large an area as possible to test in measuring the shear strength of fissured clays has been emphasized by several authors in recent years (Bishop, 1966; Lo, 1970). This has led to an increasing number of large-scale shear box tests being performed in situ (Bishop, 1966; Lo et al., 1969; Marsland, 1971; Tice and Sams, 1974; Bundred, 1975).

For the Ankara Clay the need for such large-scale tests is increased by the presence of the frequently encountered coarse particles that it contains. Various devices, for in situ shear testing in unsaturated soils, have been reported

(Handy and Fox, 1967; Biarez, 1968; Thorley et al., 1969). The large shear box test, which presently appears to be the soundest means of measuring the shear strength along a prescribed shear plane particularly when stones are present (Schmertmann, 1975), suffers from the serious drawback of being too cumbersome for routine testing: it requires dead weights in addition to at least two hydraulic jacks and two load cells, and cannot conveniently be performed in a test pit of limited dimensions.

The test described in Chapter 4 has been developed as a simpler and more versatile alternative to the large shear box test. Although conceived and applied before the publication of the paper by Fagnoul and Bonnchère (1970), this test may be looked upon as a modified and simplified version of the special, large-scale tests described by these authors. It can be performed by two men in four to six hours using equipment not exceeding 85 kg in total weight. For practical purposes, four such tests using at least one other test mould, weighing about 15 kg, are sufficient to yield a shear strength envelope for unsaturated soils. The test may also be used for saturated soils if desired, and is suitable for all soils having some cohesion. The test can be conveniently performed in a pit measuring as little as 110 cm in diameter, or in any other accessible excavation, and enables the strength on a plane of any desired orientation to be measured with equal ease.

3.8 Methods of stability analysis

Since Bishop's (1955) rigorous method of slope stability

analysis, and its simplified version, nowadays frequently referred to as Bishop's Simplified Method (abbreviated here to 'BISIM') was published, a number of different methods have been proposed (Morgenstern and Price, 1965; Nonveiller, 1965; Spencer, 1967; Bell, 1968; Kogan and Lupashko, 1970; Chen and Giger, 1971; Robertson, 1971; Sarma, 1972; Janbu, 1973; Spencer, 1973). However, BISIM has remained amongst the "most widely used and considered to be most accurate" (Wright et al., 1973). Comparisons by Whitman and Bailey (1967) between solutions using BISIM and Morgenstern and Price's (1965) method, which satisfies all conditions of equilibrium, have shown that the maximum error in BISIM was 7 % and this error was generally less than 2 % for a wide range of values of slope angle, shear strength, and pore pressure. Wright et al. (1973) performed a similar comparison between the results obtained by BISIM and the values of the factor of safety obtained by calculating the linear elastic stress distribution along the critical circle given by BISIM, evaluating the factor of safety at different points along this surface, and averaging these. For a wide range of different cases studied, the maximum difference between the results was 8 %, the values obtained through the linear elastic analysis being lower. The Author believes that such a comparison would have been more valuable had the development of plastic zones (Dunlop and Duncan, 1970) been taken into account in the calculation of the stresses, but their results still are an independent check of the reliability of BISIM, and the limit equilibrium methods in general.

BISIM has accordingly been used in this thesis with Janbu's (1973) Generalized Procedure of Slices (GPS), which has been found to yield very nearly the same values of factor of safety as Morgenstern and Price's (1965) method (Wright et al., 1973), used to assess the order of magnitude of the errors involved in BISIM in the particular slopes analysed.

3.9 Concluding Remarks

In this chapter, some of the presently available experimental and mathematical techniques for a fuller treatment of the problem of short-term slope stability in unsaturated, fissured clays has been reviewed. This has been done without regard to the cost and the commercial availability of these equipment. In fact, the self-boring pressuremeter device, referred to at the end of Section 3.2, for example, presently costs about four times as much as a complete triaxial unit for testing 36 mm dia. specimens, and about twelve times as much as the equipment needed for the in situ test described in Chapter 4. Most of the equipment referred to in Section 3.3 have been developed in specific research laboratories, and have either to be almost re-discovered and built at a relatively high cost by individual users, or their use postponed until they become commercially available. Furthermore, even the most advanced of these equipment still have some shortcomings as failure to simulate the rotation of principal stress axes (Pearce, 1971), encountered in the slope stability problem (Duncan and Seed 1966(a)and(b)).

Thus although it now appears theoretically possible to

subject an undisturbed sample of the soil, in at least some zones of the potential failure surface, to an accurately calculated set of stresses, and use the measured strength and stress-strain characteristics of the soil in as elaborate a stability analysis as desired in order to study the short - term stability of slopes, the research centres where this can be done are rather limited in number. So it is natural that here, a direct solution to the problem has been sought: that of performing a model test on a slope to test its safety. In the search for this, a completely new in situ test has been developed, capable of being performed using equipment that can be easily made in any reasonably well equipped workshop, in addition to devices that are readily available on the market.

The aim of this thesis has been to demonstrate the usefulness of the developed in situ test in assessing the short-term stability of slopes in the Ankara Clay, and to compare the results with those obtained by the more conventional methods based on triaxial and laboratory shear box tests.

CHAPTER 4

THE IN SITU WEDGE SHEAR TEST

4.1 Principles

Suppose that a two-stage pit is dug in the soil, as shown in Fig. 4.1(a), and the two sides at one end are cut off in such a way as to leave a wedge of soil protruding as shown in Fig. 4.1(b). If the wedge of soil is protected against local breakage, and a gradually increasing compression, P, is applied in the direction of the arrows shown, failure will take place along ABDE, provided the angle α is within certain limits discussed in Section 3.3.1.

Fagnoul and Bonnechère (1970) have made use of a similar principle in order to measure the ultimate horizontal force that can be applied to a heterogeneous mass of soil cut in the shape of a large wedge (measuring about 3 m x 5 m x 6 m) similar to that shown in Fig. 4.1(b) but having a curved surface of rupture. Such a method, as it stands, cannot be used to determine the absolute values of the undrained shear strength parameters c and $\emptyset$ of unsaturated soils, and even if it could, cannot be recommended as a routine testing procedure.

If, however, the sliding surface is chosen as plane, the values of c and $\emptyset$ can be determined by performing a number of tests with different inclinations α of the failure plane to the direction of loading. If, furthermore, the size of the test wedge is reduced, and the applied force system made statically determinate, the test becomes simple to perform and

to interpret.

Inspired by the shape of the soil mass that is sheared, the test has been called the in situ wedge shear test (iswest).

The loading system chosen is shown in Fig. 4.2. The soil wedge is encased in a test mould TM of mild steel. Different test moulds have different angles α, but provide an equal area of shear for the soil wedge. The load is applied by means of a hydraulic jack HJ through two grooved plates, LP.1 and LP.2, with thirty 12 mm dia. steel balls held loosely in a ball cage BC in between. The hydraulic jack reacts against a mild steel plate RP through a single 18 mm dia. steel ball held in the central recesses of two mild steel ball pads BP.

The forces, displacements, and distances involved in the evaluation of the iswest results are shown in Fig. 4.3. The full lines in this diagram represent the conditions at the start of the test, and the dashed lines the position of the test mould and the three adjoining components at an intermediate stage of the test. O_1 and O_2 represent respectively the initial and intermediate positions of the centroid of the shearing plane of the test mould. O_3 represents the centroid of the remaining (corrected) area of shear, as the soil immediately above the test mould is trimmed free of the path of the test mould. For clarity, the force W has been indicated on the intermediate position of the test mould, all the remaining forces being indicated on the initial position of the equipment.

The components X and Y (Fig. 4.3), of the resultant force acting on the failure plane, which are respectively parallel and perpendicular to the direction of loading may be calculated from the following equations.

$$X = P - (W + W_{BC} + W_{LP}) \sin \theta \qquad \ldots\ldots\ldots\ldots (4.1)$$

$$Y = (W + \frac{M_B}{D}) \cos \theta + F \qquad \ldots\ldots\ldots\ldots (4.2)$$

where P = force measured through the load cell

W = total weight of soil wedge, test mould and grooved loading plate LP.1

W_{LP} = weight of grooved loading plate LP.2

W_{BC} = weight of ball cage

θ = inclination of direction of loading to the horizontal

M_B = sum of the moments, about the single ball, of weights of all components lying between the grooved face of loading plate LP.1 and the ball, when $\theta = 0$

D = perpendicular distance between the grooved face of loading plate LP.1 and the single ball

F = frictional resistance against the motion of one grooved loading plate relative to the other with the steel balls rolling in between.

F is relatively small and for all practical purposes may be calculated from the formula

$$F = \mu \cdot P \qquad \ldots\ldots\ldots\ldots\ldots\ldots\ldots\ldots (4.3)$$

where μ is the relevant coefficient of friction*.

The average normal stress σ_N and the average shear stress τ on the failure plane may then be calculated from the following equations:

$$\sigma_N = \frac{1}{A_c} \left\{ X \sin \alpha + Y \cos \alpha \right\} \quad \ldots\ldots\ldots\ldots (4.4)$$

$$\tau = \frac{1}{A_c} \left\{ X \cos \alpha - Y \sin \alpha \right\} \quad \ldots\ldots\ldots\ldots (4.5)$$

where α is the angle between the shearing plane of test mould and the direction of loading, and A_c is the corrected area of the plane of shear obtained from the relation

$$A_c = b\,(d - u) \quad \ldots\ldots\ldots\ldots\ldots\ldots\ldots\ldots (4.6)$$

where d = initial length of the failure plane (360 mm for the moulds ordinarily used in this study)

b = constant width of the failure plane (250 mm for the moulds used in this study)

u = displacement of the mould in the direction of the failure plane.

---

* For the components used in this study, the value of μ has been measured as 0.0089 with the grooves lubricated, and as 0.0125 with no lubrication. Three balls and dead loading up to 400 kg were used for these determinations.

u and the displacement v of the mould normal to the failure plane can be calculated from the following equations

$$u = \delta_x \cos\alpha + \delta_y \sin\alpha \quad \ldots\ldots\ldots\ldots (4.7)$$

$$v = \delta_y \cos\alpha - \delta_x \sin\alpha \quad \ldots\ldots\ldots\ldots (4.8)$$

where δ_x and δ_y are the displacements measured during the test in the positive directions of X and **y** (Fig. 4.3) respectively. Positive values of v indicate a rise relative to the failure plane.

To analyse the distribution of normal stress along the failure plane, and to detect zones of tension if any, the evaluation of moments M, about the centroid O_3 of the corrected area A_c, is necessary.

$$M = x.W\cos\Theta + y.W\sin\Theta + \left(\frac{M_B}{D}\cos\Theta + F\right)\left(\frac{d-u}{2}\cos\alpha + n\right)$$

$$+\left\{P - (W_{BC} + W_{LP})\sin\Theta\right\}\left(\frac{u}{2}\sin\alpha + v\cos\alpha - \Delta y_P\right) \quad \ldots (4.9)$$

where $$x = \bar{x} - \frac{u}{2}\cos\alpha \quad \ldots\ldots\ldots\ldots\ldots\ldots\ldots\ldots (4.10)$$

$$y = \bar{y} + \frac{u}{2}\sin\alpha \quad \ldots\ldots\ldots\ldots\ldots\ldots\ldots\ldots (4.11)$$

n = distance from the inner loading face of test mould to the grooved face of loading plate LP.1.

Δy_P is the amount by which the jacking equipment is raised relative to the test mould prior to the start of loading (Δy_P is zero in Fig. 4.3); $\bar{x}$, $\bar{y}$ are the coordinates

of the combined centre of gravity of the soil wedge, the test mould and the grooved loading plate LP.1, relative to the centroid of the shearing plane of the test mould. Little error will result if the values of $\bar{x}$ and $\bar{y}$ are determined, once for all, using an average value for the density of the soil.

Assuming a linear distribution of stress along the failure plane, the maximum and minimum values of the normal stress may be calculated from the following equations.

$$(\sigma_N)_{max} = \sigma_N + \frac{6\,M}{b\,(d-u)^2} \qquad \ldots\ldots\ldots\ldots \quad (4.12)$$

$$(\sigma_N)_{min} = \sigma_N - \frac{6\,M}{b\,(d-u)^2} \qquad \ldots\ldots\ldots\ldots \quad (4.13)$$

If $(\sigma_N)_{min}$ is negative, equations 4.6 , 4.12 and 4.13 are no longer valid, as soil is generally assumed unable to take any tension. If, for this condition, a length d_c of the failure plane is under compression, the following equations may be used to calculate d_c, σ_N and τ .

$$d_c = 3\left\{\frac{d-u}{2} - M / (X \sin\alpha + Y \cos\alpha)\right\} \quad \ldots\ldots (4.14)$$

$$\sigma_N = \frac{1}{bd_c}\,(X \sin\alpha + Y \cos\alpha) \qquad \ldots\ldots\ldots\ldots (4.15)$$

$$\tau = \frac{1}{bd_c}\,(X \cos\alpha - Y \sin\alpha) \qquad \ldots\ldots\ldots\ldots (4.16)$$

These equations are based on the assumption that the test mould retains its initial orientation throughout the test. It has been observed, however, that as the test proceeds, the soil wedge tilts slightly, the amount of this rotation β (Fig. 4.4) reaching a maximum value of about 1 degree by the end of the test. The same phenomenon has been observed in twelve slow shear box tests on 63 mm square specimens (Fig. 5.15(d)). The sense of the rotation is generally opposite to that shown in Fig. 4.4, and therefore tends to increase the moments acting on the failure plane in the iswest by decreasing the effective value of the initial eccentricity, Δy_p.

Examples of application of the iswest have shown that, except in the rare instance of tension developing at the leading edge of the failure plane, the neglect of β in the calculations does not affect the undrained shear strength parameters measured. But if a more rigorous analysis taking β into account is desired, the following modified equations may be used. These have been derived (Appendix A) from the geometry of Fig. 4.4 by making fair approximations.

$$\bar{u} = u + (\overline{O_3E} \cdot \cos\psi_1 \cdot \sin\alpha + \overline{O_3F} \cdot \sin\psi_2 \cdot \cos\alpha) \cdot \beta \quad ..(4.17)$$

$$\bar{v} = v + (\overline{O_3E} \cdot \cos\psi_1 \cdot \cos\alpha - \overline{O_3F} \cdot \sin\psi_2 \cdot \sin\alpha) \cdot \beta \quad ..(4.18)$$

where $\bar{u}$, $\bar{v}$ = average displacements of the test mould

u, v = displacements calculated from equations 4.7 and 4.8.

$$\overline{O_3E} = \left\{(d+u)\ \frac{\sin\alpha}{2} + t\right\} / \sin\psi_1 \quad \ldots\ldots\ldots\ldots\ldots\ldots (4.19)$$

$$\overline{O_3F} = \left\{(d-u)\ \frac{\cos\alpha}{2} + t\right\} / \cos\psi_2 \quad \ldots\ldots\ldots\ldots\ldots\ldots (4.20)$$

$$\psi_1 = \arctan\left\{\left[(d+u)\ \frac{\sin\alpha}{2} + t\right] / \left[d\cdot\cos\alpha + t - d_1 + \delta_x - (d+u)\frac{\cos\alpha}{2}\right]\right\} \quad \ldots\ldots (4.21)$$

$$\psi_2 = \arctan\left\{\left[(d\cdot\sin\alpha + t - d_2 - \delta_y - (d-u)\ \frac{\sin\alpha}{2}\right] / \left[(d-u)\ \frac{\cos\alpha}{2} + t\right]\right\} \ldots (4.22)$$

$$\beta = (\ \delta_y - \Delta y_{MP} - \Delta y_P) \ / \ (D + n + d_1 - t) \quad \text{(radians)} \ \ldots\ldots (4.23)$$

where δ_x, δ_y = same displacements as in equation 4.8, but have to be measured by dial gauges supported independently of the test mould

d_1, d_2 = respectively the initial distances from the outer right corner of the test mould at which δ_y and δ_x are measured

t = wall thickness of the test mould

Δy_{MP} = downward displacement of P relative to the instantaneous centre line of the loading face of the soil wedge ($\Delta y_{MP} = -\Delta y_P$ at start of testing),

and D, n, Δy_P have the same meaning as in equations 4.2 and 4.9.

Equations 4.3 to 4.8, 4.15, 4.16 remain unaltered; θ has, strictly, to be replaced by $(\theta + 57.3\ \beta)$ in equations 4.1, 4.2, and 4.9; u has to be replaced by $\bar{u}$ in equations 4.6, and 4.9 to 4.14; and the last expression in equation 4.9 has to be replaced by $(\Delta y_{MP} - u\cdot\sin\alpha/2)$. If the jacking

equipment is raised during the test by an amount Δy_{RB}, Δy_P in equation 4.23 has to be replaced by ($\Delta y_P + \Delta y_{RB}$).

As σ_N is not constant during the iswest as in an ordinary direct shear test, the values of τ / σ_N are generally but not necessarily indicative of the peak or the residual strength. It has been found in practice that, for large negative values of θ, τ / σ_N can continue rising slightly after the peak load has been reached (cf. the stress paths for iswests C/4/3 and C/4/5 in Fig. 7.1). The applied load is therefore a safer criterion in deciding when the peak and the residual strengths are reached.

4.2 Description of apparatus

4.2.1 Special equipment

4.2.1.1 Test mould. Fig. 4.5 shows the details of the test mould used for encassing the soil wedge to prevent it from crushing during the test. It is made out of four 10 mm thick mild steel plates, cut to size and welded together. Five moulds with angles α ranging from 25° to 45° in steps of 5° have been found sufficient.

Each mould has an inside width of 250 mm and the length of the open end is 360 mm, giving a constant initial area of 900 cm^2 for the failure plane. Each mould has the following additional features.

(1) The long sides of the open end are chamfered at 45° to form two cutting edges.

(2) There are three tapped holes A for 6.3 mm diameter screws for mounting the grooved loading plate LP.1 (Fig. 4.2) centrally (relative to the inner loading face of the mould) on to the mould.

(3) On either side of the mould, close to the edge where the loading and shearing faces meet, there are two holes B, 6.2 mm in dia. and 5 mm deep. For moulds with the smaller angles α, the chamfer on the sides of the mould may be back-filled with weld sufficiently to enable the holes B to be drilled.

(4) On the loading face of the mould, in a position identified in Section 4.4(4), there is a hole D, 7.5 mm dia. and 5 mm deep.

(5) The outer rectangular faces of the mould have a smooth finish.

(6) Two guide plates GP measuring 40 mm x 15 mm x 3 mm have been screwed and adjusted so as to enable rapid centralizing of the grooved loading plate LP.1 in screwing this on to the mould.

(7) On the chamfered sides of the mould, two marks M have been inscribed at a distance h, from the centre of the nearest hole B, equal to the perpendicular distance between this hole and the opposite inner rectangular face of the mould.

(8) If the same mould is intended for use on soils with low or zero angles of shearing resistance, the effective value

of α may be increased up to 65^{o} by duplicating the features (2) to (7) for the other rectangular face of the mould.

(9) A handle is welded in such a position as not to interfere with possible usage as in (8). This handle provides ease in transportation, and a convenient means for supporting the mould temporarily in tests in which such support is needed.

4.2.1.2 Grooved Loading plates. These were made as follows. A 300 mm x 150 mm x 22 mm plate was cut and machined out of high tensile steel (Brinell hardness No. 220). One face of this plate was ground to a smooth finish. On the opposite face five parallel grooves 300 mm long, 1 mm deep and 6 mm in radius were cut on a milling machine at a spacing of 27 mm. This plate was then cut into two 150 mm x 150 mm plates (LP.1 and LP.2 in Fig. 4.2).

The following details shown in Fig. 4.6 were then added to these plates.

(1) On plate LP.1, three 2-stage holes H for accommodating the sunk screws for fixing the plate on to the test mould were drilled. These were enlarged to diameters 2 mm larger than those of the 6.3 mm screws to enable fine adjustment in centralizing the grooved plate relative to the inner loading face of the mould.

(2) On the lower part of the plate LP.1 were fitted two rotatable brackets BR having a width of 20 mm and protruding by about 32 mm when normal to LP.1.

(3) Four swivel catches K, two on each side of the plate LP.1, were fitted to hold the ball cage BC (Fig. 4.2) and the plate LP.2 in position through the screws S (Fig. 4.6(b)) on the latter, while these are resting on the brackets BR during asembly of the loading equipment.

(4) At the centre of the flat side of the plate LP.2, a brass disc BD was screwed. This fitted into the central hole on the load cell LC (Fig.4.2) and enabled rapid centralizing of the rest of the loading equipment.

(5) A hole F was tapped in the middle of one of the sides perpendicular to the grooves on plate LP.2 for enabling an eye bolt to be screwed on to this plate during a friction test for determining the value of the coefficient μ in equation (4.3).

4.2.1.3 Pivoting and jacking frame. To enable the test mould to be jacked over the soil wedge squarely and without undue disturbance to the soil, the frame shown in Fig. 4.7 has been devised. This has been cut and welded out of 30 mm x 30 mm x 4 mm angle bars. It has three levelling screws LS, six clamp screws CS, two set screws SS the tips of which have been turned to a diameter of 6 mm, and a jacking screw JS of at least 16 mm dia. whose tip has been turned to 7 mm dia.

4.2.1.4 Apparatus for raising the jacking equipment during the test. This apparatus, shown in Fig. 4.8, can be used instead of the plain reaction plate RP in Fig. 4.2, in order to minimize the moments acting on the shear plane during

the test. It consists of two mild steel plates RPG and BPG, measuring 250 mm x 250 mm x 20 mm and 100 mm x 100 mm x 25 mm respectively. Six parallel grooves of depth 1 mm and radius 6 mm have been cut along the whole length of each plate. For ease of manufacture, these grooves can be cut along a 350 mm x 100 mm x 10 mm steel plate, which is then cut into two parts: one part, measuring 100 mm x 100 mm x 10 mm, is screwed on to a 100 mm x 100 mm x 20 mm steel plate, and the remainder on to a 250 mm x 250 mm x 20 mm steel plate. Between the grooved plates RPG and BPG there is a ball cage BC.2 carrying forty-two 12 mm dia. steel balls which can rotate freely in their housing situated at the nodes of a 16 mm x 13 mm rectangular grid. BC.2 is similar in construction to that shown in Fig. 4.9. A raising screw RS, 185 mm long, 8 mm in dia., can rotate freely, without axial motion, in a bracket screwed on RPG. RS passes through a hole in BPG. This hole is threaded along a length of 25 mm so that as RS is rotated, BPG and hence the whole jacking equipment is raised. The lower end of RS can rotate freely in a hole on a second bracket, which protects RS against bending during transport. The adoptors AD.1 and AD.2 facilitate the alignment of the hydraulic jack, the load cell, and a steel ball pasted centrally on to BPG. A handle of 10 mm dia. reinforcement steel is welded to RPG to provide ease in transportation. A bracket of 80 mm x 20 mm x 2 mm brass strip may be screwed on top of RPG, to one side of the handle, to aid the recording of the amount Δy_{RB} by which the jacking system is raised during the test.

the corresponding test mould, and that of the other limb is equal to the length of the other inner rectangular face of the same mould.

(2) Inverted gauging stool (GS in Fig. 4.12(d)).(Optional.) This is a simple wooden device with four legs, on which lines have been inscribed denoting the depth of the loading pit corresponding to each test mould. By a similar means as shown in Fig. 4.10, its length can be made adjustable to enable the use of different loading equipment. It provides a rapid means of checking the dimensions of the loading pit.

(3) Ball pads (BP in Fig. 4.2). Two 100 mm x 20 mm mild steel plates, each with a central, conical recess of a depth of 5 mm and a base diameter of 20 mm.

(4) Reaction plate (RP in Fig. 4.2). A mild steel plate measuring 270 mm x 250 mm x 20 mm.

(5) Centralizer (CR in Fig. 4.12(j)). This is a wooden frame with cross-pieces so shaped as to enable the load cell LC, the hydraulic jack HJ and the two ball pads BP (Fig.4.2) to lie concentrically when placed in their appropriate positions. The overall length of the frame is slightly less than the total length of the equipment to be aligned, its width is about 240 mm and height 70 mm. The frame rests on and is reinforced by a 2 mm thick steel lamina on which four nuts have been welded. Through these pass the levelling screws (8 mm dia., 150 mm long wing bolts with rotatable cup washers at the tips). For soft soils, where the jacking equipment may

tend to slip down upon loosening the levelling screws, it is advantageous to make the rear part (carrying the ball pad in contact with the reaction plate RB, Fig. 4.12(j)) detachable and provide it with two additional levelling screws.

If the device shown in Fig. 4.8 is to be used, a centralizer is not needed, but if the soil is soft, a simpler frame sufficiently long to support the hydraulic jack alone may be useful.

(6) Reference plate for dial micrometers (RL in Fig.4.12(j)). A 200 mm x 16 mm x 0.2 mm aluminium plate bent into an L-shaped cross-section with 100 mm long limbs.

(7) Supports to reference plate (Fig. 4.12(j)). Two 360 mm long, two 240 mm long and one 400 mm long slotted angle bars measuring 30 mm x 20 mm x 1.3 mm in cross-section.

(8) Wooden set squares (Figs 4.12(a)and(b)). Five wooden wedges measuring about 40 mm across the triangular faces and about 200 mm in length, with the smallest angles ranging from 5° to 25° at 5-degree intervals.

(9) Wooden blocks. Two 250 mm x 100 mm x 100 mm, two 250 mm x 100 mm x 50 mm and two 250 mm x 50 mm x 15 mm wooden blocks.

(10) Wooden strut and wedge (Fig. 4.12(e)). A 150 mm wide by 15 mm thick wooden strut measuring slightly less than the length of the loading pit minus 20 mm, and a 100 mm wide wooden wedge, tapering from about 30 mm to 2 mm in a length of 150 mm. One end of the strut is also cut so that one of the

longer edges measures about 30 mm shorter than the other.

(11) Steel bars (Fig. 4.12(h)). Two 300 mm long and one 600 mm long steel reinforcement bars of about 10 mm diameter.

(12) Stabilizing plate. A 460 mm x 240 mm x 1.5 mm lamina for placing on the base of the loading pit to prevent the levelling screws of the pivoting frame and of the centralizer from sinking into the ground in cases where ground water seeps and softens the base of this pit.

(13) Raising boards. Three or four 360 mm x 300 mm x 20 mm boards are sometimes useful in rapid adjustment of the elevation of the loading equipment.

(14) Gauging board. When the mode of loading shown in Fig. 4.11(a) is to be used, a gauging board is needed to enable the pivoting frame (Fig. 4.7) to be clamped into position, before mounting the test mould on to this frame. This is a 280 mm x 250 mm x 15 mm board, enlarged to a width of 270 mm for the last 30 mm at the end where holes are drilled for the set screws SS (Fig. 4.7) to engage, and is marked with a set of lines at the distances h (Fig. 4.5) from these holes.

(15) Reinforcing strips. Eight 320 mm x 20 mm x 2 mm brass strips bent to the cross-section of a right-angled channel with two 100 mm long limbs.

(16) Supports for dial gauges. If the dial gauges are

to be supported independently of the test mould, two 600 mm long slotted angle bars 60 mm x 40 mm x 2 mm in cross-section are needed.

(17) Shelf. If the test is to be performed in a test pit, a shelf suspended in the side of the pit is useful. A convenient shelf can be made by connecting two 250 mm wide, 30 mm thick boards, one side measuring 640 mm the other 900 mm, by four 450 mm long, 8 mm dia. steel bars near the corners (Fig. 5.17).

(18) Supports for reaction plate. If the mode of loading shown in Fig. 4.11(a) is to be used, two 600 mm long slotted angle bars, 30 mm x 20 mm x 1.3 mm in cross-section, are needed to be driven into the side of the test pit to support the reaction plate.

4.2.2.2 Equipment available commercially

(1) A flat faced electrical load cell (LC in Fig. 4.2) and the ancillary equipment. With the size of test moulds described here, a 2000 kg capacity load cell has been found satisfactory for the softer soils, and one of 5000 kg capacity for the stiffer soils.

(2) A hydraulic jack (HJ in Fig. 4.2), with the jacking unit connected to the hand pump by means of a flexible hose. One of 10 000 kg capacity is adequate.

(3) Depending on the type of test envisaged (see Section 4.3), two to four dial gauges, 0.01 mm divisions, 50 mm

travel, mounted on supports with magnetic bases.

(4) A stop-watch.

(5) A spirit level of length about 200 mm.

(6) (Optional.) An adjustable spirit level for checking any desired inclination.

(7) A 500 mm steel rule, graduated in mm.

(8) A carpenter's square.

(9) Tools for scraping, excavating and cutting, for shaping the loading pit and the soil wedge.

(10) A screw driver.

(11) A small container of vaseline.

(12) A small container of light grade oil.

(13) An 18 mm dia. steel ball. For ease in transport and handling, this may be pasted into the central recess on one of the ball pads BP (Fig. 4.2).

(14) Four 40 mm long wood screws; three 6.3 mm dia., 18 mm long screws; four 4.8 mm dia., 15 mm long screws with wing nuts.

(15) Two cellophane sheets, measuring about 1.5 m x 1.0 m, for covering the test area if left temporarily for some hours before testing, and for placing instruments on.

(16) If the test is to be performed in a test pit, means

of excavating and keeping it free of ground water.

(17) A thermometer for recording the soil temperature, moisture content boxes, sellotape .

4.3 Planning the test

4.3.1 Choice of suitable test moulds

There are two limitations on the value of the mould angle α (Fig. 4.2) that can be used in the iswest . Firstly, if α is too large, the soil at the more critical end of the loading pit will fail in three-dimensional passive resistance. Secondly, if α is too low, failure may take place along a surface inclined at an average angle λ to the direction of loading, where $\lambda > \alpha$, and there is no guarantee that this surface will be plane. Both these limits depend on the value of the undrained shear strength parameters c and $\emptyset$ of the soil (which are to be determined through the iswests), on the inclination of the direction of loading, and on the weight and frictional properties of the loading equipment used.

The curves in Figs 4.13 and 4.14 have been derived (Appendix B) by combining equations 4.1 to 4.5 with the Mohr-Coulomb failure criterion, neglecting the area correction and side friction, and using the actual values for the weights of the loading equipment used in this study.

Fig. 4.13 shows the variation with α of the theoretical force P_f required to cause shear failure along the prescribed plane (ABDE in Fig. 4.1(b), for six different values of $\emptyset$ and

two different values each of c and θ. The dots on the dashed curves and the thick dashes across the continuous curves represent one-half of the ultimate bearing capacity of a 250 mm square plate at the surface of a semi-infinite medium as calculated from Terzaghi's (1943) bearing capacity factors for the appropriate Ø values. These dots and dashes therefore represent the approximate limits beyond which three-dimensional shear failure may take place before failure along the plane ABDE (Fig. 4.1(b)) can occur. More accurate positions for these points will depend on the exact configuration used in the test.

In their lower extremities the curves in Fig. 4.13 have been terminated to conform with the relationships given in Fig. 4.14. These represent, for different c and θ values, the relationships between the mould angle α and the minimum value of Ø that the soil must have to ensure that failure will not take place along a plane inclined at $\lambda > \alpha$ to the direction of loading. The intersection of these lines with the $\emptyset = 0$ axis gives the minimum value of α that can be used for a fully saturated soil for the particular values of c and θ.

Due to friction between the sides of the test mould and the soil wedge, it is likely that in practice the minimum required values of Ø will be somewhat less than given in Fig. 4.14.

If the approximate undrained shear strength parameters of the soil are known, the curves in Figs 4.13 and 4.14 may be used to select a suitable range of test moulds. For example, for

$\theta = -90^{\circ}$ (vertical loading), $c = 0.3$ kg/cm^2 and $\phi = 10^{\circ}$, moulds with angles α between 40° and 65° could be used; for $\theta = 0$, $c = 0.05$ kg/cm^2 and $\phi = 30^{\circ}$, moulds with α between 25° and 50° are suitable. A 45 degree mould can be used for any type of soil having sufficient cohesion to be shaped as in Fig. 4.1(b). Thus for soils whose properties are completely unknown, it is best to start testing with a mould of $\alpha = 45^{\circ}$ and continue with moulds having decreasing angles α. If in any test the soil fails at an angle larger than α to the direction of loading and the surface of failure is nearly plane, calculations may be performed using the actual inclination of the failure plane. The remaining tests can then be carried out using moulds with α larger than 45°.

For soils whose approximate undrained shear strength properties have been established by previous tests, two moulds with as widely different angles α as possible are sufficient to enable the undrained shear strength envelope to be determined, for as many tests as the desired accuracy warrants may be performed using these moulds and a mean straight line drawn through the points obtained.

4.3.2 Selection of the mode of loading

If the peak shear strength parameters are required for the solution of a slope stability problem, the stress conditions in the iswest will be closest to those in the actual problem if the mode of loading shown in Fig. 4.11(a) is adopted. In weaker soils, particularly if the undrained residual strength parameters are also required, a more certain mode of loading

to adopt is that shown in Figs 4.11(b) and (c). In this case, the shear strength is measured under the same normal stress as in Fig. 4.11(a), but the orientation of principal stresses at failure is different. The influence of this difference on the measured strength can, however, be estimated by comparing the results of tests using the two main modes of loading. By the use of both modes of loading, the shear strength on any plane can be measured.

4.3.3 Minimizing moments on the shear plane

4.3.3.1 When a plain reaction plate is used

In order to minimize the moments and hence the non-uniformity of stress along the failure plane, an initial upward displacement, here referred to as the initial eccentricity, Δy_p, can be applied to the jacking system relative to the test mould, before the start of the test. The value of Δy_p to be used in any series of tests can be decided after performing one or two tests with a nominal value of $\Delta y_p = 5$ mm, say, and evaluating, from equation (4.9), the value of Δy_p required to make the resultant moment on the failure plane zero at peak strength. This value of Δy_p can then be adopted as the initial eccentricity to be used in future tests on the same material. The value of Δy_p required for large negative values of θ (e.g., Fig. 4.11(a)) is generally about one-half of that required for positive values of θ (Figs 4.11(a) and (c)).

4.3.3.2 When the device for raising jacking equipment during test is used

A more effective means of reducing moments on the failure plane is to raise the jacking equipment during the test by means of the device in Fig. 4.8, in accordance with a set of pre - calculated curves correlating Δy_{MP} (required to make M in equation 4.9 zero when v and β are neglected) with P for different values of δ_x. Such curves can be calculated for each intended value of α and θ from the following equation.

$$\Delta y_{MP} = \delta_x \frac{\tan \alpha}{2} - \frac{xW\cos\theta + yW\sin\theta + (\frac{M_B}{D}\cos\theta + F)(\frac{d\cos\alpha - \delta_x + n}{2})}{P - (W_{BC} + W_{LP})\sin\theta} \quad ..(4.24)$$

4.3.4 Measurement of the mould rotation β

If the peak shear strength parameters are required for a routine stability analysis, and particularly if the computations are to be performed by hand, it is not necessary to measure the slight rotation β of the mould during the test. If, however, a more comprehensive interpretation of the test is desired, β will have to be measured.

4.4 Test procedure

Whichever of the modes of loading explained in Section 4.3.2 is selected, the test procedure is essentially as follows.

(1) A shallow pit about 500 mm wide is formed as in Fig. 4.12 (a) or (b) such that AB is parallel to the proposed failure plane, DB is parallel to the proposed direction of loading and

equal to the combined length of the top of the soil wedge and the jacking equipment, and DE is at least 80 mm.

(2) Using the adjustable frame (Section 4.2.1.6) as a guide, a loading pit is cut to a depth equal to the height of the loading face of the soil wedge plus about 10 mm (Fig. 4.12(c)). The guide frame is then removed, and the loading face of the test wedge accurately trimmed perpendicular to the upper face, the L-plate (Section 4.2.2.1(1)) being used to facilitate this procedure. The sides of the loading pit are then cut by a further 20 to 30 mm for a distance of about 80 mm measuring from the test wedge end. The dimensions of the loading pit are eventually checked by means of the gauging stool GS (Fig. 4.12(d)).

(3) The reaction plate RP is then placed at the end of the pit, and the L-plate is held in position by a wooden strut while the sides of the soil wedge are trimmed using the L-plate as a guide (Fig. 4.12(b)). If the soil is soft, a stabilizing plate is placed on the base of the loading pit.

(4) The inner walls of the test mould are smeared with vaseline. The pivoting and jacking frame is mounted on to the test mould through the set screws SS (Fig. 4.7) engaging the holes B on the mould (Fig. 4.5). The set screws are adjusted until the jacking screw JS is coaxial with the hole D on the mould when the pivoting frame is held in a position perpendicular to the loading face of the mould. The levelling screws LS and the clamp screws CS on the pivoting frame,

together with wooden blocks placed along the sides of the loading pit, are used to clamp this frame in the position shown in Fig. 4.12(f) with the marks M, on the chamfered edges of the test mould, level with the top of the soil wedge. (If the mode of loading shown in Fig. 4.11(a) is to be used, the pivoting and jacking frame should be clamped into position by means of the gauging board (Section 4.2.2.1 (14)) before mounting the test mould on this frame.)

(5) The test mould is rotated about the set screws SS (Fig. 4.7), until the upper inner face of the mould just touches the upper face of the soil wedge. During this rotation the cutting edges of the test mould trim off the excess soil on the two sides of the test wedge. The jacking screw JS (Fig. 4.7) is then screwed forward until it engages the hole D on the test mould (Fig. 4.12(g)). The set screws SS are then unscrewed until they are clear of the test mould. A hydraulic jack is inserted between the upper part of the loading face of the mould and the reaction plate. The test mould is jacked forward by the simultaneous operation of the jacking screw and the hydraulic jack until resistance is felt on both these units. If the test mould tends to slide back when left unsupported, support is provided, by a steel reinforcement bar bearing on the handle of the mould and held by two other bars driven into the soil on either side of the mould (Fig. 4.12(h)), before the pivoting frame and the hydraulic jack are removed.

(6) The section AB (Fig. 4.12(a)and(b)) is flattened

slightly as in Fig. 4.2. This is important for ensuring consistent test results, and to avoid ambiguity about the area correction applied in the evaluation of the test. In the softer soils, it is advisable to reinforce the flattened section AB by some eight reinforcing strips (Section 4.2.2.1 (15)), with the two limbs driven at 30 mm intervals into the soil, and the tops lying along AB. The possibility of a local passive failure in this zone is thus eliminated.

(7) The grooved loading plate LP.1 (Fig. 4.6(a)) is screwed on to the test mould using the plates GP (Fig. 4.5) as a guide. The ball cage BC (Fig. 4.9) and the second grooved plate LP.2 (Fig. 4.6(b)) are then placed on the rotatable brackets BR of the grooved plate LP.1, and fastened on to the latter by means of the swivel catches K on LP.1 engaging the screws S on LP.2. The grooves are lubricated with a light grade oil.

(8) The load cell LC, the hydraulic jack HJ, and two ball pads BP with an 18 mm dia. steel ball in between are then placed into their appropriate positions on the centralizer CR. The whole is lowered into the loading pit and the levelling screws of the centralizer adjusted until the jacking equipment is coaxial with the brass disc BD on the grooved plate LP.2 (Fig. 4.6(b)).

(9) The reference plate RL is mounted on a slotted angle bar supported by two others driven into the soil on either side of the mould. Two dial gauges on magnetic bases are

positioned to measure the displacements of the mould parallel and perpendicular to the direction of loading (Fig. 4.12(j)). For the reason given at end of Section 7.1.1.3, it is advisable to mount the latter near the plane of symmetry of the test mould. If it is desired to measure the slight rotation β of the mould (Section 4.3.4), these dial gauges should be supported independently of the test mould, and adjusted such that the distances d_1 and d_2 in equations 4.21 and 4.22 are about 120 mm and 10 mm respectively, and a third dial gauge be set to record the relative movement between the mould and LP.2.

(10) If the set up shown in Fig. 4.8 is to be used (Section 4.3.3.2), a fourth dial gauge is used to record the amount by which the jacking equipment is raised during the test.

(11) The zero readings of the dial gauges and of the balancing unit for the load cell are taken, and then a small load (about 15 kg) is applied through the hydraulic jack. The brackets BR and the catches K on the grooved plate LP.1 are turned free of the second grooved plate LP.2. The jacking equipment is raised until the desired initial eccentricity (Δy_p) is obtained (Section 4.3.3.1).

(12) Soon after the loading is resumed, the levelling screws on the centralizer, except those supporting the detachable rear part if provided, are loosened. (In soft soils, particularly when the available jack is unduly heavy, it may be necessary to adjust these levelling screws

continuously in order to enable the jacking equipment to remain normal to the loading face of the test mould, but if this is done, M_B in equations 4.2 and 4.9 should be taken as zero.) A displacement rate of about 0.125 mm/minute in the direction of loading is used until failure occurs. The displacement rate is then increased to 0.25 mm/minute until about twice the failure displacement is reached, when the rate is increased again to about 2.5 mm/minute. Readings are taken at about 2 minute intervals.

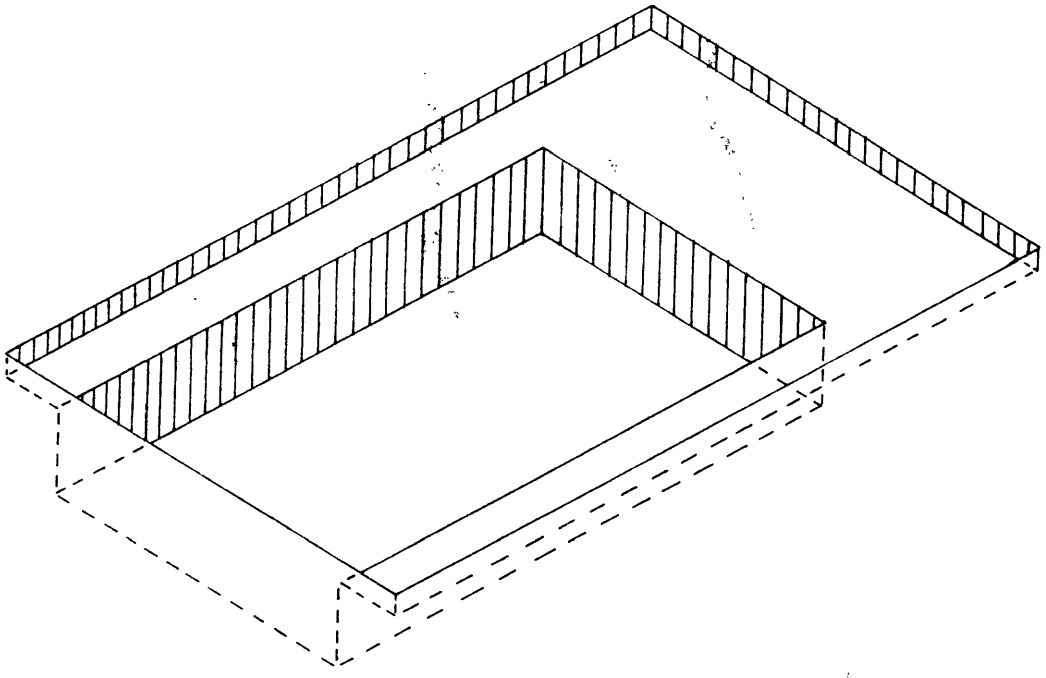

(a)

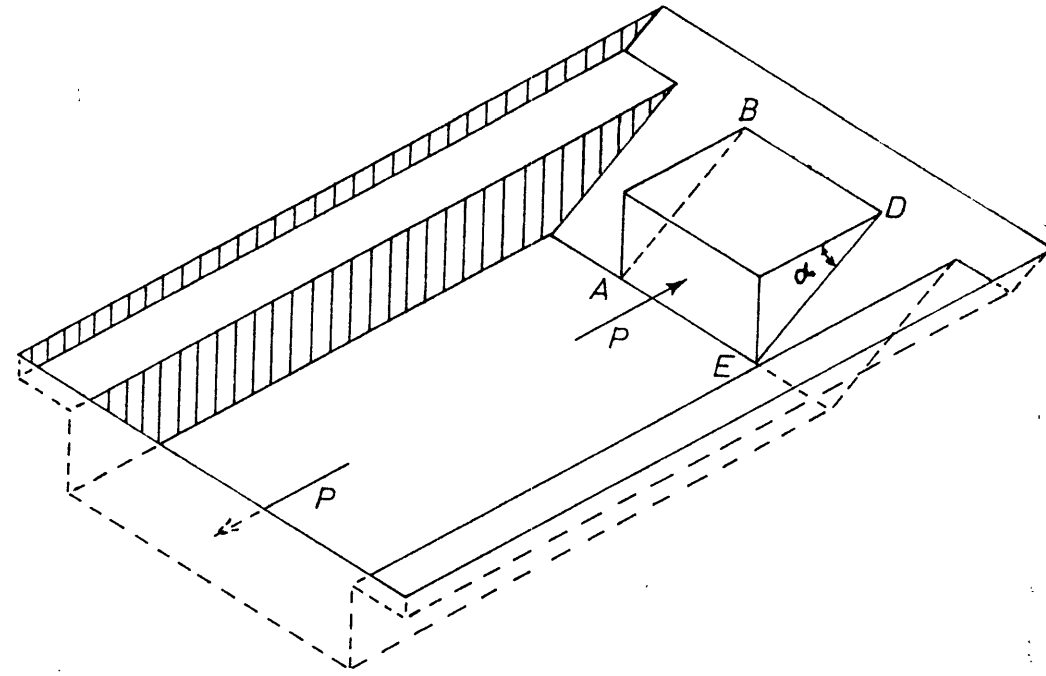

(b)

Fig. 4.1. : Illustration of principle of the iswest

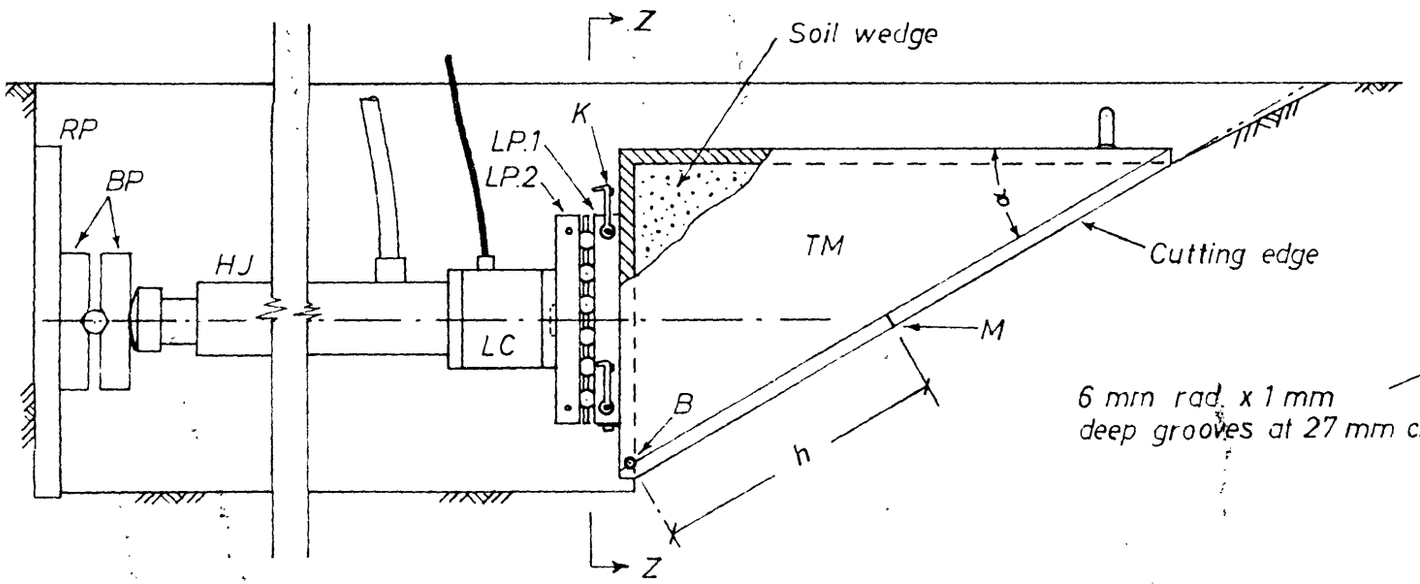

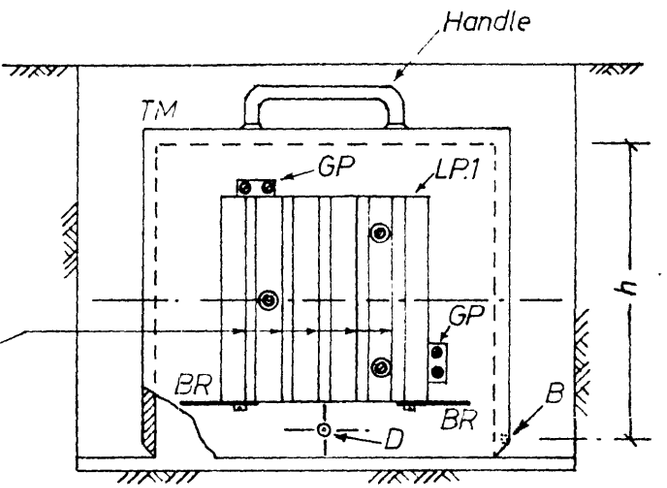

6 mm rad. x 1 mm
deep grooves at 27 mm crs.

View on Z - Z

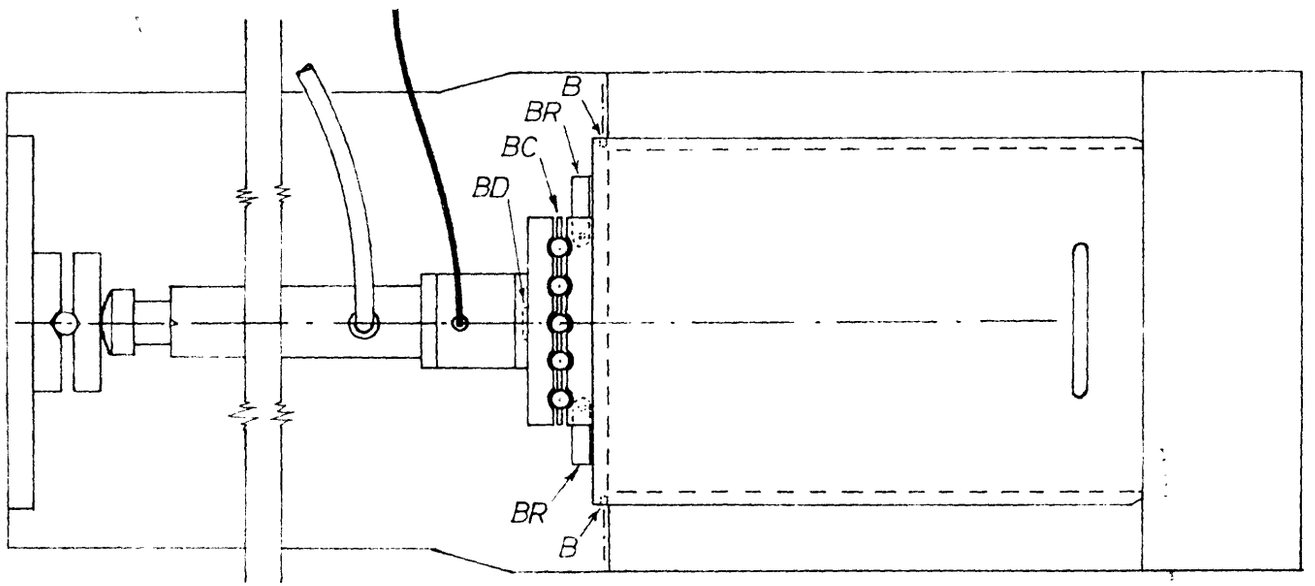

Fig. 4.2. Loading system used in the iswest

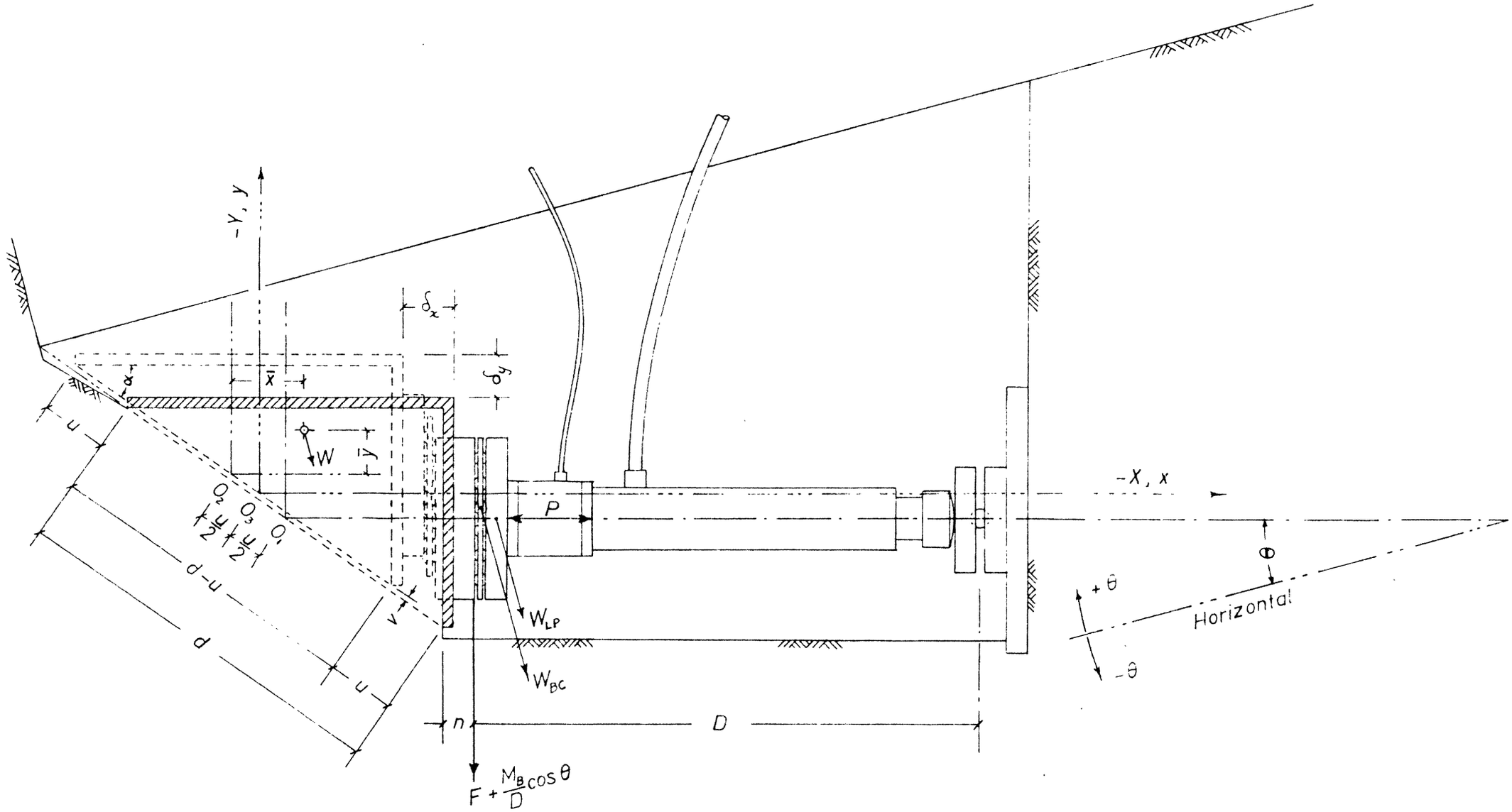

Fig 4.3. Forces, displacements, and distances involved in the evaluation of test results

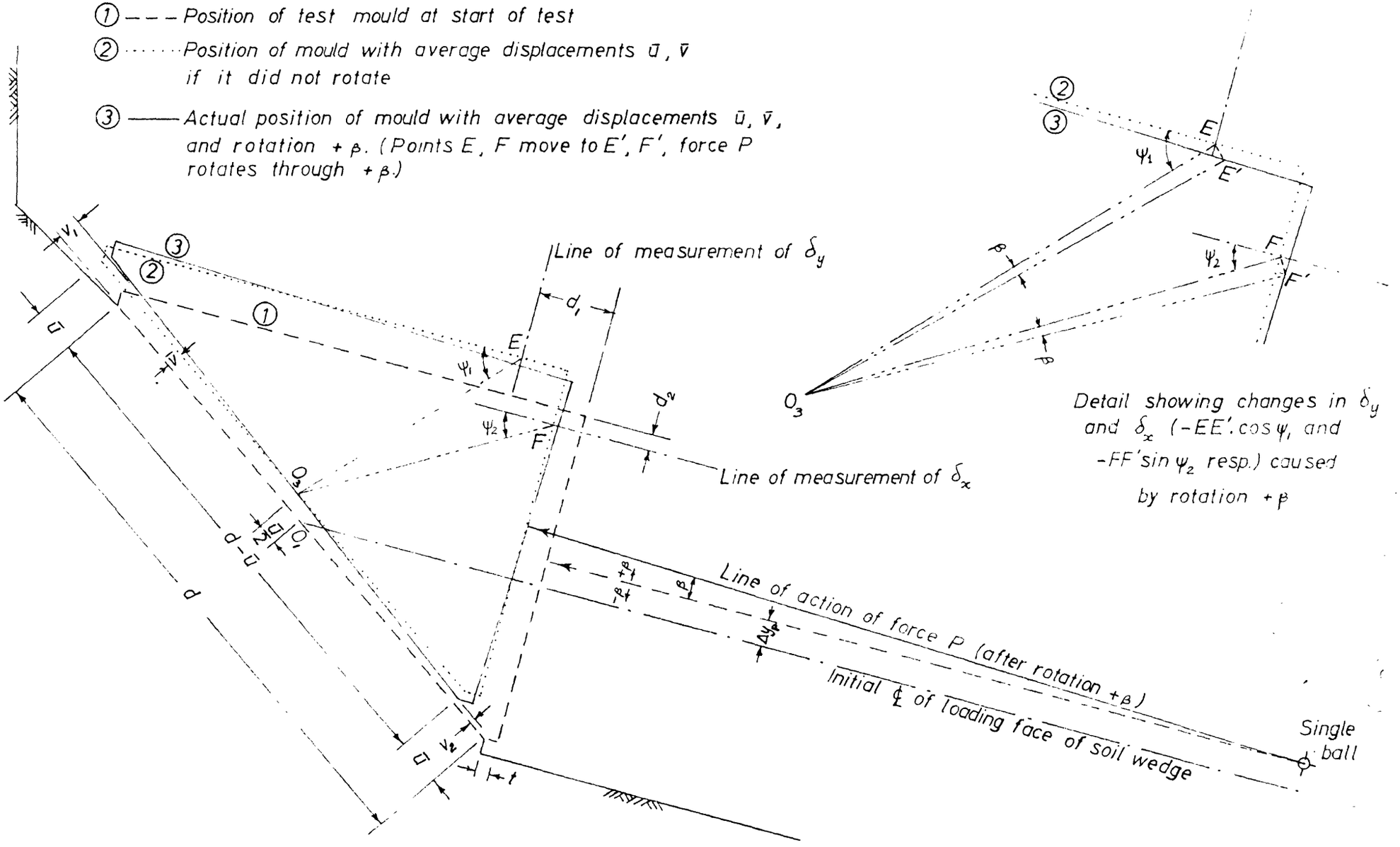

Fig. 4.4. Diagrammatic illustration of the effect of mould rotation on the effective values of Δy_p, δ_x and δ_y

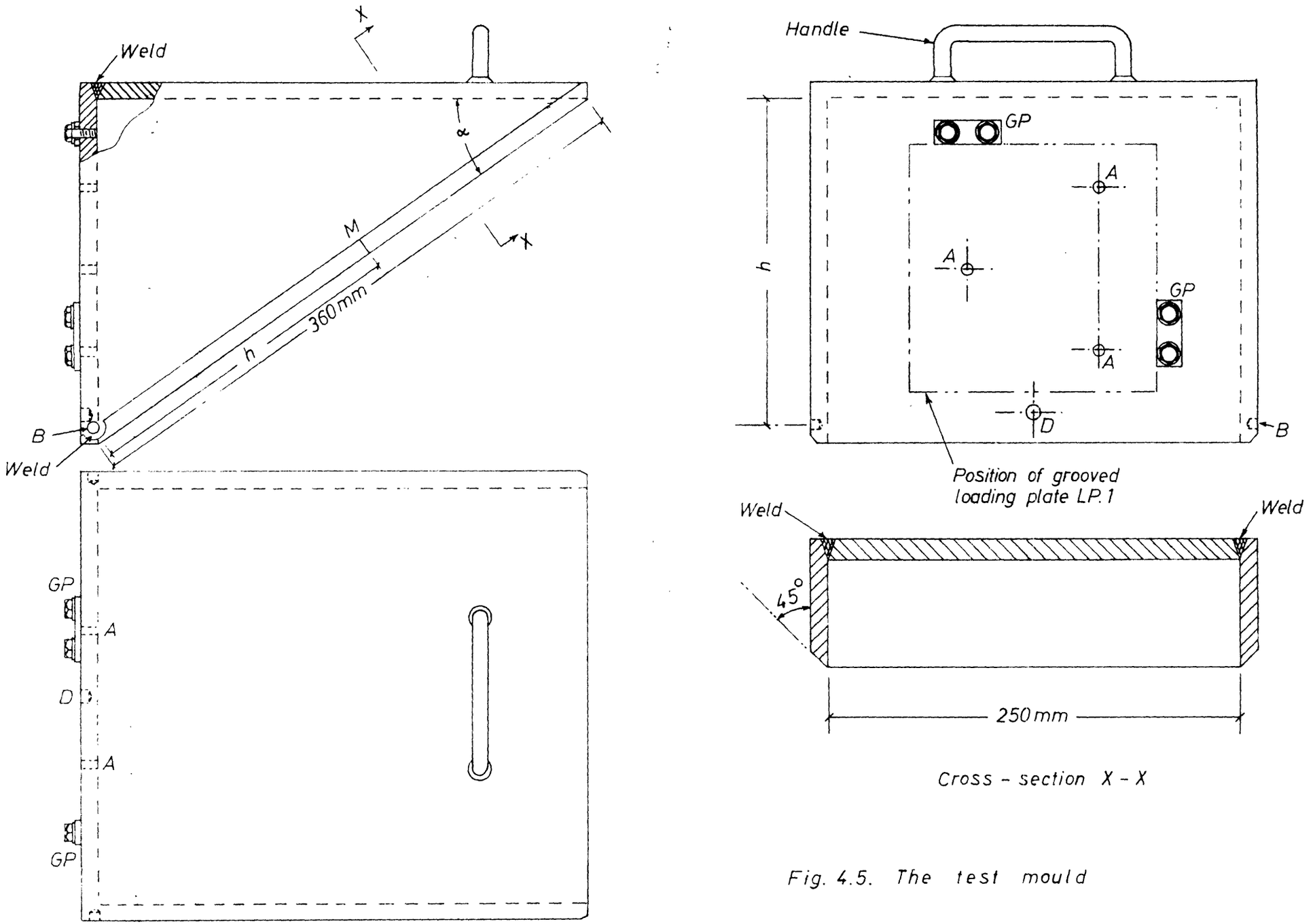

Fig. 4.5. The test mould

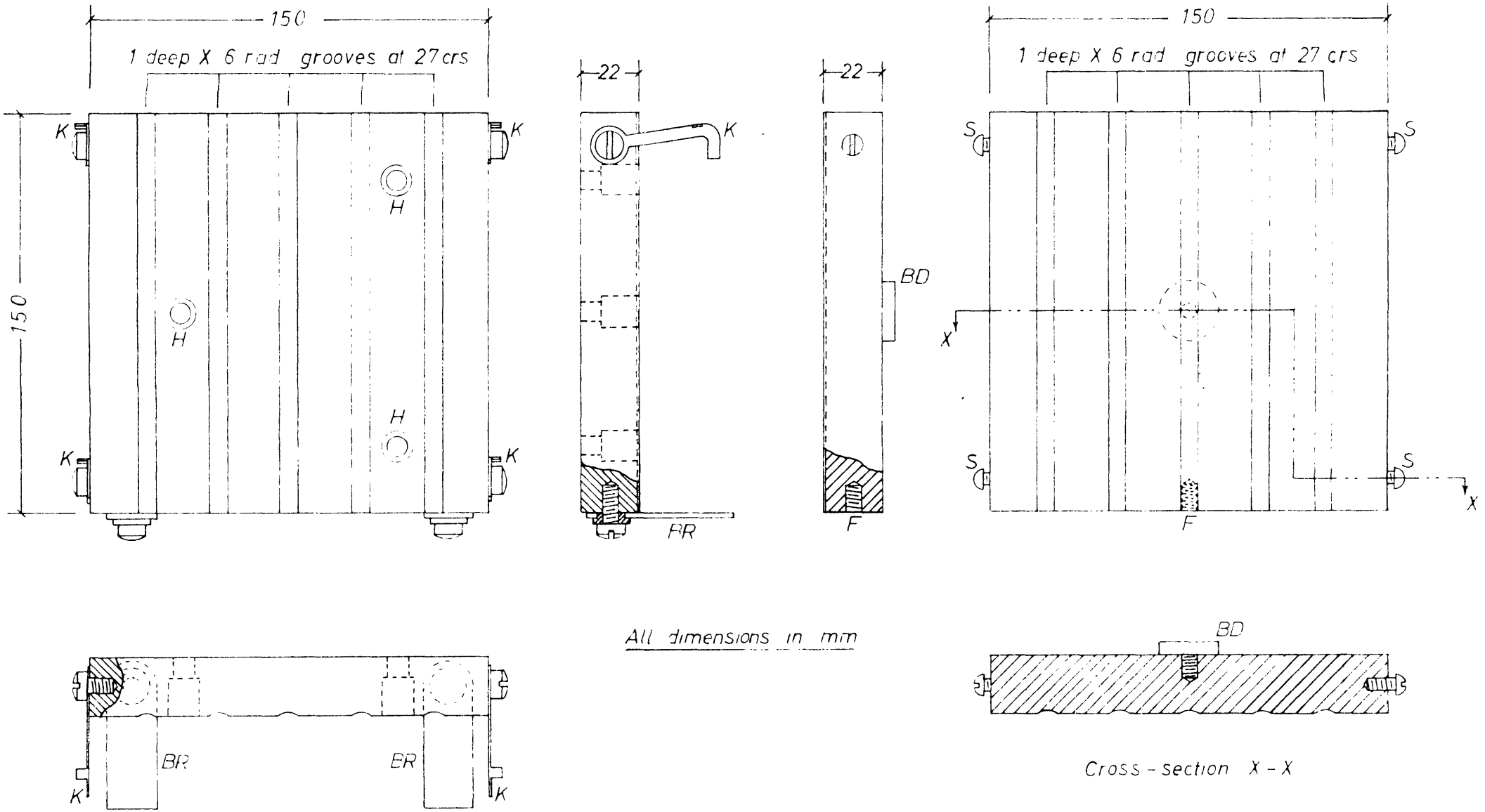

(a) Grooved loading plate LP 1

(b) Grooved loading plate LP 2

Fig 4.6. Details of the grooved loading plates

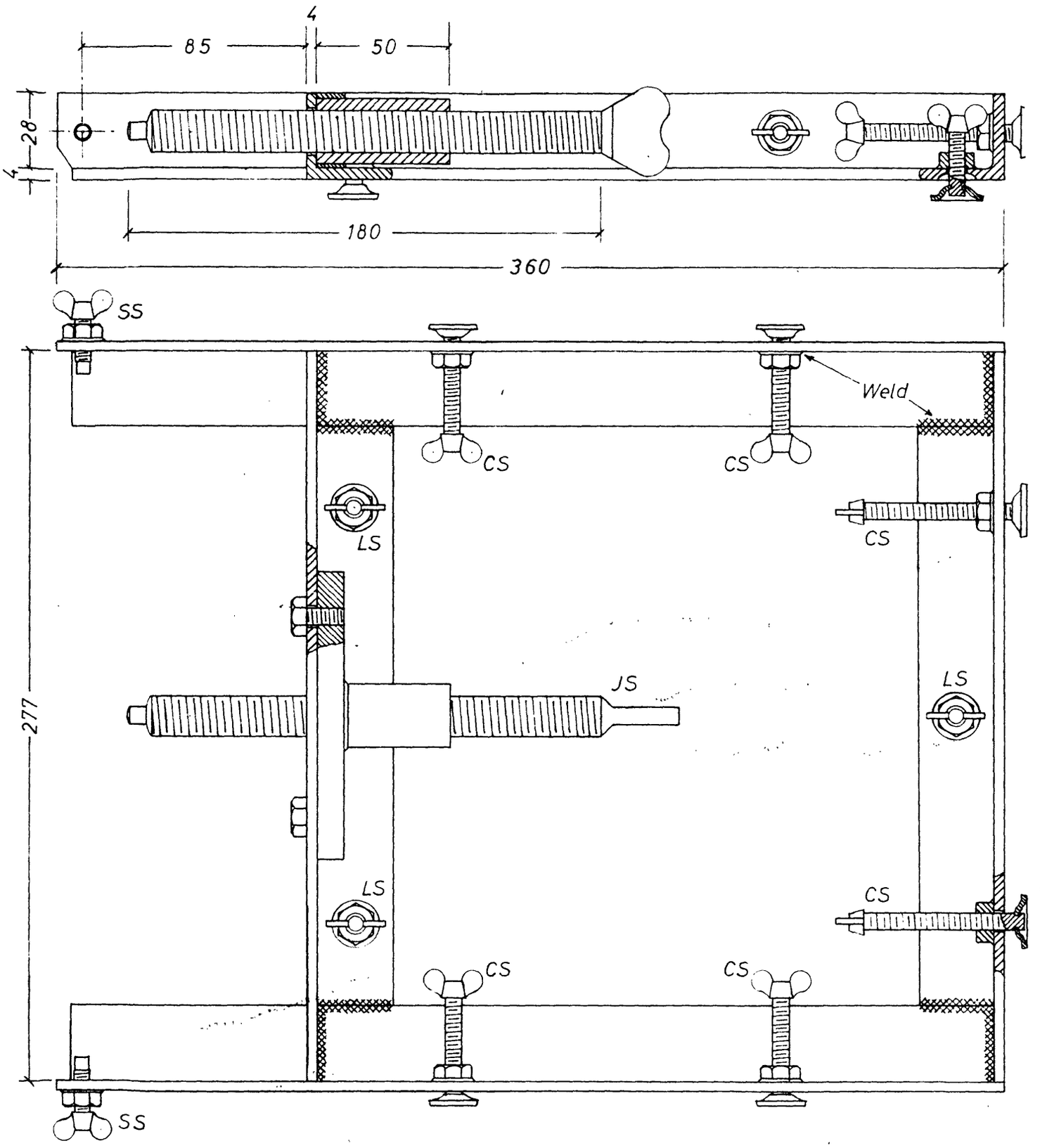

All dimensions in mm

Fig. 4.7 Pivoting and jacking frame

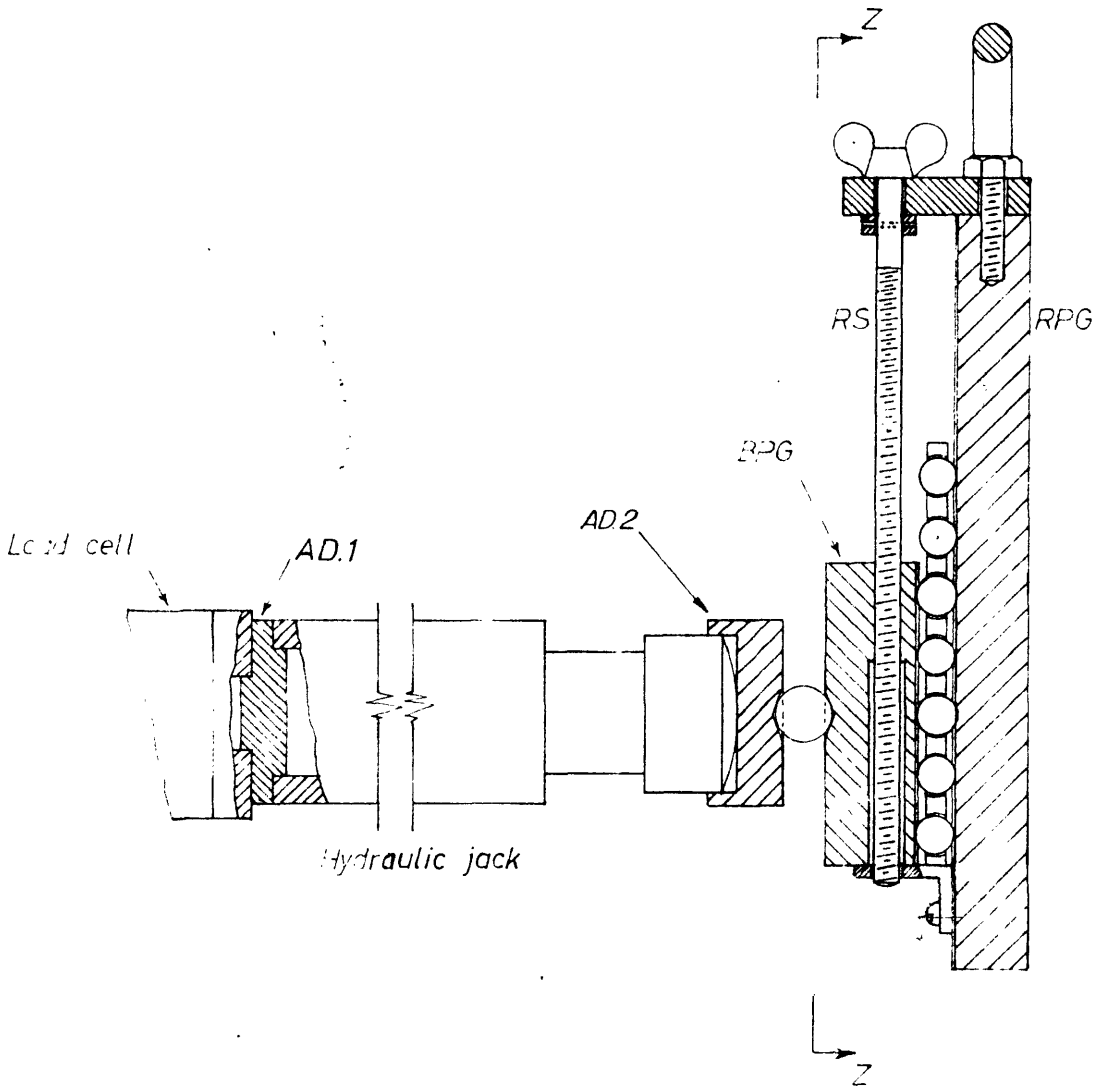

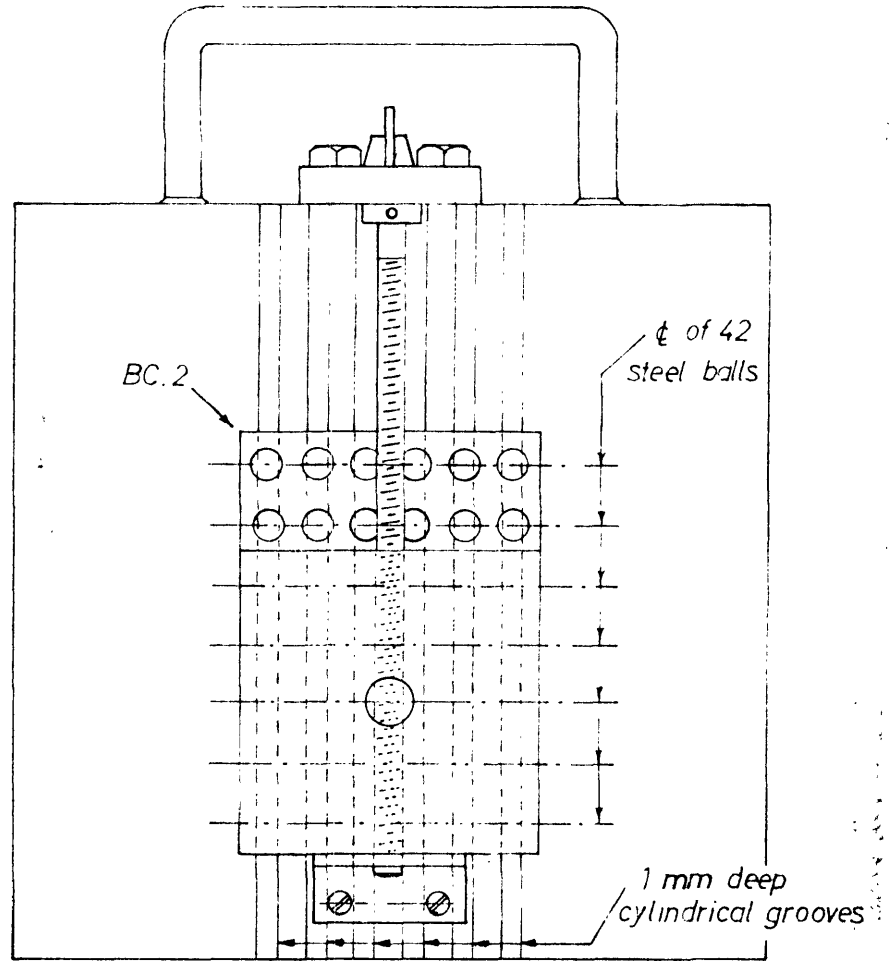

View on Z - Z

FIG 4.8. Mechanism for minimizing moments on the shear plane at large strains

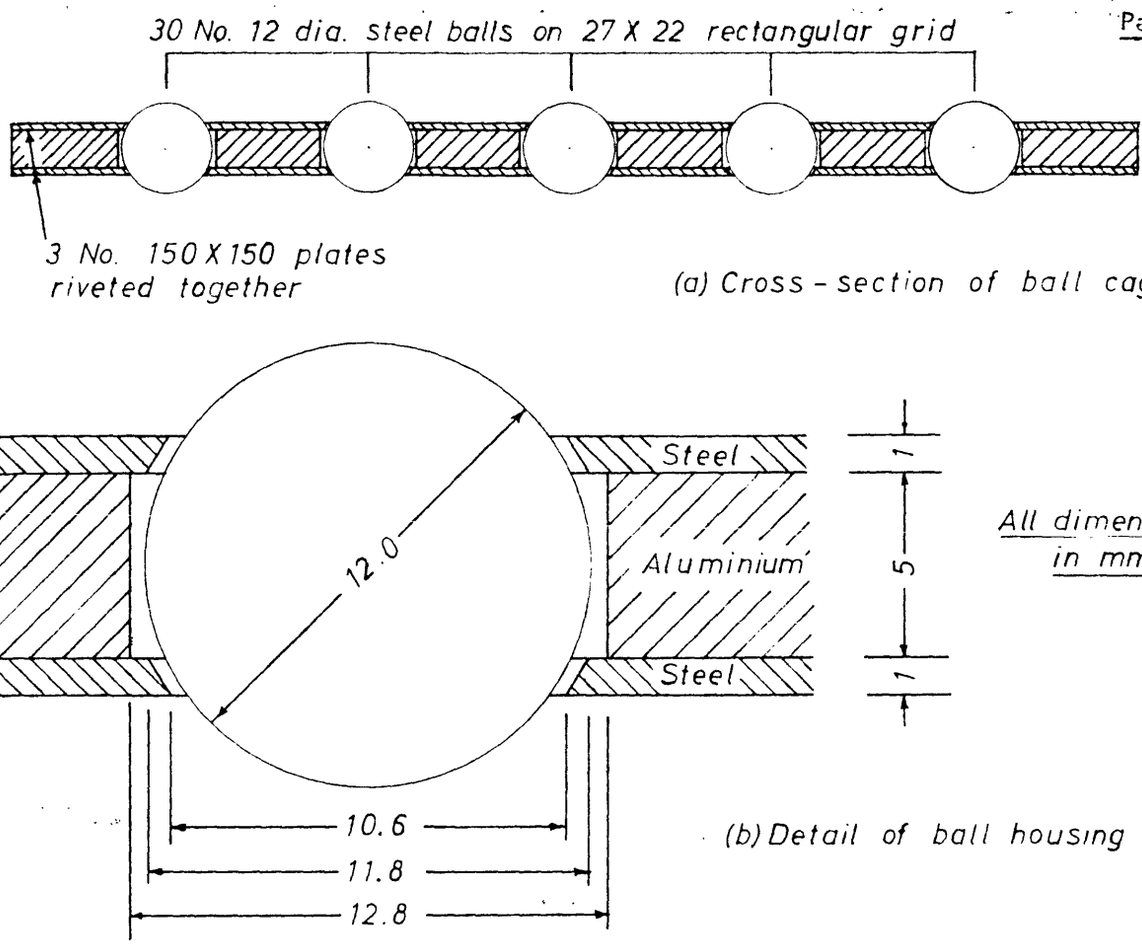

Fig. 4.9. The ball cage

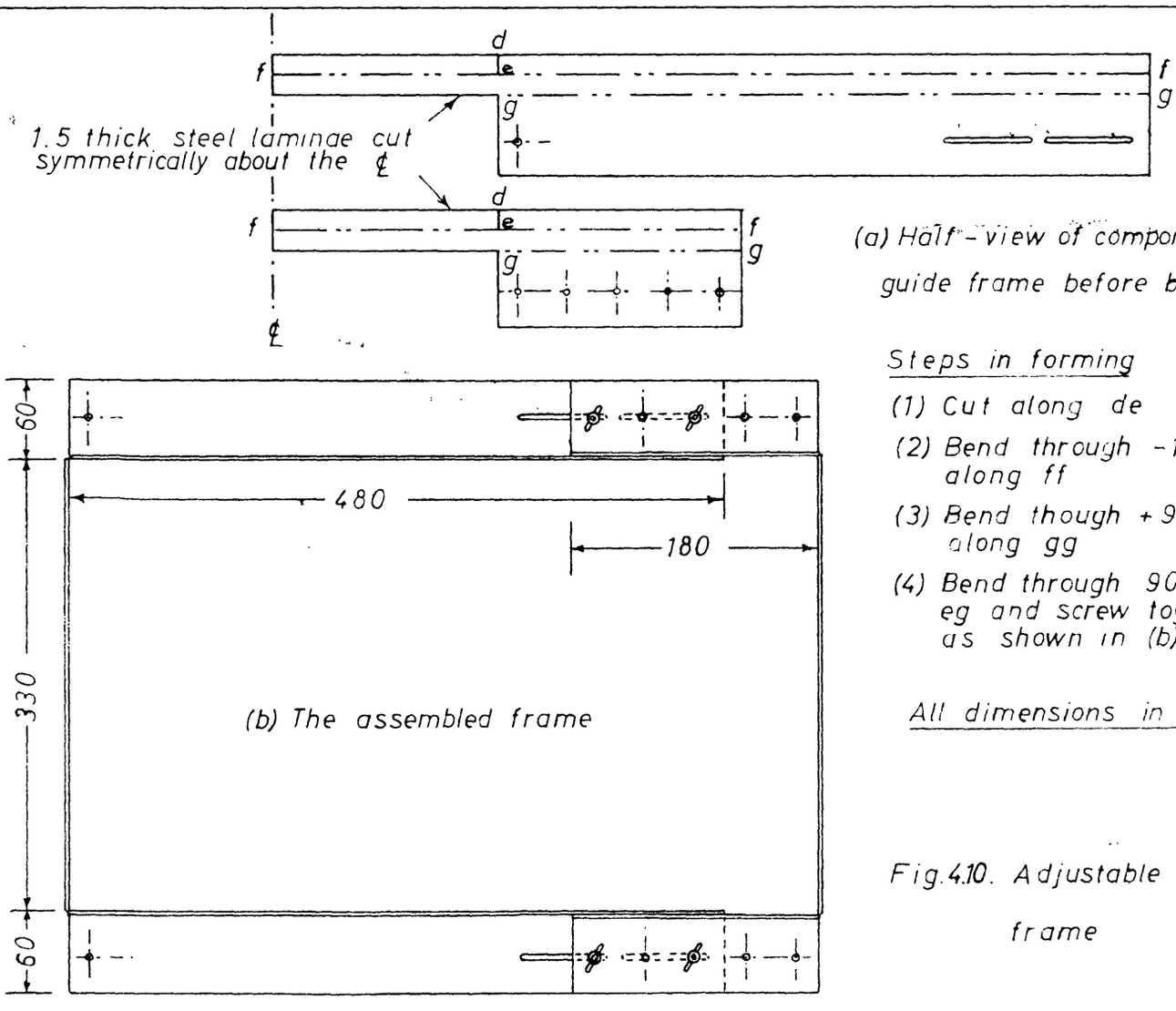

Fig. 4.10. Adjustable guide frame

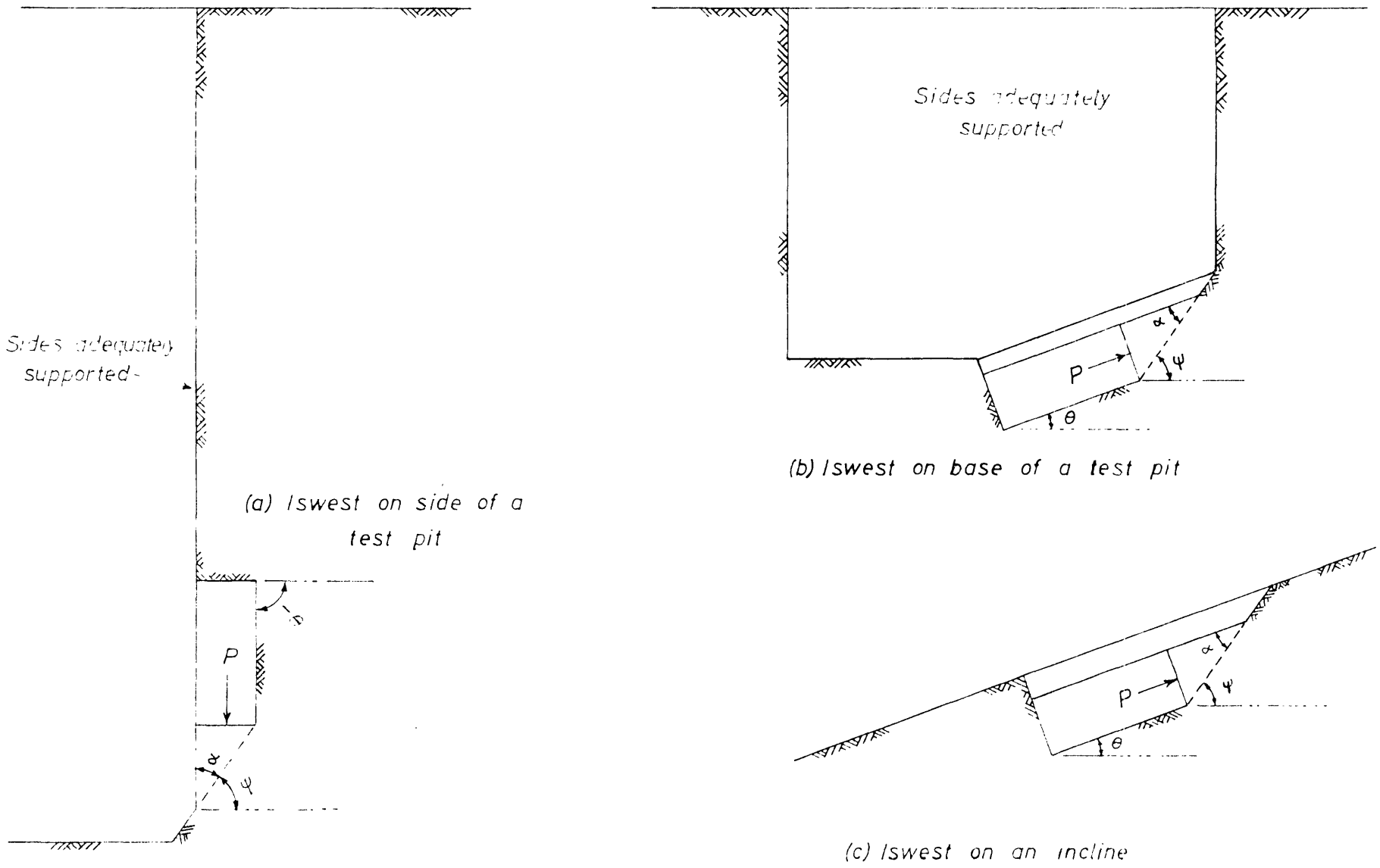

(a) Iswest on side of a test pit

(b) Iswest on base of a test pit

(c) Iswest on an incline

Fig. 4.11. Different ways of measuring shear strength on a given plane by iswests

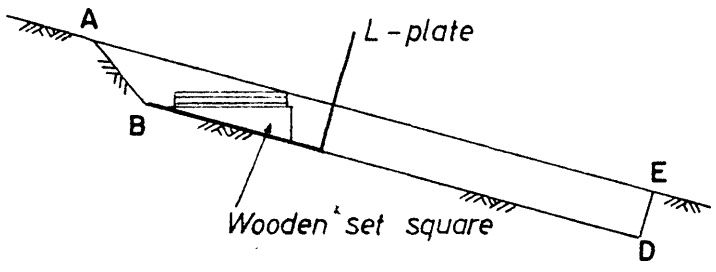

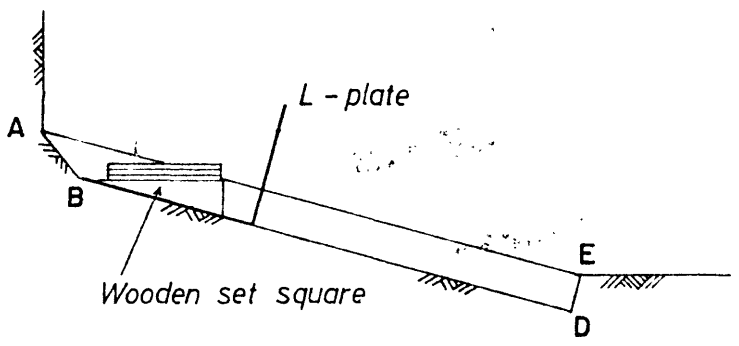

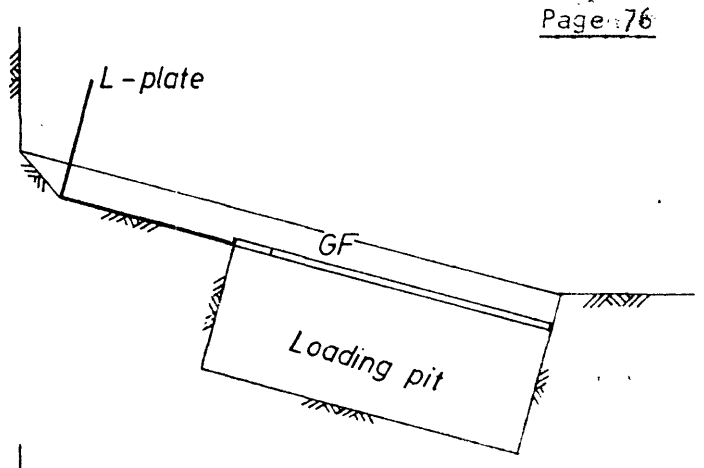

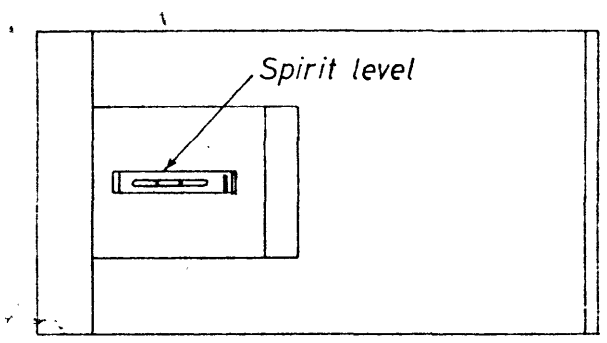

(a) Preparation of test area (on an incline)

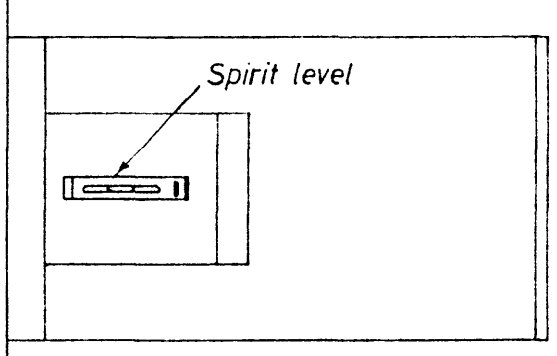

(b) Preparation of test area (in a test pit)

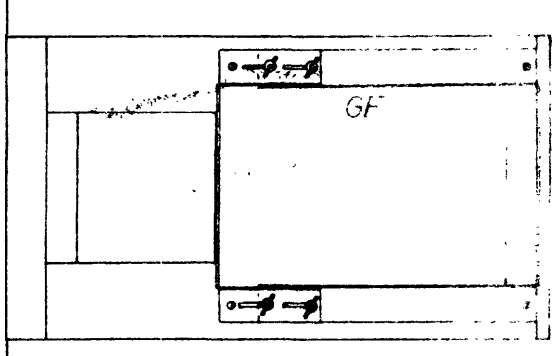

(c) Excavation of loading pit

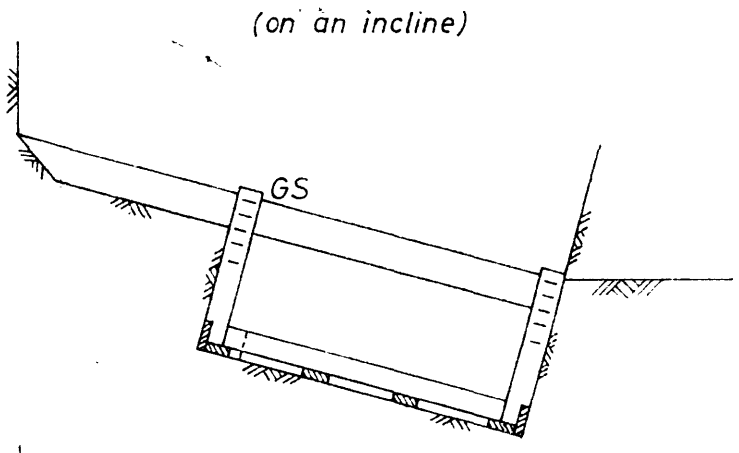

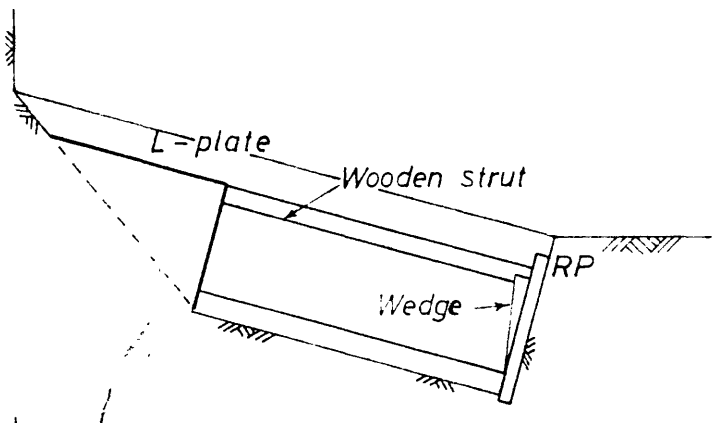

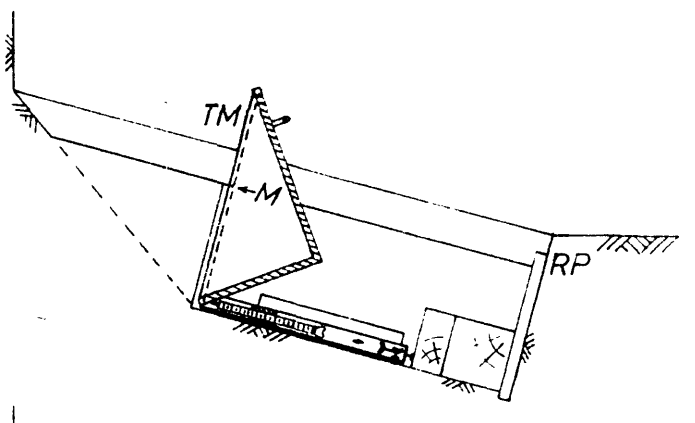

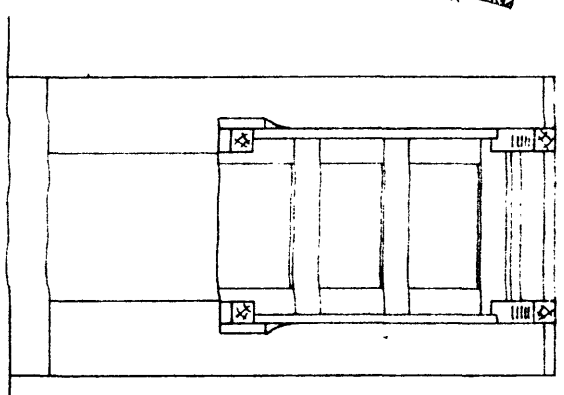

(d) Checking dimensions of loading pit

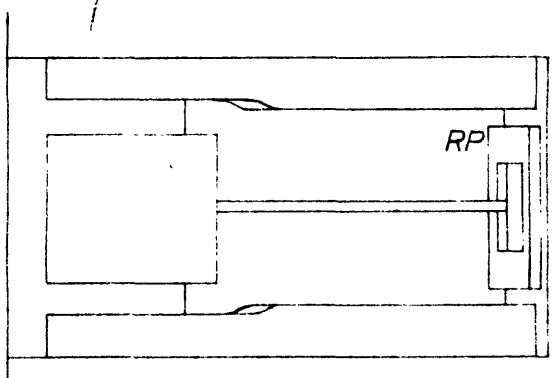

(e) Cutting sides of soil wedge

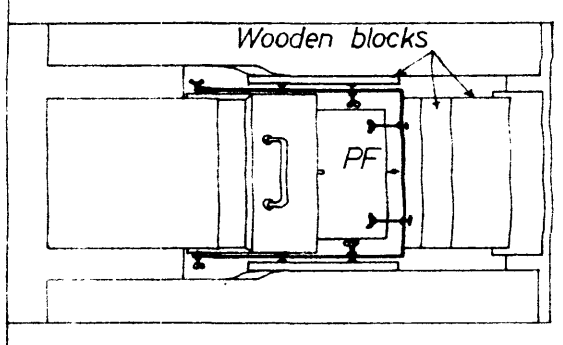

(f) Clamping the pivoting and jacking frame in position

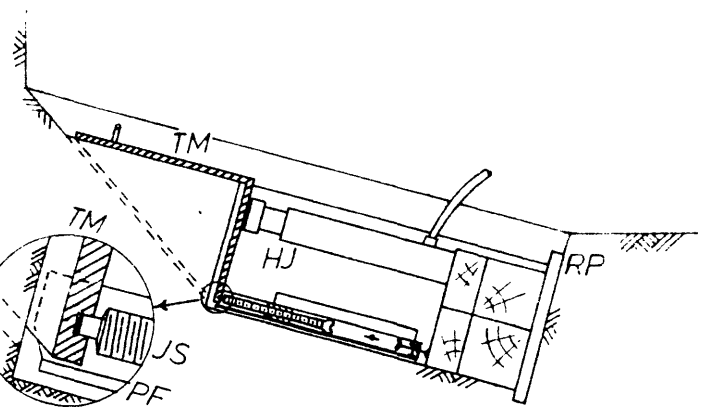

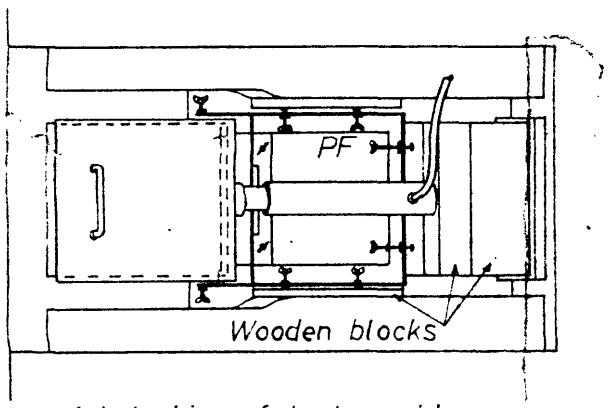

(g) Jacking of test mould over the soil wedge

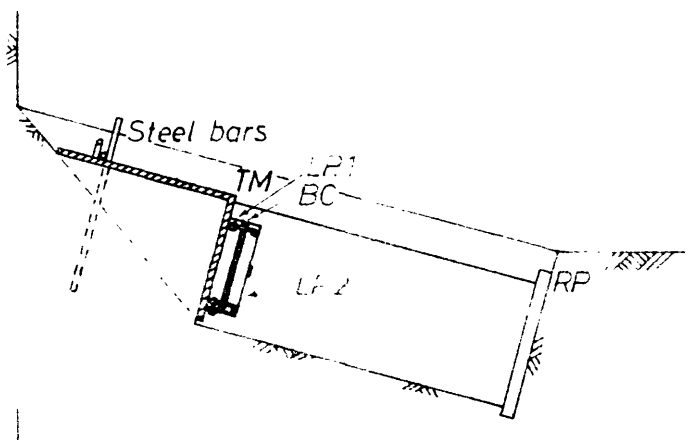

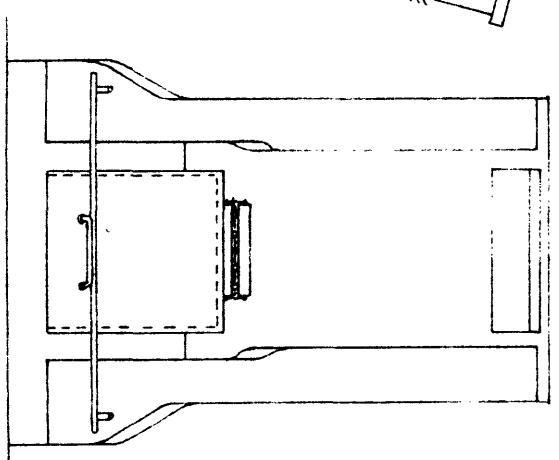

(h) Grooved loading plates in position

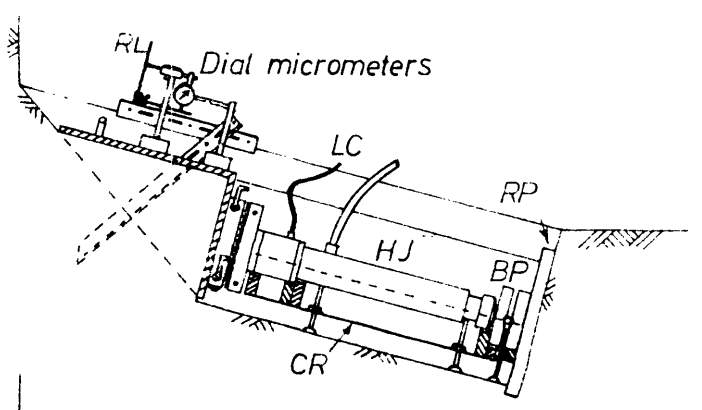

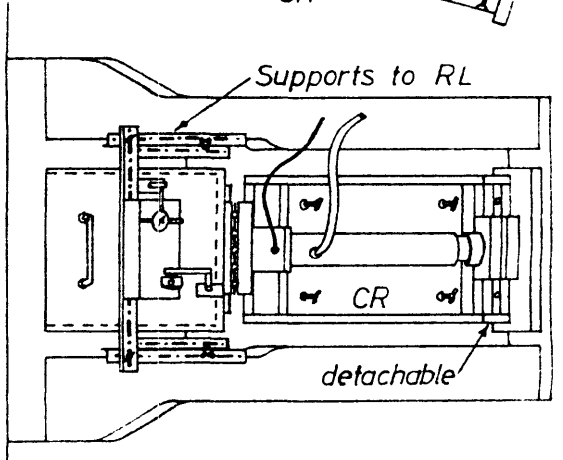

(j) Loading

Fig. 4.12. Stages in performing an iswest

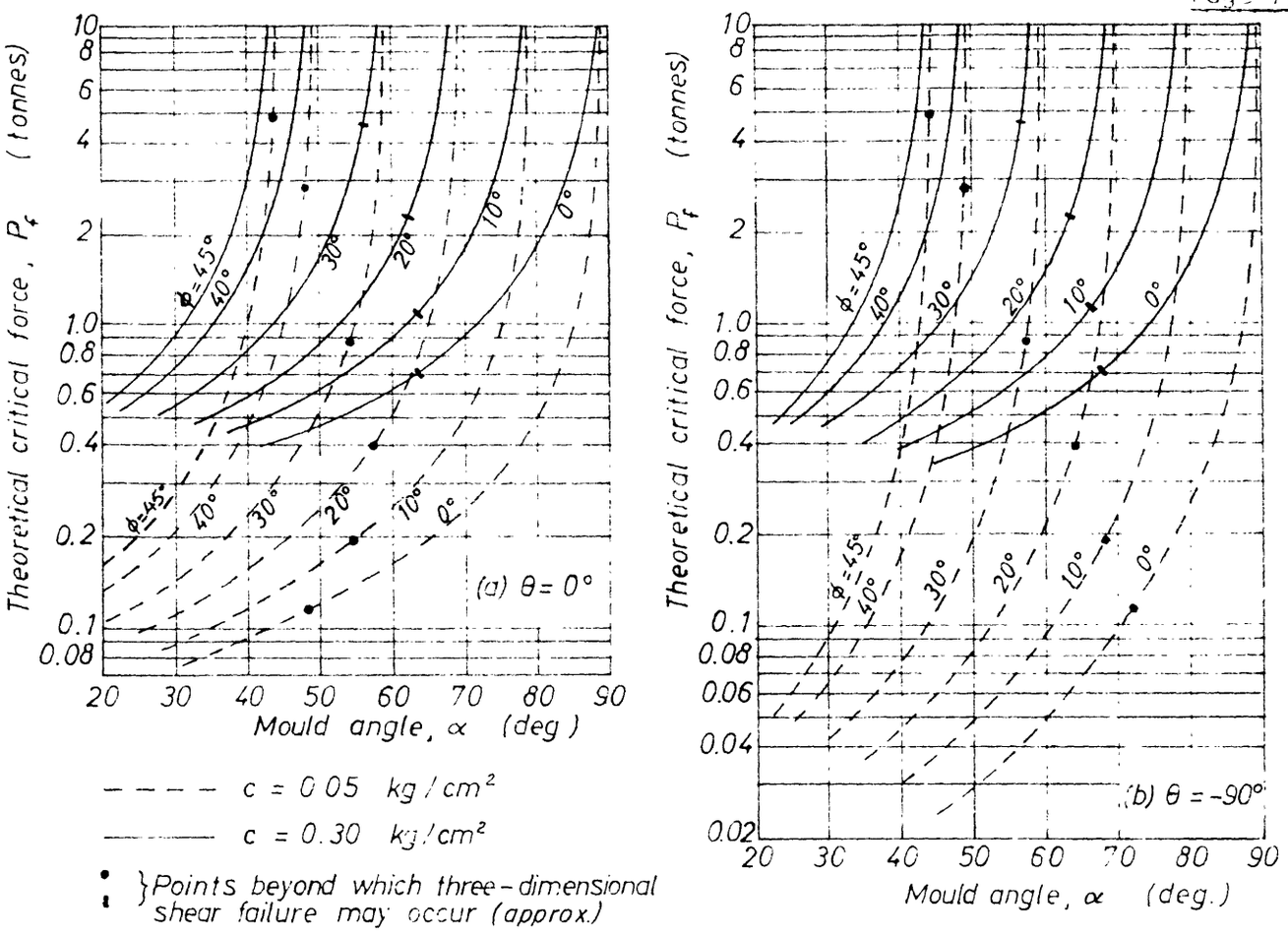

Fig 4.13 Theoretical variation with α of force P_f required to shear soil wedge along ABDE (Fig. 4.1(b))

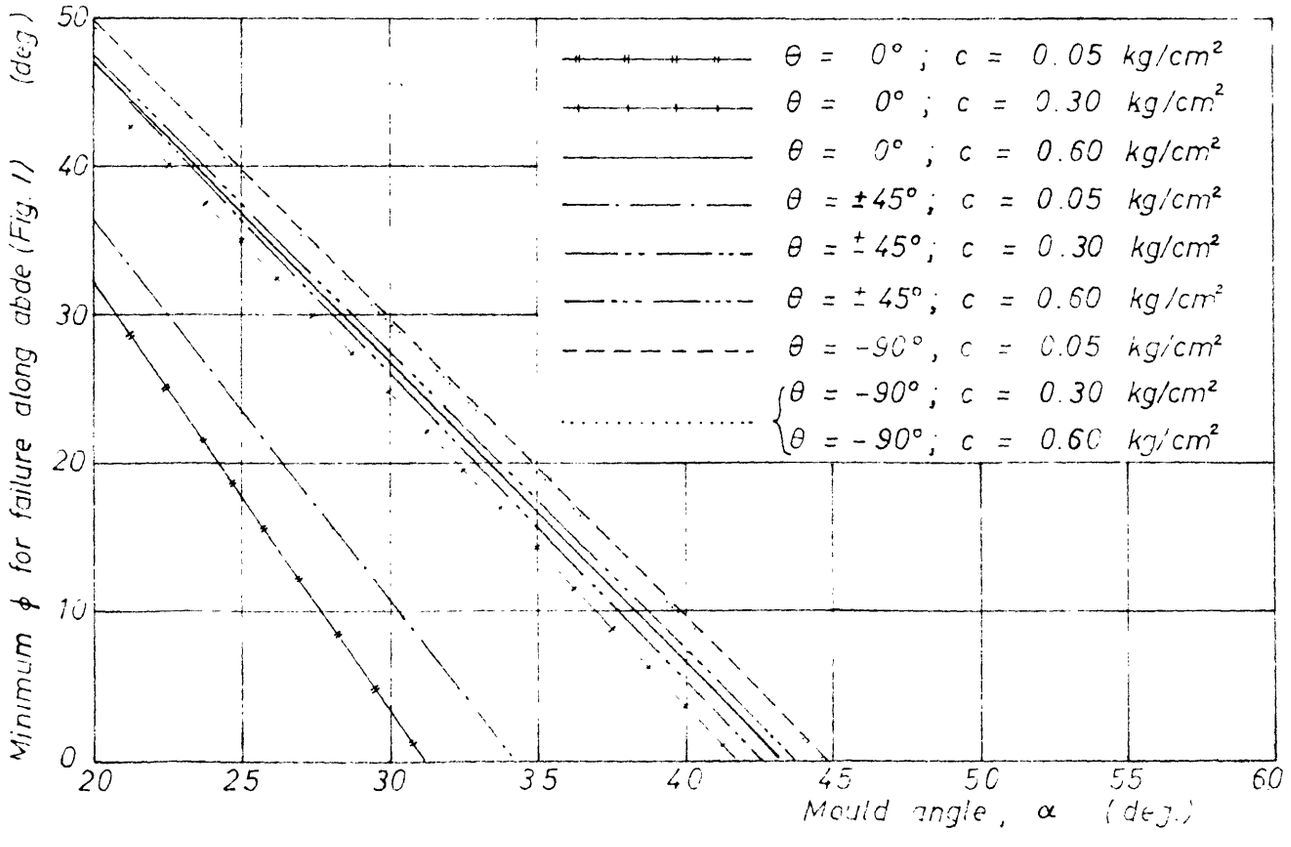

Fig. 4.14. Theoretical variation with α of minimum φ required for soil wedge to fail along ABDE (Fig. 4.1(b))

CHAPTER 5

ANALYSIS OF SLIPS BY THE IN SITU WEDGE SHEAR TEST

5.1 Slips analysed

Three slips have been analysed directly through iswests . The factor of safety of a fourth slip has been evaluated using the results of iswests performed for a nearby slip.

5.1.1 Slips at Site B

About Christmas 1970, a slip (Slip 1 at Site B, Fig. 5.1) occurred on the vertical side of a 5.5 m deep excavation, made some 10 weeks before. At this location raking shores (Fig. 5.2) had been erected as an empirical measure of safety during the performance of two iswests using the mode of loading shown in Fig. 4.11(a). Weather conditions prevented their subsequent removal. Rain water pooling at the base of the excavation softened the soil to the extent that the pegs supporting the right-hand panel of shoring were uprooted during the slide. All elements of this panel were recovered intact. The pegs for the left-hand panel stood, but this panel failed to support the whole of the sliding mass by itself, three of the four struts breaking into two. The slip was apparently caused by a gravel-filled, buried stream channel (Fig. 5.2) which crossed the top of the side of the excavation at this point; this acted as a water collector particularly during the heavy rains of the preceding weeks and softened the

underlying clay. This view was substantiated by a second slip (Slip 2, Fig. 5.1) which occurred during the excavation of an adjacent section on 9 April 1971, revealing a similar cross-section of sandy gravel (Fig. 5.3).

After the promising results (Fig. 5.4) obtained from the first series of iswests (Section 5.2.1), a second series were performed for the study of Slip 1, but the start of construction prevented the performance of further iswests for the study of Slip 2.

5.1.2 Slip at Site C

The second slip studied through iswests had occurred on 1 November 1968 on the Middle East Technical University (M.E.T.U.) campus (Fig. 5.5), soon after the completion of an excavation for the extension of an existing service gallery. The slip surface was surveyed and hand cut block samples were taken from near this surface on 11 November 1968 (Fig. 5.6). A drainage channel which discharged into the ditch at the side of the road (Fig. 5.5) had been temporarily diverted towards the northwest, but was running close to the top of the slip.

5.1.3 Slip at Site D

The last slip studied through iswests had occurred on 20 July 1966 also on the M.E.T.U. campus (Fig. 5.7), soon after the completion of an excavation for a service gallery. The slip surface was surveyed roughly, on 22 July 1966, the estimated dimensions being verified subsequently by the

information supplied by the M.E.T.U. Directorate of Planning and Design. The slip circle shown in Fig. 5.8 was drawn by anology to Slip 1 at Site B (Fig. 5.2). Amongst the notes taken on 22 July 1966 was that water was seeping out of the 45 cm thick upper layer of sandy gravel placed as stabilizer for the old road to the Physics Department, and exposed at the slip surface.

5.2 Iswests performed

The essential features of the fourty-nine iswests successfully performed so far are summarized in Table 5.1. Besides the study of the slips described in Section 5.1, these were aimed at the development of the test into the form described in Chapter 4. The developments introduced in the different series of iswests are outlined in the following sub-sections. All shear strength envelopes have been fitted by polynomial regression (POLRG) programmed for the electronic computer (IBM, 1969).

5.2.1 Iswest series B/H

The test, in its simplest form, was first performed at the base of an open excavation at the northeast corner of Site B (Fig. 5.1), between 18 September and 6 October 1970. Horizontal loading was employed in all five of these tests, and hence the series designated B/H.

The load was applied through thirty-six 7 mm diameter steel balls held by a ball cage and interposed directly between the loading face of the test mould and a 250 mm x 250 mm x 20 mm

steel plate. As both this plate and the test mould were made of mild steel, after a certain load, the steel balls indented the surfaces sufficiently to become locked between the plate and the test mould.

The test mould was placed over the test wedge by hand. Quite severe blows had to be applied, and the uniformity of placement was not perfect, one side of the mould usually ending up about 1 cm above the other.

The undrained shear strength envelope shown in Fig. 5.4 was obtained by making an approximate allowance for the locking of the steel balls between the loading plate and the mould at some stage of the test, estimated from the positions of the indentations on the loading face of the moulds. The dashed line in Fig. 5.4 represents the shear strength envelope obtained from slow shear box tests (Section 6.3). The proximity of these envelopes was sufficient encouragement for further work on the iswest , for the soil was stiff and unsoftened, implying that pore pressures in both field and laboratory tests were probably very low or negative, and that the effect of fissures on strength was small; although the failure plane in iswest B/H/1 coincided completely with a fissure plane, the strength measured in this test was not lower than given by the mean envelope (Fig. 5.4).

5.2.2 Iswest series B/10°

From the two tests performed at the point indicated in Fig. 5.2, little was deduced except that the mode of loading

shown in Fig. 4.11 (a) was possible, but should, for reasons of safety, preferably be performed on the side of a test pit.

Between 24 March and 6 April 1971, five iswests were performed at an average distance of 20 m from Slip 1 at Site B, on a ramp inclined at 10° to the horizontal (Fig. 5.1). Surface wetting during the preceding rainy months had produced the same average moisture content at this point as at Slip 1, and other geotechnical properties of the soil at the two locations were very similar (Table 6.6, Rows 8 to 14). The mode of loading shown in Fig. 4.11(c) was used. Thus the inclination to the horizontal of the failure plane in the iswests ranged between 35° and 55° as compared to the range of 45° to 75° for the major part of the actual slip surface. The devices described in Sections 4.2.1.2, 4.2.1.3, and 4.2.1.5 were used for the first time in these tests. Fig. 5.9 shows the peak and residual shear strength envelopes obtained.

5.2.3 Iswest series C/1, D, C/2

The next three series of iswests were conducted between 7 and 23 June 1971, 30 May and 23 June 1972, and 3 and 21 July 1972 at the locations C/1 (Fig. 5.5), D (Fig. 5.7), and C/2 (Fig. 5.5) respectively. These tests were performed in a test pit 1.62 m x 1.53 m in plan, and as shown in Figs 5.6 and 5.8, the orientation of the failure plane for each test was chosen to conform with the inclination of the actual slip surface at the corresponding elevation. The mould angles α were generally chosen to make the magnitude of the average normal stress in

the iswests follow approximately the same pattern of variation with depth as along the actual slip surface.

The mode of loading shown in Fig. 4.11(a) was used in iswests D/7, C/2/4, and C/2/8 (Table 5.1), and the mode of loading in Fig. 4.11(b) in the remaining tests. Fig. 5.10 shows one of the latter type in progress. Based on the results of previous tests, an initial eccentricity Δy_p (Section 4.3.3.1) was applied in iswest D/4 and subsequent tests (Table 5.1). To study the effect of the area of shear, iswests D/3 and C/2/3 were performed using a test mould with a length of shearing plane 1.5 times larger than that of the rest of the test moulds, but with the same width. Figs 5.11 to 5.13 show the peak and residual strength envelopes obtained from iswest series C/1, D, and C/2 respectively. Fig. 5.14 shows typical curves of τ / σ_N and normal displacement versus shear displacement, and the success of the method explained in Section 4.3.3.1 in reducing non-uniformity of normal stress on the shear plane.

5.2.4 Iswest series C/3

These tests, performed in a shallow test pit at the location C/3 (Fig. 5.5), were intended for the investigation of the effect of mould rotation β on the test results (Fig. 5.15), and for the demonstration that two moulds are sufficient to define a failure envelope (Fig. 5.16). The device in Fig. 4.8 was used for the first time in iswest C/3/7 on 10 May 1973.

5.2.5 Iswest series C/4

Iswest series C/2 had originally been intended to be performed at the location C/2A (Fig. 5.5), but it was found impossible to deepen a pit at this point to more than about 1.0 m due to the water, infiltrating from a nearby drainage channel, causing instability of the sides of the pit if left unsupported.

To be able to excavate a pit at this site closer to the slip than C/1 and C/2, a safer and more practical means of temporary support for the sides of a test pit than the timbering shown in Figs 5.6 and 5.10 was required. This was provided by the use of the 400 mm high cylindrical rings shown in Fig. 5.17. These were made of 3 mm thick mild steel plate, and were left with a slit which could be expanded by two turnbuckles of the type shown in Fig. 5.18. Fitted at each end of a diameter perpendicular to the one through the slit, was a dual purpose steel bar, 8 mm dia., bent to the shape shown in Fig. 5.19. This acted as a handle when in the vertical position, and as a step when horizontal. A rotatable catch helped to hold the handle in the vertical position during transport and when one ring was to be passed through another.

Eight such rings were made, their minimum diameters ranging from 1033 mm to 1255 mm at about 30 mm intervals. For each size, a separate guide ring, about 25 mm larger in dia. than the minimum dia. of the corresponding expansible

ring, bent out of 30 mm wide strip of 1.5 mm thick lamina and reinforced by two orthogonal, 8 mm dia. steel bars, aided in excavating the pit to the right diameter. For every 400 mm that the pit was deepened, the next smaller ring was contracted to its minimum diameter, lowered through the rings already placed, and then expanded in position. Removal of the rings as the pit was back-filled was a reversal of this procedure. The rings were so dimensioned as to fit into each other up to the level of the handles, and thus to occupy a minimum of space during storage and transport. Each ring was light enough to be hauled and mounted into position comfortably by two men.

Using this method of support, it became possible not only to excavate a test pit at the location C/4 in Fig. 5.5, but also to perform tests using the mode of loading in Fig. 4.11(a) with as much comfort as those using the mode of loading in Fig. 4.11(b). Ten iswests , two of each type at five different levels, were performed. The same rules as in Section 5.2.3 were observed in the selection of the test moulds and the orientation of the shear plane at the different levels.

The method given in Section 4.3.3.2 for minimizing moments on the shear plane was employed successfully in most of these tests (Table 5.1, Columns 11 and 15). With the actual values of v and β measured in these tests, it could have been theoretically possible to keep the maximum deviation of normal stress on the shear plane to within about $\pm$ 10.0 % of the average normal stress. The devices described in Sections

4.2.2.1(15) and (17) were used for the first time in these tests, and the procedure given in brackets in Section 4.4(12) was applied in the last three tests of this series, as the hydraulic jack available for this series was of 20 tonnes capacity and unnecessarily heavy. In all these tests, by recording the displacement of the mould perpendicular to the direction of loading at two different points, using a fifth dial gauge, the rotation of the mould in a plane normal to the direction of loading was calculated. This rotation was found to be of the order of $\pm$ 1.0°.

Fig. 5.20 shows the peak shear strength envelopes obtained from the tests using the two different modes of loading, together with the peak and residual strength envelopes given by all the ten tests.

5.3 Stability of the slopes by iswest results

The factor of safety F_s of the failed slopes was calculated by using the peak shear strength parameters measured in the iswests in a total stress type of stability analysis, assuming horizontal interslice forces (following Bishop, 1955). This was in effect Bishop's simplified method (BISIM) adapted for total stresses. Unless otherwise stated, all values of F_s presented have been obtained by BISIM.

The depth of tension cracks (Table 6.6, Row 7) was estimated on the assumption that in practice such cracks generally extend to about one-half (Gibson, 1963) of the depth given by Rankine's theory, and for convenience was taken equal

to the depth of the lowest point of the uppermost slice obtained by dividing the sliding mass into equally wide slices, one greater in number than shown in Table 6.6, Row 6.

In calculating F_s for Slip 1 at Site B, the raking shores (Fig. 5.2) were assumed to be merely leaning against the vertical cut, with zero friction between the timbering and the dry and loose face of the cut, and the additional restoring moments due to the increased normal stress along the circular arc and due to the horizontal reaction from the shores were taken into account, as also was the weakening effect and the reduction in weight caused by the loading holes for the two iswests performed on the face of this cut. The net effect on F_s of considering these factors was found to be less than 1 %.

The values of F_s obtained by assuming the tension cracks to be vertical and to be filled with water are given in Table 6.6, Row 20, where, for the two cases for which a convergence was obtained, the values of F_s calculated by Janbu's (1973) GPS, through a computer program by Öner (1974), are also given. The thrust lines assumed for the latter solutions are shown in Figs 5.3 and 5.6. In Table 6.6, Row 21 are given the values of F_s calculated by assuming the tension crack to be of the same depth as for Row 20, but to follow the circular arc used in the stability analyses.

A simple program was written to study, for a given geometry for the slices, the effect on F_s of the assumed

depth h_c of a vertical tension crack, and the depth h_w of water in such a crack, as well as the effect of the depth of a curved tension crack. The continuous curves in Fig. 6.26 show the results of this analysis.

Table 5.1 - Essential features of the iswests

1	2	3	4	5	6	7	8	9	10	11	12	13	14	15
		Mean depth below					At peak strength				At residual strength			
Iswest Series	Test No.	ground surface (m)	top of slip (m)	α (deg)	θ (deg)	Δy_p (mm)	β* (deg)	u (mm)	v (mm)	$\delta\sigma_N/\sigma_N$ (%)	β* (deg)	u (mm)	v (mm)	$\delta\sigma_N/\sigma_N$ %
B/H	1	6.8	3.5	25	0	0	-	6.3	-0.2	19.3	-	23.6	1.1	74.8
	2	6.8	3.5	35	0	0	-	4.7	-0.4	12.6	-	27.1	1.1	47.8
	3	6.8	3.5	30	0	0	-	4.5	-0.2	16.3	-	19.2	4.8	55.4
	4	6.8	3.5	40	0	0	-	7.3	-3.2	8.8	-	19.2	2.8	55.0
	5	6.8	3.5	45	0	0	-	5.7	-2.0	7.6	-	18.3	1.8	26.0
B/10°	1	3.8	3.8	40	10	0	-	10.2	3.7	36.0	-	21.6	6.8	55.6
	2	4.0	4.0	25	10	0	-	7.1	-0.2	48.2	-	15.7	7.5	79.6
	3	4.8	4.8	30	10	0	-	10.9	-0.9	36.5	-	25.7	1.8	70.8
	4	5.3	5.3	35	10	0	-	5.3	-1.9	21.2	-	16.9	5.0	51.1
	5	5.3	5.3	45	10	0	-	8.9	-2.1	14.2	-	20.7	0.4	30.8
C/1	1	2.2	1.2	25	45	0	-	8.9	-2.9	62.6	-	26.2	2.0	100
	2	2.7	1.7	45	20	0	-	6.1	-1.9	26.1	-	20.7	-2.7	58.9
	3	3.2	2.2	40	15	0	-	16.9	-9.1	22.5	-	42.2	-10.9	48.3
	4	3.6	2.6	45	0	0	-	12.5	-1.6	25.5	-	30.4	-1.2	44.6
	5	4.1	3.1	35	0	0	-	10.1	-3.7	30.7	-	28.8	-2.4	54.8
	6	4.4	3.4	30	0	0	-	14.2	-2.4	50.8	-	42.1	-0.3	77.0
D	1	1.5	2.0	25	45	0	-	1.3	-0.1	100	-	7.9	0.7	100
	2	2.3	2.8	30	30	0	-	4.0	-2.0	56.5	-	9.9	-0.8	100
	3	2.4	2.9	30**	30	0	-	6.7	-3.5	16.0	-	48.9	7.7	100
	4	2.7	3.2	35	20	10	-	5.8	-3.1	-13.8	-	30.0	-0.7	41.8
	5	3.1	3.6	40	10	10	-	20.5	-7.8	-12.3	-	70.6	-3.3	55.8
	6	3.1	3.6	45	0	10	-	7.1	-3.7	-13.8	-	47.8	-7.9	20.8
	7	3.1	3.6	25	-70	10	-	11.3	-2.5	-28.6	-	20.9	5.7	4.0
C/2	1	1.6	1.1	25	45	15	-	2.2	-0.3	-11.4	-	52.8	3.1	75.5
	2	2.2	1.7	30	30	15	-	8.1	-1.6	0.72	-	56.7	4.6	62.5
	3	2.2	1.7	30**	30	20	-	14.4	-5.0	-3.36	-	78.2	0.3	50.3
	4	2.2	1.7	30	-90	15	-	4.2	-0.4	-53.0	-	-	-	-
	5	2.7	2.2	40	15	15	-	10.2	-4.2	-12.3	-	28.5	-1.0	10.0
	6	3.4	2.9	45	0	15	-	16.8	-4.9	-9.9	-	70.4	-6.1	33.0
	7	3.8	3.3	35	0	15	-	10.2	-4.6	-3.7	-	79.1	0.9	63.1
	8	3.8	3.3	35	-70	10	-	7.8	-1.6	-18.7	-	34.6	-4.6	-24.6
	9	4.1	3.6	30	0	15	-	11.4	-2.7	-20.9	-	77.9	2.4	30.1
C/3	1	0.4	-0.6	25	15	10	-	9.0	-1.0	7.4	-	35.2	2.7	52.9
	2	0.4	-0.6	45	15	15	-	19.7	-6.1	-13.8	-	40.7	-6.8	2.5
	3	0.6	-0.4	45	15	15	-	14.7	-5.7	-15.2	-	48.9	-8.3	8.3
	4	0.8	-0.2	25	15	15	-	11.9	1.5	10.8	-	44.7	6.9	61.9
							-0.86	10.1	0.2	35.8	-1.06	42.6	4.7	93.4
	5	0.8	-0.2	45	15	14	-	14.0	-1.1	-7.7	-	44.7	2.0	23.8
							-0.95	11.4	-0.7	13.3	-1.17	41.7	2.2	52.6
	6	0.8	-0.2	25	15	12.5	-	5.1	0.9	14.1	-	40.6	7.1	70.0
							-0.82	3.4	-0.3	37.1	-1.13	38.3	5.1	100
	7	1.0	0.0	45	15	0†	-	23.6	-1.0	3.9	-	100.7	0.5	-72.5
							-0.26	23.1	-0.9	10.9	-1.68	97.3	0.5	-8.5
C/4	1	1.6	1.0	25	40	0†	-	25.9	-1.3	81.0	-	78.0	-3.1	100
							0.76	26.7	-1.9	50.8	2.53	80.8	-3.7	32.2
	2	1.6	1.0	25	-90	0†	-	2.2	0.0‡	-49.3	-	4.0	0.0‡	-57.4
	3	2.6	2.0	40	10	15†	-	12.6	-5.1	-22.0	-	80.0	-2.5	6.2
							+0.53	13.7	-5.4	1.3	3.44	87.0	-2.2	-50.5
	4	3.1	2.5	45	0	15†	-	10.3	-2.4	-38.5	-	134.4	-5.3	-7.9
							-0.17	10.0	-2.4	-2.4	0.81	135.9	-5.4	15.1
	5	2.6	2.0	40	-90	-3.8†	-	2.5	0.0	-9.6	-	33.4	1.6	-88.5
							-0.18	2.1	0.1	-13.8	-0.96	31.3	1.9	-83.7
	6	3.2	2.6	35	5	15.2†	-	6.7	-1.7	-33.5	-	72.1	-0.7	-19.3
							-0.92	4.7	-1.5	24.9	-0.10	71.9	-0.8	28.2
	7	3.1	2.5	45	-90	-6.0†	-	7.0	-0.9	16.1	-	61.6	1.5	-72.7
							0.07	7.1	-1.0	2.4	-1.66	58.5	2.7	-55.9
	8	3.2	2.6	35	-75	0†	-	5.9	0.3	2.3	-	29.9	4.8	-51.6
							-0.11	5.7	1.3	4.5	-1.85	26.6	5.3	-24.2
	9	4.0	3.4	30	0	15†	-	10.8	-3.1	-62.2	-	114.6	-1.8	-71.9
							-2.30	6.0	-3.4	29.9	-4.61	104.8	6.4	81.8
	10	3.9	3.3	30	-60	8†	-	5.1	0.6	-30.8	-	89.6	16.8	-77.9
							0.42	5.9	0.5	-21.4	-1.66	87.0	15.8	-45.5

* *Where value of β is unrecorded or neglected, this is shown by a dash, and the values of u, v, and $\delta\sigma_N/\sigma_N$ evaluated by assuming β as zero.*

** *Test mould has area of shear 1.5 times larger than the rest.*

† *Jacking equipment raised during test.*

‡ *Assumed values.*

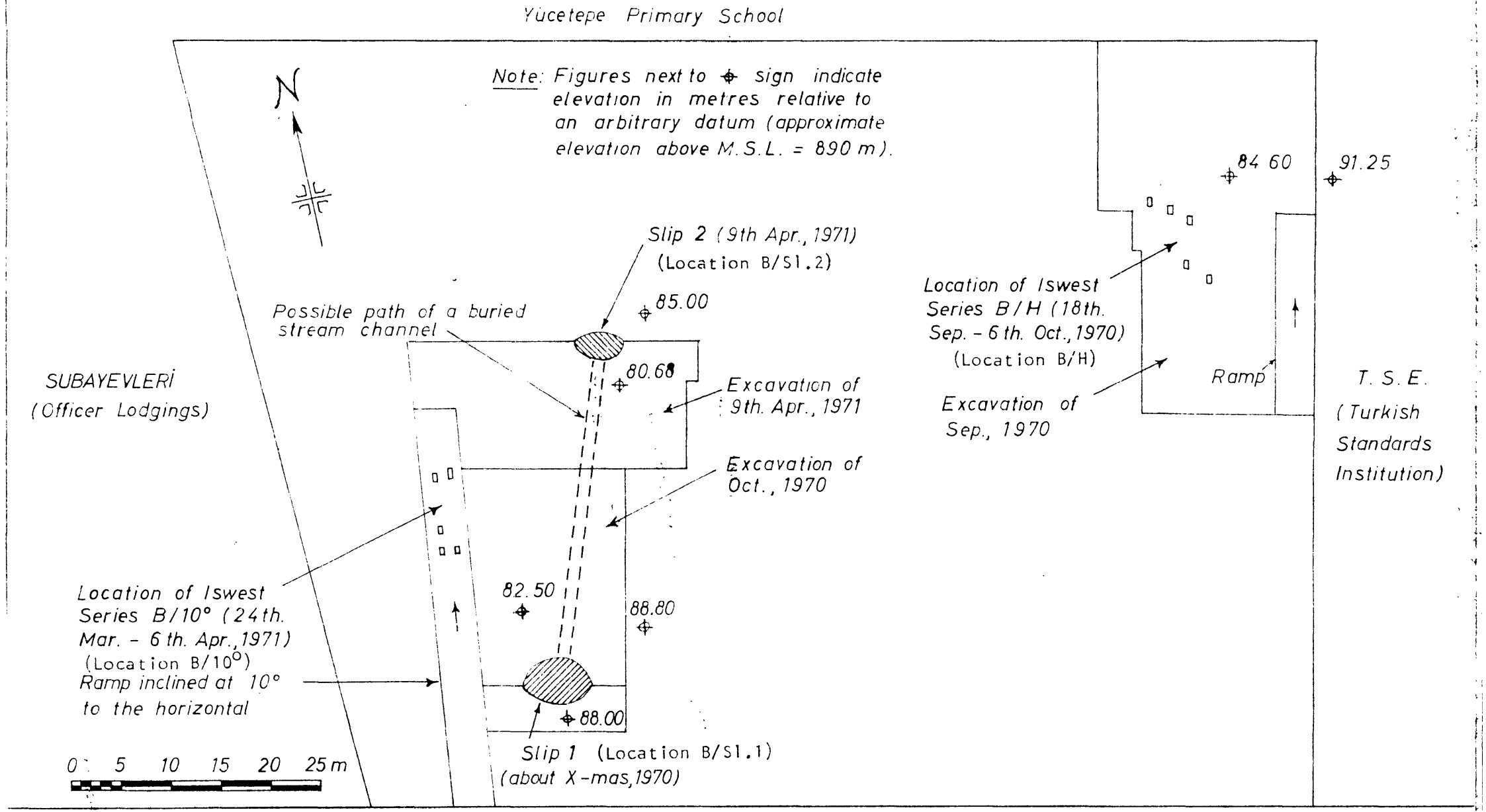

Fig. 5.1. Site plan of the Institute of Public Administration for Turkey and the Middle East (T.O.D.A.İ E.) showing the position of the two slips and the location of the iswests
(Site D, Figs 2.1 and 2.2)

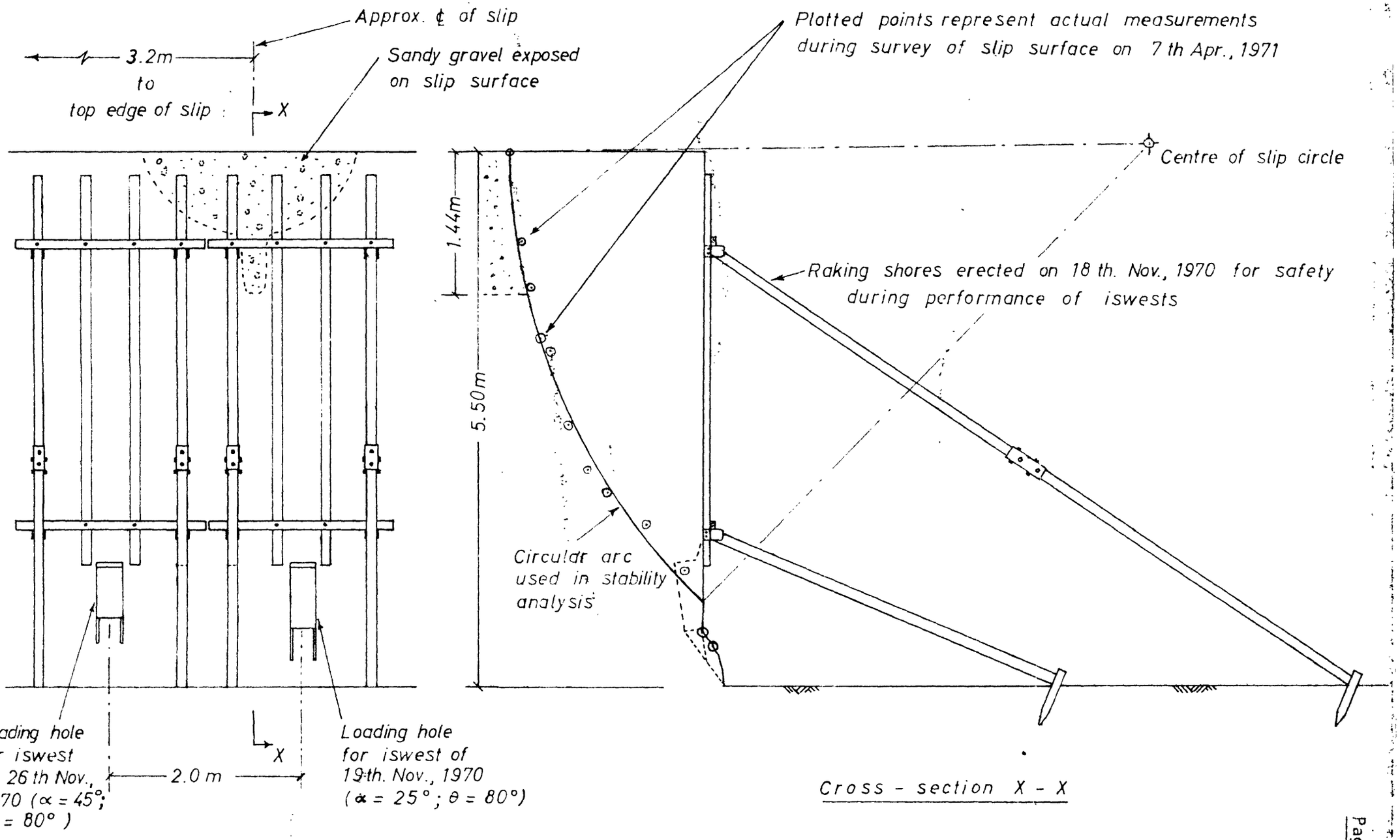

Fig. 5.2. Front view and cross-section of vertical cut at Site B showing conditions before failure of about Christmas 1970 and the slip surface

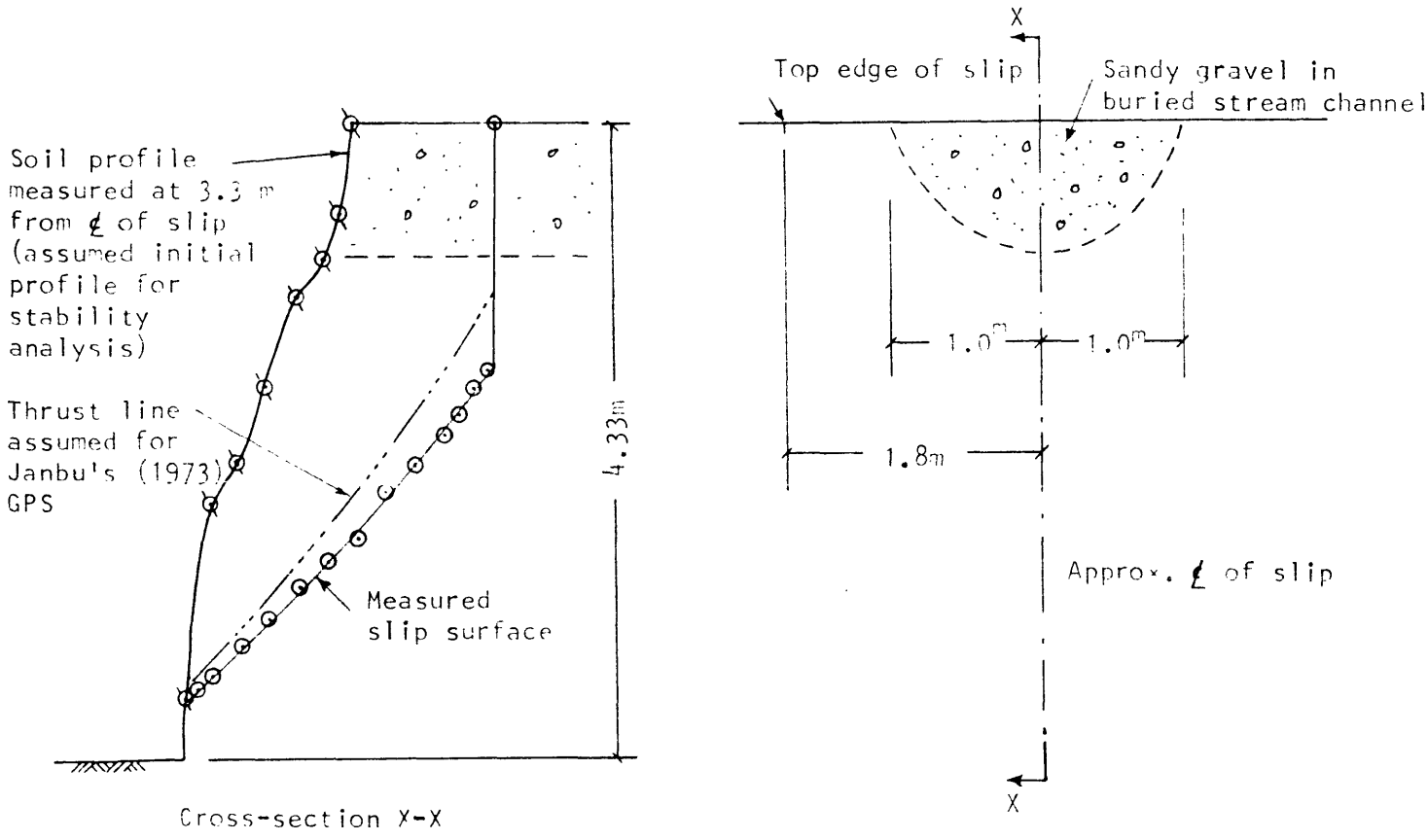

Fig. 5.3. Front view and cross-section of Slip 2 at Site B

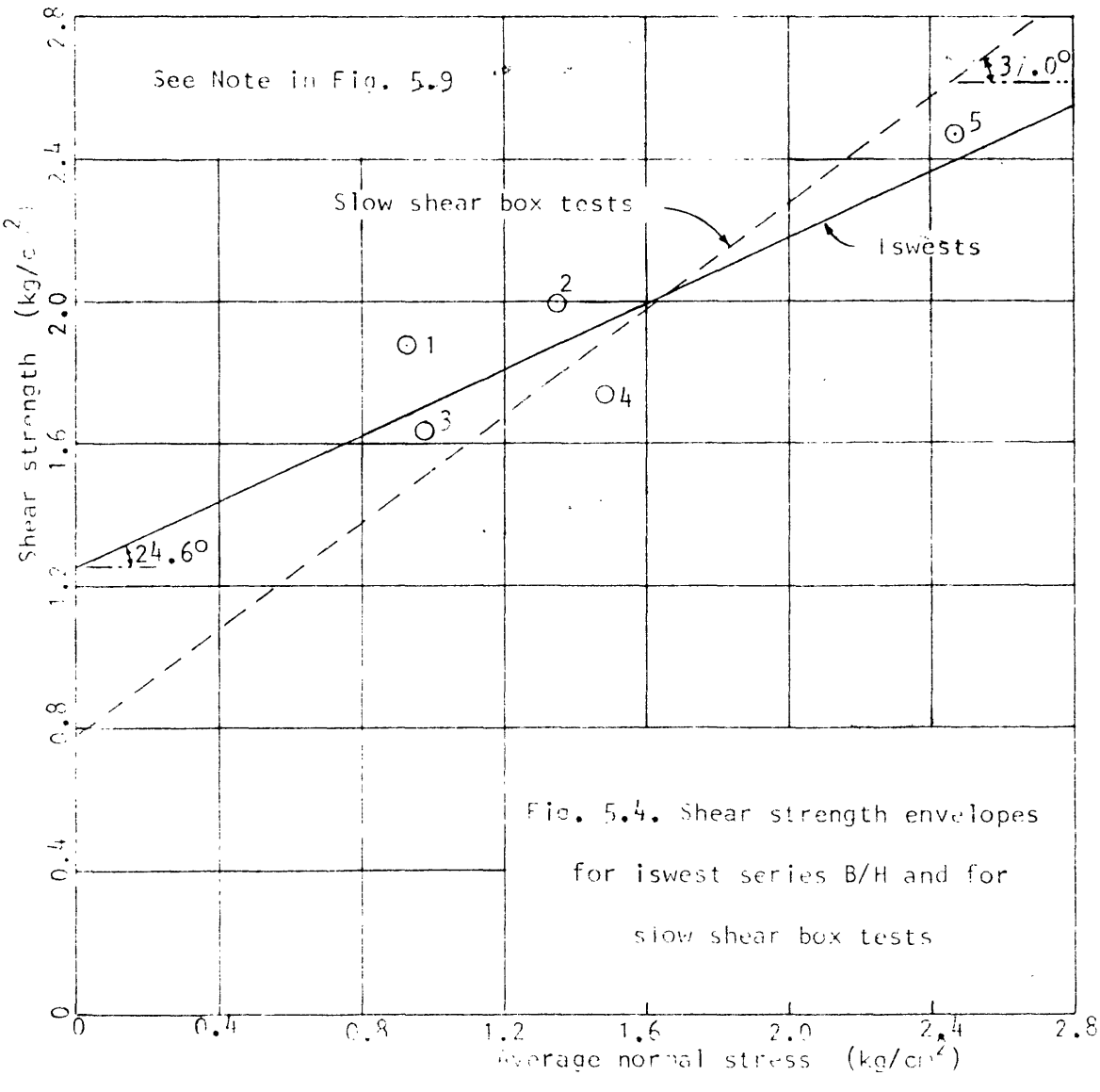

Fig. 5.4. Shear strength envelopes for iswest series B/H and for slow shear box tests

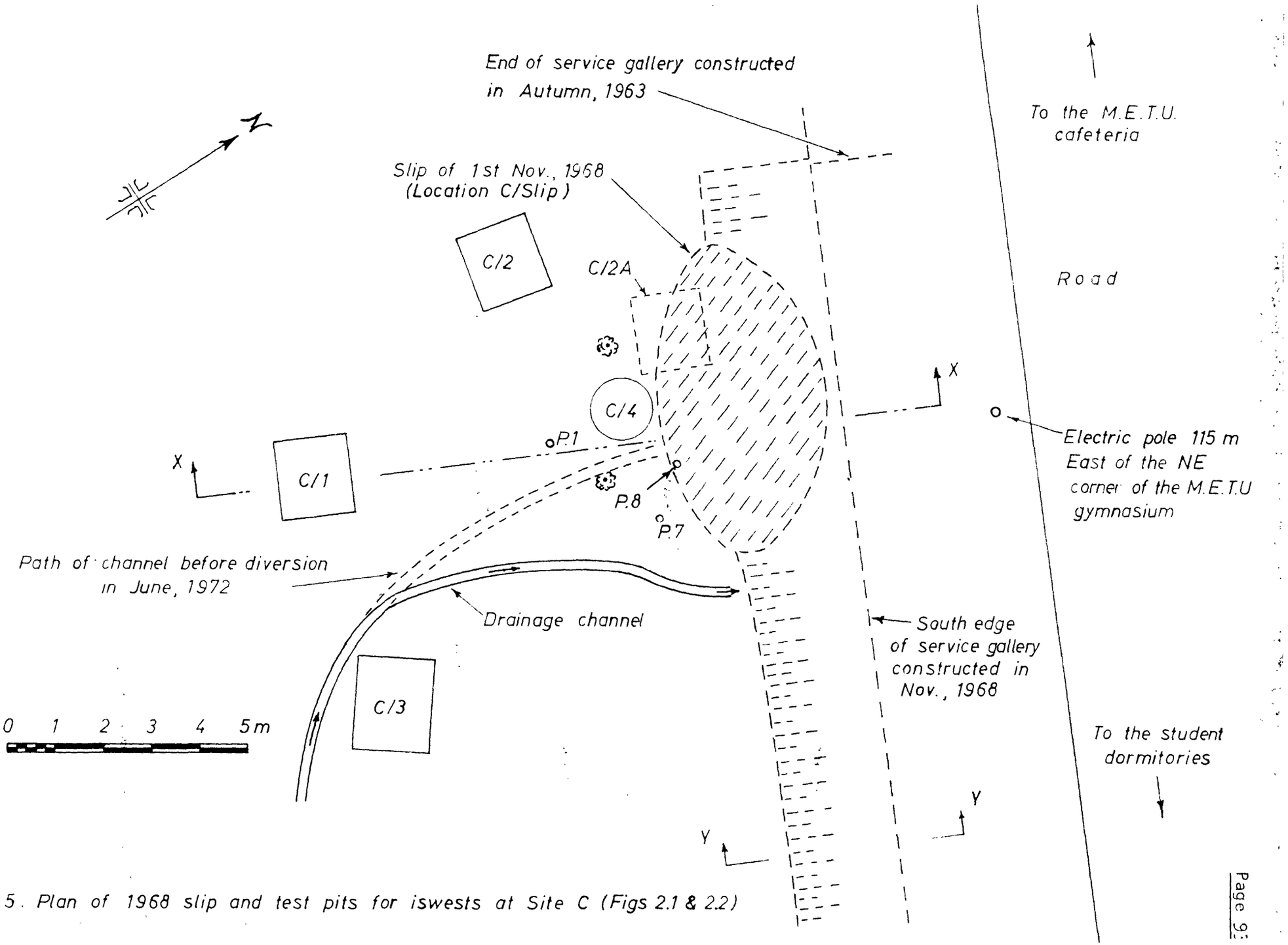

Fig. 5.5. Plan of 1968 slip and test pits for iswests at Site C (Figs 2.1 & 2.2)

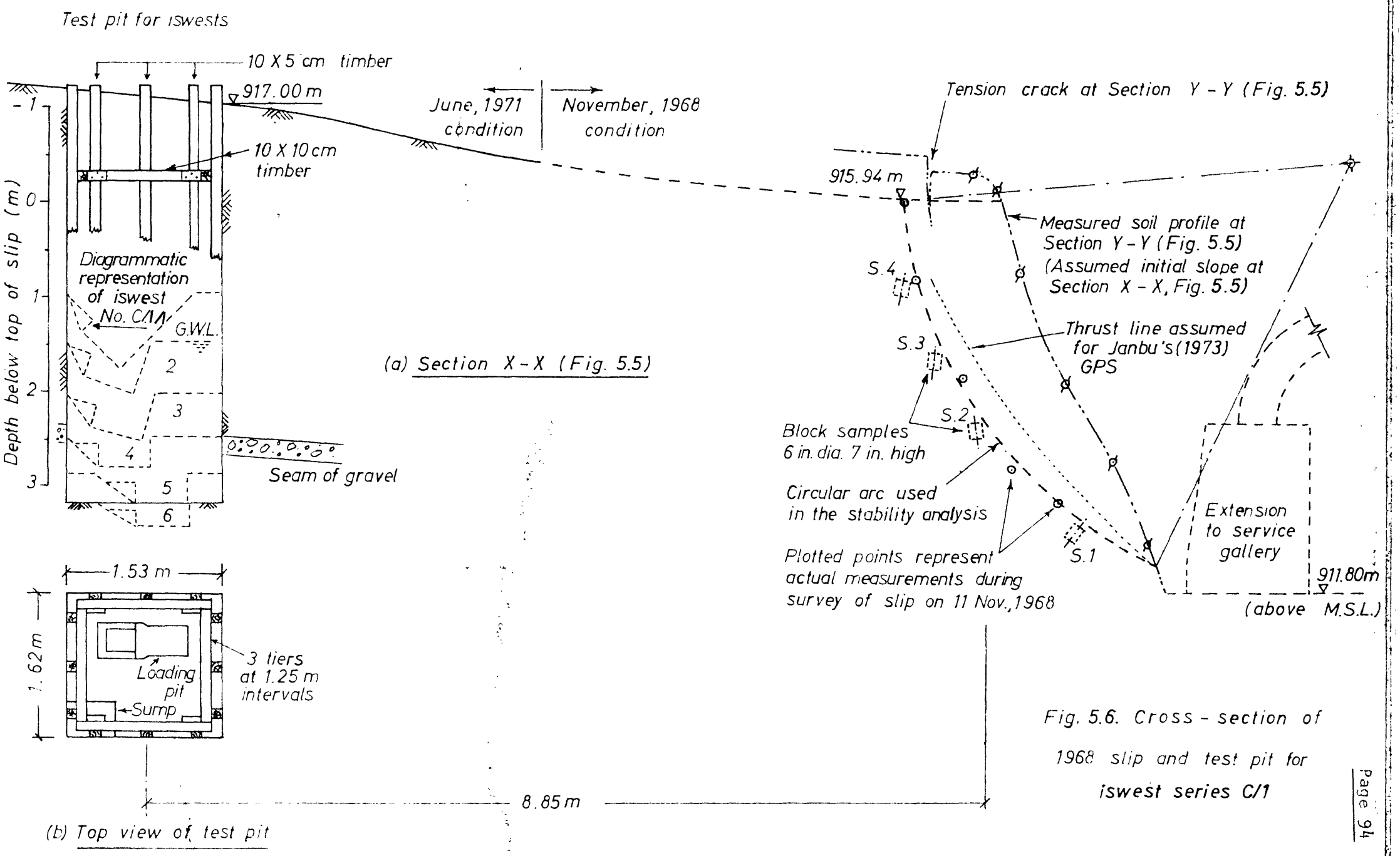

Fig. 5.6. Cross - section of 1968 slip and test pit for iswest series C/1

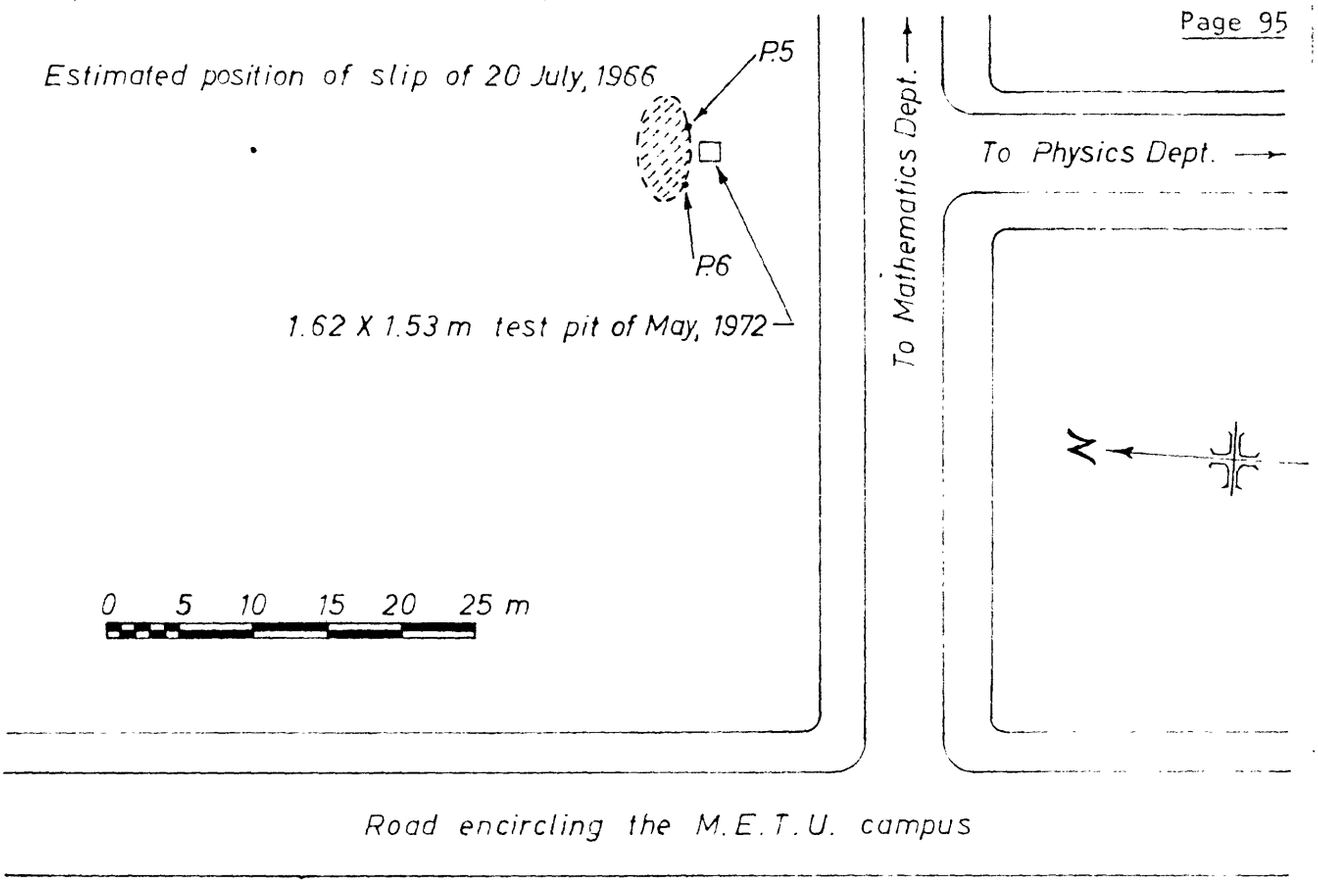

Fig. 5.7. Location of 1966 slip and test pit for iswests at Site D (Figs 2.1 and 2.2)

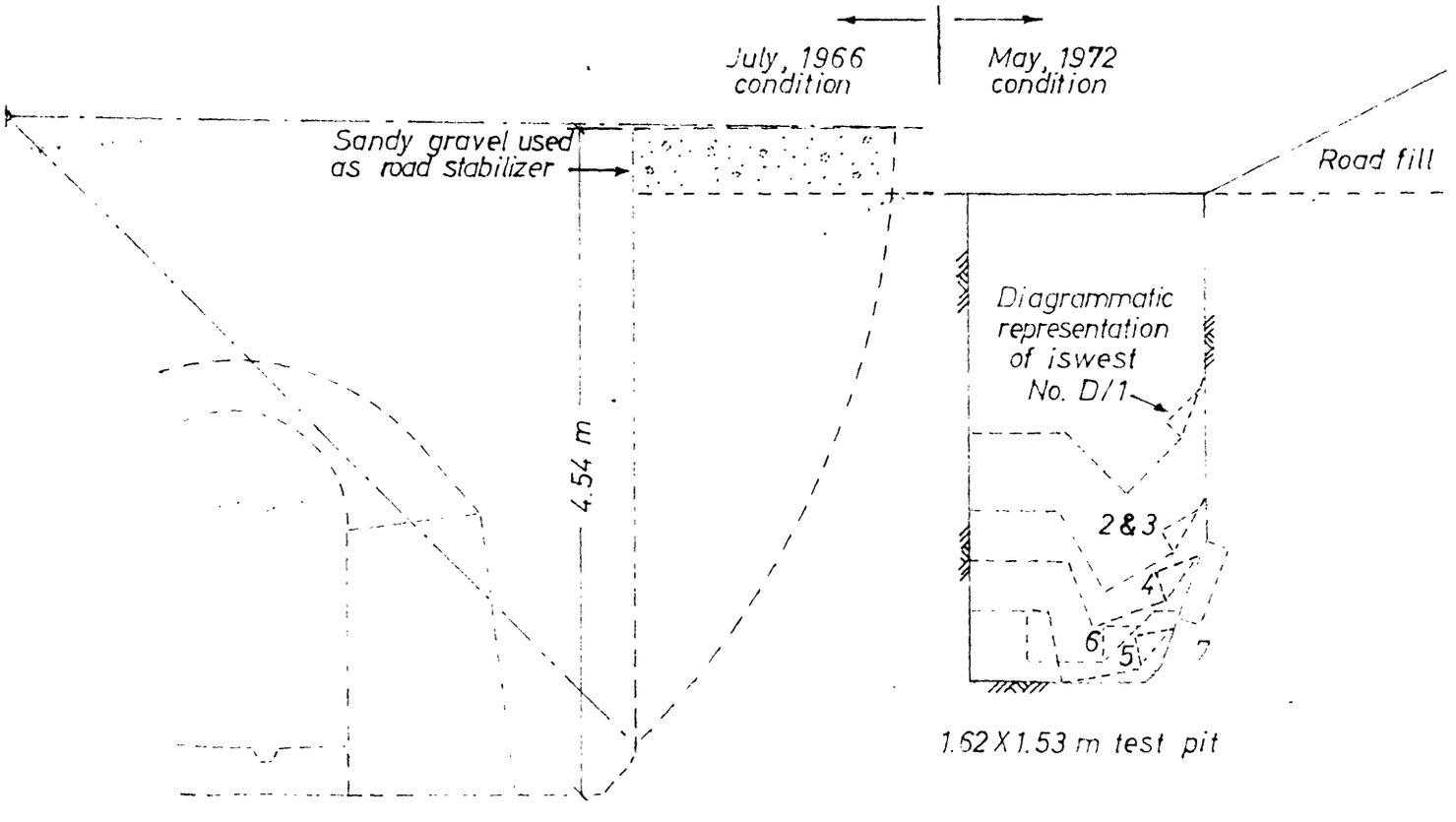

Fig. 5.8. Cross-section of 1966 slip and test pit for iswests at Site D

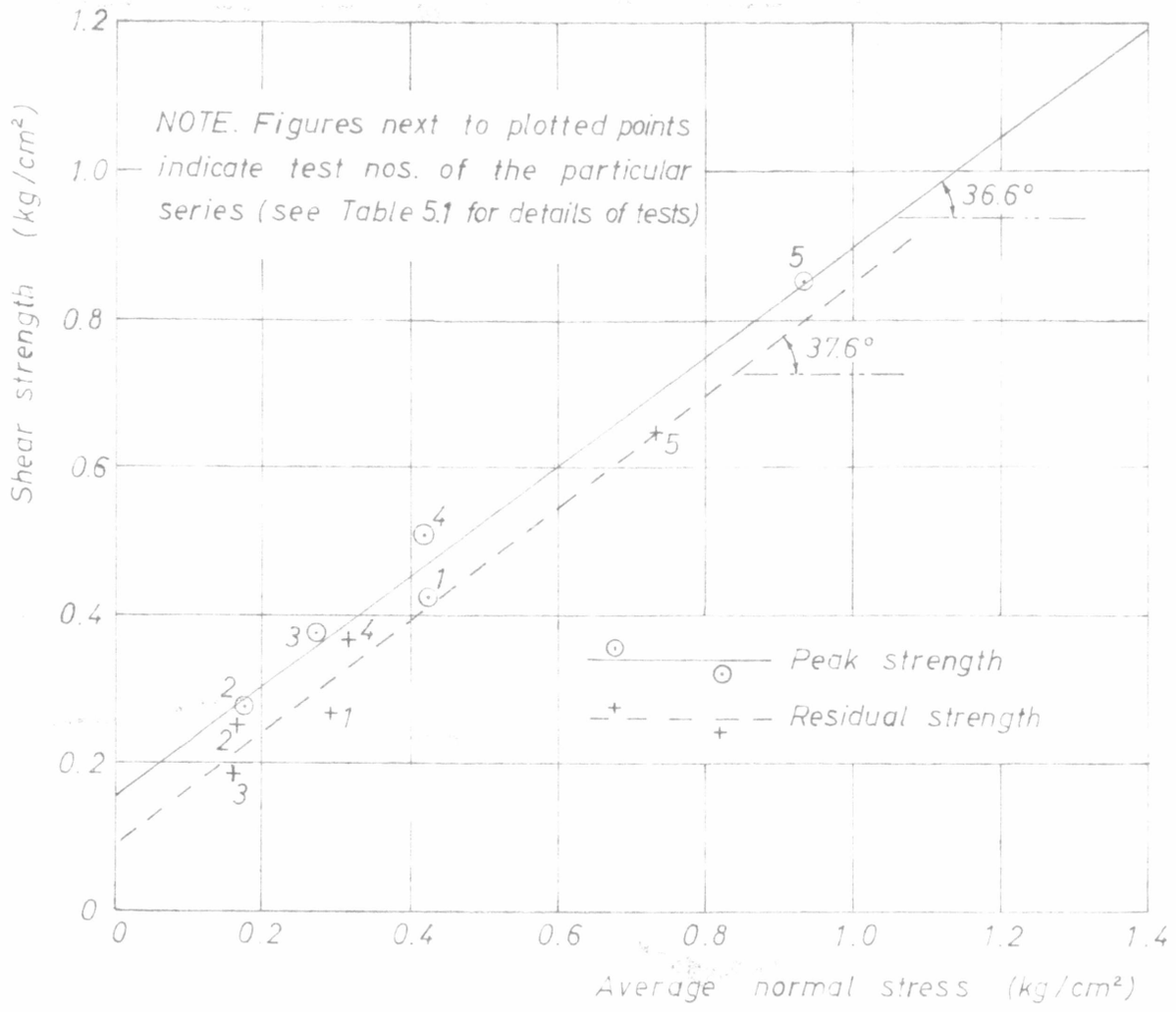

Fig. 5.9. Peak and residual undrained shear strength envelopes for iswest series B/10°

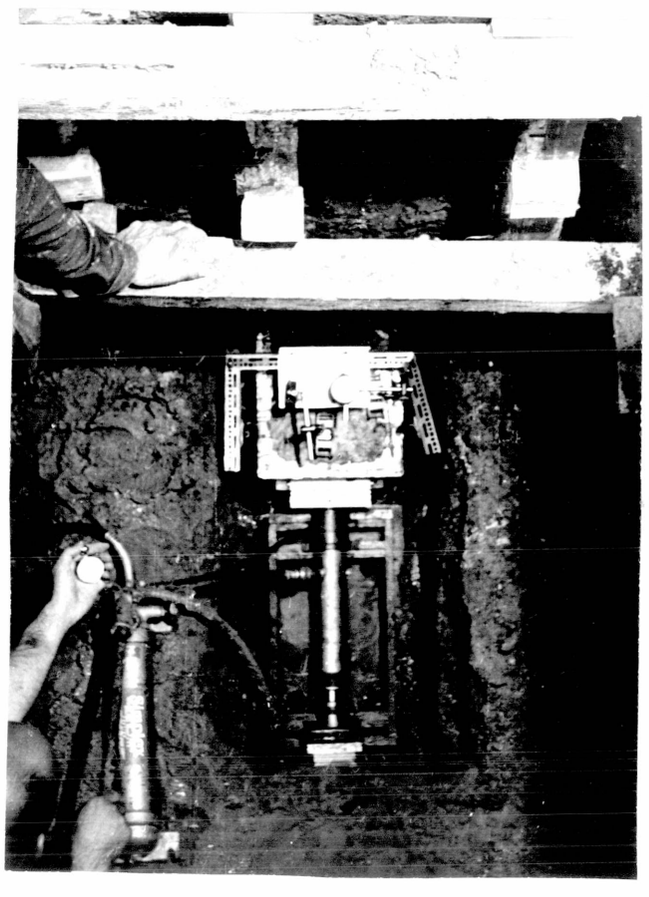

Fig. 5.10. Iswest No. C/1/3 in 1.62 x 1.53 m test pit in progress

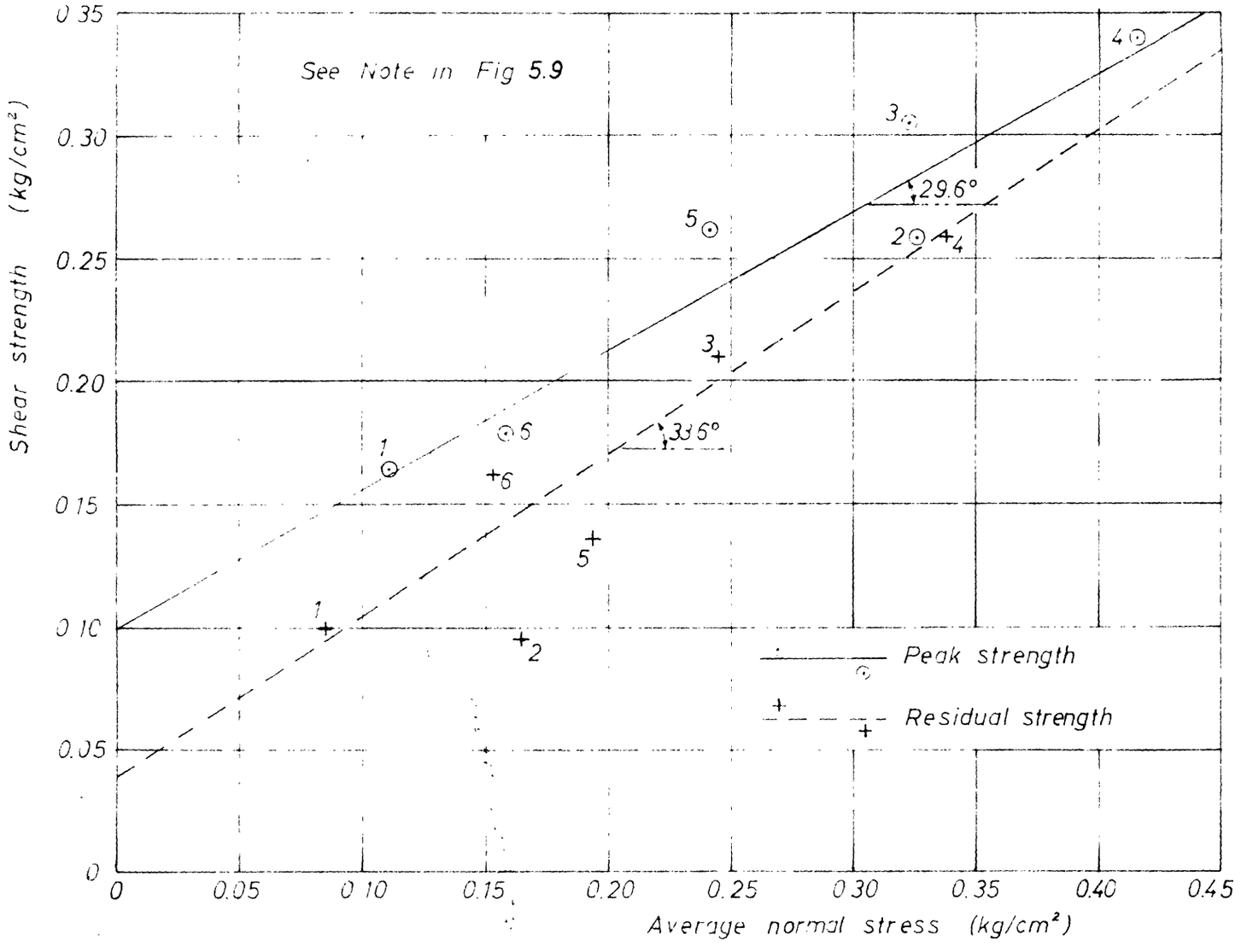

Fig. 5.11. Peck and residual undrained shear strength envelopes for iswest series C/1

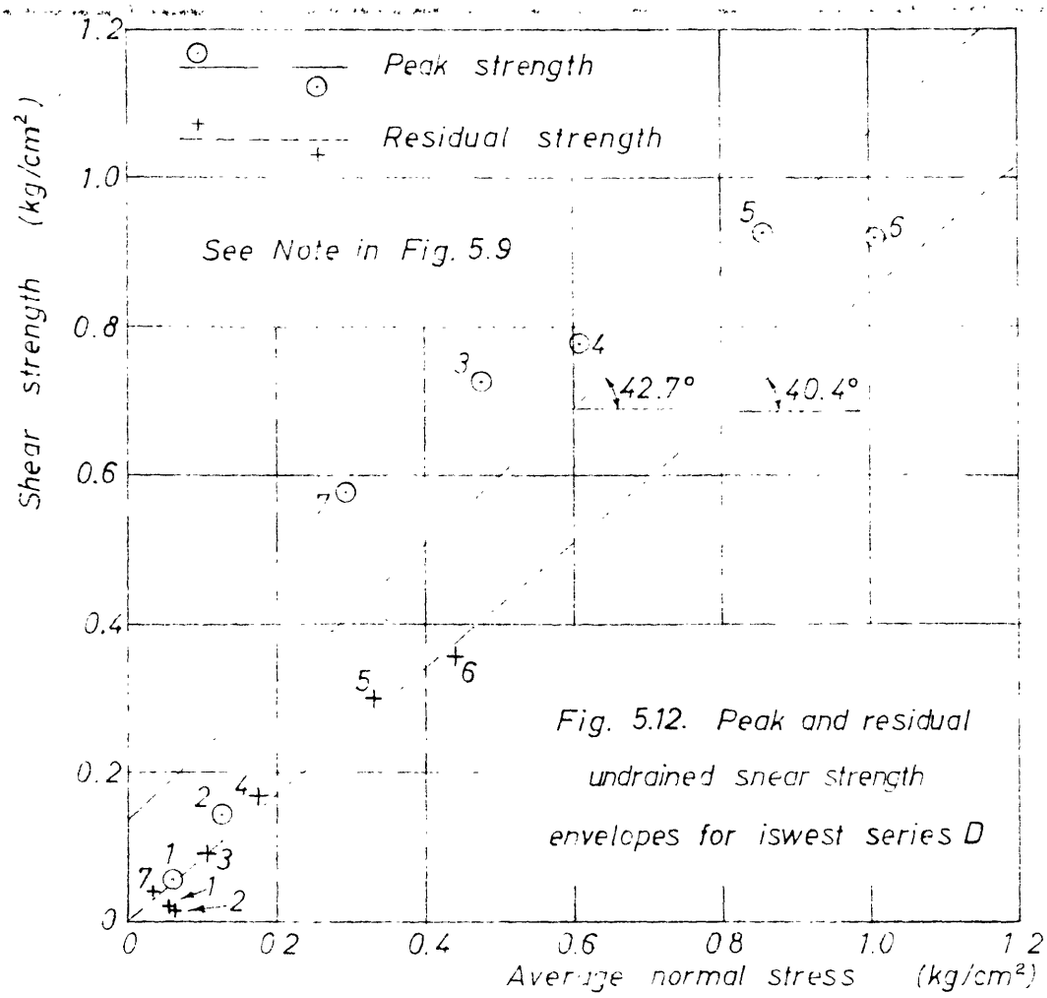

Fig. 5.12. Peak and residual undrained shear strength envelopes for iswest series D

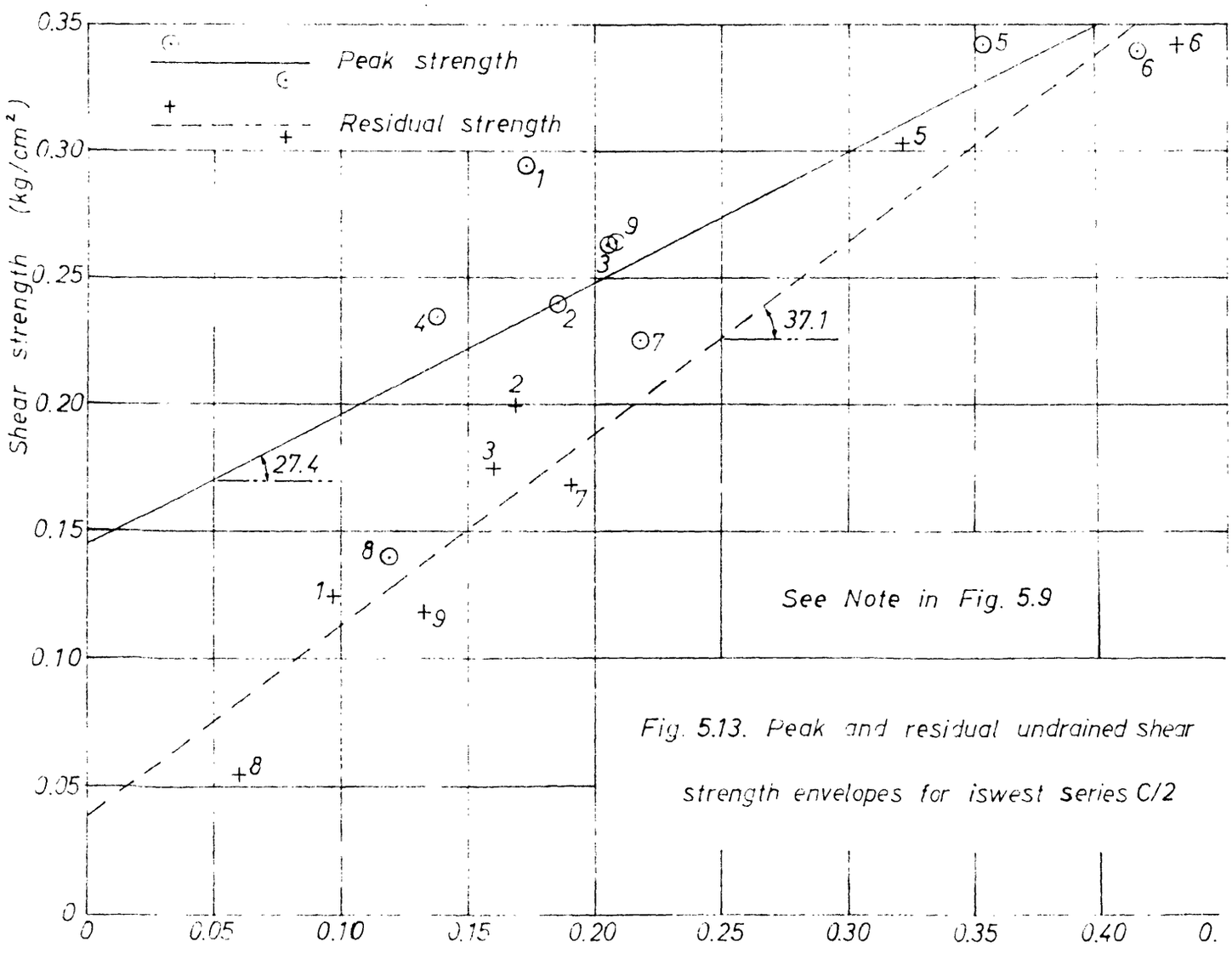

Fig. 5.13. Peak and residual undrained shear strength envelopes for iswest series C/2

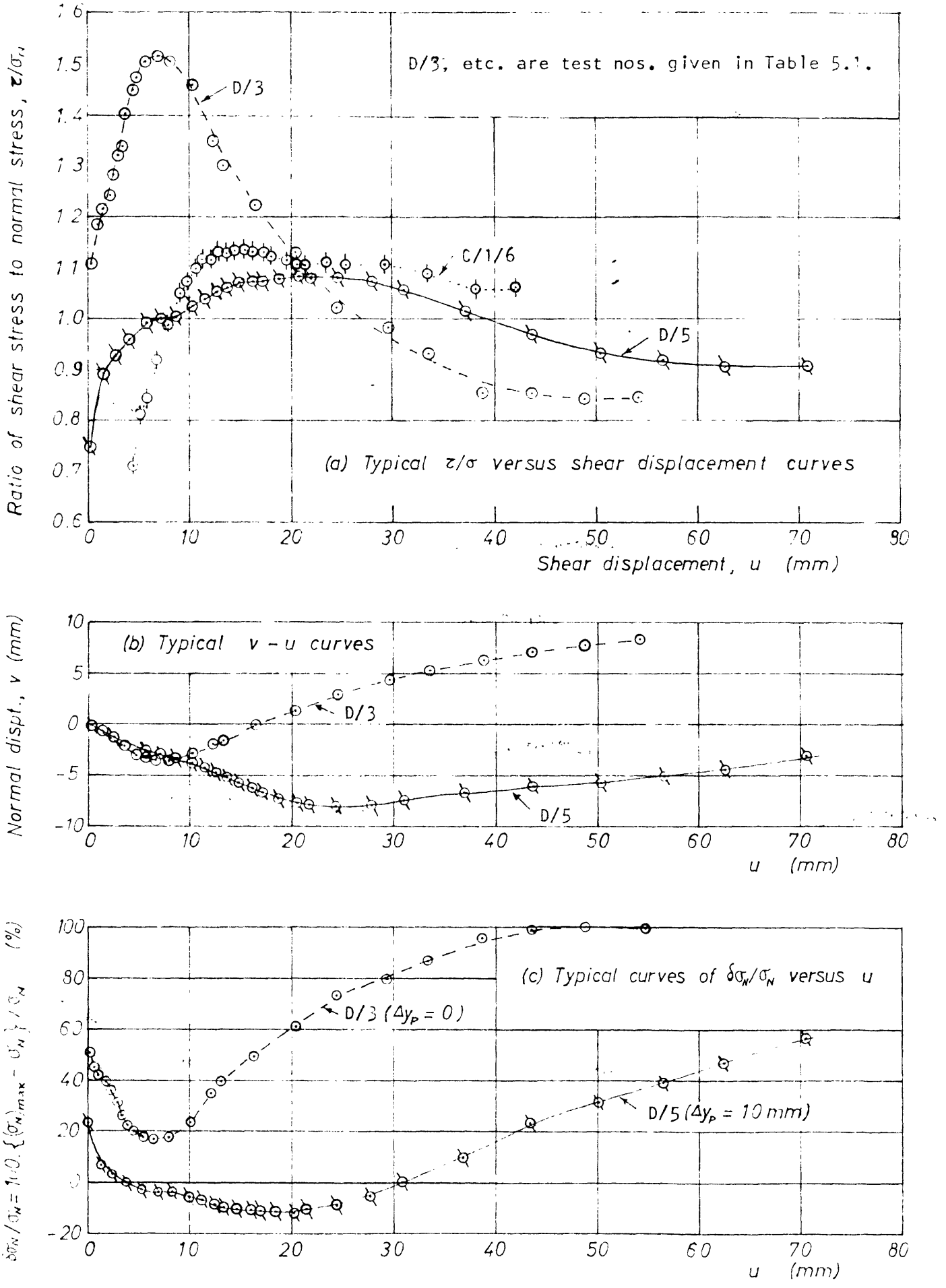

Fig. 5.14. Typical curves of τ/σ_N, normal displacement, and $\delta\sigma_N/\sigma_N$ versus shear displacement

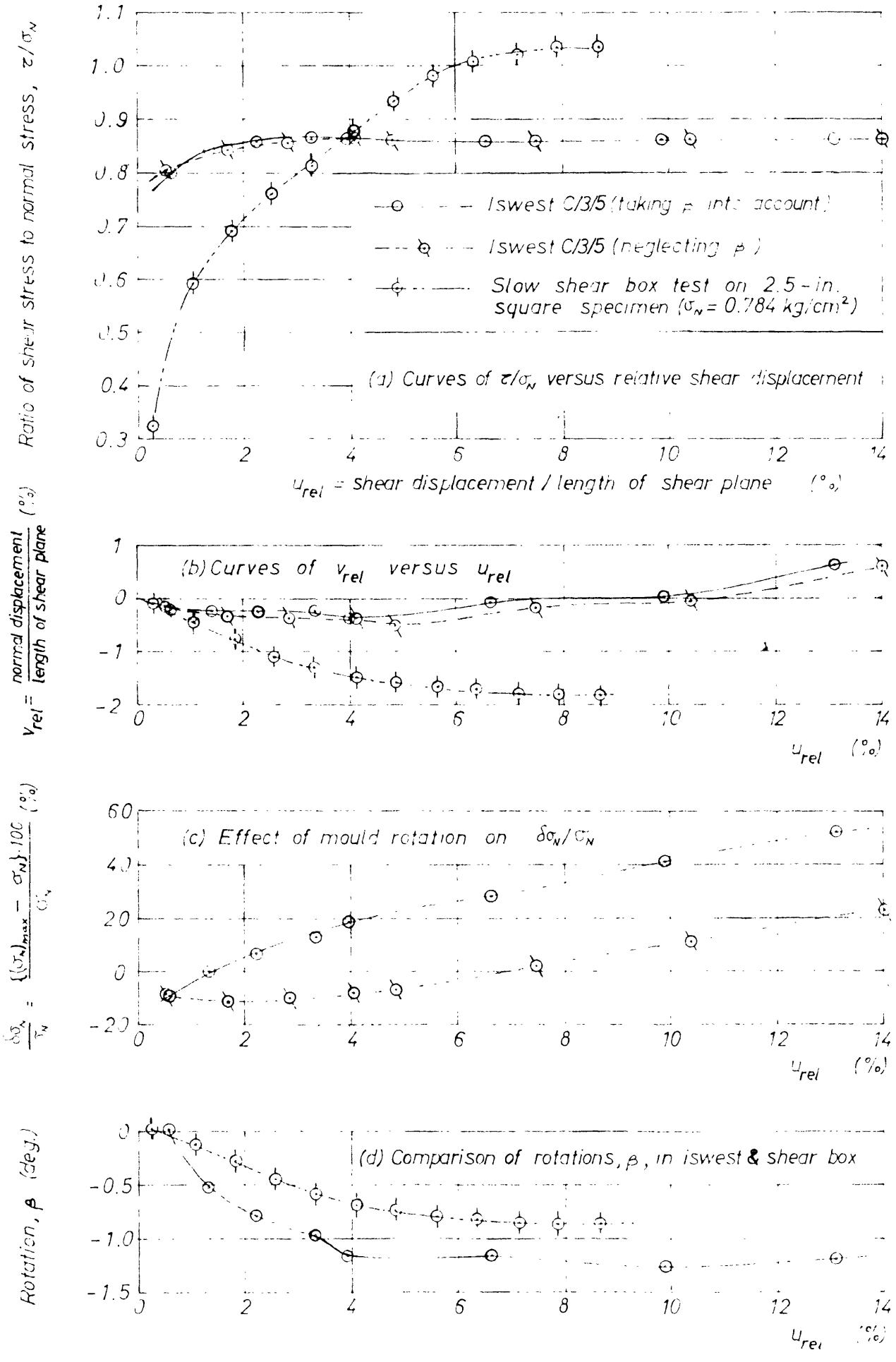

Fig 5.15. Comparison of rotations β in iswest and shear box test and the effect of β on measured τ/σ_N, normal displacement, and $\delta\sigma_N/\sigma_N$ in iswests

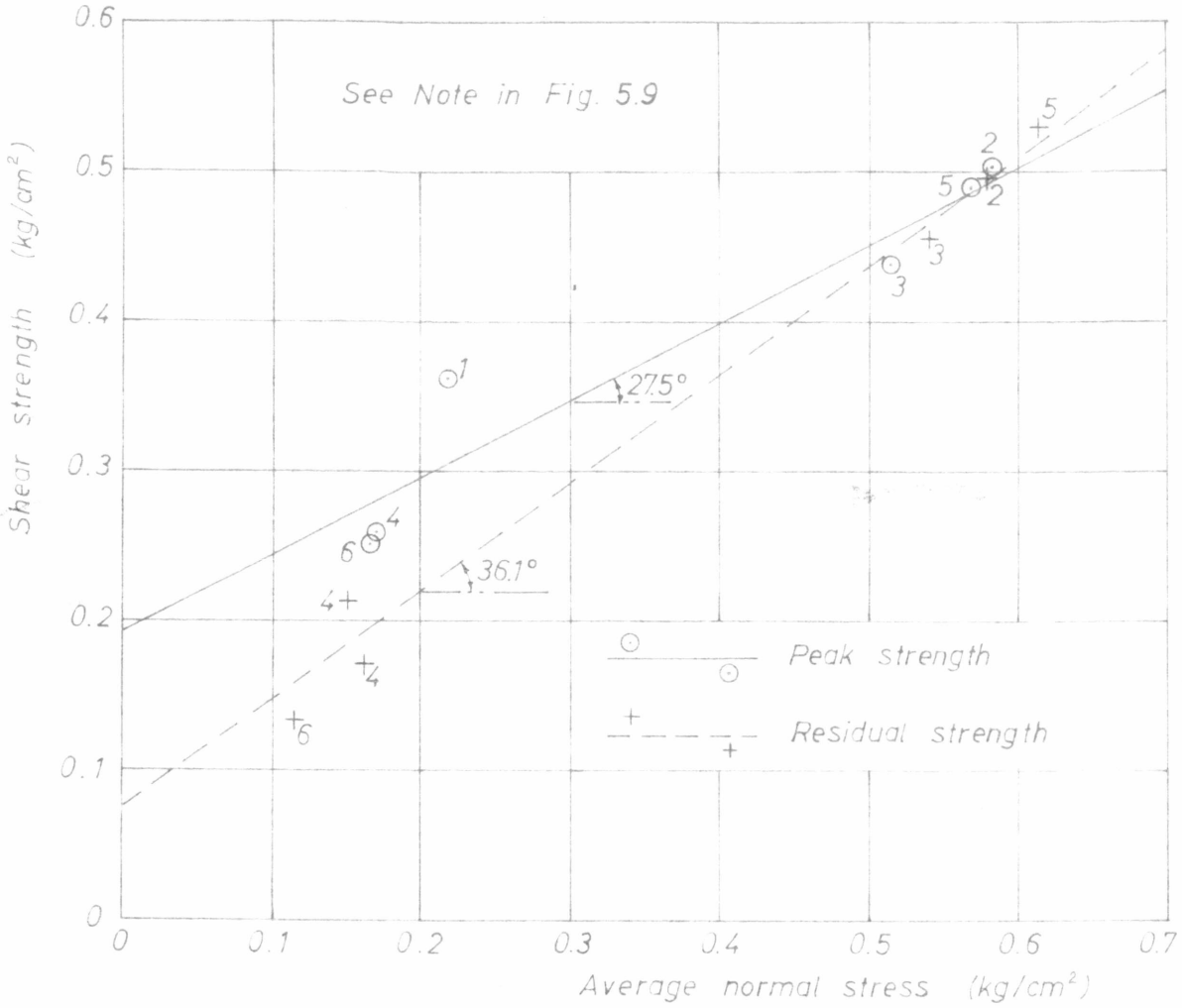

Fig. 5.16. Peak and residual undrained shear strength envelopes for Iswest series C/3 using two moulds only

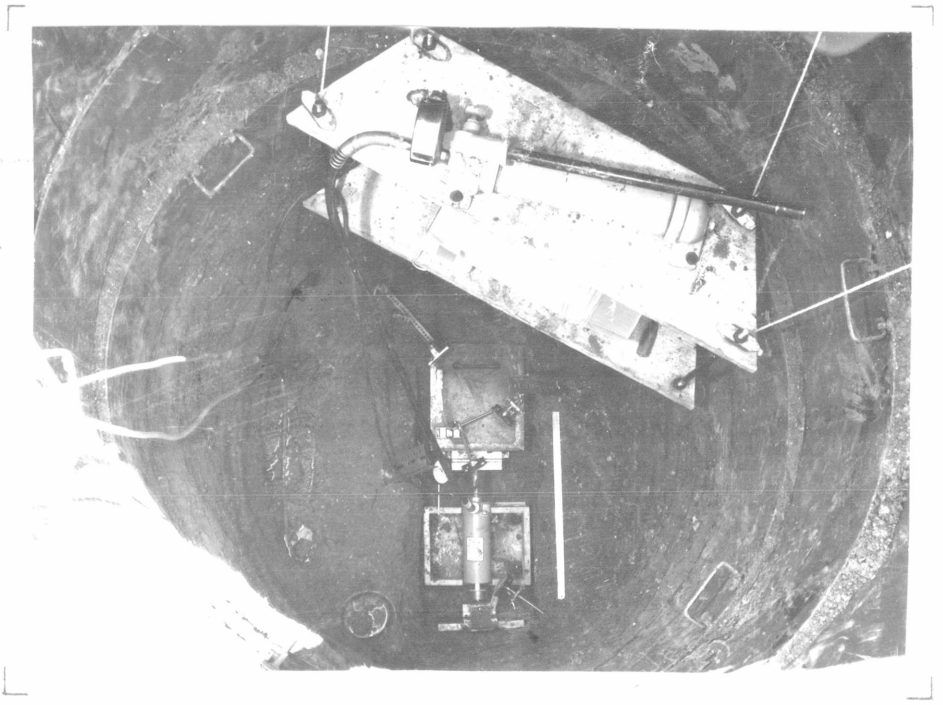

Fig. 5.17. Iswest C/4/6 in 1.20 m diameter test pit supported by expansible steel rings

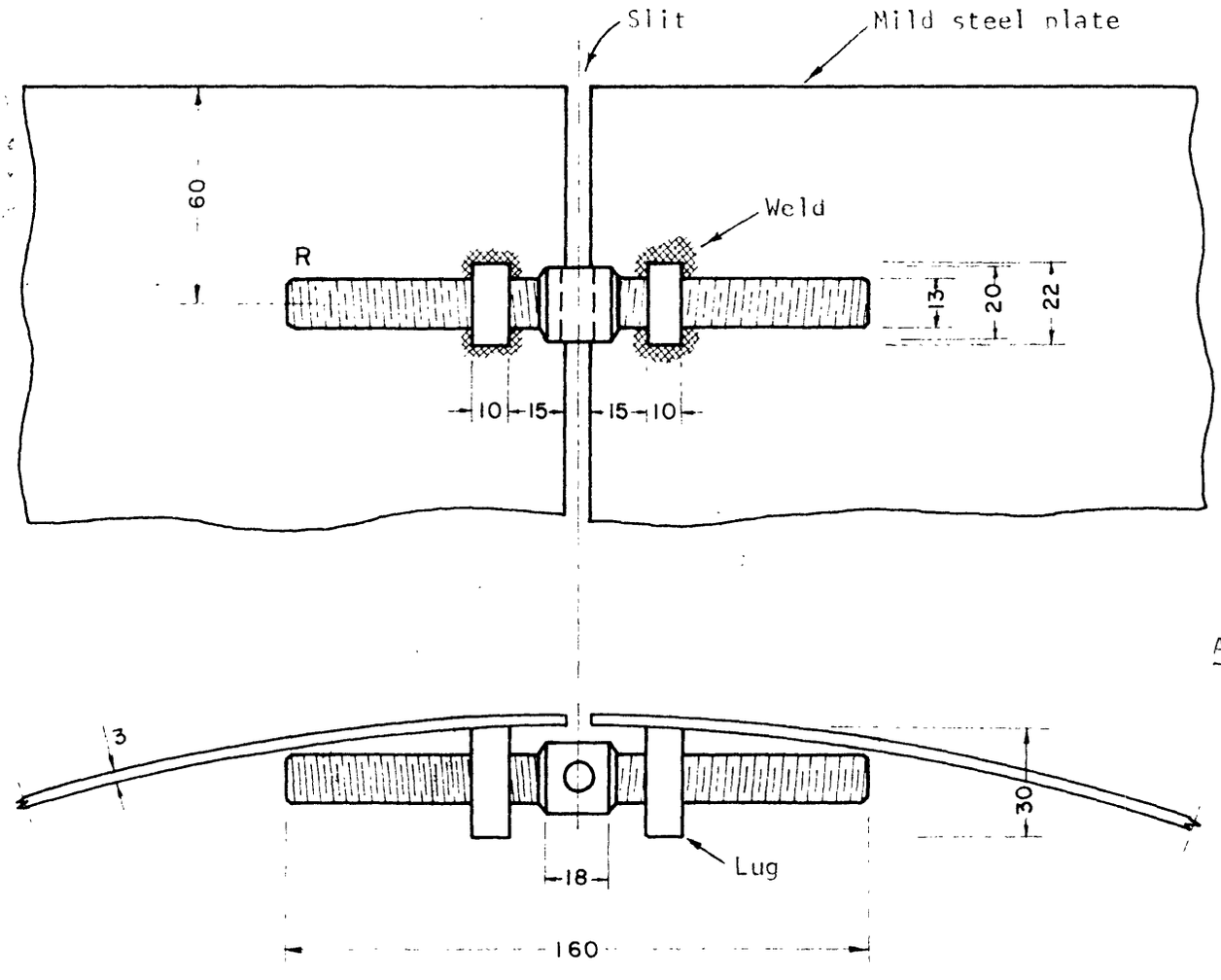

Fig. 5.19. Turnbuckle used in the expansible steel rings for support of tes pit walls

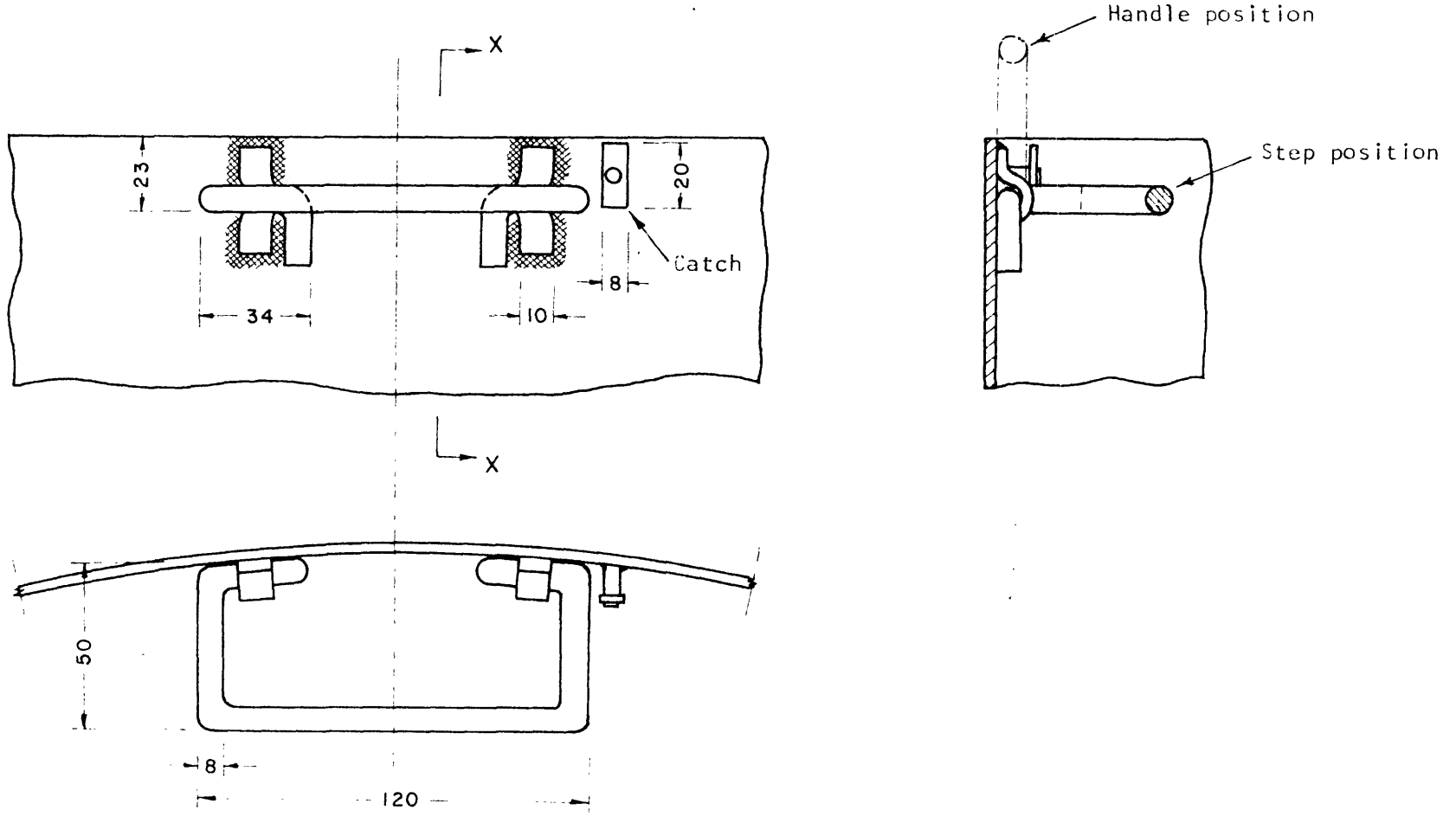

Fig. 5.19. Combined step and handle used in the expansible steel rings for support of test pit walls

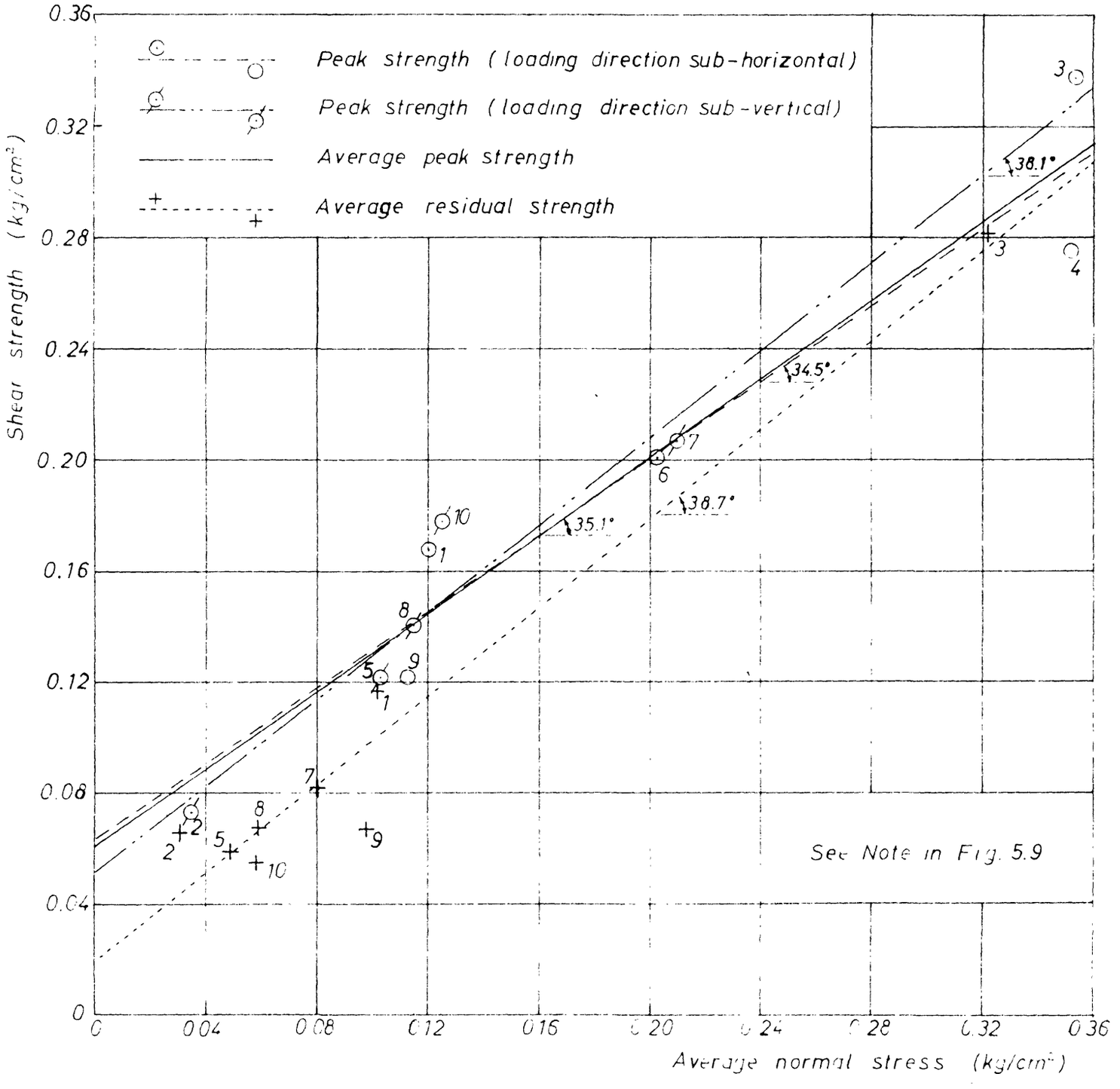

Fig. 5.20. Peak and residual undrained shear strength envelopes for iswest series C/4

CHAPTER 6

ANALYSIS OF SLIPS BY CONVENTIONAL METHODS

6.1 Introduction

In this chapter the stability of the four slips described in the previous chapter is analysed through triaxial tests and the effective stress type of stability analysis. The results of analyses based on slow shear box tests are also presented.

6.2 Triaxial Tests

Tables 6.1 to 6.3 summarize the particulars of the nine series of triaxial tests performed. Test series 4 were done on 102 mm dia. specimens, the remainder on 36 mm dia. specimens. All tests were run at a room temperature held constant between 22 °C and 24 °C, at slow enough a rate of strain to enable 95% equalization of pore pressures based on values of coefficient of consolidation, c_v, measured in a number of triaxial tests (Table 6.4, Column 18).

Except series 9, which consisted of two multi-stage tests, all tests have been performed by keeping the axial stress σ_1 constant and decreasing the cell pressure σ_3 as recommended by Bishop and Henkel (1962) for partly saturated soils.

The calibration, testing, and calculation procedures are outlined in the following sub-sections, with particular reference to the problems believed to have been solved in an original way.

6.2.1 Pre-testing operations

6.2.1.1 Calibration of proving rings

As the means for checking the calibration of the proving rings were not available, the calibration tables provided by the manufacturers were assumed as correct. The plot of the tabulated values gave the constants for the 180 kg and 2250 kg capacity proving rings, used for the tests on 36 mm dia. and 102 mm dia. specimens, as 0.0738 kg/10^{-4} in and 1.365 kg/10^{-4}in respectively.

6.2.1.2 Calibration of pressure gauges

All pressure gauges used in this study were re-calibrated by means of a dead weight tester. This device operated on the principle of balancing the force exerted by oil pressure on a piston of known area against dead weights of known mass, and was claimed to have an accuracy of 0.1 %. A mercury manometer (Section 6.2.1.3) was used for the calibration of gauge nos. 2 and 4 over the negative pressure range. Gauge No. 2 was permanently balanced against a mercury manometer and always showed a positive reading. The calibrations of the gauges were as follows.

Gauge No. 1 (for cell pressure, 36 mm dia. specimens):

$$\sigma_3 = 0.0703\ p_1 - 0.039 \quad \ldots\ldots\ldots\ldots\ldots\ldots \quad (6.1)$$

Gauge No. 2 (for pore pressure, 36 mm dia. specimens):

$$u_s = p_2 + (C_{01}+C_{11}\cdot p_2 + C_{21}\cdot p_2^2 + C_{31}\cdot p_2^3 + C_{41}\cdot p_2^4) \ldots \quad (6.2)$$

Gauge No. 3 (for cell pressure, 102 mm dia. specimens):

$$\sigma_3 = 0.0703\ p_3 + 0.037 \quad \ldots\ldots\ldots\ldots\ldots\ldots \quad (6.3)$$

Gauge No. 4 (for pore pressure, 102 mm dia. specimens and for test series 8):

$$u_s = 0.06715\ (\ p_4 - p_o\ ) - 0.010 \quad \ldots\ldots\ldots\ldots \quad (6.4)$$

where σ_3, u_s = corrected cell pressure (kg/cm^2) and pore pressure (kg/cm^2) respectively, making due allowance for the head difference between the centre of the relevant pressure gauge and the mid-height of the specimen

p_1, p_3, p_4 = pressure recorded on gauge nos. 1, 3 and 4 respectively (lb/in^2)

p_2 = pressure recorded on gauge no. 2 (kg/cm^2)

p_o = pressure recorded on gauge no. 4 with a 1 mm thick layer of water on the lower pedestal (lb/in^2)

C_{ij} = coefficients given in Table 6.5 for i= 0 to 4, and j = 1.

The expression, obtained by POLRG (IBM, 1969), inside the brackets in equation 6.2 adds to the observed reading a correction which changes evenly from 0.024 kg/cm^2 at a pressure of - 0.6 kg/cm^2 observed pressure to zero at 1.2 kg/cm^2, drops to a minimum of - 0.076 kg/cm^2 at 5.6 kg/cm^2, and then rises to - 0.050 kg/cm^2 at 8.4 kg/cm^2. If calculations are to be performed by hand, it is quicker to plot a curve showing this

variation and read off values of this correction from this curve. This applies to all polynomials quoted in this thesis whose coefficients are given in Table 6.5.

6.2.1.3 Pressure equivalence of manometer readings.

It is generally assumed that pressures measured by a manometer are more reliable than those given by a Bourdon gauge; Blight (1961), for instance, reports that a manometer was used to measure pressures below 20 lb/in^2. This assumption is true only if, as presumed by some manufacturers of such manometers (whose only one limb at a time can be read against the graduations provided), the mercury rises in one limb by the exact amount by which it falls in the other. The Author's observations have shown that this property of manometers is not to be taken for granted; for the manometer used in this study for tests on 36 mm dia. specimens, the value of δM, the sum the readings of the level of mercury in the two limbs, was found to vary between - 2.1 cm/2 when M_L was 66.9 cm/2 to 1.2 cm/2 when M_R was 50.0 cm/2

where

$$\delta M = M_L + M_R \quad \ldots\ldots\ldots\ldots\ldots\ldots \quad (6.5)$$

M_L = reading of the mercury level in the left-hand limb (cm/2)

M_R = reading of the mercury level in the right-hand limb (cm/2).

At the time of the study of the behaviour of the manometer, when M_R was zero, δM was 0.7 cm/2, so that

if pressures were to be evaluated by assuming δM constant at this value and reading only one limb of the manometer, an error ranging from - 0.0063 kg/cm^2 to 0.0354 kg/cm^2 over the quoted range of manometer readings would result. At this point, it should be explained that above the mercury in the right-hand limb, connected to the automatic pore pressure balancing unit, was machine oil of specific gravity 0.902, and above that in the left-hand limb, connected to a small water reservoir, was water (the total variation of water level in this reservoir over the full range of the manometer was 10 mm, and therefore this level was assumed as constant in calculating pressures).

The true pressure at the mid-height of the specimen, calculated by reading both limbs of the manometer and correlating this pressure to the readings of each limb in turn, was given by the following equations.

$$u_s = 0.01283 \, (M_L + C_L) + 0.0560 \quad \ldots\ldots\ldots\ldots \quad (6.6)$$

$$u_s = -0.01249 \, (M_R - M_{Ro}) - 0.0044 \quad \ldots\ldots\ldots\ldots \quad (6.7)$$

where C_L = a correction to be determined by comparison with the corrected pressure gauge readings (equation 6.2)

and M_{Ro} = reading of right-hand limb of manometer with a 1 mm thick layer of water on the lower pedestal (cm/2).

Had the value of δM in equation 6.5 been assumed constant at its value for $M_R = 0$, the numerical value of the

first coefficient in both of equations 6.6 and 6.7 would have been 0.01265. The fact that the value of δM was not constant was discovered after fifty triaxial tests had been completed. Thus in twenty of these tests in which the pore pressures had been based on M_L readings, and computer cards punched accordingly, although simultaneous pressure gauge readings had been taken, it was found quicker to determine the value of C_L in equation 6.6 by equating the values of u_s obtained by equations 6.2 and 6.6 for one stage of each test, and to use the latter equation for the evaluation of pore pressures for that test. So in this study, values of pore pressure evaluated through the use of equation 6.6 were only as accurate as those obtained by the pressure gauge.

No manometer readings were used in the evaluation of the tests on 102 mm dia. specimens.

6.2.1.4 Properties and adjustment of cell ram

6.2.1.4.1 Cell for 36 mm diameter specimens

The cell used for the testing of 36 mm dia. specimens was of the rotating bushing type. No change in proving ring dial readings could be observed on reversing the direction of axial strain, with the cell filled with water and the cell pressure constant. This showed that friction between the rotating bushing and ram was negligible. Wade (1968) has shown that even when a lateral force, as in the case of a specimen deforming unsymmetrically, is applied to the ram, the friction in this type of bushing is negligible.

The top of the cell was held in position by three tie bars screwed to the collar at the base of the perspex cylinder, as illustrated by Bishop and Henkel (1962), Fig. 16. The nuts at the upper end of these tie bars were tightened evenly to bring the ram to a central position, and these were then covered with sealing wax to avoid inadvertent subsequent turning.

The weight of the ram was 420 g. The weight of the perspex top cap (33 g) and that of the ceramic disc (13 g), used in tests with top drainage, were taken into account in the calculations.

The cross-sectional area of the ram was 1.983 cm^2.

6.2.1.4.2 Cell for 102 mm diameter specimens

The principal feature of the cell, used for the testing of 102 mm dia. specimens, was a rolling diaphragm type of seal between the lower part of an expanded section near the lower end of the ram, and the lower end of the collar attached to the cell top and housing this expanded section. Leakage between the ram and the top of the cell was therefore completely arrested. The upper part of the ram passed through a cylindrical guide provided with a ball bushing for free axial motion. The friction between the ram and the bushing was found, by a similar test as in Section 6.2.1.4.1, to be negligible. Work by Olson and Campbell (1967) has indicated that lateral loads on the ram produce a negligible increase in ram friction for this type of bushing as well.

The tie bars, attaching the top of the cell to the lower collar in this case, were tightened by sunk nuts which could not inadvertently be turned out of adjustment.

The effective cross-sectional area of the ram was determined by measurement of the uplift on the ram under different cell pressures, and by the measurement of the volume of the displaced cell fluid under constant cell pressure at different axial displacements. This area was 18.40 cm^2. The weight of the ram was estimated as 1.15 kg, and the weight of the steel top cap (2.20 kg) and the ceramic disc (0.10 kg), used in tests with top drainage, were taken into account in the calculations.

6.2.1.5 Rate of leakage past ram

As explained in Section 6.2.1.4.2, there was no problem of leakage of cell fluid past the ram in the cell used for the testing of 102 mm dia. specimens.

The rate of leakage of castor oil between the ram and bushing in the small cell was determined under different cell pressures with the bushing rotated, and when this was stationary. The weight of castor oil leaking past the ram was determined by drawing most of this oil into a small, weighed, hypodermic syringe, and wiping off the remainder by means of a weighed piece of linen. The specific gravity of castor oil was determined as 0.965.

With the bushing rotated, the average rate of leakage past the ram was found to be 0.0001467 cm^3/min per kg/cm^2

cell pressure. With the bushing stationary, this figure dropped to 0.0000973 $cm^3/min/kg/cm^2$. The latter figure was used in correcting for leakage in determining the volume change characteristics of the cell. The former figure was used in the calculation of volume changes in the specimen during the test. The weight W_{cl} of castor oil leaking past the ram was determined at the end of each test, and this was checked against the weight W_{cc} calculated by the use of the figure of 0.0001467 $cm^3/min/kg/cm^2$. Reasonable agreement resulted. But when all the test results had to be re - evaluated to allow for the anomalous behaviour of the manometer (Section 6.2.1.3), the opportunity was taken to calculate a corrected value of rate of leakage L_r per unit pressure, by multiplying the figure of 0.0001467 by the ratio of W_{cl}/W_{cc}. The values of L_r so obtained (Table 6.6, Column 22) ranged between 0.0001215 and 0.0002570 $cm^3/min/kg/cm^2$, and as expected, perfect agreement between W_{cl} and the new values of W_{cc} resulted.

6.2.1.6 Volume change characteristics of cells

6.2.1.6.1 Elastic volume change

As the specimens were to be sheared by decreasing the cell pressure, the cells were calibrated under similar conditions. Each cell was filled with de-aired water, and the cell pressure raised to a typical value to be used during actual testing. The cell was kept under this initial nominal (as observed on the cell pressure gauge) cell pressure $(\sigma_3)_o$ for a period long enough to enable all air bubbles, trapped within the cell

during filling and/or the introduction of castor oil, to be dissolved completely in the water. No observable creep of the small cell occurred. The creep behaviour of the large cell is presented in Section 6.2.1.6.2.

The cell pressure was then reduced in steps, and the flow of water out of the cell observed by means of a twin 25 ml burette volume change measurement device, containing a low viscosity silicone oil as the immiscible fluid. The change in volume of the small cell was negligibly small after about ten minutes, and stopped completely after about an hour. No correction was therefore applied to account for this time dependent adaptation of the cell to the new pressure. The rebound of the large cell, however, took about twenty-four hours to complete; the correction to be applied to volume change readings to account for this property of the large cell is treated in Section 6.2.1.6.3.

The cumulative decrease in volume of the cell was determined at each step until zero cell pressure was reached, and then each of these values were deducted from the cumulative decrease in volume corresponding to zero cell pressure. The resulting values of fictitious increase in volume were correlated with the cell pressure by POLRG (IBM, 1969). Equations 6.8 and 6.9 represent the relationships obtained for the small cell for $(\sigma_3)_o$ = 40 lb/in^2 and 80 lb/in^2 respectively.

$$\delta V_{el} = C_{02} + C_{12} \cdot \sigma_3 + C_{22} \cdot \sigma_3^2 \quad \ldots\ldots\ldots \quad (6.8)$$

$$\delta V_{eh} = C_{03} + C_{13} \cdot \sigma_3 + C_{23} \cdot \sigma_3^2 \quad \ldots\ldots\ldots\ldots \quad (6.9)$$

The corresponding relationships for the large cell are given in equations 6.10 and 6.11 for $(\sigma_3)_o$ = 80 lb/in^2 and 120 lb/in^2 respectively.

$$\delta V_{el} = C_{04} + C_{14} \cdot \sigma_3 + C_{24} \cdot \sigma_3^2 \quad \ldots\ldots\ldots\ldots \quad (6.10)$$

$$\delta V_{eh} = C_{05} + C_{15} \cdot \sigma_3 + C_{25} \cdot \sigma_3^2 \quad \ldots\ldots\ldots\ldots \quad (6.11)$$

where δV_{el}, δV_{eh} = fictitious elastic increase in volume (cm^3) of the cell for the lower and higher values of $(\sigma_3)_o$ respectively

σ_3 = true cell pressure at the mid-height of the cell (kg/cm^2)

C_{ij} = coefficients given in Table 6.5 for i = 0 to 2, and j = 2 to 5.

The elastic changes in volume of the cell, for any other value of $(\sigma_3)_o$ than those used for the calibration of the cell in question, were obtained by linear interpolation (or extrapolation) between the appropriate pair of equations 6.8 to 6.11 (Section 6.2.4.2.1).

6.2.1.6.2 Creep of large cell

For calculating the volume changes in the specimen between the start of testing and the first set of readings, the creep characteristics of the large cell had to be known. These were determined under two different cell pressures, and are given by equations 6.12 and 6.13 for $(\sigma_3)_o$ = 80 lb/in^2

and 120 lb/in^2 respectively.

$$\delta V_{crl} = C_{16} \cdot t_m + C_{26} \cdot t_m^2 \quad \ldots\ldots\ldots\ldots\ldots\ldots (6.12)$$

$$\delta V_{crh} = C_{17} \cdot t_m + C_{27} \cdot t_m^2 \quad \ldots\ldots\ldots\ldots\ldots\ldots (6.13)$$

where δV_{crl} , δV_{crh} = increase in volume (cm^3) of the cell due to creep under the lower and higher values of $(\sigma_3)_o$ respectively

t_m = time elapsed from start of deviator stress application (min)

C_{ij} = coefficients given in Table 6.5 for i = 1 and 2, and j = 6 and 7.

The relationship corresponding to any other value of $(\sigma_3)_o$ was determined by linear interpolation (or extrapolation) between equations 6.12 and 6.13 (Section 6.2.4.2.1).

6.2.1.6.3 Time dependent rebound of large cell

On reducing the cell pressure (in decrements of 20 lb/in^2 from 120 lb/in^2, and of 15 lb/in^2 from 80 lb/in^2), it was noticed that after a very rapid decrease in volume within the first 10 minutes, the cell continued to shrink at a gradually decreasing rate for the next 24 hours. This additional decrease in volume was 0.75 cm^3 for an average pressure decrement of 17.5 lb/in^2. The equation of the curve drawn through the rather scattered points, correlating the additional decrease in volume δV_{rb} (cm^3) with the time t_r (minutes) in excess of the first 10 minutes after the decrease in cell pressure, was as follows.

$$\delta V_{rb} = C_{08} + C_{18} \cdot t_r + C_{28} \cdot t_r^2 + C_{38} \cdot t_r^3 + C_{48} \cdot t_r^4 + C_{58} \cdot t_r^5 \quad \text{.....(6.14)}$$

where C_{ij} = coefficients given in Table 6.5 for i = 0 to 5 and j = 8.

As the equations 6.10 and 6.11 were based on the equilibrium condition of the cell, no correction was applied to the changes in volume measured at $t_r \geq 1400$ minutes. For $t_r < 1400$ minutes, a correction C_{rb} (cm^3), given by the following equation, was deducted from the decrease in volume calculated via equations 6.10 and 6.11.

$$C_{rb} = (0.75 - \delta V_{rb}) \cdot \delta\sigma_3 / 17.5 \quad \text{.....} \quad (6.15)$$

where $\delta\sigma_3$ = decrease in cell pressure (lb/in^2) at t_r = -10 min.

6.2.1.7 Elastic elongation of cell tie bars

During the determination of the volume change characteristics of the cells, it was noticed that the strain dial, registering the relative movement between the top of the cell and the ram, did not deflect as much as the proving ring dial, indicating the absolute displacement of the ram. The difference was due to the elastic elongation of the tie bars holding the top and bottom of the cell together, and this had to be allowed for in determining the true compression of the specimen. The necessary correction, δL_e (10^{-3} in), to be added to the strain dial readings are given in equations 6.16 and 6.17 for the small and the large cells respectively.

$$\delta L_e = 0.038 \quad \Delta\sigma_{3c} \quad \text{.....} \quad (6.16)$$

$$\delta L_e = 0.037 \quad \Delta\sigma_{3c} \quad \ldots\ldots\ldots\ldots\ldots\ldots\ldots \quad (6.17)$$

where $\Delta\sigma_{3c}$ = cumulative decrease in cell pressure from start of deviator stress application (lb/in^2).

6.2.1.8 Calibration of lateral strain indicator to measure change in area of specimen on initial cell pressure application

The method of determining the change in area of the specimen on initial cell pressure application, based on the assumption of isotropic strain and either the measurement of the change in volume or the optical determination of the change in height of the specimen, as recommended by Bishop and Henkel (1962), has been observed to suffer from a number of indeterminate factors. The first two of these factors apply only to the cases where volume changes are measured in a conventional cell, as in the present study, and not when mercury inside an inner perspex cylinder is used to surround the specimen. Firstly, some air bubbles invariably remained trapped in the cell during filling and/or the injection of castor oil. These bubbles did not dissolve completely in the inially de-aired cell water until the initial cell pressure, $(\sigma_3)_o$, was applied and maintained for at least twenty-four hours. It was impossible to gauge the volume of these bubbles accurately. Secondly, although a method of correction for the volume of air trapped between the specimen and the rubber membrane is given by Bishop and Henkel (1962), more recent observations quoted by the same authors indicate that in tests lasting more than a few hours in the conventional

triaxial cell, a significant proportion of this air as well as that in the pore space of the soil may be lost by diffusion through the rubber membrane into the surrounding de-aired water. Thirdly, it is known that on initial application of an axial load to a specimen, some of the axial shortening is due to bedding down of the ends of the test specimen and to closing up of open laminations and fissures (Ward et al., 1959). Although this observation is based on the particularly low Young's modulus values observed in the initial stages of deviator stress application, it is reasonable to expect, and it has been verified here, that not all of the volume change and axial shortening observed on the application of an all-round pressure will be due to a decrease in the volume of the specimen. Lastly, the assumption of isotropic strain may not be true. A novel method of determining the change in area of the specimen on initial cell pressure application has accordingly been employed in the present study. For this purpose, a lateral strain indicator (LSI), as illustrated by Bishop and Henkel (1962), has been used for 102 mm dia. specimens, except that the short graduated perspex tube was replaced by one measuring 80 mm in length. A short length of plastic tubing was attached to the top of this perspex tube to prevent inadvertent loss of mercury, and a clearly readable millimetre scale was fixed behind the perspex tube. For 36 mm dia. specimens, a similar device, manufactured for 38 mm dia. specimens, was used by pasting two pieces of 0.12 mm thick brass foil on each of the radiused pads; attaching a similar plastic tube

and scale on the graduated perspex tube, which was in this case of adequate length (4.4 mm); and adding suitable coils of lead on the counterweights, required to keep the device in equilibrium.

De-aeration of the space enclosing the mercury in the LSI presented a problem. It was found impossible to accomplish this merely by the application of a vacuum as recommended by Bishop and Henkel (1962); mercury would rise in the graduated tube as the trapped air bubbles expanded under the vacuum, and fall when the vacuum was removed, thus preventing escape of such bubbles. Finally, the following method was adopted for this purpose, and proved effective. The rubber diaphragm was removed, and the resulting opening was blocked by the finger, while vacuum was applied to the of a 2 to 3 m length of plastic tubing connected to the upper end of the graduated tube. The device was then dipped into a bowl of mercury, the finger removed, and air-free mercury drawn through the device. The plastic tubing was then bent and pressed at a point close to the device, the vacuum was removed, and the rubber diaphragm carefully replaced. The long plastic tubing was replaced by the short length of tubing mentioned earlier, this was filled with de-aired water, and the amount of mercury adjusted, using a hypodermic needle, so that with no pressure on the diaphragm, the mercury level stood at the base of the graduated tube. Very little air remained in the system after this procedure, the mercury in the graduated tube being depressed only by a few millimetres under a pressure of 120 lb/in^2. The remaining air apparently

escaped by diffusion through the rubber membrane on keeping the device in the triaxial cell filled with de-aired water under a pressure of 120 lb/in^2 for several days. The mercury level was unaffected by subsequent changes in cell pressure.

To calibrate the LSI to measure changes in the area of the specimen, this procedure was followed. The triaxial cell was assembled with the LSI around the specimen, and the mercury level adjusted to a low elevation on the graduated scale. Cell pressure was applied in increments, and the rise δL_s in the LSI reading, and the pore pressure were recorded until steady readings were obtained under each cell pressure. The readings were stopped when further increments in cell pressure produced no change in the LSI reading, indicating full saturation of the specimen. Axial strain was then started, and readings of the LSI and the strain dial were taken until the LSI reading was restored to the value before the application of cell pressure; the strain ε_o, corresponding to this value of LSI reading, was then used in the following equation for the calculation of fictitious strains ε_n (numerically negative).

$$\varepsilon_n = \varepsilon - \varepsilon_o \quad \ldots\ldots\ldots\ldots\ldots\ldots\ldots \quad (6.18)$$

where ε = strain measured at intermediate stages of the calibration test.

These values of ε_n were then used in an analogous equation to that used for calculating the corrected area

of a specimen whose volume remains unchanged in a triaxial test (Bishop and Henkel, 1962), in order to calculate the area a_u of the specimen at intermediate stages of the calibration test in terms of the area a_{oc} corresponding to the strain ε_o :

$$a_u = a_{oc} \frac{1}{1 - \varepsilon_n} \quad \ldots\ldots\ldots\ldots\ldots\ldots \quad (6.19)$$

The values of the ratio a_u/a_{oc} calculated from equation 6.19 were then plotted against the equivalent values of the rise in LSI reading, obtained as the difference between the reading corresponding to ε_o and the readings corresponding to the other values of ε_n . A straight line relationship or a very slight curve resulted. This was assumed to hold true for the cell pressure application stage of the test, and hence the values of a_u/a_{oc} corresponding to each σ_s were read off from this graph, using, if necessary, the corrected zero for the equivalent rise in LSI readings (Fig. 6.1). Finally, the values of a_u/a_{oc} were plotted against the calculated increase $\Delta\sigma'_3$ in the effective all-round stress on the specimen. The value of a_u/a_{oc} read off this curve for the appropriate value of $\Delta\sigma'_3$ in an actual test on all specimens from the same location was taken as the ratio F_u of the area of the specimen at the end of the undrained application of cell pressure to the initial area, a_o. The error introduced by the variations in the properties of the specimens from the same location was believed to be much smaller than the errors in any values based on volume change and/or axial strain measurement, neglecting the indeterminate

factors enumerated at the beginning of this sub-section (see also Section 6.2.2.1.3). The error in the LSI readings caused by the air trapped between the specimen and the rubber membrane was believed to be negligible due to the slight pressure exerted by the LSI pads driving any trapped air to other parts of the specimen.

Typical curves of a_u/a_{oc} versus the equivalent rise in LSI reading, and of a_u/a_{oc} versus $\Delta\sigma'_3$ are given in Figs 6.1 and 6.2 respectively. The scale of ε_n and ε have also been indicated on the right of Fig. 6.1. The lowest value of ε, below which the LSI showed practically no deflection, is an indication of the order of the 'seating' errors due to the initial eccentricity of the top cap relative to the cell ram. This is treated in more detail in Section 6.2.2.3.

After the calibration of the LSI, the specimen was sheared in the usual way, attention being paid to the likelihood of the LSI bearing on the walls of the cell due to excessive bulging of the specimen in the later stages of the test. The limited clearance between the LSI and the walls of the cell prevented the use of the LSI in tests where top drainage was intended.

6.2.1.9 Calculation of specimen dimensions at start of shear

The determination of the area of the specimen at the end of the undrained application of cell pressure has been explained in the previous section. The additional change in area of the specimen during consolidation, in tests where the

specimen was partially consolidated prior to shear, was initially estimated from the volume of water, gauged by a burette, draining from the specimen, by assuming isotropic strain and full saturation of the specimen. The change in area so calculated was generally an over-estimate because any air that occupied a negligible volume under pressure, and some of the air, initially dissolved in the pore water under pressure, occupied a finite volume in the drainage lines. The resultant error was, however, small and affected only the calculations for adjusting the cell pressure to keep the axial stress constant during the test. For the evaluation of the test results, the change δa_c in area during consolidation was calculated from the following equation based on the same assumptions of isotropic strain and full saturation.

$$\frac{\delta a_c}{a_o} = \frac{2}{3} \left(\frac{\delta W}{V_o}\right) \quad \ldots\ldots\ldots\ldots \quad (6.20)$$

where δW = difference in weight of specimen before and after the test (g)

V_o = initial volume of specimen (cm^3)

The ratio F_{rs} of the area a_s of the specimen at the start of shear to the initial area a_o was calculated from

$$F_{rs} = F_u - \frac{\delta a_c}{a_o} \quad \ldots\ldots\ldots\ldots\ldots\ldots \quad (6.21)$$

where F_u was determined as explained in Section 6.2.1.8. Thus

$$a_s = F_{rs} \cdot a_o \quad \ldots\ldots\ldots\ldots\ldots\ldots \quad (6.22)$$

The decrease δh_o in the height of the specimen during the undrained application of cell pressure and consolidation, if any, was calculated from the following equation, also based on the assumption of isotropic strain.

$$\delta h_o = \frac{1}{2} (1 - F_{rs}) . h_o \quad \ldots\ldots\ldots\ldots\ldots\ldots \quad (6.23)$$

where h_o = initial height of the specimen.

The height h_s of the specimen at the start of shear was thus obtained from

$$h_s = h_o - \delta h_o \quad \ldots\ldots\ldots\ldots\ldots\ldots\ldots\ldots \quad (6.24)$$

The corresponding decrease δV_o in the volume of the specimen was likewise calculated from

$$\delta V_o = \frac{3}{2} (1 - F_{rs}) . V_o \quad \ldots\ldots\ldots\ldots\ldots\ldots \quad (6.25)$$

The volume V_s of the specimen at the start of shear was calculated simply from

$$V_s = a_s . h_s \quad \ldots\ldots\ldots\ldots\ldots\ldots\ldots\ldots\ldots\ldots \quad (6.26)$$

6.2.1.10 Deciding on rate of strain

Dissipation tests (Table 6.4, Columns 16 to 18) were performed on at least one specimen from each site in accordance with the procedure given by Bishop and Henkel (1962).

Trial tests were run to determine the order of magnitude of the axial strain at failure. The required time to failure and hence the rate of strain was calculated as explained by Bishop and Henkel (1962) for 95 % equalization of pore

pressures. For the earlier tests, no side drains were used, partly due to the non-availability of filter paper of known properties (such as Whatman's No. 54), and partly due to the remarks by Bishop and Henkel (1962) about the difficulty of estimating accurately the restraint imposed by side drains and the inefficiency of side drains in partly saturated soils. The required time to failure for 36 mm dia. specimens in such tests was about 19 hours, and the tests had therefore to be left running overnight, when the rate of strain was temporarily reduced by one-fifth to avoid a failure during the unattended hours. In the later tests, when, during the dissipation stage of the partly consolidated-undrained tests, lower c_v values than measured in the earlier dissipation tests were observed, it was decided to use side drains cut from the available filter paper, and the properties of this paper was estimated subsequently by comparison with Whatman's No. 54 filter paper (see Section 6.2.2). Side drains were observed to be more efficient than expected, for although the soil was initially partly saturated, under the $(\sigma_3)_o$ values that had to be applied in order to obtain a satisfactory failure envelope, most of the specimens became fully saturated or very nearly so (see Table 6.2, Column 25, where the maximum pore pressure in the specimen is given as a fraction of the approximate theoretical pore pressure required to cause full saturation, based on Boyle's law and Henry's law of solubility (Bishop and Eldin, 1950)). Thus, the shearing stage of the tests on 36 mm dia. specimens could be completed in a working day. Tests on 102 mm dia. specimens were run at the lowest

available rate of strain of the machine, and took on the average some 17 days to complete. The rate of strain used for each test is given in Table 6.2, Column 5.

6.2.1.11 Precalculated curves

6.2.1.11.1 For failure by bulging

Bishop and Henkel (1962) give the following expression for the cell pressure σ_3 required to keep the axial stress σ_1 constant and equal to the initial cell pressure $(\sigma_3)_{oc}$:

$$\sigma_3 = \left\{ (\sigma_3)_{oc} - \frac{N \cdot p_r + W_r}{a_t} \right\} \left\{ \frac{1}{1 - a_r/a_t} \right\} \quad \ldots\ldots (6.27)$$

where N = proving ring factor expressed as a force per division

p_r = proving ring deflection in divisions from zero load

W_r = weight of ram

a_r = area of ram

a_t = area of the specimen at the instant considered.

For a specimen failing by bulging (Fig. 6.3 (a)), a_t is given by the following equation (Bishop and Henkel, 1962).

$$a_t = a_s \frac{1 + \Delta V/V_s}{1 - \varepsilon} \quad \ldots\ldots\ldots\ldots\ldots\ldots (6.28)$$

where ΔV = change in volume of specimen during shear (incease considered as positive)

ε = axial strain

and a_s, V_s denote the same quantities as in Section 6.2.1.9.

By taking the partial derivative of σ_3 in equation 6.27 with respect to p_r it follows that, if over any interval of the test, a_t is assumed as constant, the ratio of the decrease $\delta\sigma_3$ that has to be applied to the cell pressure for keeping σ_1 constant to the increase δp_r in proving ring deflection in the same interval can be expressed as:

$$\frac{\delta\sigma_3}{\delta p_r} = \frac{N}{a_t - a_r} \quad \ldots\ldots\ldots\ldots\ldots\ldots \quad (6.29)$$

For each nominal area a_n of the specimens to be tested, using equations 6.28 and 6.29 a set of curves similar to those illustrated by Bishop and Henkel (1962), Fig. 105, were calculated correlating $\delta\sigma_3 / \delta p_r$ with ε for values of $a_s = a_n$, 0.99 a_n, 0.98 a_n, and for $\Delta V/V_s$ = 0, + 2 % and - 2 %. Of these curves only the ones for $\Delta V/V_s = 0$ (Fig. 6.6), have been used for simplicity, as the volume changes in the specimen during shear were generally well below $\pm$ 1 % at failure (Table 6.3, Column 8).

The use of such curves during the test requires clarification. The value of p_r in equation 6.27 includes the effect of uplift due to cell pressure at the end of the ram. Thus, the calculation of δp_r for use with the pre-calculated curves should be based on the proving ring deflection immediately before the last adjustment of σ_3, and not this value corrected for the decrease in uplift resulting from this adjustment. The latter method was erroneously applied in the majority of the tests (those performed after 18 October 1973 (Table 6.1, Column 9)), and

resulted in an average decrease in σ_1 at failure of about 12 % (Table 6.3, Column 9). Even when the former method was employed, an average decrease in σ_1 of about 4 % (excluding test 1/4 where an arithmetical error was made and test 1/7 where the specimen did not fail until well after the cell pressure was reduced to zero) occurred because of the neglect, in the calculations performed during the test, of the volume increase in the specimen and the various corrections given in Section 6.2.2. It was not considered practical to apply corrections for membrane and side drains during the test, but the δp_r values were corrected for the increase in the area of the specimen between one adjustment of σ_3 and the next, in the later stages of most of the tests. This last correction also helped indicate the point of failure of the specimens failing by bulging. It is believed, however, that the slight decrease in σ_1 during the test is a closer simulation of the cutting of a slope, where a certain amount of decrease in σ_1 would generally occur.

6.2.1.11.2 <u>For failure along single slip plane</u>

For specimens failing along a single slip plane Fig.6.3(b), the curves in Section 6.2.1.11.1 could not be used directly. For such cases, the following method was devised, but was used on very few occasions due to the slip plane generally appearing immediately before failure, when further adjustment to σ_3 was no longer necessary. The corrected area of the specimen was calculated for different additional axial strains δ after the development of the slip plane, using equations

6.41 to 6.44, and neglecting volume changes. These areas were expressed as a ratio F_r of the area at the instant of development of the slip plane. Values of equivalent strain ε_{ns} (numerically negative) in a bulging specimen, necessary to produce the same relative decrease in area, were then calculated using the following equation.

$$\varepsilon_{ns} = \frac{F_r - 1}{F_r} \qquad \ldots\ldots\ldots\ldots\ldots\ldots (6.30)$$

The values of ε_{ns} were then plotted against the further axial shortening after the development of the slip plane. During the actual test, the corresponding values of ε_{ns} could be read off this graph, and then added to the strain, reached at the instant of development of the slip plane, to give a value for which the required $\delta\sigma_3/\ \delta p_r$ value could be read from the curves in Section 6.2.1.11.1, extended if necessary for negative values of ε. The significantly higher restraint of the rubber membrane in this mode of failure should be borne in mind (see Table 6.3, Column 16, tests 1/2 and 3/5).

6.2.1.11.3 Failure along a number of planes

Quite a few of the specimens failed by squeezing out of one or more wedges of soil along fissure planes (see Fig. 6.3(c), and Table 6.3, Column 2). As this occurred after a certain amount of bulging, and no simple analysis of such cases is known, these tests were evaluated assuming the specimens to have failed by simple bulging, and the curves in Section 6.2.1.11.1 were used for the adjustment of σ_3

during the test. This assumption was also used in the evaluation of the test results, although perhaps assuming that the cross-sectional area of the specimen stops changing upon the appearance of such planes would have been more correct. The effect of such specimens on the final results is believed to be insignificant.

6.2.2 Corrections

6.2.2.1 Corrections for failure by bulging

6.2.2.1.1 Area correction

For specimens failing by bulging, the corrected area a_t during shear was calculated using equation 6.28, the values of a_s and V_s being determined as explained in Section 6.2.1.9.

6.2.2.1.2 Correction for filter paper side drains

The value of $(\Delta\sigma_1)_{fp}$ given by the following equation suggested by Duncan and Seed (1967) was deducted from the measured axial stress to correct for the restraint imposed by filter paper side drains.

$$(\Delta\sigma_1)_{fp} = K_{fp} \left(\frac{P_{fp}}{a_t}\right) \quad \ldots\ldots\ldots\ldots\ldots\ldots \quad (6.31)$$

where K_{fp} = load carried by filter paper covering a unit length of the specimen perimeter

P_{fp} = length of perimeter covered by filter paper.

The value of K_{fp} for Whatman's No. 54 filter paper was calculated from the data given by Bishop and Henkel (1962) as 0.18 kg/cm (and not as 0.19 kg/cm found by

Duncan and Seed (1967) from the same data).

The other type of filter paper used in this study had slight corrugations which mostly evened out on wetting. The side drains were accordingly cut to 0.972 of the required length perpendicular to the general trend of the corrugations, and 0.980 of the required height parallel to this trend, before giving them the shape illustrated by Bishop and Henkel (1962). The corresponding reduction factor in the dimensions, in the dry state, of Whatman's No. 54 filter paper was 0.996 in any direction. The K_{fp} value of the corrugated filter paper was estimated from the value for Whatman's No.54 filter paper by direct proportion of the dry weights of the side drains, cut in this way, out of the two types of filter paper; this value was 0.15 kg/cm.

Duncan and Seed (1967) have observed that the load carried by the side drains increases to its maximum value at 2 % to 3 % axial strain and remains constant thereafter. The quoted values of K_{fp} were accordingly taken to be applicable for total axial strains ε_{at} above 2.5 %, ε_{at} being calculated from the following equation.

$$\varepsilon_{at} = \delta h_o / h_o + \varepsilon_c \quad \ldots\ldots\ldots\ldots\ldots\ldots \quad (6.32)$$

where ε_c = corrected axial strain during shear calculated from equation 6.54 and δh_o and h_o denote the same quantities as in equation 6.23.

For values of ε_{at} less than 2.5 %, the restraint due to the side drains was assumed to follow the same trend

of variation with ε_{at} as that given by Larochelle (1967) for axial strains caused by the displacement on a single slip plane. So for $0 \leqslant \varepsilon_{at} \leqslant 2.5$ %, K_{fp} in equation 6.31 was replaced by K_{fe} given by the following equation.

$$K_{fe} = 1.135\ K_{fp}(C_{09}+C_{19}\cdot \varepsilon_{at}+C_{29}\cdot \varepsilon_{at}^{2}+C_{39}\cdot \varepsilon_{at}^{3}+C_{49}\cdot \varepsilon_{at}^{4}) \quad \ldots\ldots\ldots (6.33)$$

where C_{ij} = coefficients given in Table 6.5 for i = 0 to 4 and j = 9.

For Whatman's No. 54 filter paper, equation 6.33 represents equivalent values of K_{fp} given by LaRochelle's (1967) curve with all ordinates multiplied by 1.135 to make K_{fe} = 0.18 kg/cm at ε_{at} = 2.5 %.

6.2.2.1.3 Correction for rubber membrane

The membrane corrections $(\Delta\sigma_1)_m$ and $(\Delta\sigma_3)_m$, to be deducted from the measured values of axial and radial stress respectively, were based on the following form of the equations given by Duncan and Seed (1967).

$$(\Delta\sigma_1)_m = \frac{2\ P_{om}\cdot M_e}{3\ a_o(1+\varepsilon_v)}\left(1 + 2\ \varepsilon_{at} - \sqrt{\frac{1+\varepsilon_v}{1-\varepsilon_{at}}}\right) \ldots (6.34)$$

$$(\Delta\sigma_3)_m = \frac{4\ M_e}{3\ d_o(1+\varepsilon_v)}\left(2 + \varepsilon_{at} - 2\sqrt{\frac{1+\varepsilon_v}{1-\varepsilon_{at}}}\right) \ldots (6.35)$$

where P_{om} = initial average perimeter of the membrane

M_e = extension modulus of the membrane

ε_{at} = total axial strain defined by equation 6.32

ε_v = total volumetric strain (contrary to the sign convention used by Duncan and Seed (1967), an increase in volume is taken here as positive volumetric strain)

and d_o = initial diameter of the specimen.

ε_v was calculated from the following equation.

$$\varepsilon_v = (\Delta V - \delta V_o) / V_o \quad \ldots\ldots\ldots\ldots\ldots (6.36)$$

where ΔV = increase in volume during shear and a_o, δV_o and V_o denote the same quantities as in Section 6.2.1.9.

Examining Duncan and Seed's (1965) derivations of equations 6.34 and 6.35 in the light of the discussion in 6.2.1.8, has lead to the following modified form of these equations. These have been obtained by replacing ε_{at} by ε_{ab} in expressions dependent on the axial shortening of the membrane, and leaving ε_{at} intact in expressions where it was used for the calculation of the lateral strain of the specimen. Used for the latter purpose only, ε_v was also left intact.

$$(\Delta\sigma_1)_m = \frac{2 P_{om} \cdot M_e}{3 a_o (1+\varepsilon_v)} \left(1+2\varepsilon_{ab} - \sqrt{\frac{1+\varepsilon_v}{1-\varepsilon_{at}}}\right)\left(\frac{1-\varepsilon_{at}}{1-\varepsilon_{ab}}\right) \quad \ldots\ldots (6.37)$$

$$(\Delta\sigma_3)_m = \frac{4 M_e}{3 d_o (1+\varepsilon_v)} \left(2+\varepsilon_{ab} - 2\sqrt{\frac{1+\varepsilon_v}{1-\varepsilon_{at}}}\right)\left(\frac{1-\varepsilon_{at}}{1-\varepsilon_{ab}}\right) \quad \ldots\ldots (6.38)$$

where $\varepsilon_{ab} = \varepsilon_{at} + \varepsilon_b$ ..... (6.39)

and ε_b = apparent axial strain of specimen due to bedding.

Observations through a cathetometer during the application of cell pressure in triaxial test series 8 have indicated that ε_b could be correlated approximately with the initial nominal cell pressure $(\sigma_3)_o$ (in lb/in^2) by the equation:

$$\varepsilon_b = 0.000073\ (\sigma_3)_o \quad \ldots\ldots\ldots\ldots\ldots\ldots \quad (6.40)$$

The use of equations 6.37 to 6.40 for the calculation of the membrane corrections for triaxial test series 8 have resulted in values of $(\Delta\sigma_1)_m$ 0.002 kg/cm^2 to 0.004 kg/cm^2 greater, and in values of $(\Delta\sigma_3)_m$ 0.001 kg/cm^2 greater than the corresponding values that would have been found from equations 6.34 and 6.35, neglecting the effect of bedding. Although the effect of these differences on the measured strength is almost negligible, for consistency, equation 6.40 was assumed to be true for all the previous tests and the membrane corrections calculated by using equations 6.37 and 6.38. The amount of bedding, based on equation 6.40, is given in mm in Table 6.2, Column 8; and as a percentage of the initial axial strain $\delta h_o/h_o$ and the axial strain at failure in Table 6.2, Column 9 and in Table 6.3, Column 5 respectively.

6.2.2.2 Corrections for failure on single slip plane

In this study all the specimens that have eventually failed by shearing along a slip plane, the slip along the single plane started after a certain amount of bulging. So the corrections, calculated here by using modified forms of LaRochelle's (1967) and Pachakis' (1976) equations, have been

based on the specimen dimensions at the estimated instant of the development of the slip plane. The membrane and drain corrections calculated here were added on to the corresponding corrections due to bulging of the specimen up to the point of development of the slip plane.

6.2.2.2.1 Area correction

The corrected area a_t after the development of the slip plane was calculated from this equation:

$$a_t = \frac{d_p^2}{4} (\theta_p - \sin \theta_p) \quad \ldots\ldots\ldots\ldots\ldots\ldots \quad (6.41)$$

where d_p = diameter of specimen at the instant of appearance of the slip plane

and $$\theta_p = 2 \cos^{-1} (\delta h_p / d_p \cdot \tan \alpha_p) \quad \ldots\ldots\ldots \quad (6.42)$$

where δh_p = axial shortening of specimen due to displacement along of the slip plane

α_p = angle between the slip plane and the horizontal.

δh_p is calculated from the following equation.

$$\delta h_p = h_s \cdot \delta \quad \ldots\ldots\ldots\ldots\ldots\ldots \quad (6.43)$$

where h_s = height of specimen at the start of deviator stress application

and δ = axial strain due to displacement along the slip plane.

δ was calculated from the following modified and corrected version of an equation given by LaRochelle (1967).

$$\delta = C_{sn} + (\varepsilon_c - \varepsilon_p) + \left(\frac{\Delta V - \Delta V_p}{3 h_s \cdot a_p}\right) \quad \ldots\ldots\ldots \quad (6.44)$$

where ε_c = total corrected axial strain occurring during deviator stress application calculated from equation 6.54

ε_p = value of ε_c at the point of appearance of the slip plane

ΔV = measured change in volume of specimen (contrary to the sign convention used by LaRochelle (1967), increase in volume is assumed here as positive)

ΔV_p = value of ΔV at the point of appearance of the slip plane

a_p = corrected cross-sectional area of the specimen at the point of appearance of the slip plane

C_{sn} = axial strain that must take place before the slip plane may become visible.

In the original equation given by LaRochelle (1967), the constant in the denominator of the last expression is 2, and h_s has been omitted. LaRochelle (1967) suggests that C_{sn} be taken as 0.25 %. As however it is not practical to watch the specimen continuously throughout the test, here the slip plane has been assumed to have both developed and 'appeared' immediately after the reading preceeding the one at which the slip plane was noticed, and the value of C_{sn} has been taken as zero. However, with the frequency of readings employed, the equivalent value of C_{sn} inherent in this assumption was of the order of 0.25 % (Fig. 6.4).

6.2.2.2.2 Correction for filter paper side drains

LaRochelle's (1967) previously mentioned (Section

6.2.2.1.2) curve gives the variation of the deviator stress caused by the restraint due to the filter paper side drains with δ. It has been assumed here that, the side drains affect only the axial stress measured, and the values of K_{fer}, to be substituted for K_{fp} in a similar expression to equation 6.31 for the calculation of $(\Delta\sigma_1)_{fpr}$, the additional correction due to side drains, were determined from the following equation fitted to LaRochelle's (1967) curve up to $\delta = 6\ \%$.

$$K_{fer} = K_{fp} (C_{09} + C_{19} \cdot \delta + C_{29} \cdot \delta^2 + C_{39} \cdot \delta^3 + C_{49} \cdot \delta^4) \quad ..(6.45)$$

where C_{ij} = coefficients given in Table 6.5 for i = 0 to 4 and j = 9

K_{fp} was taken as 0.18 kg/cm for Whatman's No. 54 filter paper and 0.15 kg/cm for the other type of filter paper used (Section 6.2.2.1.2).

The values of $(\Delta\sigma_1)_{fpr}$ were calculated from

$$(\Delta\sigma_1)_{fpr} = K_{fer} \left(\frac{P_{fp}}{a_t}\right) \quad \ldots\ldots\ldots\ldots\ldots \quad (6.46)$$

and the overall correction $(\Delta\sigma_1)_{fpt}$ due to side drains from

$$(\Delta\sigma_1)_{fpt} = (\Delta\sigma_1)_{fpp} + (\Delta\sigma_1)_{fpr} \quad \ldots\ldots\ldots\ldots\ldots \quad (6.47)$$

where $(\Delta\sigma_1)_{fpp}$ is the value of $(\Delta\sigma_1)_{fp}$ calculated from equation 6.31 for the point of development of the slip plane.

6.2.2.2.3 Corrections for rubber membrane

Pachakis (1976), by considering the equilibrium of one

half of a dummy specimen cut along a plane inclined at $(90 - \alpha_p)$ to the axis, with the friction on the slip plane eliminated and forces P_a, P_m and P_r, all due to the restraint of the rubber membrane, acting respectively along the axis, along the slip plane and normal to the slip plane, has shown that a correction has to be applied to the ambient stress in the plane of movement as well as the deviator stress. He has derived corrections in terms of the force P_a acting on the dummy specimen, and suggested that these corrections be superimposed on the additional stresses applied to a real soil specimen during loading. It is thus implicitly assumed that P_r would always be normal to the slip plane, as in the dummy specimen.

The Author believes that in superimposing the restraint of the rubber membrane on to the other forces acting on a soil specimen, one has to consider the correct orientation of P_r. Acting on the slip plane in a soil specimen, there will generally be a cohesive force C_p and a reaction R_p that is inclined to the normal to the slip plane at the angle of shearing resistance $\emptyset$, in terms of total stresses, obtaining at the instant considered. Both these forces will act in such a direction as to oppose the relative movement between the two halves of the specimen. C_p is independent of the external forces acting on the soil specimen, and the inclination of R_p is independent of the nature of these forces. The reaction P_r due to the restraint of the rubber membrane has therefore to be included in R_p and as such is also inclined at $\emptyset$ to the normal to the slip plane.

With this reasoning, the equations given by Pachakis (1976) for the corrections $(\Delta\sigma_1)_{mr}$ and $(\Delta\sigma_3)_{mr}$ to be deducted from the uncorrected values of axial stress and cell pressure respectively can be written as follows.

$$(\Delta\sigma_1)_{mr} = \frac{P_m}{a_t}(\sin\alpha_p + \cos\alpha_p/\tan(\alpha_p - \phi) - \cos\alpha_p/\tan\alpha_p) \quad \ldots(6.48)$$

$$(\Delta\sigma_3)_{mr} = -\frac{P_m}{a_t}(\cos\alpha_p / \tan\alpha_p) \quad \ldots\ldots\ldots\ldots\ldots\ldots(6.49)$$

LaRochelle (1967) presents a theoretical expression, subsequently corrected algebraically (LaRochelle, 1970), for the calculation of P_m. The values of P_m calculated from this expression have, however, to be multiplied by a factor of 0.614 if the deviator stress due to the rubber membrane calculated from equations (6.48) and (6.49) is to fit the experimental value measured by LaRochelle (1967) on a perspex specimen with the friction on the slip plane eliminated by steel balls. The Author believes that this reduction in P_m, calculated by LaRochelle's (1967) theory, is reasonable, for in his derivation LaRochelle has evaluated the force required to stretch unit width of the membrane in the central plane of movement, and multiplied this force by the length of the periphery of the slip plane, whereas the mode of deformation of the membrane changes on moving away from the central plane of movement, and may well result in a lower force per unit length. Accordingly, the value of P_m for use in equations (6.48) and (6.49) was calculated from the following modified form of LaRochelle's equation.

$$P_m = \frac{0.614\,\pi \cdot d_p}{\sin \alpha_p \cos \alpha_p} \sqrt{M_e \cdot f \cdot \delta h_p \cdot \sin \alpha_p} \quad \ldots\ldots(6.50)$$

where f = unit friction between the membrane and the specimen.

LaRochelle (1967) gives a semi-logarithmic plot of the value of f for a specimen of London Clay and for a perspex specimen as a function of normal pressure. From this plot it is seen that the value of f is not so sensitive to the nature of the surface in contact with the rubber membrane. So the values of f for Ankara Clay have been calculated from the following equation which represents LaRochelle's (1967) plot for London Clay.

$$f = 0.0143 + 0.2263 \log_e (10.\ \sigma_3) \quad \ldots\ldots\ldots\ldots (6.51)$$

where both f and the true cell pressure σ_3 are in kg/cm^2.

In view of the considerable scatter of the results expressed in terms of total stresses, the value of ϕ for use in equation (6.48) has been taken as 20^o for all the specimens of Ankara Clay that have failed by shearing along a single plane, with a lower limit of 10^o for $(\alpha_p - \phi)$, which had only to be applied in test 8/4.

The total membrane corrections $(\Delta\sigma_1)_{mt}$ and $(\Delta\sigma_3)_{mt}$ to be deducted from the measured axial and radial stresses respectively were calculated from the following equations.

$$(\Delta\sigma_1)_{mt} = (\Delta\sigma_1)_{mp} + (\Delta\sigma_1)_{mr} \quad \ldots\ldots\ldots\ldots (6.52)$$

$$(\Delta\sigma_3)_{mt} = (\Delta\sigma_3)_{mp} + (\Delta\sigma_3)_{mr} \quad \ldots\ldots\ldots\ldots \quad (6.53)$$

where $(\Delta\sigma_1)_{mp}$, $(\Delta\sigma_3)_{mp}$ are the values of $(\Delta\sigma_1)_m$ and $(\Delta\sigma_3)_m$ calculated from equations 6.37 and 6.38 respectively for the point of development of the slip plane.

6.2.2.3 Seating correction

On raising the cell to bring the top cap into contact with the cell ram, it was noticed in almost every test that when the proving ring started deflecting, the top cap and ram were not coaxial. This eccentricity of the top cap was due to non-uniform deformation of the specimen during the application of cell pressure and /or partial consolidation, and was generally more marked in specimens containing stones (Table 6.1, Column 18, Table 6.2, Columns 9 and 12) and where lateral cracks on one side of the specimen, as illustrated by Terzaghi and Peck (1948), Fig. 119(c), caused during the driving of the core cutter into the block sample for preparation of the specimen (Section 6.2.3), were visible to the naked eye (test nos. 4/2, 5/5, 8/1).

If the start of deflection of the proving ring were to be taken as the point of zero axial strain for deviator stress application, during the test when the half ball on the top cap steadily (Fig. 6.4(a)), but sometimes in the form of jerks (Fig. 6.4(b)), seated itself coaxially in the cup-shaped housing at the end of the ram, the additional amount by which the cell is raised to effect this seating would erroneously be recorded as part of the axial strain of

the specimen. This error was partly eliminated by applying an initial loading - unloading cycle to each specimen by raising the cell manually until there was a definite increase in the rate of increase of the proving ring dial readings. This, however, did not eliminate the seating error completely, for when the cell was lowered until the initial proving ring dial reading was restored, part of the eccentricity, largely eliminated during the manual loading, reappeared. The amount of this mechanical correction $\Delta\varepsilon_{so}$ for seating is given in mm, as apparent strain, and as a percentage of the total seating correction in Table 6.2, Columns 10, 12, and 14 respectively. The need for a further correction $\Delta\varepsilon_s$ for seating, was discovered after all the triaxial tests had been completed; so the values of axial strain used for the adjustment of cell pressure during the test included this part of the error due to seating. The values of $\Delta\varepsilon_s$ used to correct the apparent strain ε_a, recorded during the test and corrected as in Section 6.2.1.7, were obtained by producing the steeply rising portion of the deviator stress versus ε_a curve to intersect the ε_a axis as shown in Fig. 6.4(a), and taking the point of intersection as the correct origin for axial strain. If the top cap, as rarely occurred, seated itself in the ram housing in jerks, the cumulative value of $\Delta\varepsilon_s$ was obtained as in Fig. 6.4(b). A stepped seating correction would have clearly been better for the earlier readings in this case. The corrected axial strain ε_c during the application of deviator stress was calculated from

$$\varepsilon_c = \varepsilon_a - \Delta\varepsilon_s \quad \ldots\ldots\ldots\ldots\ldots\ldots\ldots \quad (6.54)$$

where

$$\varepsilon_a = (\ \delta h + \delta L_e) \ / \ 0.00254\ h_s \quad \ldots\ldots\ldots\ldots \quad (6.55)$$

where δh = strain dial deflection observed during shear (10^{-3} in)

δL_e = correction given by equation 6.16 or 6.17 (10^{-3} in)

h_s = height of specimen at start of shear (cm).

To precevnt ε_c given by equation 6.54 from becoming negative, ε_c was limited by the value of ε_a obtained by putting $\delta h = 0$ in equation 6.55. The corrected deviator stress versus ε_c curves are shown by dashed lines in Fig. 6.4. The values of $\Delta\varepsilon_s$ are given in Table 6.2, Column 13. The amount of this graphical seating correction is given in mm in Table 6.2, Column 12, and the total seating correction, expressed as a percentage of ε_c at failure, is given in Table 6.3, Column 6.

6.2.3 Sampling and preparation of specimens

Unless otherwise stated, all samples, from which triaxial test specimens were prepared, were cylindrical block samples taken by hand, following the procedure recommended in U.S.B.R. (1960), and using a Proctor compaction mould (except for the locations D and [illegible] (Table 6.1, Column 2) where CBR moulds were used to confine the sample. These were immediately wrapped with a moist cloth and after transport to the laboratory, which usually took less than half an hour, were kept in a cabin where the relative humidity was kept above

about 90 % by manual mositening of the floor and concrete walls. The samples or the specimens prepared from these samples were waxed as soon as possible, but not later than two days after sampling. Test specimens were prepared by jacking thin-walled core cutters (having an area ratio of 16 % for 36 mm dia. and 12 % for 102 mm dia. specimens, the larger tubes having, in addition, an inside diameter 1 % larger than at the cutting edge) into the sample while confined in the appropriate mould. 36 mm dia. specimens were weighed and then waxed by repeated dipping into molten paraffin wax as recommended by Akroyd (1957). The larger samples, taken in CBR moulds, were waxed before the preparation of the test specimen, and were further covered by a layer of waxed cheese cloth. 36 mm dia. specimens prepared from such samples were re-waxed in the usual way before being tested; 102 mm dia. specimens were prepared one at a time, and were taken directly to test without re-waxing. The specimen nos. given in Table 6.1, Column 3 generally contain a figure which represents the angle α of the test mould used in the iswest performed at the level from which the sample was taken.

The dates of sampling, waxing and/or specimen preparation are given in Table 6.1, Columns 6 to 8. The starting date of the test on each specimen is given in Column 9. The only moisture content specimen taken at the time of sampling was from the failure surface of the iswest performed at the same level (except for location C/Slip . where a moisture content specimen was taken from near one of the samples). Thus the percentage difference (Column 12) between the moisture content

of such specimens (Column 10) and the moisture content of the trimmings produced during specimen preparation (Column 11) give only a rough guide to any changes that may have occurred in moisture content between sampling and specimen preparation, because of the local variations in moisture content. This also applies to the differences between Column 11 and the final average moisture content of the specimen given in Table 6.2, Column 16. These differences are given for unconsolidated-undrained (UU) tests and partly consolidated - undrained (PCU) tests in Table 6.2, Columns 17 and 18 respectively.

The change in weight (Table 6.2, Column 21) of the specimen is a better indication, for UU tests, of any wetting (e.g. through a punctured rubber membrane, or cavitation taking place in the pore pressure measurement lines), or drying between the unwaxing of the specimen and sealing in a rubber membrane, and during weighing after the test. For specimens tested on and after 24 January 1974 (Table 6.1, Column 9), practically no such drying could have occurred, for the specimen was unwaxed, weighed, its diameter and height measured, and sealed in a rubber membrane, mounted on a membrane stretcher, in a cabin where the relative humidity was kept close to 100 % by an electrically operated humidifier fitted with a humidistat, before being transferred into the triaxial testing laboratory; the specimen was re-weighed after the test in the same cabin. For specimens tested before that date, these operations meant an exposure to atmosphere for about 2 to 3 minutes, and with the low relative

humidity in Ankara (averaging at 60 % over the years 1973 - 1975)*, to a rate of drying of about 0.02 g/min. Some of the apparent loss in weight of the specimen may have been due to some soil particles remaining stuck on the lower pedestal after the test, or falling off during handling.

The bulk density γ and hence the initial degree of saturation S_r (Table 6.1, Columns 15 and 16) were determined for each waxed specimen using the BS 1377 (1967) weight in water method. For the 102 mm dia. specimens, these values were determined using a smaller block (about the size of the small specimens), cut from the same sample. The few values of S_r which have turned out to be greater than 100 % were probably caused by local variations in moisture content. The other index properties of the soil (Table 6.6, Rows 8 to 12) were also determined by the procedures given in BS 1377 (1967), except that the liquid limit was determined by five single determinations at different mositure contents, as repeat tests at the same moisture content always gave a higher blow count due to the low relative humidity in Ankara.

6.2.4 Routine testing and calculations

6.2.4.1 Testing procedures

The testing procedures followed were generally those recommended by Bishop and Henkel (1962), with the following modifications.

---

* From data supplied by the General Directorate of Turkish State Meteorological Office.

6.2.4.1.1 Testing of rubber membranes for punctures

"Although we take every care to maintain an acceptable standard of product, it is difficult and uneconomic in time to test every individual membrane." This is taken from the letter received from a world-renowned firm of manufacturers of soil mechanics equipment, on reporting to them that a number of tests had been ruined due to holes in freshly acquired membranes. Thus for tests performed on or after 16 December 1973 (Table 6.1, Column 9), each rubber membrane was tested for punctures before every test. This was done by sealing one end on to a plain end cap, the other on to a top cap with a drainage connection, and blowing the membrane up under water to observe the escape of air. Some ten triaxial tests were saved in this way, but a few membranes either had tiny holes which escaped detection during the control test, or developed such holes during the triaxial test itself. If not discarded, and with the exception of those wetted for the reasons given in Section 6.2.4.1.4, these tests are identified by an increase in the weight of the specimen in the UU tests (Table 6.2, Columns 21 and 17). No such occurrence has been suspected in the PCU tests (Table 6.2, Column 18), except test 3/1 (Table 6.2, Column 3).

6.2.4.1.2 Testing for water separation in the pore pressure ducts

As a perspex null indicator attached directly to the cell base was used for all pore pressure measurements, only any air bubbles sucked into the pore pressure ducts between

the null indicator and the high air entry value ceramic disc cemented on the base pedestal, or any separation in the water in these ducts due to cavitation could not be detected by eye. To test for such water separation, the pore pressure device was operated and the pore pressure recorded with a film of water covering the base pedestal to prevent the ceramic disc from drying. Any water separation was indicated by anomolous pore pressure readings. When this occurred, the ceramic disc and the pore pressure ducts were re-saturated by the method suggested by Bishop and Henkel (1962), p.185, before proceeding with the test. It must be admitted that, but for the fear of drying the ceramic disc, the procedure given by Bishop and Henkel (1962), p.186 would have been a more certain way of checking separation in the pore pressure ducts.

6.2.4.1.3 Unwaxing of specimens

The paraffin wax, used for preserving the specimens, formed a fairly stiff crust, about 2 - 3 mm thick, on cooling to room temperature, and tended to peel off some of the soil during removal. The waxed specimen was therefore dipped into warm water for about a minute to enable the wax coating to soften and facilitate its removal without damage to the specimen.

6.2.4.1.4 Placement of filter paper side drains around specimen

According to the procedure given in Bishop and Henkel (1962), p.81, the filter paper side drain (FPSD) is soaked

in water before being wrapped round the specimen. This procedure was used in all tests in which a FPSD was used prior to 16 July 1974 (Table 6.1, Column 9; Table 6.2, Column 24). It was observed that some 0.55 g of water entered the specimen in this way, due to the difference between the final weight of the FPSD and its weight when sufficiently moist to remain on the specimen during assembly for testing. This was feared to produce a marked decrease in the strength of the partly saturated samples of the Ankara Clay, particularly in the UU tests. So in triaxial test nos. 5/7, 7/3, 8/1 and 8/2, when freshly cut FPSD were used, after soaking, these were pressed between two dry sheets of filter paper. So the weight of water entering the specimen was reduced to less than 0.20 g. In all the other tests performed after 16 July 1974, the FPSD used in the previous test was re-used, and the net quantity of water entering the specimen was reduced practically to zero. Keeping the FPSD, in this fairly dry state, around the specimen, while the rubber membrane was slipped over the specimen, was not so easy. The simplest and the best method of achieving this, eventually adopted, was to hold the FPSD around the specimen (with a ceramic disc, if top drainage was to be used, and a plain end cap[¤] on top) by means of a thin card, measuring about 140 mm x 85 mm x 0.2 mm, wrapped tightly around the specimen with about 10 mm protruding above the top cap, and sticking the overlapping

---

[¤]The periphery of both the top cap and the pedestal was smeared with a thin film of castor oil as an added precaution against leakage between these surfaces and the rubber membrane.

ends together by means of a stationery type of glue. The stretched rubber membrane could then be easily slipped over the specimen, and the restraining card pulled out. If top drainage was to be used, the plain top cap was replaced by one with a drainage connection, after transferring the specimen to the triaxial cell. For 102 mm dia. specimens for which the membrane stretcher was not of the split cylinder type, the drainage connection to the top cap was made after removal of the membrane stretcher.

6.2.4.1.5 Mechanical seating correction

Before the start of deviator stress application, a mechanical seating correction was applied as explained in Section 6.2.2.3.

6.2.4.1.6 Partly consolidated-undrained tests

In consolidating specimens to extend the range of effective stresses, full dissipation of pore pressures was not waited, for two reasons: firstly, to gain time; secondly, to avoid cavitation in the later stages of the shear test, as the specimen was brought to failure by decreasing the cell pressure.

6.2.4.2 Routine calculations

All calculations for the evaluation of the triaxial test results, except those for the determination of the specimen dimensions at the start of shear to enable the adjustment of cell pressure to keep the axial stress constant

during the test, were performed on the electronic computer through a program based on the equations given earlier in this chapter and the ones given below.

6.2.4.2.1 Calculation of volume change of specimen

For each test performed with an initial nominal cell pressure $(\sigma_3)_o$, a ratio R was calculated from the following equation.

$$R = \left\{ (\sigma_3)_o - (\sigma_3)_L \right\} / \left\{ (\sigma_3)_H - (\sigma_3)_L \right\} \quad \ldots\ldots(6.56)$$

where $(\sigma_3)_L$, $(\sigma_3)_H$ = lower and higher nominal initial cell pressures respectively, for which the calibrations in Section 6.2.1.6.1 have been performed (lb/in^2).

The fictitious elastic increase δV_e in volume of the small cell was calculated from

$$\delta V_e = C_{0S} + C_{1S} \cdot \sigma_3 + C_{2S} \cdot \sigma_3^2 \quad \ldots\ldots\ldots\ldots(6.57)$$

where

$$C_{iS} = C_{i2} + R \left(C_{i3} - C_{i2} \right) \quad \ldots\ldots\ldots\ldots\ldots\ldots(6.58)$$

where C_{i2}, C_{i3} = coefficients given in Table 6.5 for i = 0 to 2, and j = 2 and 3.

Likewise, for the large cell,

$$\delta V_e = C_{0L} + C_{1L} \cdot \sigma_3 + C_{2L} \cdot \sigma_3^2 \quad \ldots\ldots\ldots\ldots\ldots(6.59)$$

where

$$C_{iL} = C_{i4} + R \left(C_{i5} - C_{i4} \right) \quad \ldots\ldots\ldots\ldots\ldots\ldots(6.60)$$

where C_{i4} , C_{i5} = coefficients given in Table 6.5, for i = 0 to 2, and j = 4 and 5.

The total elastic volumetric shrinkage S_v of the cell from the start of shear was calculated from

$$S_v = \delta V_{eo} - \delta V_e \quad \ldots\ldots\ldots\ldots\ldots\ldots\ldots\ldots \quad (6.61)$$

where δV_e = volume calculated from the appropriate equation (6.57 or 6.59) for the particular cell pressure σ_3 at the instant considered

δV_{eo} = initial value of δV_e obtained by substituting $\sigma_3 = (\sigma_3)_o$ in the appropriate equation (6.57 or 6.59).

Note that the coefficient C_{OS} or C_{OL} cancels out in equation (6.61).

The volumetric displacement D_r of cell water due to the corrected axial movement of the ram was calculated from

$$D_r = a_r (\delta h + \delta L_e) / 0.00254 \quad \ldots\ldots\ldots\ldots\ldots \quad (6.62)$$

where a_r is the effective cross-sectional area of the ram, given in Section 6.2.1.4, and δh, δL_e denote the same quantities as in equation (6.54).

The increase ΔV in volume, during shear, of the specimen tested in the small cell was calculated from

$$\Delta V = F_o - S_v - D_r + V_c \quad \ldots\ldots\ldots\ldots\ldots\ldots\ldots \quad (6.63)$$

where F_o = volume of water flowing out of cell as gauged by the volume change measurement device

V_c = cumulative volume of castor oil leaking between ram and bushing, calculated from :

$$V_c = V_{co} + L_r \cdot (\sigma_3)_t \cdot \delta t \quad \ldots\ldots\ldots\ldots\ldots (6.64)$$

where V_{co} = value of V_c before the last adjustment of cell pressure (cm^3)

L_r = rate of leakage per unit pressure determined as in Section 6.2.1.5 ($cm^3/min/kg/cm^2$)

δt = time elapsed since the last adjustment of cell pressure (min)

$(\sigma_3)_t$ = water pressure at top of cell (kg/cm^2 calculated from :

$$(\sigma_3)_t = \sigma_3 - 0.0125 \quad \ldots\ldots\ldots\ldots\ldots\ldots\ldots (6.65)$$

The volume increase of the specimen, tested in the large cell, before the first adjustment of cell pressure was calculated from

$$\Delta V = F_o - D_r + \delta V_{cr} \quad \ldots\ldots\ldots\ldots\ldots\ldots\ldots (6.66)$$

where

$$\delta V_{cr} = C_{1c} \cdot t_m + C_{2c} \cdot t_m^2 \quad \ldots\ldots\ldots\ldots\ldots (6.67)$$

where

$$C_{ic} = C_{i6} + R\,(C_{i7} - C_{i6}) \quad \ldots\ldots\ldots\ldots\ldots (6.68)$$

where C_{i6} , C_{i7} = coefficients given in Table 6.5 for $i = 1$ and 2, and $j = 6$ and 7.

The volume increase of the specimen, tested in the large cell, at subsequent stages of the test was calculated from

$$\Delta V = F_o - S_v - D_r + C_{rb} \quad \ldots\ldots\ldots\ldots\ldots\ldots \quad (6.69)$$

where C_{rb} = correction given by equation 6.15.

6.2.4.2.2 Calculation of corrected stresses

The corrected axial strain ε_c of the specimen was calculated from equation 6.54. The corrected cross-sectional area a_t was calculated by putting $\varepsilon = \varepsilon_c$ in equation 6.28 until a single slip plane develcped, when equation 6.41 was used. The uncorrected axial stress σ_1 was calculated from

$$\sigma_1 = (N \cdot p_r + W_r + W_{tc} + W_{cd} - a_r \cdot \sigma_3) / a_t + \sigma_3 \quad \ldots (6.70)$$

where W_{tc} , W_{cd} = weight of top cap and ceramic disc (if used) respectively (kg).

Up to the development of a single slip plane, the corrected axial total stress σ_{1c} and the corrected lateral total stress σ_{3c} were calculated from the following equations.

$$\sigma_{1c} = \sigma_1 - (\Delta\sigma_1)_{fp} - (\Delta\sigma_1)_m \quad \ldots\ldots\ldots\ldots\ldots \quad (6.71)$$

$$\sigma_{3c} = \sigma_3 - (\Delta\sigma_3)_m \quad \ldots\ldots\ldots\ldots\ldots\ldots\ldots \quad (6.72)$$

where $(\Delta\sigma_1)_{fp}$, $(\Delta\sigma_1)_m$ and $(\Delta\sigma_3)_m$ are the corrections given by equations 6.31, 6.37 and 6.38 respectively.

The values of σ_{1c} and σ_{3c} after the development of a single slip plane were calculated from

$$\sigma_{1c} = \sigma_1 - (\Delta\sigma_1)_{fpt} - (\Delta\sigma_1)_{mt} \quad \ldots\ldots\ldots \quad (6.73)$$

$$\sigma_{3c} = \sigma_3 - (\Delta\sigma_3)_{mt} \quad \ldots\ldots\ldots\ldots\ldots \quad (6.74)$$

where $(\Delta\sigma_1)_{fpt}$, $(\Delta\sigma_1)_{mt}$ and $(\Delta\sigma_3)_{mt}$ are given by equations 6.47, 6.52 and 6.53 respectively.

6.2.4.2.3 Determination of the peak shear strength parameters in terms of effective stresses

The values of the average effective normal stress p' and half the deviator stress q were calculated from :

$$p' = (\sigma_{1c} + \sigma_{3c}) / 2 - u_s \quad \ldots\ldots\ldots\ldots \quad (6.75)$$

$$q = (\sigma_{1c} - \sigma_{3c}) / 2 \quad \ldots\ldots\ldots\ldots\ldots \quad (6.76)$$

For each test of any one series, the peak value q_f of q was plotted against the corresponding value p'_f of p'. Figs 6.5 to 6.13 show these plots together with the K_f-line fitted to the plotted points by POLRG (IBM, 1969), except where otherwise stated. The peak shear strength parameters in terms of effective stresses (c' , $\emptyset'$) were calculated from the intercept a_f on the q_f axis and the inclination α_f of the K_f-line using the following relationships (see, e.g. Lambe and Whitman, 1969).

$$\emptyset' = \sin^{-1}(\tan \alpha_f) \quad \ldots\ldots\ldots\ldots\ldots \quad (6.77)$$

$$c' = a_f / \cos \emptyset' \quad \ldots\ldots\ldots\ldots\ldots\ldots \quad (6.78)$$

The values of c' and $\emptyset'$ so calculated are given in Table 6.6, Rows 22 and 23.

6.2.5 Estimation of pore pressures in the slopes

6.2.5.1 Theory and assumptions

In view of the assumption stated in Section 3.6, 'pore pressure' implies 'pore water pressure' in the remainder of the thesis.

6.2.5.1.1 Estimation of horizontal geostatic stress

It has been established (Skempton, 1961) that the horizontal stresses in an overconsolidated clay can be greater than the vertical. Skempton (1961) gives a number of different methods for estimating the horizontal stresses in saturated, overconsolidated clays by means of laboratory tests. So far as the Author is aware there is at present no such method applicable to unsaturated soils.

Hendron, Brooker and Ireland (quoted by Lambe and Whitman, 1969), by measuring the lateral as well as the vertical stress in oedometer tests, have developed relationships among the coefficient of earth pressure at rest (K_o), overconsolidation ratio (R_{oc}), and plasticity index (I_p). These relationships, being based on direct measurement of horizontal stresses, have been assumed here to be applicable to partly saturated soils as well. For the particular value of I_p for each of the slopes studied, the values of K_o corresponding to different values of R_{oc} were read off the curves reproduced by the latter authors, and correlated by POLRG (IBM, 1969) as follows.

$$K_o = C_{oj} + C_{1j} \cdot R_{oc} + C_{2j} \cdot R_{oc}^2 + C_{3j} \cdot R_{oc}^3 \quad \ldots\ldots\ldots (6.79)$$

where C_{ij} = coefficients given in Table 6.5 for i = 0 to 3 and j = 10 to 13 for the Locations B/Sl.1, B/Sl.2 and C/Slip, D, and E respectively.

The preconsolidation pressure, p_c' at Site B was determined as 10.0 kg/cm^2, using Schmertmann's (1955) method. The value of p_c' for Site C was found as 7.0 kg/cm^2 by Ildız (1974), using the same method. These figures differ from each other by very nearly the submerged density of the Ankara Clay multiplied by the difference in the ground elevation at the two sites, and expressed in the same units. The values of p_c' at Sites D and E were accordingly estimated by assuming the same correlation between ground elevation and p_c'. The values so found are given in Table 6.6, Row 4.

For any point considered, the value of R_{oc} to be used in equation 6.79 is given by

$$R_{oc} = p_c' / (p_{ob} - u_{ko}) \quad \ldots\ldots\ldots\ldots\ldots\ldots (6.80)$$

where p_{ob} = vertical geostatic total stress at the point considered

u_{ko} = pore pressure under p_{ob} and the horizontal geostatic total stress q_{ob} given by

$$q_{ob} = K_o (p_{ob} - u_{ko}) + u_{ko} \quad \ldots\ldots\ldots (6.81)$$

So, unless u_{ko} is determined by in situ pore pressure measurements, whether u_{ko} is measured in the triaxial test by applying an extension to the specimen or calculated from

the results of tests on isotropically loaded triaxial specimens, the solution of equations 6.79 to 6.81 is possible only by successive approximations, although in the latter case it has been found that a sufficiently accurate solution is possible by replacing u_{ko} in equation 6.81 by u_o, the pore pressure measured in the triaxial test under an isotropic stress equal to p_{ob} .

6.2.5.1.2 Estimation of pore pressures under geostatic stresses

The attachments necessary to apply an extension to the triaxial specimen (Bishop and Henkel, 1962), for the direct measurement of u_{ko} in equation 6.80, did not become available until a late stage in this research, and so could only be used as a check on the procedure that has been adopted here, based on the measurement of u_o under an isotropic stress equal to p_{ob} (Fig. 6.14(a)), and the calculation of the changes in pore pressure produced on increasing the horizontal stress to the geostatic value q_{ob} (Fig. 6.14(b)).

Skempton (1954) gives the following expression for the relation between the pore pressure change Δu in the triaxial test and the changes $\Delta\sigma_1$ and $\Delta\sigma_3$ in the major and minor principal total stress respectively.

$$\Delta u = B\left\{\frac{1}{3}(\Delta\sigma_1 + 2\,\Delta\sigma_3) + \frac{3A-1}{3}(\Delta\sigma_1 - \Delta\sigma_3)\right\} \quad \ldots\ldots(6.82)$$

where A, B = pore pressure coefficients.

Here, the assumption has been made that the coefficients

A and B measured in the triaxial test will be applicable to the general triaxial state of stress, and the qualifications for $\Delta\sigma_1$, $\Delta\sigma_2$, and $\Delta\sigma_3$, namely the major, intermediate and minor changes in principal total stress respectively, suggested by Duncan and Seed (1966(a)) have been used. Thus $2\ \Delta\sigma_3$ in equation 6.82 was replaced by $(\Delta\sigma_2 + \Delta\sigma_3)$, and the resulting equation used for all calculations of pore pressure changes:

$$\Delta u = B\left\{\frac{1}{3}(\Delta\sigma_1 + \Delta\sigma_2 + \Delta\sigma_3) + \frac{3A-1}{3}(\Delta\sigma_1 - \Delta\sigma_3)\right\} \quad ..(6.83)$$

By comparison of Figs 6.14(a) and (b) it is seen that on moving from the condition of an isotropic stress

$$p_{ob} = \gamma h_{ob} \quad ..... (6.84)$$

where γ = average bulk density

h_{ob} = height of overburden above the point considered,

to the geostatic state of stress,

$$\Delta\sigma_1 = q_{ob} - p_{ob} \quad ..... (6.85)$$

$$\Delta\sigma_2 = \Delta\sigma_1 \quad ..... (6.86)$$

$$\Delta\sigma_3 = 0 \quad ..... (6.87)$$

where q_{ob} is given by equation 6.81.

The change Δu_{ko} in pore pressure on moving from condition (a) to condition (b) in Fig. 6.14, was calculated from the following equation obtained by substituting equations 6.84 to 6.87 in equation 6.83, and replacing B by B_o, the

value determined, as in Section 6.2.5.3, at the initial degree of saturation; and A by A_e, the value determined, as in Section 6.2.5.4, for the initial stages of deviator stress application.

$$\Delta u_{ko} = B_o \left\{ \frac{2}{3} (q_{ob} - \gamma h_{ob}) + \frac{3A_e - 1}{3} (q_{ob} - \gamma h_{ob}) \right\} \quad \ldots \quad (6.88)$$

The pore pressure u_{ko} in equation 6.81 was calculated from

$$u_{ko} = u_o + \Delta u_{ko} \quad \ldots\ldots\ldots\ldots\ldots\ldots \quad (6.89)$$

where u_o is the pore pressure measured under a cell pressure equal to p_{ob} as in Section 6.2.5.2 .

6.2.5.1.3 Estimation of pore pressure changes due to excavation

Mineiro (1969) has presented a method for predicting the pore pressures in a plane strain problem from the results of triaxial tests; this analysis, however, assumes the soil to be fully saturated. So here once again equation 6.83 was used for calculating the further change Δu_e in pore pressure due to the excavation of a slope. As shown in Fig. 6.14(c), the further assumptions were made that the horizontal stress normal to the slope would be zero and that the vertical stress would be reduced by the pressure γh_t of the overburden removed above the point considered. By comparing Figs 6.14(b) and (c), it is seen that upon excavation the further major and minor changes in total principal stress are respectively given by

$$\Delta\sigma_1 = - \gamma h_t \quad \ldots\ldots\ldots\ldots\ldots\ldots\ldots \quad (6.90)$$

$$\Delta\sigma_3 = - q_{ob} \quad \ldots\ldots\ldots\ldots\ldots\ldots\ldots \quad (6.91)$$

The intermediate change $\Delta\sigma_2$ in total principal stress is then obtainable by the use of elastic theory :

$$\Delta\sigma_2 = \nu(\Delta\sigma_1 + \Delta\sigma_3) \quad \ldots\ldots\ldots\ldots\ldots\ldots \quad (6.92)$$

where ν = Poisson's ratio, determined as in Section 6.2.5.5.

Δu_e was calculated from the following equation obtained by substituting equations 6.90 to 6.92 in equation 6.83, and replacing B by B_o, and A by A_f, the value determined, as in Section 6.2.5.4, for the deviator stress corresponding to failure.

$$\Delta u_e = B_o \left\{ - \frac{1+\nu}{3} (\gamma h_t + q_{ob}) + \frac{3 A_f - 1}{3} (q_{ob} - \gamma h_t) \right\} \ldots (6.93)$$

The pore pressure u_f at any point in the slope was calculated from

$$u_f = u_o + \Delta u_{ko} + \Delta u_e \quad \ldots\ldots\ldots\ldots \quad (6.94)$$

6.2.5.2 Determination of the pore pressure u_o

Fig. 6.15 shows examples of the results of tests (Table 6.4) performed for estimating the pore pressure u_o in 36 mm dia. triaxial specimens under a cell pressure equal to the vertical geostatic total stress p_{ob}. The solid circles in Fig. 6.15 indicate the pore pressure readings under a cell pressure of p_{ob}, the remainder being taken under a cell pressure of 0.044 kg/cm^2. The results for test 1/6 (Fig.6.15)

is typical of most of such determinations, where a curve was plotted through the last reading under p_{ob}, following the general trend of the pore pressure - time curve under the lower cell pressure. The ultimate value of u_o was taken to be equal to the value at which the former curve became parallel to the time axis. The values so found are given in Table 6.4, Column 9. As a measure of the accuracy of these determinations, the amount of extrapolation E_p (%) was calculated from the following equation and given in Table 6.4, Column 10.

$$E_p = 100 (u_o - u_{or}) / u_o \quad \ldots\ldots\ldots (6.95)$$

where u_{or} = last reading taken under a cell pressure p_{ob}, given in Table 6.4, Column 8.

Test 7/3 (Fig. 6.15), which consists of a single reading some twenty-four hours after the application of cell pressure, represents the least accurate of such determinations; test 5/1 in which no extrapolation was needed was the best. Test 6/1 was the only one in which the extrapolation was done differently, as shown in Fig. 6.15, thus giving a negative value to E_p defined by equation 6.95.

6.2.5.3 Determination of pore pressure coefficient B_o

Fig. 6.16 shows two typical curves of the variation of pore pressure with cell pressure. As,in most tests, the cell pressure was increased before the pore pressure readings reached an equilibrium under the cell pressure p_{ob} (Section 6.2.5.2), the pore pressure reading u_{or} corresponding to a

cell pressure p_{ob} was corrected for the drop in pore pressure that would have taken place under p_{ob} by the time the pore pressure reached equilibrium under the next increment of cell pressure. In test 2/8 (Fig. 6.16) the lower pore pressure vs. cell pressure curve has been drawn through the point so corrected. For Test 7/2, no such correction was needed. In all cases the value of B_o was obtained as the slope of the tangent to the pore pressure vs. cell pressure curve at the cell pressure p_{ob}. The values of B_o so obtained are given in Table 6.4, Column 11.

6.2.5.4 Determination of pore pressure coefficients A_e, A_f

As the specimens were brought to failure by keeping the axial stress constant and decreasing the cell pressure, it was necessary to predict the change in pore pressure due to the decrease in all-round stress, and deduct this change from the overall change in pore pressure in order to obtain the value of the shear induced pore pressure.

Fig. 6.17 shows the steps followed in such determinations. Before the start of deviator stress application, the cell pressure was decreased in steps, and then re-increased, reading the equilibrium pore pressure at each step (dashed curve in Fig. 6.17). This enabled the value B_s (Table 6.4, Column 12) of Skempton's (1954) pore pressure coefficient B, applicable during the test to be determined. In a few tests, this value was checked for the effect of deformation of the specimen by measuring the value B_f (Table 6.4, Column 13) of B after the specimen had failed and the deviator stress been removed

(chain-dotted curve in Fig. 6.17). The difference between the pore pressure, read at any stage of the shear test, and the value given by the dashed curve, for the particular value of cell pressure at that stage, gave the value of the shear induced pore pressure. Such values have been plotted against the deviator stress in Fig. 6.18, for another test. For the calculation of the initial value A_e and the final value A_f of the pore pressure coefficient A, the plotting of such curves as in Fig. 6.18 was not necessary. These values were calculated from

$$A_e = (u_e - u_{eb}) / 2 q_e \cdot B_s \quad \ldots\ldots\ldots\ldots\ldots (6.96)$$

$$A_f = (u_{ft} - u_{fb}) / 2 q_f \cdot B_s \quad \ldots\ldots\ldots\ldots\ldots (6.97)$$

where u_e = pore pressure reading prior to the first adjustment of cell pressure

u_{eb} = pore pressure under the maximum cell pressure before the start of shear

q_e = half the deviator stress corresponding to the pore pressure u_e

u_{ft} = pore pressure at failure

u_{fb} = pore pressure corresponding to the cell pressure at failure on the dashed curve in Fig. 6.17

q_f = half the deviator stress at failure.

The values of A_e and A_f so calculated are given in Table 6.4, Columns 14 and 15 respectively.

6.2.5.5 Measurement of Poisson's ratio

If, in the expression, based on elastic theory, correlating Poisson's ratio ν with the stress and strain changes in a triaxial specimen (see, e.g., Lambe and Whitman, 1969), the change in lateral strain is equated to zero, the following expression results.

$$\nu = \Delta\sigma_{3o} / (\Delta\sigma_{3o} + \Delta\sigma_{1o}) \quad \ldots\ldots\ldots \quad (6.98)$$

where $\Delta\sigma_{3o}$ = change in cell pressure required to prevent lateral yield on increasing the axial stress by $\Delta\sigma_{1o}$.

Using an LSI to indicate the condition of no lateral yield, ν was measured in the tests 4/3 and 6/2 (Table 6.4). The specimen was first loaded and unloaded under no lateral yield conditions. This operation was repeated after performing an intermediate loading - unloading cycle for the determination of Young's modulus.* The starting cell pressure in all cycles was set to p_{ob}. The value of ν, calculated from equation 6.98 by taking the starting values of cell pressure and axial stress in each loading and unloading stage as the basis of calculation of the changes in these quantities, ranged between 0.28 and 0.33 with an average value of 0.31 in test 4/3 and between 0.28 and 0.41 with an average value of 0.33 in test 6/2. A similar determination by the Author for another site** about one-third of the way between Sites D

---

* Young's modulus on reloading and unloading were respectively 330 kg/cm^2 and 596 kg/cm^2 in test 4/3, and 364 kg/cm^2 and 496 kg/cm^2 in test 6/2.

** w_L=75 %, w_P= 28 %, w_N= 31 %, S_r= 98 %, depth=6.5 m (Tümerdem, 1973)

and C had also given a value of $\nu = 0.30$. So, for the other sites, for which no direct determination was made, the value of ν for use in equation 6.92 was taken as 0.3 .

6.2.5.6 Effect of temperature on pore pressure

In Table 6.6, Row 17 are given the values of mean soil temperature taken after the completion of each of the iswests . These show that the soil temperature obtaining during the iswests , and probably also during the actual slips, was appreciably lower than the average laboratory temperature of 23 ^{o}C during the triaxial tests. So the effect of temperature on the pore pressure in three specimens was investigated and the results obtained are shown in Fig. 6.19. Although these specimens are wetter than the average specimen encountered in the slips studied, and cannot be taken to reflect the true behaviour of the soil in the slips, they do show a clear tendency of the pore pressure to drop with decrease in temperature, and this is in conformity with the tendency observed, for example, by Plum and Esrig (1969) on a remoulded, saturated clay.

6.2.5.7 Testing the reasonableness of pore pressure estimates

An examination of Table 6.4, Columns 5 and 9 shows that there is no clear correlation between depth and the u_o value measured in triaxial specimens. So the mean value of u_o given in Table 6.4 for each location, together with the mean values of B_o, A_e and A_f (entered in Table 6.6, Rows 24 to 27 respectively) have been used in equations 6.79 to 6.94 for

the calculation of the pore pressure u_f at the base of each slice used in the stability analysis (Table 6, Row 6). The mean values of Δu_{ko}, Δu_e and u_f for the slices of any one slope are given in Table 6.6, Rows 28 to 30 respectively. Comparison of these values with the values of u_o in Row 24 indicates that the values of u_f are very close to u_o. So the accuracy of the stability analysis depends largely on the accuracy with which u_o has been determined. Also the calculated changes Δu_e in pore pressure due to the excavation appear rather low. It was therefore desired to examine the effect of applying the geostatic stress state to the triaxial specimen; to check the pore pressures, measured on triaxial specimens, with in situ pore pressure measurements; and to observe, in situ, the changes in pore pressure produced by the excavation in an actual cut slope.

6.2.5.7.1 Extension tests

In all, eight tests were performed in which an extension T was applied to the specimen by means of the special top cap and ram fitting illustrated by Bishop and Henkel (1962), and a counterbalanced pulley system designed for mounting on the rigid steel strain rods of the 1 ton compression test machine. The value of T to be applied to the specimen was calculated initially from

$$T = (\sigma_3)_{ex} (a_o - a_r) - p_{ob} \cdot a_o \quad \ldots\ldots\ldots\ldots (6.99)$$

where $(\sigma_3)_{ex}$ = new value of cell pressure calculated from the following equation.

$$(\sigma_3)_{ex} = K_o (p_{ob} - u_o) + u_o \quad \ldots\ldots\ldots\ldots\ldots (6.100)$$

where u_o is the equilibrium pore pressure measured under an isotropic pressure p_{ob}, the total overburden pressure for the point from which the specimen was taken; K_o is read off the appropriate curve represented by equation 6.79; a_o and a_r are the cross-sectional areas of the specimen and ram respectively.

If on applying T and $(\sigma_3)_{ex}$ the pore pressure was altered to u_{ex}, u_o in equation (6.100) was replaced by u_{ex}, and T re-calculated from equation 6.99. This procedure of successive approximation was repeated until the pore pressure u_{ko} corresponding to the geostatic stress state was obtained.

Unfortunately, out of the eight specimens tested in this way, only one, that from above piezometer P.7 (Section 6.2.5.7.2) at Site C (which was itself wetter than the earlier specimens from this site), ended up with the same weight as at the start of the test, all the rest having taken up water in quantities ranging from 0.44 g to 3.5 g. In most cases the leakage appeared to have taken place between the relatively rough peripheral surface of the special top caps and the rubber membrane; in some the packing of the klinger valve was loose, and in one case the rubber membrane was punctured during the test (a number of newly acquired cells and top caps were used for the first time in these tests). So here only the results on the one of the earlier specimens with the least change in water content is presented (Fig. 6.20). This test, as well as the ones not presented, but which had developed a fairly

steady pore pressure before the application of extension, showed that the values of Δu_{ko} (Table 6.6, Row 28) calculated as in Section 6.2.5.1.2 were fairly reasonable.

6.2.5.7.2 In situ pore pressure measurements

In situ pore pressure measurements were made following the procedure outlined by Vaughan and Walbancke (1973). The problem that had to be solved was how to apply this procedure in the time and by the means available.

The various equipment devised for this purpose are shown in Fig. 6.21. A satisfactory piezometer tip was formed as shown in Fig. 6.21(a), by means of the attachments shown, and a high air entry value ceramic cup (used for the tensiometers mentioned in Section 2.5, and available at 90 US cents by July 1974 prices). A brass sleeve was cemented on to the neck of the ceramic cup. A fiber-reinforced rubber gasket was introduced between the top of the cup and a brass disc, through which passed two 1.5 mm bore brass tubes. These were tapered externally from a diameter of 2.30 mm to 2.05 mm over the 12 mm protruding from the disc, and were soldered on to this disc. On to these tubes were forced the ends of 2 mm bore, 3.3 mm external diameter nylon tubing (as against the polythene covered nylon tubing used by Vaughan and Walbancke (1973), which is clearly preferable owing to the permeability of nylon to water vapour (Blight, 1961)). One of the brass tubes extended below the disc with a similar taper and carried a short length of nylon tubing. This was used as the inlet during the saturation

of the piezometer. A brass adaptor screwed on to the sleeve, thus sealing the disc on to the ceramic cup. To the upper end of this adaptor could be screwed the collar of 20 mm dia. galvanized iron (GI) pipe, through which the nylon tubing led to the ground surface and were connected to valves.

After cementing the brass sleeve on, the ceramic cup was de-aired by boiling in distilled water. The parts of the piezometer tip were then assembled, the nylon tubing passed through the GI pipe of the appropriate length with collars at both ends, the valves attached, and the system completely saturated with warm de-aired water in the laboratory. The piezometer tip was kept immersed and detached from the GI pipe to avoid breakage during transport.

The borehole was drilled by means of a 10 cm dia. hand auger. The bottom of the hole was shaped with the tool shown in Fig. 6.21(b), and cleaned with the tool shown in Fig. 6.21(c). The piezometer tip was then attached to the GI pipe. 70 g of plaster of Paris was mixed in 72.5 g of water, taking about 5 minutes for this operation, and the mixture poured into the borehole, followed by the introduction of the piezometer into its position. A small torch attached to a length of string was introduced into the borehole to aid both these operations. The hole was then filled with cement - bentonite grout consisting of 68.3 % water, 13.2 % bentonite and 18.5 % cement by weight. This mix was chosen after preparing five trial mixes based on the triangular diagram given by Jones (1963), and testing these with the laboratory

vane shear device. It was desired to recover the piezometers after use. For this purpose, a 22 mm dia. hole was drilled through a 7.5 cm dia., worn, and otherwise disused hand auger, and this was screwed on to a 40 mm dia. GI pipe of sufficient length. The grout used was accordingly selected to set sufficiently in about twenty-four hours to form a satisfactory seal, and not to slump out of the drilled auger during subsequent removal, but not to exhibit an excessive shrinkage on setting, and not to be stiffer than could be removed by this auger within two months after installation. The valves were housed in a split box, 250 mm x 250 mm x 200 mm high, made of 3 mm thick steel lamina, capable of being clamped together internally after engaging the GI pipe below the collar, and having a lockable lid.

Pressure measurement was by a mercury manometer mounted on a portable frame together with a null indicator and a valve block carrying a screw piston.

The first in situ pore pressure measurement was done on 4 November, 1974 at a depth of 2.5 m below the ground surface at the point P.1 at Site C (Fig. 5.5), three days after the installation of the piezometer. The pore pressure at this depth was recorded as - 0.041 kg/cm^2. No further readings could be taken, as there were signs of unauthorized disturbance to the equipment.

Three piezometers were then installed along a proposed 3.70 m wide by 3.10 m deep excavation for a service gallery at Site E (Figs 2.1 and 2.2) at the points indicated as P.2,

P.3, and P.4 in Figs 6.22(a) and (b). The intention was to position these piezometers along a potential slip surface in the proposed cut, but owing to a slight re-alignment of the cut, and the impossibility of deepening further the borehole for piezometer P.4 due to the presence of stones, the positions shown in Fig. 6.22(b) resulted.

Piezometers P.2 and P.3 were installed on 8 September 1975, followed by P.4 the next day, and readings were continued for some 42 days. The excavation was completed in two stages as shown in Figs 6.22(a) and (c). Stage I extended to the final depth at piezometers P.2 and P.3, but terminated 3.8 m east of P.2; at Piezometer P.4 it was only 2.15 m deep.

Fig. 6.22(d) shows the piezometer readings. Cavitation occurred in the nylon tubing at the ground surface above P.2. So the pore pressures recorded by this piezometer do not reflect the full magnitude of the negative pore pressures at this point, nor do they indicate any changes in pore pressure that might have occurred upon excavation. Piezometers P.3 and P.4 registered reasonable pore pressures, as ground water had collected in a 3.5 m deep drainage channel 22.4 m west of P.4. Even so, no appreciable change in pore pressure was observed at these points due to either stage of the excavation. The gradual drop in pore pressure at P.3, starting about 4 days after Stage I of the excavation, is believed to be partly due to drying and partly to the drop in average temperature (Section 6.2.5.6), although why a

similar drop did not occur at P.4 is open to question. This may be due to the presence, at the level of P.4, of a gravelly seam, which retarded the rate of moisture transfer to the face of the cut by capillarity, and due to the smaller area of exposure around this piezometer.

During the placement of each of the piezometers P.2 and P.3, a 36 mm dia. sample had been taken from about 10 cm above the intended level of the piezometer tips, by driving a thin-walled core cutter attached to a special adaptor screwed on to the auger rods. The ends of these samples were sealed by paraffin wax immediately on recovery. Triaxial specimens were prepared in a cabin of nearly 100 % relative humidity. Pore pressure tests 9/1 and 9/2 (Table 6.4) were performed on these specimens. The pore pressures measured under a cell pressure of p_{ob} have also been plotted in Fig. 6.22(d), which shows that cavitation occurred in the measuring system in both these tests. Hence the actual negative pore pressure in both specimens have been under-estimated; the value of B_o given in Table 6.4, Column 9, and hence the absolute value of Δu_e (Table 6.6, Row 29) for Site E is an over-estimate, since after cavitation in the measuring system, some water is sucked by the specimen, this causing a higher rise in pore pressure than would otherwise occur on subsequent increments in cell pressure. So the value of the comparison, between the field measurements of pore pressure at this site and the laboratory estimates, is unfortunately limited. It does however show that the pore pressures

estimated by the methods outlined in Sections 6.2.5.1 to 6.2.5.5 could not be very much in error.

Similar observations of in situ pore pressures, and comparisons with measurements on laboratory specimens from above the piezometers, were made at the points P.5 and P.6 at Site D (Fig. 5.7), and the points P.7 and P.8 at Site C (Fig. 5.5). Piezometers P.5 and P.6 were installed on 23 October 1975, P.7 and P.8 on the following day, at the depths of 1.34 m, 2.38 m, 2.04 m, and 2.94 m below the ground surface respectively. Figs 6.23(a) and (b) show the field and laboratory observations.

For Site C, the agreement between the field observations and laboratory measurements, particularly for the point P.8, where the laboratory specimen was subjected to the estimated geostatic stresses by applying extension to the specimen (Section 6.2.5.7.1), is remarkable. Comparison of the laboratory measurements with those on the specimens taken at the time of Slip C (Table 6.6, Row 24) shows that the conditions at the points P.7 and P.8 in 1975 were much wetter than those at the time of the slip.

For Site D, cavitation occurred both in the piezometer tubes and in the laboratory test, before the last readings. But extrapolation using the earlier field observations yields the average pore pressure at Site D as - 0.533 kg/cm^2. Comparing the rainfall (Fig. 6.24) in the months preceding the piezometer readings with that preceding the iswests of June 1972, when the earlier samples were taken, it is seen

that the laboratory estimate of u_o at this site (Table 6.4, Column 9) is reasonable. A similar comparison, between the rainfall in the months preceding the iswests and the slip of 20 July 1966, shows that the same order of pore pressures must have existed at this site before the excavation.

Due to the stony nature of Site D, out of the four tube samples taken from the piezometer holes, anly one proper specimen could be prepared; one other heavily patched specimen, which acquired some 3.5 g of water apparently by leakage between the top cap and the rubber membrane, was, after the pore pressures became steady, used for the temperature effect study explained in Section 6.2.5.6.

6.2.6 Stability of the slopes by triaxial test results

As the data given in Table 6.6, Rows 22, 23 and 30 produced no convergence by Janbu's (1973) GPS, all values of factor of safety F_s have been obtained by BISIM. For purposes of comparison, the same depths of tension cracks as in Section 5.3 have been assumed (Table 6.6, Row 7). The pore pressures were calculated as explained at the beginning of Section 6.2.5.7. The values of F_s given in Table 6.6, Row 31 were calculated using the pore pressures so obtained, and the parameters in Rows 22 and 23; those in Row 32 were calculated similarly but are the only values of F_s based on the shear strength parameters (not presented) derived by the use of the maximum principal effective stress ratio criterion.

Fig. 6.25 shows the variation of F_s with the average

pore pressure assumed. The dashed curves in Fig. 6.26 show the effect on F_s of the depth of tension cracks and the depth of water in such cracks.

6.3 Stability of the slopes by strength parameters from slow shear box tests and pore pressures from triaxial tests

In testing the partly saturated Ankara Clay in the shear box, the Author was faced with a dilemma: if the specimen was not flooded with water during shear, the negative pore pressures, which existed and/or could develop in the soil particularly under the lower normal stresses (see, e.g., Fig. 6.16), could not dissipate; if the specimen was flooded after the application of the normal load, the moisture content of the specimen increased even under normal stresses as much as 4.0 kg/cm^2, and higher stresses were beyond the capacity of the available machines. So, of the ten series of shear box tests, nine were performed without flooding the specimen with water, but taking adequate precautions against drying. These tests have therefore been qualified as 'slow' rather than drained .

Each series consisted of seven tests, except one series, which consisted of four tests performed by flooding the specimen after the normal stress application.

The orientation of the failure plane was generally parallel to the failure plane in the corresponding iswests or slips, except the four specimens derived coaxially from samples S.2 to S.4 (Fig. 5.6), and the specimens from the

location B/S 1.1 (Fig. 5.1), which were derived from blocks that had become detached from the slip surface through a secondary slide, their correct orientation thus becoming uncertain. The specimens were 20 mm thick and mostly 63 mm in dia., specimens from locations C/2 and C/3 (Fig. 5.5) being 63 mm square.

Following the findings by Cullen and Donald (1971), no area correction was applied. Believing that in comparisons with the triaxial test results, in which practically no volume change occurred during shear (Table 6.3, Column 8), the shear strength parameters with a dilatancy correction (Bishop, 1950), and in comparisons with iswest results and in estimates of factor of safety F_s of the slopes based on the shear box tests, the parameters without a dilatancy correction would be more appropriate, both were calculated.

The peak and the quasi-residual strength parameters (measured at a shear displacement about 7 times the displacement at peak strength) with and without a dilatancy correction (c_{spc} , $\emptyset_{spc}$, c_{src} , $\emptyset_{src}$, c_{sp} , $\emptyset_{sp}$, c_{sr} , $\emptyset_{sr}$) are given in Table 6.6, Rows 33 to 40 respectively. Fig. 6.27 shows typical peak and quasi-residual shear strength envelopes, without a dilatancy correction, obtained from slow shear box tests for the location B/10^{o} (continuous and dashed lines respectively), together with the envelopes obtained by flooding the specimens after the normal stress application. The moisture content increased by between 1.6 % and 11.4 % of the initial moisture content of the specimens in the latter

tests.

The values of F_s given in Table 6.6, Rows 41 to 44 have been calculated by assuming the parameters in Rows 33 to 40 to be 'drained' shear strength parameters, and the pore pressures calculated from triaxial tests as in Section 6.2.5.7 to be effective; assuming the same depth for tension cracks as in Section 5.3 (Table 6.6, Row 7); and using BISIM. Fig. 6.28 shows, for two of the slopes, the variation of F_s with the pore pressure ratio r_u for the less optimistic range of average pore pressures (- 0.19 kg/cm^2 to 0.06 kg/cm^2 for Slip 1 at Site B, - 0.09 kg/cm^2 to 0.03 kg/cm^2 for Slip C). The F_s values obtained by iswests have also been plotted to enable a visual comparison.

Table 6.1. Triaxial shear tests: Particulars of specimens

1	2	3	4	5	6	7	8	9	10	11	12	13	14	15	16	17	18	19
Series/test No.	Location	Spec. No.	Depth below G.L. (m)	Inclination* of axis to horiz. (deg)	Date sample taken	Date sample waxed	Date specimen waxed	Date specimen taken for test	Moisture content at time of sampling (%)	Moisture content during preparation of spec. (%)	Ch. in m/c bet. sampling & spec. preparation (%)	Dia. of spec. (cm)	Height of spec. (cm)	Initial bulk density, γ (g/cc)	Initial degr. of satn., S_r (%)	Cavities filled (%)	Particles > 4.8 mm (%)	Particles > 3.2 mm (%)
1/1		1						8.9.73	-	35.8	-	3.605	7.125	1.845	96.9	0.00	-	-
1/2		2						27.5.73	-	35.7	-	3.575	7.120	1.863	98.7	0.00	-	-
1/3		5						31.8.73	-	36.5	-	3.580	7.125	1.861	99.5	0.00	-	-
1/4		8						4.9.73	-	34.6	-	3.585	7.125	1.863	97.2	0.00	-	-
1/5		12						7.9.73	-	36.1	-	3.580	7.110	1.853	98.2	0.00	-	-
1/6	B/S1.1	17	2.5-4.5	random	9.4.71	-	10.4.71	11.9.73	-	36.3	-	3.580	7.120	1.859	99.1	0.00	-	-
1/7		21						14.9.73	-	35.5	-	3.580	7.125	1.850	97.1	0.00	-	-
1/8		3						31.8.73	-	36.0	-	3.590	7.125	1.847	97.4	0.00	-	-
1/9		16						16.11.73	-	35.9	-	3.600	7.120	1.861	98.8	0.00	-	-
1/10		18						21.11.73	-	36.3	-	3.585	7.120	1.868	100.0	0.00	-	-
1/11		19						26.11.73	-	35.5	-	3.585	7.130	1.840	96.1	0.00	-	-
2/1		45/1/1	2.7	100	10. 6.71	-	10. 6.71	1.10.73	-	33.0	-	3.580	7.120	1.897	97.7	0.00	1.1	2.6
2/2		45/2/3	3.6	90	21. 6.71	-	24. 6.71	5.10.73	-	28.3	-	3.565	7.110	1.962	96.6	0.00	4.1	6.3
2/3		30/4	4.4	65	23. 6.71	-	24. 6.71	9.10.73	-	31.9	-	3.580	7.150	1.902	95.7	0.00	0.6	1.9
2/4		25/2	2.2	90	8. 6.71	-	8. 6.71	12.10.73	34.0	34.5	1.62	3.585	7.135	1.895	98.8	0.00	1.0	2.0
2/5		25/3	2.2	90	8. 6.71	-	8. 6.71	16.10.73	34.0	35.2	3.65	3.590	7.130	1.892	99.5	0.00	3.7	5.1
2/6	C/1	35/2	4.1	90	22. 6.71	-	24. 6.71	19.10.73	-	32.7	-	3.570	7.120	1.892	95.4	0.00	0.5	1.0
2/7		45/1/3	2.7	100	10. 6.71	-	10. 6.71	23.10.73	-	35.4	-	3.575	7.120	1.900	101.4	0.00	1.4	2.4
2/8		25/1	2.2	90	8. 6.71	-	8. 6.71	6.11.73	34.0	35.0	-2.94	3.580	7.130	1.896	96.7	0.00	2.4	4.0
2/9		45/1/2	2.7	100	10. 6.71	-	10. 6.71	9.11.73	-	33.3	-	3.570	7.130	1.857	93.9	0.00	0.6	2.0
2/10		30/1	4.4	65	23. 6.71	-	24. 6.71	13.11.73	-	32.9	-	3.590	7.120	1.902	97.2	0.00	1.3	5.7
2/11		35/M/5	4.1	90	22. 6.71	-	24. 6.71	27.11.73	-	33.8	-	3.600	7.125	1.872	95.0	0.00	0.0	0.5
3/1		1.4/40/4	3.1	90	16. 6.72	17. 6.72	19.12.73	19.12.73	28.1	29.3	4.27	3.580	7.120	1.944	97.0	0.00	1.4	1.9
3/2		1.4/25/1/1	1.4	120	30. 5.72	31. 5.72	24. 1.74	29. 1.74	32.0	33.2	3.75	3.585	7.110	1.895	97.7	0.14	1.7	3.4
3/3		1.4/40/1	3.1	90	16. 6.72	17. 6.72	19.12.73	14. 2.74	28.1	27.3	-2.85	3.610	7.115	1.967	96.1	0.04	0.9	1.9
3/4	D	1.4/25/1/3	1.4	120	30. 5.72	31. 5.72	24. 1.74	13. 3.74	32.0	26.6	-16.88	3.580	7.115	1.932	91.0	0.00	1.1	2.8
3/5		1.4/40/2	3.1	90	16. 6.72	17. 6.72	19.12.73	21. 3.74	28.1	28.7	2.14	3.590	7.100	1.964	98.2	0.00	2.3	3.4
3/6		1.4/40/3	3.1	90	16. 6.72	17. 6.72	19.12.73	2. 4.74	28.1	27.4	-2.49	3.590	7.115	1.953	94.7	0.09	0.6	1.2
3/7		1.4/25/1/2	1.4	120	30. 5.72	31. 5.72	24. 1.74	5. 4.74	32.0	28.9	-9.69	3.585	7.120	1.881	89.6	2.22	2.6	4.6
4/1		4/35/5	2.7	90	10. 6.72	10. 6.72	-	24. 1.74	31.2	30.0	-3.85	10.10	20.32	1.934	97.0	-	0.0§	1.1§§
4/2		4/40/7	3.1	90	16. 6.72	17. 6.72	-	1. 2.74	28.1	28.7	2.14	10.21	17.95	1.964	98.2	-	0.0§	0.5§§
4/3	D	4/30/3	2.4	90	5. 6.72	6. 6.72	-	19. 2.74	30.1	31.6	4.98	10.21	20.30	1.911	97.0	-	1.6§	2.5§§
4/4		4/35/6	2.7	90	10. 6.72	10. 6.72	-	8. 3.74	31.2	29.7	-4.81	10.20	19.48	1.933	96.5	-	0.0§	2.4§§
4/5		4/45/9	3.1	90	19. 6.72	20. 6.72	-	27. 3.74	25.0	29.4	17.60	10.21	18.50	1.940	96.7	-	3.2§	7.1§§
4/6		4/30/4	2.4	90	5. 6.72	6. 6.72	-	15. 4.74	30.1	31.0	2.99	10.17	18.87	1.921	97.2	-	1.1§	6.0§§
5/1		30/2	4.8	10	1. 4.71	-	2. 4.71	6. 6.74	-	35.7	-	3.585	7.120	1.871	97.8	0.00	-	-
5/2		45/4	5.3	10	6. 4.71	-	8. 4.71	11. 4.74	30.8	32.3	4.87	3.590	7.120	1.879	93.2	0.00	0.3	0.4
5/3		30/1	4.8	10	1. 4.71	-	2. 4.71	24. 4.74	35.7	35.9	0.56	3.590	7.120	1.868	97.7	0.00	0.0	0.1
5/4	B/10°	45/3	5.3	10	6. 4.71	-	8. 4.71	30. 4.74	30.8	31.6	2.60	3.600	7.120	1.854	90.3	0.00	-	-
5/5		45/2	5.3	10	6. 4.71	-	8. 4.71	8. 7.74	30.8	33.3	8.12	3.585	7.120	1.761	83.9	0.00	0.0	0.0
5/6		25/2	4.0	0	30. 3.71	-	31. 3.71	13. 7.74	36.6	36.5	-0.27	3.570	7.120	1.850	96.6	0.00	0.2	0.4
5/7		25/1	4.0	0	30. 3.71	-	31. 3.71	16. 7.74	36.6	37.2	1.64	3.570	7.125	1.860	98.5	0.00	0.8	1.2
6/1		1/3	3.4	129				11. 1.74	-	33.1	-	3.600	7.120	1.825	91.2	0.00	0.1	0.9
6/2		1/2	3.4	129				8. 5.74	-	32.6	-	3.585	7.120	1.853	93.4	0.00	3.8	5.5
6/3		1/1	3.4	129				15. 5.74	-	34.6	-	3.595	7.125	1.840	94.7	1.45	0.3	1.3
6/4	C/Slip	1/4	3.4	129	11.11.68	12.11.68	3. 8.71	22. 5.74	-	33.9	-	3.655	7.125	1.827	92.5	1.14	4.3	7.8
6/5		2/2	2.4	84				24. 5.74	-	33.7	-	3.590	7.120	1.888	98.5	1.87	2.7	5.3
6/6		3/2	1.6	95				31. 5.74	-	30.5	-	3.585	7.120	1.877	92.5	1.82	5.9	9.0
6/7		4/1	0.9	103				4. 6.74	34.1	33.6	-1.47	3.575	7.130	1.793	88.4	0.48	1.5	3.6
7/1**		25/1/2	1.6	90	10. 6.74	-	11. 6.74	11. 6.74	37.1	35.7	-3.77	3.580	7.130	-	-	0.00	0.9	2.2
7/2		40/1/M/1	2.6	100	18. 6.74	-	19. 6.74	20. 6.74	37.5	36.2	-3.47	3.570	7.125	1.881	101.4	0.00	12.8	14.3
7/3		35/1/3	3.2	90	27. 6.74	-	29. 6.74	18. 7.74	38.2	36.5	-4.45	3.565	7.125	1.864	99.6	0.00	0.0	0.8
7/4	C/4	35/1/M/2	3.2	95	27. 6.74	-	29. 6.74	20. 7.74	38.2	37.7	-1.31	3.600	7.125	1.841	98.6	0.00	1.0	1.8
7/5		45/2/3	3.1	90	28. 6.74	-	29. 6.74	23. 7.74	39.2	36.2	-7.65	3.600	7.120	1.876	100.4	0.00	1.3	2.1
7/6		40/1/1	2.6	90	21. 6.74	-	21. 6.74	25. 7.74	37.5	38.1	1.60	3.585	7.130	1.844	99.5	0.00	2.2	3.7
7/7		45/2/2	3.1	90	28. 6.74	-	29. 6.74	27. 7.74	39.2	31.2	-20.41	3.595	7.140	1.871	93.0	0.00	1.4	3.0
8/1		U/11	1.7					31.10.75	-	34.0	-	3.560	7.130	1.837	92.6	0.00	-	-
8/2		U/6	1.7					4.11.75	-	32.2	-	3.580	7.125	1.881	94.6	0.00	0.2	1.3
8/3		L/6	3.5					6.11.75	-	28.8	-	3.600	7.125	1.932	95.2	0.16	-	-
8/4	B/S1.2	L/1	3.5	90	10. 4.71	-	12. 4.71	7.11.75	-	27.7	-	3.580	7.135	1.947	95.0	0.00	-	-
8/5		U/2	1.7					13.11.75	-	33.3	-	3.590	7.130	1.877	95.8	0.00	0.0	0.4
8/6		U/8	1.7					14.11.75	-	32.0	-	3.600	7.140	1.888	95.1	0.00	0.0	0.5
8/7		U/12	1.7					17.11.75	-	33.2	-	3.590	7.125	1.851	93.0	0.01	0.0	0.3
9/1**	E	P.2/1	1.2	90	8. 9.75	8. 9.75	-	10. 9.75	-	23.0	0.00+	3.490	7.120	-	-	0.00	3.4	7.8
9/2		P.3/1	1.6	90	8. 9.75	8. 9.75	10. 9.75	18. 9.75	-	16.0	0.00+	3.490	7.115	2.079	83.4	0.00	0.0	0.2

* Measured in same sense as makes the inclination of the slip surface < 90°.
§ Particles larger than 19.1 mm. §§ Particles larger than 9.6 mm.
** Specimen tested without prior waxing.
+ Sampling tube sealed immediately after sampling.

Table 6.2. Triaxial shear tests: main features

1	2	3	4	5	6	7	8	9	10	11	12	13	14	15	16	17	18	19	20	21	22	23	24	25
Series/test No.	$(\sigma_3)_o$ (lb/in²)	Degr. of consdn. (%)	Pore press. at start of shear (kg/cm²)	Strain rate (in/min)	F_{rs} (ratio)	Initial axial strain (%)	Bedding (mm)	Bedding (% of (7))	Med 1 seating corr. (mm)	(10) as apparent strain (%)	Graphical seating corr. (mm)	(12) as apparent strain (%)	Ratio of (10) to total seating corr. (%)	Time to failure (hrs)	Final aver. m/c (%)	Ch. in m/c in UU tests (%)	Ch. in m/c in PCU tests (%)	Diffce in m/c bet. base and (16) (%)	Diffce in m/c bet. mid. and ends (%)	Ch. in weight of spec. (g)	L_r (10^{-4} cc/min/kg/cm²)	M_e (kg/cm)	R_{in} (kg/cm)	Fraction of p.p. for full satn.
1/1	29	0.0	[illegible]	.0122	.9357	[illegible]	0.15	98.[illegible]	.00	.00	0.72	1.02	0.0	[illegible]	[illegible]	-6.33	-	4.51	-0.55	-	1.350	.140	-	0.06
1/2	60	0.0	[illegible]	.0041	.9935	0.23	0.31	134.[illegible]	.10	.14	0.07	0.09	59.6	[illegible]	33.5	-5.33	-	4.06	4.06	-	1.320	.369	-	[illegible]
1/3	45	0.0	2.142	.0041	.9980	0.10	[illegible]	328.[illegible]	.00	.00	0.42	0.59	0.0	30.5	36.1	-1.06	-	2.20	-0.67	1.08	1.370	.369	-	9.08
1/4	55	0.0	1.680	.0041	.9950	0.25	0.29	160.6	.10	.14	1.35	1.90	6.8	24.5	36.3	4.88	-	1.90	5.39	-	1.390	.369	-	[illegible]
1/5	35	0.[illegible]	[illegible].777	.0041	.9993	0.04	0.18	729.[illegible]	.00	.00	0.34	0.48	6.0	[illegible]	34.8	[illegible].58	-	-5.89	3.31	1.38	1.306	.369	-	2.09
1/6	50	0.0	0.344	.0041	.9936	0.32	0.26	114.[illegible]	[illegible]	.06	0.05	0.07	48.4	[illegible]	[illegible]	-1.36	-	-3.09	1.75	0.08	1.306	.195	-	[illegible]
1/7	40	0.0	-.072	.0041	.9939	0.21	0.21	95.[illegible]	.04	.06	0.45	0.63	6.3	27.5	36.0	1.48	-	-0.15	2.44	-0.47	1.215	.195	-	[illegible]
1/8	70	0.0	0.782	.0041	.9922	0.39	0.36	131.[illegible]	.00	.00	1.27	1.80	0.0	27.3	34.0	-5.68	-	-0.33	1.66	0.08	1.381	.234	-	[illegible]
1/9	60	0.0	1.374	.0041	.9946	0.17	0.31	162.[illegible]	.02	.02	0.00	0.00	100.0	25.3	[illegible]	[illegible].49	-	-4.78	3.84	0.24	1.271	.234	-	[illegible]
1/10	110	[illegible]	4.948	.0041	.9948	0.26	0.27	308.8	[illegible]	.11	0.16	0.22	32.3	31.8	[illegible]	[illegible].50	-	-6.18	-0.26	-0.09	1.472	.206	-	
1/11	115	68.[illegible]	[illegible].276	.0041	.9886	0.57	0.60	147.[illegible]	[illegible]	.02	1.04	1.47	1.4	28.0	[illegible]	-	0.88	-3.26	0.62	-0.93	1.254	.206	-	2.17
2/1	45	[illegible]	1.620	.0061	.9966	0.17	[illegible]	[illegible]	[illegible]	.00	0.00	0.00	0.0	41.8	34.4	4.35	-	-2.85	2.23	-0.08	1.336	.234	-	1.37
2/2	70	0.0	2.612	.0061	.9918	0.41	0.36	124.[illegible]	.00	.00	0.00	0.00	[illegible]	[illegible]	30.0	[illegible]	-	0.15	2.88	-0.10	1.618	.234	-	[illegible]
2/3	40	[illegible]	-.142	.0061	.9936	0.32	[illegible]	91.[illegible]	.07	.10	0.27	0.38	[illegible]	[illegible]	32.[illegible]	0.93	-	-5.29	[illegible]	0.20	[illegible]	.234	-	[illegible]
2/4	50	[illegible]	[illegible]	.0061	.9968	[illegible]	[illegible]	[illegible]	[illegible]	[illegible]	[illegible]	0.00	[illegible]	[illegible]	[illegible]	-2.94	-	-1.14	[illegible]	-	[illegible]	.234	-	[illegible]
2/5	55	[illegible]	[illegible]	.0061	.9942	[illegible]	[illegible]	[illegible]	[illegible]	[illegible]	[illegible].17	[illegible]	[illegible]	[illegible]	[illegible]	[illegible]	-	.97	1.36	-0.07	1.448	.234	-	[illegible]
2/6	60	0.0	[illegible]	.0061	.9892	[illegible]	[illegible]	[illegible]	[illegible]	.00	[illegible]	[illegible]	[illegible]	24.[illegible]	[illegible]	[illegible]	-	[illegible]	6.23	-	1.406	.234	-	[illegible]
2/7	65	[illegible]	[illegible]	.0061	[illegible]	0.25	[illegible]	[illegible]	[illegible]	.04	[illegible]	0.20	[illegible]	[illegible]	[illegible]	[illegible]	-	.16	4.21	[illegible]	1.433	[illegible]	-	
2/8	80	[illegible]	[illegible]	.0061	[illegible]	[illegible]	[illegible]	[illegible]	[illegible]	[illegible]	[illegible]	[illegible]	11.3	[illegible]	[illegible]	-	[illegible]	[illegible]	3.14	[illegible]	1.720	.234	-	[illegible]
2/9	90	[illegible]	[illegible]	.0061	.9887	0.57	[illegible]	[illegible]	[illegible]	[illegible]	[illegible]	[illegible]	[illegible]	[illegible]	[illegible]	-	-2.76	1.31	2.52	[illegible]	1.682	.234	-	[illegible]
2/10	110	59.4	[illegible]	.0061	.9880	0.60	[illegible]	133.[illegible]	.05	[illegible]	0.45	0.63	[illegible]	[illegible]	[illegible]	-	[illegible]	-0.01	1.74	[illegible]	1.795	.234	-	[illegible]
2/11	50	[illegible]	[illegible]	.0061	[illegible]	0.38	[illegible]	[illegible]	.37	[illegible]	[illegible]	0.40	[illegible]	6.8	[illegible]	[illegible]	-	0.23	6.53	[illegible]	1.547	.230	-	[illegible]
3/1	50	11.[illegible]	[illegible]	.0030	[illegible]	0.62	[illegible]	[illegible]	[illegible]	[illegible]	[illegible]	0.24	[illegible]	[illegible]	[illegible]	-	[illegible]	0.43	[illegible]	0.72	1.670	.288	-	[illegible]
3/2	110	[illegible]	[illegible]	.0030	.9740	1.30	[illegible]	61.[illegible]	[illegible]	.08	0.16	0.23	24.5	[illegible]	[illegible]	-	[illegible]	[illegible]	1.92	[illegible]	1.725	.151	-	[illegible]
3/3	100	63.[illegible]	[illegible]	.0041	.9745	1.28	[illegible]	57.[illegible]	.21	.29	0.48	0.68	[illegible]	31.4	27.[illegible]	-	[illegible]	[illegible]	1.92	[illegible]	1.852	.230	.15	[illegible]
3/4	50	0.0	1.534	.0041	.9900	[illegible]	[illegible]	[illegible]	.08	.11	0.11	0.16	40.8	30.4	[illegible]	28.50	-	3.51	-1.59	0.77	1.755	.230	.15	[illegible]
3/5	90	69.3	1.032	.0041	.9766	[illegible]	[illegible]	56.[illegible]	[illegible]	.13	0.61	[illegible]	[illegible]	[illegible]	[illegible]	-	-1.31	5.54	-0.94	0.07	1.986	.190	.15	[illegible]
3/6	80	41.7	2.040	.0041	.9824	0.38	[illegible]	[illegible]	[illegible]	.15	0.54	0.77	[illegible]	23.2	[illegible]	-	[illegible]	0.86	3.77	-0.28	1.816	.190	.15	[illegible]
3/7	70	0.0	1.811	.0041	.9846	0.77	0.36	[illegible]	[illegible]	.19	0.43	0.60	[illegible]	[illegible]	[illegible]	19.26	-	-3.92	4.03	0.43	1.823	.328	.15	[illegible]
4/1	50	0.0	[illegible]	.0006	.9914	0.43	[illegible]	84.[illegible]	[illegible]	.00	0.19	[illegible]	0.0	101.1	[illegible]	[illegible]	-	-1.85	-6.22	0.0	0.000	.463	-	1.27
4/2	110	36.[illegible]	[illegible]	.0006	[illegible]	[illegible]	[illegible]	[illegible]	[illegible]	[illegible]	[illegible]	[illegible]	[illegible]	160.9	[illegible]	-	[illegible]	2.60	[illegible]	[illegible]	0.000	.576	.15	[illegible]
4/3	60	[illegible]	[illegible]	.0006	.9822	0.39	[illegible]	[illegible]	.50	.25	0.00	[illegible]	100.0	166.1	[illegible]	0.27	-	2.00	-2.67	8.0	0.000	.463	.15	[illegible]
4/4	120	40.[illegible]	[illegible]	.0006	[illegible]	[illegible]	[illegible]	[illegible]	.60	[illegible]	[illegible]	[illegible]	45.8	[illegible]	[illegible]	-	[illegible]	7.30	-1.27	-29.2	0.000	.576	.15	[illegible]
4/5	100	46.[illegible]	[illegible]	.0006	.9820	[illegible]	[illegible]	81.[illegible]	[illegible]	.14	[illegible]	[illegible]	[illegible]	[illegible]	[illegible]	-	2.76	5.60	[illegible]	[illegible]	0.000	.536	.15	[illegible]
4/6	80	[illegible]	[illegible]	.0006	.9885	[illegible]	[illegible]	101.[illegible]	[illegible]	.00	0.40	0.21	0.0	74.2	[illegible]	1.28	-	16.46	[illegible]	10.0	0.000	.576	.15	2.36
5/1	50	[illegible]	[illegible]	.0041	.9947	0.27	0.26	[illegible]	[illegible]	.15	0.29	[illegible]	27.4	9.5	[illegible]	-8.38	-	-8.83	[illegible]	0.49	1.384	.190	.15	1.24
5/2	110	[illegible]	[illegible]	.0041	.9896	0.52	0.57	[illegible]	[illegible]	.06	0.84	1.18	[illegible]	24.8	[illegible]	3.22	-	-2.27	2.08	0.94	1.958	.204	-	[illegible]
5/3	70	[illegible]	[illegible]	.0041	[illegible]	0.19	[illegible]	268.[illegible]	[illegible]	.04	0.03	[illegible]	50.8	[illegible]	[illegible]	1.27	-	0.53	-2.13	-0.01	1.640	.204	-	2.17
5/4	100	[illegible]	[illegible]	.0041	.9928	0.36	[illegible]	[illegible]	.10	.14	0.24	0.34	[illegible]	10.9	[illegible]	4.98	-	-0.36	5.41	-0.03	1.513	.197	-	0.38
5/5	90	[illegible]	[illegible]	.0061	[illegible]	0.27	[illegible]	[illegible]	[illegible]	[illegible]	1.59	2.24	[illegible]	13.5	[illegible]	2.08	-	[illegible]	-0.89	0.57	1.464	.235	[illegible]	0.18
5/6	80	[illegible]	[illegible]	[illegible]	.9900	0.50	0.42	[illegible]	.04	.05	0.36	1.36	3.6	11.1	36.8	-	0.69	-4.13	1.12	-0.81	1.695	.204	.15	2.71
5/7	60	[illegible]	2.629	.0061	.9975	[illegible]	[illegible]	[illegible]	[illegible]	.03	0.17	[illegible]	[illegible]	[illegible]	36.7	[illegible]	-	-0.50	1.27	0.15	1.620	.235	.15	3.78
6/1	100	53.3	[illegible]	.0061	.9725	1.38	[illegible]	53.1	.01	[illegible]	0.13	0.19	3.7	8.2	34.0	-	2.86	4.03	4.38	-2.20	1.860	.273	-	[illegible]
6/2	70	[illegible]	[illegible]	.0061	.9919	[illegible]	0.36	126.1	.00	.00	0.06	0.09	[illegible]	2.9	36.4	11.51	-	-0.74	-0.50	0.49	1.508	.204	-	[illegible]
6/3	70	[illegible]	[illegible]	[illegible]	[illegible]	[illegible]	[illegible]	[illegible]	[illegible]	.07	0.08	0.11	39.7	[illegible]	[illegible]	8.88	-	10.18	1.34	-0.13	1.739	.197	-	1.24
6/4	80	30.3	[illegible]	.0061	.9788	1.06	[illegible]	55.1	[illegible]	.06	1.13	1.60	[illegible]	21.4	[illegible]	-	-3.83	10.87	0.16	[illegible]	2.109	.204	-	[illegible]
6/5	110	62.[illegible]	[illegible]	.0061	.9715	1.43	[illegible]	56.4	[illegible]	.07	0.17	0.25	21.7	[illegible]	[illegible]	-	-2.27	4.74	2.64	-2.33	2.570	.204	.15	[illegible]
6/6	90	[illegible]	[illegible]	.0061	.9535	2.33	[illegible]	[illegible]	.66	.94	0.80	1.15	44.9	[illegible]	29.1	-	-4.50	3.08	-5.21	-4.55	2.119	.197	.15	1.33
6/7	70	46.4	2.147	.0091	.9571	2.15	0.36	[illegible]	[illegible]	.02	0.90	1.29	1.7	[illegible]	33.0	-	-1.81	-6.30	0.90	-4.35	1.647	.204	.15	0.35
7/1	60	0.0	3.416	.0091	[illegible]	0.11	[illegible]	417.[illegible]	.33	.46	0.52	0.73	38.5	[illegible]	37.3	4.42	-	-4.63	[illegible]	[illegible]	1.577	[illegible]	.15	-
7/2	100	65.9	1.846	.0091	.9695	1.53	0.52	[illegible]	.05	.07	0.78	1.10	[illegible]	[illegible]	34.0	-	-5.99	-4.76	0.49	-2.62	1.991	.204	[illegible]	∞
7/3	50	0.0	1.486	.0091	.9914	0.43	0.26	85.4	.02	.02	0.00	0.00	[illegible]	7.5	37.6	3.13	-	0.47	-3.71	-0.04	1.476	.224	.18	7.60
7/4	70	55.1	1.369	.0091	.9759	1.20	0.36	[illegible]	.27	.38	0.45	0.64	37.4	4.8	36.2	-	-4.07	-2.83	1.20	-1.66	1.706	.273	.18	4.79
7/5	90	37.8	2.395	.0091	.9792	1.04	0.47	[illegible]	[illegible]	.30	0.34	0.49	37.8	4.8	33.8	-	-6.68	-1.08	-1.97	-1.43	1.534	.224	.18	∞
7/6	80	50.6	1.656	.0091	.9706	1.47	0.42	[illegible]	[illegible]	.10	0.18	0.26	28.8	7.9	32.5	-	-14.78	4.07	1.59	-2.24	1.467	.273	.18	13.2
7/7	110	72.[illegible]	1.432	.0091	.9678	1.61	0.57	[illegible]	.08	.12	0.26	0.37	23.7	3.2	31.7	-	1.54	1.79	2.17	-2.43	2.016	.283	.18	[illegible]
8/1	50	0.0	-.033	.0061	.9804	0.98	0.26	37.3	.01	.02	1.53*	2.13	0.6	32.6	34.0	0.07	-	-0.56	0.01	0.06	1.567	.396	.18	-.01
8/2	60	0.0	0.142	.0091	.9800	1.00	0.31	43.8	[illegible]	.43	0.30	0.42	50.7	5.7	31.4	-2.34	-	-4.71	1.18	-0.02	1.347	.391	.18	0.05
8/3	70	0.0	0.350	.0091	.9780	1.10	0.36	46.5	.36	.50	0.53	0.75	40.1	5.7	27.6	-4.04	-	3.02	4.59	-0.27	1.403	.396	.18	0.15
8/4	80	0.0	0.464	.0091	.9780	1.10	0.42	53.1	.56	.80	0.46	0.66	54.9	6.6	26.7	-3.47	-	-0.84	-0.50	-0.01	1.334	.358	.18	0.19
8/5	90	97.5	0.027	.0091	.9719	1.41	0.47	46.8	.00	.00	0.45	0.63	0.0	4.1	31.9	-	-4.33	3.15	-1.55	-0.54	1.823	.396	.18	[illegible]
8/6	100	88.0	0.142	.0091	.9716	1.42	[illegible]	51.[illegible]	.14	.21	0.23	0.33	38.4	4.9	31.4	-	-1.93	2.60	-2.26	-0.52	1.823	.358	.18	0.49
8/7	110	68.7	0.729	.0091	.9727	1.36	[illegible]	58.8	.23	.33	0.23	0.33	49.4	5.6	33.1	-	-0.16	-1.58	0.62	-0.47	1.693	.300	.18	0.67
	20	0.0	0.139				0.10	36.5	.12	.16	0.00	0.00	100.0	7.1										0.04
9/1	40	0.0	1.632	.0457	.9920	0.40	0.21	73.0	.00	.00	0.00	0.00	0.0	1.3	22.8	-0.70	-	3.45	-13.61	0.34	0.000	.430	-	0.50
	60	0.0	2.722				0.31	109.5	.00	.00	0.00	0.00	0.0	0.6										0.84
	50	80.7	0.238	.0457	.9808	0.96	0.26	38.0	.12	.17	0.00	0.00	100.0	3.4										0.03
9/2	70	87.0	0.228	.0457	.9688	1.56	0.36	32.[illegible]	.00	.00	0.00	0.00	0.0	1.2	18.8	-	17.24	0.43	-1.59	-0.97	0.000	.396	.18	0.19
	100	91.0	0.130	.0203	.9615	1.93	0.52	37.9	.00	.00	0.00	0.00	0.0	1.6										0.16

* Seating correction applied during shear.

Table 6.2

Table 6.3. Triaxial shear tests: conditions at failure

1	2	3	4	5	6	7	8	9	10	11	12	13	14	15	16	17	18	19	20	21
Series/test No.	Failure mode (Fig. 6.3)	α_p (deg)	δ (%)	Bedding (ℓ of (7))	Total seating corr. (% of (7))	Corrected axial strain (%)	Volumetric strain during shear (%)	Deviation from initial σ_1 (%)	Membrane corr. to σ_1 due to bulging (kg/cm^2)	Additional membr. corr. to σ_1 (kg/cm^2)	Membrane corr. to σ_3 due to bulging (kg/cm^2)	Additional membr. corr. to σ_3 (kg/cm^2)	Corr. to σ_1 due to FPSD for bulging (kg/cm^2)	Addl. corr. to σ_1 due to FPSD (kg/cm^2)	Corr. to deviator stress due to membr. (%)	Corr. to deviator stress due to FPSD (%)	Error in B.sh.'s membr. corr. to deviator stress (%)	Pore pressure (kg/cm^2)	p_f' (kg/cm^2)	q_f (kg/cm^2)
1/1	3.	-	-	6.0	29.0	3.51	0.67	-2.9	0.006	-	0.000	-	-	-	0.4	-	-6.5	-0.183	1.415	0.709
1/2	2.	38.5	0.12	165.5	35.8	0.26	-0.09	-1.7	0.005	0.110	0.002	-0.055	-	-	19.3	-	-74.6	0.906	2.767	0.436
1/3	3.	-	-	6.9	12.2	4.79	-0.04	-7.8	0.021	-	0.001	-	-	-	0.9	-	-5.6	-0.182	2.013	1.056
1/4	1.	-	-	14.4	68.2	2.78	0.12	14.9	0.014	-	0.001	-	-	-	0.3	-	-14.4	-0.397	2.915	1.870
1/5	3.	-	-	5.3	9.3	4.87	-0.13	-6.0	0.020	-	0.000	-	-	-	1.3	-	-3.0	0.128	1.379	0.773
1/6	1.	-	-	12.1	2.3	3.02	0.37	-0.8	0.008	-	0.001	-	-	-	0.2	-	-14.3	-0.507	2.350	1.607
1/7	1.	-	-	8.7	18.9	3.36	0.39	5.5	0.008	-	0.000	-	-	-	0.3	-	-11.2	-0.344	2.029	1.441
1/8	2.	31.4	0.00	21.4	75.3	2.38	-0.05	-13.1	0.009	0.000	0.002	0.000	-	-	0.3	-	-22.5	0.071	2.836	1.345
1/9	1.	-	-	13.1	0.0	3.33	0.54	-20.2	0.010	-	0.001	-	-	-	0.3	-	-13.3	-0.227	1.952	1.603
1/10	3.	-	-	15.7	4.4	0.11	-0.15	-8.9	0.014	-	0.001	-	-	-	0.3	-	-15.1	1.476	3.607	1.910
1/11	1.	-	-	43.5	76.9	1.92	-0.29	-4.8	0.009	-	0.002	-	-	-	0.1	-	-38.0	-0.323	5.274	2.686
2/1	3.	-	-	3.0	0.0	10.85	-0.04	-10.6	0.028	-	0.000	-	-	-	1.8	-	-8.2	0.174	1.832	0.786
2/2	2.	52.3	0.00	14.4	0.0	3.56	0.23	-3.3	0.012	0.000	0.001	0.000	-	-	0.7	-	-17.3	1.870	2.052	0.788
2/3	1.	-	-	8.7	11.3	3.37	0.08	-3.6	0.011	-	0.001	-	-	-	0.4	-	-11.2	-0.339	1.698	1.316
2/4	2.	51.5	0.00	11.0	0.0	3.31	-0.06	-2.2	0.010	0.000	0.001	0.000	-	-	0.7	-	-3.4	1.291	1.417	0.702
2/5	3.	-	-	5.2	3.1	7.71	-0.01	-4.3	0.021	-	0.001	-	-	-	1.4	-	-8.3	1.128	1.800	0.740
2/6	1.	-	-	12.3	3.4	3.58	0.85	-11.0	0.012	-	0.001	-	-	-	0.3	-	-18.3	-0.583	2.578	1.719
2/7	3.	36.3	0.00	19.1	7.9	2.48	0.00	-7.6	0.009	0.000	0.000	0.000	-	-	0.6	-	-18.1	1.914	1.617	0.646
2/8	2.	46.2	0.00	10.4	9.0	5.39	-0.13	-8.0	0.017	0.000	0.001	0.000	-	-	1.0	-	-12.0	2.507	1.872	0.757
2/9	1.	-	-	19.0	19.1	2.45	0.03	-12.6	0.013	-	0.002	-	-	-	0.4	-	-22.8	0.855	3.165	1.461
2/10	1.	-	-	19.1	15.0	4.21	0.23	-16.1	0.016	-	0.002	-	-	-	0.3	-	-22.0	-0.018	4.245	2.209
2/11	3.	51.1	0.00	15.6	16.9	2.34	-0.05	-12.3	0.009	0.000	0.001	0.000	-	-	0.4	-	-19.0	0.139	2.021	0.900
3/1	1.	-	-	5.6	3.7	6.49	0.28	-11.5	0.025	-	0.002	-	-	-	1.0	-	-14.8	-0.030	1.895	1.202
3/2	1.	-	-	15.0	4.3	5.36	0.39	-13.6	0.015	-	0.002	-	-	-	0.3	-	-27.6	-0.047	4.368	2.310
3/3	1.	-	-	20.6	19.2	3.65	0.49	-11.8	0.017	-	0.004	-	0.081	-	0.3	1.8	-33.1	-0.019	3.850	2.250
3/4	1.	-	-	7.7	3.3	4.74	0.22	-16.4	0.015	-	0.001	-	0.081	-	0.6	3.4	-13.7	-0.173	1.870	1.175
3/5	2.	53.4	0.17	8.6	11.4	7.64	0.53	-10.5	0.012	0.378	0.003	-0.132	0.074	0.079	13.7	4.0	-90.3	-0.144	3.808	1.893
3/6	1.	-	-	20.2	26.6	2.89	0.22	-17.4	0.011	-	0.002	-	0.082	-	0.2	2.2	-29.8	-0.170	2.854	1.874
3/7	1.	-	-	16.3	19.3	3.13	0.09	-10.4	0.018	-	0.003	-	0.082	-	0.7	3.9	-24.1	0.756	2.505	1.046
4/1	1.	-	-	23.8	6.0	1.53	-0.05	-18.4	0.005	-	0.001	-	-	-	0.2	0.0	-33.3	0.064	1.775	1.072
4/2	1.	-	-	48.3	110.4	1.66	-1.14	-9.6	0.013	-	0.005	-	0.030	-	0.3	1.0	-52.6	2.481	2.971	1.553
4/3	1.	-	-	15.4	0.0	2.84	-0.04	-16.2	0.009	-	0.002	-	0.029	-	0.3	1.3	-31.0	0.329	2.207	1.074
4/4	1.	-	-	35.4	14.8	2.47	0.18	-17.2	0.013	-	0.003	-	0.029	-	0.2	0.6	-42.1	0.148	4.483	2.396
4/5	1.	-	-	39.9	24.8	1.83	0.11	-16.7	0.009	-	0.002	-	0.029	-	0.2	0.7	-45.4	0.520	3.345	2.031
4/6	1.	-	-	55.7	20.4	1.05	-0.01	-14.3	0.007	-	0.002	-	0.029	-	0.2	1.1	-50.6	0.960	2.561	1.341
5/1	2.	64.3	0.00	21.2	23.6	1.72	0.00	-13.7	0.005	0.000	0.001	0.000	0.084	0.000	0.2	3.2	-21.8	-0.433	2.111	1.304
5/2	1.	-	-	65.1	95.7	1.23	-0.06	-12.3	0.007	-	0.002	-	-	-	0.1	-	-48.6	0.423	4.153	2.156
5/3	3.	-	-	32.9	2.5	1.55	-0.11	-15.9	0.006	-	0.001	-	-	-	0.1	-	-27.2	-0.195	2.507	1.790
5/4	2.	48.1	0.00	47.8	22.4	1.53	0.08	-10.7	0.006	0.000	0.001	0.000	-	-	0.1	-	-36.4	-0.138	4.420	1.940
5/5	1.	-	-	23.7	80.9	2.77	-0.21	-9.9	0.010	-	0.001	-	0.073	-	0.3	2.5	-21.1	0.764	3.388	1.479
5/6	1.	-	-	16.3	37.8	3.59	0.09	-14.6	0.012	-	0.001	-	0.082	-	0.3	2.6	-21.4	0.213	2.935	1.572
5/7	2.	51.6	0.00	14.1	7.5	3.11	0.17	-13.6	0.010	0.000	0.000	0.000	0.073	0.000	0.4	3.5	-12.1	0.744	1.818	1.034
6/1	2.	53.0	0.00	35.8	9.2	2.04	0.09	-9.1	0.017	0.000	0.005	0.000	-	-	0.4	-	-46.9	1.666	3.144	1.521
6/2	3.	55.7	0.00	60.7	10.7	0.84	-0.04	4.3	0.005	0.000	0.001	0.000	-	-	0.3	-	-48.6	2.953	1.561	0.568
6/3	2.	46.6	0.00	17.5	3.7	2.92	0.13	0.8	0.008	0.000	0.001	0.000	-	-	0.6	-	-16.9	2.780	1.520	0.615
6/4	1.	-	-	18.3	50.3	3.18	-0.15	-4.0	0.013	-	0.003	-	-	-	0.5	-	-29.7	1.442	2.881	1.026
6/5	3.	-	-	32.7	10.1	2.46	0.04	-11.0	0.014	-	0.004	-	0.084	-	0.3	2.5	-44.9	0.720	4.364	1.675
6/6	1.	-	-	14.4	25.3	4.57	0.15	-7.0	0.022	-	0.006	-	0.084	-	0.5	2.8	-36.3	0.620	3.649	1.480
6/7	1.	-	-	9.4	23.7	5.45	0.19	-9.9	0.024	-	0.005	-	0.083	-	0.9	4.2	-32.2	1.179	2.134	0.988
7/1	1.	-	-	9.7	16.2	4.53	-0.02	-4.8	0.013	-	0.001	-	0.080	-	1.5	9.6	-8.5	2.692	0.857	0.418
7/2	3.	-	-	29.5	44.7	2.47	0.18	-12.7	0.015	-	0.004	-	0.085	-	0.3	2.4	-45.5	0.813	3.396	1.798
7/3	2.	39.8	0.00	7.1	0.0	5.15	0.06	-13.0	0.015	0.000	0.001	0.000	0.097	0.000	1.0	6.7	-10.1	0.083	2.174	0.723
7/4	3.	-	-	22.4	28.1	2.29	0.03	-12.6	0.016	-	0.004	-	0.100	-	0.5	4.7	-38.4	0.720	2.401	1.055
7/5	2.	47.6	0.00	29.8	22.0	2.21	-0.04	-12.4	0.012	0.000	0.003	0.000	0.099	0.000	0.4	4.4	-37.8	1.266	3.007	1.138
7/6	1.	-	-	12.0	5.4	4.85	0.01	-13.2	0.025	-	0.005	-	0.098	-	0.8	3.9	-27.3	0.798	2.671	1.271
7/7	2.	52.5	0.00	96.0	44.6	0.84	-0.18	-8.6	0.016	0.000	0.007	0.000	0.105	0.000	0.3	3.3	-71.1	1.096	4.216	1.603
8/1	1.	-	-	8.9	52.2	4.11	0.52	9.7	0.027	-	0.004	-	0.098	-	0.8	3.6	-20.7	-0.188	2.524	1.360
8/2	1.	-	-	19.5	18.7	2.25	-0.06	4.0	0.020	-	0.005	-	0.100	-	0.4	3.0	-34.2	-0.241	2.778	1.667
8/3	2.	43.6	0.00	24.5	36.1	2.09	-0.29	-9.0	0.021	0.000	0.006	0.000	0.101	0.000	0.4	2.7	-37.4	-0.261	2.740	1.863
8/4	2.	19.1	0.00	20.2	22.8	2.89	0.55	-16.7	0.022	0.000	0.005	0.000	0.099	0.000	0.4	2.4	-34.1	-0.416	2.888	2.087
8/5	2.	53.9	0.00	72.4	69.9	0.91	0.89	0.1	0.018	0.000	0.006	0.000	0.104	0.000	0.3	2.6	-65.8	-0.040	4.163	2.039
8/6	1.	-	-	43.9	19.9	1.66	1.22	-15.5	0.020	-	0.005	-	0.100	-	0.3	2.1	-53.6	-0.224	3.640	2.377
8/7	3.	-	-	33.2	13.8	2.42	0.11	-11.0	0.020	-	0.006	-	0.101	-	0.3	2.3	-44.1	0.403	4.139	2.183
9/1*	1.	-	-	2.8	0.0	5.18	-0.43	150.2	0.029	-	0.003	-	-	-	1.3	-	-7.8	0.538	1.832	1.006
				5.1	0.0	5.76	-0.01	13.1	0.032	-	0.002	-	-	-	1.3	-	-9.9	1.794	2.112	1.135
				7.0	0.0	6.30	-0.11	1.4	0.036	-	0.002	-	-	-	1.5	-	-11.6	3.083	2.235	1.141
9/2*	1.	-	-	4.6	0.0	7.93	-0.41	138.5	0.045	-	0.005	-	0.100	-	0.9	2.2	-15.6	1.184	4.512	2.225
				4.6	0.0	11.21	-0.12	28.7	0.065	-	0.007	-	0.097	-	0.9	1.6	-20.1	0.484	7.509	3.119
				5.3	0.0	13.82	-0.53	15.3	0.083	-	0.009	-	0.096	-	1.0	1.2	-23.2	0.940	9.908	3.866

* Multiple stage tests.

Table 6.4. Summary of results of pore pressure and dissipation tests and other special tests

1	2	3	4	5	6	7	8	9	10	11	12	13	14	15	16	17	18	19	20
Series/test No.	Location	Spec. No.	Triax. shear test No.	Depth below G.S. (m)	Inclination* of axis to horiz. (deg)	Initial degree of saturation, S_r (%)	Pore press. u_o under $\sigma_3 = p_{ob}$			Pore press. parameter B			Pore press. parameter A		Dissipation tests			$\Delta\sigma_3$ vs. a_u/a_{oc} reln. det'd using LSI	Remarks
							Last reading, u_{or} (kg/cm^2)	Extrapolated value, u_o (kg/cm^2)§	Extrapolated amount, E_p (%)	B_o (at initial S_r)	B_s (before start of shear)	B_f (after failure)	A_e (at start of shear)	A_f (at failure)	Cell pressure (kg/cm^2)	Max. pore press. (kg/cm^2)	c_v (10^{-4} cm^2/sec)		
1/1		6	-			98.9	-	-	-	-	-	-	-	-	4.038	1.018	2.42	-	
1/2		11	-			99.2	-	-	-	-	-	-	-	-	-	-	-	✓	Spec. gained .55 g water.
1/3	B/S1.1	17	1/6	2.5-4.5	random	99.1	-.225	-.295	23.7	0.056	-	-	-	-	-	-	-	-	
1/4		16	1/9			98.9	-	-	-	-	0.453	-	0.912	0.051	-	-	-	-	Spec. gained .24 g water.
1/5		18	1/10			100.0	-	-	-	-	0.839	-	0.562	0.151	-	-	-	-	
1/6		19	1/11			96.1	-.477	-.490	2.7	0.036	-	-	-	-	-	-	-	-	
2/1		35/3	-	4.1	90	92.9	-	-	-	-	-	-	-	-	4.179	0.489	4.01	-	
2/2		30/2	-	4.4	65	98.8	-	-	-	-	-	-	-	-	4.179	1.296	2.88	-	
2/3		45/1/1	2/1	2.7	100	97.7	-	-	-	0.184	-	-	-	-	-	-	-	✓	
2/4		45/2/3	2/2	3.6	90	96.6	-.266	-.280	5.0	0.149	-	-	-	-	-	-	-	✓	
2/5		30/4	2/3	4.4	65	95.7	-.345	-.425	18.8	-	-	-	-	-	-	-	-	-	
2/6	C/1	25/2	2/4	2.2	90	98.8	-.468	-.575	18.6	-	-	-	-	-	-	-	-	-	Spec. gained .20 g water.
2/7		25/3	2/5	2.2	90	99.5	-.430	-.530	18.9	-	-	-	-	-	-	-	-	-	
2/8		35/2	2/6	4.1	90	95.4	-.473	-.542	12.7	0.045	-	-	-	-	-	-	-	✓	
2/9		45/1/3	2/7	2.7	100	101.4	-.423	-.547	22.7	-	-	-	-	-	-	-	-	-	
2/10		35/M/5	2/11	4.1	90	95.0	-	-	-	0.035	0.627	-	0.698	0.301	-	-	-	-	
3/1	D	1.4/40/4	3/1	3.1	90	97.0	-.410	-.415	1.2	0.076	-	-	-	-	2.773	1.223	1.56	-	Spec. gained .72 g water apparently during shear.
3/2		1.4/25/1/1	3/2	1.4	120	97.7	-	-	-	-	-	-	-	-	7.694	4.521	0.78	-	
3/3		1.4/25/1/3	3/4	1.4	120	91.0	-.470	-.480	2.1	0.063	0.737	-	0.799	0.334	-	-	-	-	Spec. gained .77 g water.
4/1		4/35/5	4/1	2.7	90	97.0	-	-	-	-	-	-	-	-	-	-	-	✓	
4/2	D	4/30/3	4/3	2.4	90	97.0	-	-	-	-	-	-	-	-	-	-	-	✓	
4/3		4/30/4	4/6	2.4	90	97.2	-	-	-	-	0.825	0.846	0.672	0.267	-	-	-	-	ν measured as 0.31
5/1		40/1	-	3.8	10	88.9	-.384	-.384	0.0	0.032	-	-	-	-	-	-	-	-	
5/2	B/10°	30/2	5/1	4.8	10	97.8	-.164	-.177	7.3	-	-	-	-	-	-	-	-	-	Spec. gained .55 g water.
5/3		30/1	5/3	4.8	10	97.7	-	-	-	0.075	0.727	-	0.642	0.241	-	-	-	✓	
5/4		45/3	5/4	5.3	10	90.3	-.423	-.472	10.4	0.026	0.554	-	0.946	0.336	-	-	-	✓	
6/1		1/3	6/1	3.4	129	91.2	-.189	-.182	-3.8§	0.242	-	-	-	-	2.773 6.991	1.174 5.118	8.06 2.04	-	
6/2	C/Slip	1/2	6/2	3.4	129	93.4	-.147	-.147	0.0	0.229	0.931	0.961	0.485	0.627	-	-	-	✓	ν measured as 0.33
6/3		1/1	6/3	3.4	129	94.7	-.128	-.150	14.7	0.255	0.947	0.962	0.598	0.669	-	-	-	✓	
6/4		2/2	6/5	2.4	84	98.5	-.145	-.180	19.4	-	-	-	-	-	-	-	-	-	Overwet FPSD used.
7/1		25/1/2	7/1	1.6	90	-	-.244	-.255	4.3	0.112	1.000	-	0.732	0.445	-	-	-	-	Spec. gained .55 g water.
7/2	C/4	40/1/M/1	7/2	2.6	100	101.4	-.370	-.374	1.1	0.278	-	-	-	-	-	-	-	-	Overwet FPSD used.
7/3		35/1/M/2	7/4	3.2	90	98.6	-.118	-.175	32.6	-	-	-	-	-	-	-	-	-	
7/4		45/2/2	7/7	3.1	90	93.0	0.015	0.016	6.3	-	-	-	-	-	-	-	-	-	
8/1		L/4	-	3.5	90	94.5	-.303	-.330	8.2	0.021	-	-	-	-	-	-	-	✓	
8/2	B/S1.2	L/1	8/4	3.5	90	95.0	-.224	-.265	15.5	-	0.132	-	0.848	-.076	-	-	-	-	
8/3		L/5	-	3.5	90	94.2	-	-	-	-	-	-	-	-	5.585	0.640	3.87	-	
9/1	E	P.2/1	9/1	1.2	90	-	-.443	-	-	-	0.747	-	0.818	0.289	-	-	-	-	Cavitation occurred
9/2		P.3/1	9/2	1.6	90	83.4	-.330	-	-	0.069	-	-	-	-	3.476	1.232	1.46	-	Cavitation occurred

* Measured in same sense as makes the inclination of the slip surface < 90°.
§ *Extrapolation in reverse sense (Fig. 6.15).*

Table 6.5. List of coefficients C_{ij} in computer-fitted polynomials

Equation No.	j	0	1	2	3	4	5
6.7	1	$0.256\ 011\ 8\times10^{-1}$	$-0.922\ 645\ 3\times10^{-2}$	$-0.105\ 291\ 1\times10^{-1}$	$0.233\ 770\ 3\times10^{-2}$	$-0.128\ 063\ 8\times10^{-3}$	-
6.8	2	$-0.470\ 304\ 5\times10^{-1}$	$0.104\ 363\ 0\times10^{1}$	$-0.158\ 386\ 0\times10^{-1}$	-	-	-
6.9	3	$-0.221\ 824\ 6\times10^{-1}$	$0.105\ 590\ 2\times10^{1}$	$-0.102\ 178\ 6\times10^{-1}$	-	-	-
6.10	4	$-0.986\ 862\ 2\times10^{0}$	$0.633\ 830\ 0\times10^{1}$	$-0.101\ 854\ 4\times10^{0}$	-	-	-
6.11	5	$-0.104\ 646\ 3\times10^{1}$	$0.592\ 548\ 8\times10^{1}$	$-0.397\ 262\ 1\times10^{-1}$	-	-	-
6.12	6	-	$0.386\ 383\ 6\times10^{-3}$	$-0.194\ 677\ 8\times10^{-7}$	-	-	-
6.13	7	-	$0.628\ 782\ 7\times10^{-3}$	$-0.299\ 293\ 2\times10^{-7}$	-	-	-
6.14	8	$0.155\ 390\ 5\times10^{-1}$	$0.274\ 891\ 2\times10^{-2}$	$-0.424\ 200\ 7\times10^{-5}$	$0.311\ 735\ 7\times10^{-8}$	$-0.105\ 663\ 5\times10^{-11}$	$0.131\ 860\ 3\times10^{-15}$
6.33, 6.45	9	$0.890\ 231\ 1\times10^{-2}$	$0.113\ 189\ 0\times10^{3}$	$-0.511\ 252\ 7\times10^{4}$	$0.966\ 358\ 8\times10^{5}$	$-0.640\ 144\ 8\times10^{6}$	-
6.79	10	$0.531\ 800\ 3\times10^{0}$	$0.147\ 868\ 8\times10^{0}$	$-0.500\ 432\ 4\times10^{-2}$	$0.703\ 453\ 1\times10^{-4}$	-	-
	11	$0.477\ 396\ 5\times10^{0}$	$0.186\ 282\ 2\times10^{0}$	$-0.924\ 333\ 9\times10^{-2}$	$0.159\ 443\ 5\times10^{-3}$	-	-
	12	$0.494\ 356\ 2\times10^{0}$	$0.186\ 521\ 4\times10^{0}$	$-0.960\ 091\ 5\times10^{-2}$	$0.167\ 888\ 8\times10^{-3}$	-	-
	13	$0.603\ 670\ 1\times10^{0}$	$0.159\ 037\ 1\times10^{0}$	$-0.770\ 652\ 3\times10^{-2}$	$0.131\ 059\ 6\times10^{-3}$	-	-

Table 6.6. Summary of test results for different locations and the factors of safety for the slopes studied (Note. Unless othewise stated, all F_s values assume Row 7)

1	Site studied		B (Fig. 5.1)				C (Fig. 5.5)					D(Fig. 5.7)	E (Fig. 6.22
2	Slip studied		Slip 1			Slip 2	C					D	-
3	Location		B/S1.1	B/-	B/10°	B/S1.2	C/Slip	C/1	C/2	C/3	C/4	D	E.2,E.3
4	Estimated preconsolidation press. (kg/cm²)		10.0	10.0	10.0	10.0	7.0	7.0	7.0	7.0	7.0	7.8	6.1
5	Average normal sress along slip surface (kg/cm²)		0.209	-	-	0.149	0.116	-	-	-	-	0.201	0.147
6	Number of slices used in stability analysis		7	-	-	5	9	-	-	-	-	9	7
7	Assumed depth of water-filled, vertical tension crack (m)		1.57	-	-	1.70	1.20	-	-	-	-	1.38	1.06
8	Liquid limit, w_L (%)		91	63	92	76	77	78	82	73	-	79	55
9	Plastic limit, w_P (%)		33	22	32	28	29	30	30	24	-	26	18
10	Natural moisture content, w_N (%)		34	26	34	33	35	33	33	32	36	29	23
11	Clay fraction, C (%)		63	44	63	56	57	56	57	50	-	52	38
12	Specific gravity of solids, G_s		2.73	2.74	2.78	2.75	2.74	2.77	2.74	2.74	2.73	2.75	2.73
13	Bulk density, γ (t/m³)		1.86	1.97	1.83	1.90	1.83	1.87	1.87	1.81	1.86	1.95	1.97
14	Degree of saturation, S_r (%)		98	95	93	95	93	96	94	88	98	97	91
15	Date of slip		25.12.70 (approx)	-	-	9.4.71	1.11.68	-	-	-	-	20.7.66	-
16	Dates of iswests		-	18.9-6.10.70	24.3-6.4.71	-	-	7-23.6.71	3-21.7.72	11.10-16.11.72, 10.5.73	19.6-3.7.74	30.5-23.6.72	-
17	Mean soil temp. in iswests (°C)		-	13.9	12.0	-	-	15.0	16.1	15.1	16.1	18.0	-
18	Shear strength parameters measured in iswests	c_{is} (kg/cm²)	-	1.257	0.156	-	-	0.100	0.144	0.192	0.061	0.138	-
19		ϕ_{is} (deg)	-	24.6	36.6	-	-	30.0	27.4	27.5	35.1	42.7	-
20	Facfor of safety, F_s by peak strength from iswests		-	-	1.07	1.26* / 1.24#	-	1.26	1.54	-	1.08 / 1.03#	1.13	-
21	F_s by peak strength from iswests assuming a curved tension crack		-	-	1.02	-	-	1.20	1.47	-	1.02	1.09	-
22	Shear strength parameters, pore pressure coefficients, and pore pressures obtained from triaxial tests	c' (kg/cm²)	0.280	-	0.247** / 0.657	0.427** / 0.857	0.041	0.079† / 0.026††	-	-	0.047	0.250 / 0.001§	0.436
23		φ' (deg)	26.4	-	27.0** / 19.0	28.5** / 20.3	23.3	29.8† / 30.5††	-	-	24.3	28.9 / 33.1§	20.9
24		Average values from Table 6.4 u_o (kg/cm²)	-0.393	-	-0.344	-0.298	-0.165	-0.483	-	-	-0.197	-.448	-0.400@
25		B_o	0.046	-	0.044	0.021	0.242	0.103	-	-	0.195	0.070	0.069
26		A_e	0.791	-	0.794	0.848	0.542	0.698	-	-	0.732	0.736	0.818
27		A_f	0.101	-	0.289	-0.076	0.648	0.301	-	-	0.445	0.301	0.289
28		Δu_{ko} (kg/cm²)	0.029	-	0.028	0.014	0.079	0.040	-	-	0.079	0.032	0.026
29		Δu_e (kg/cm²)	-0.036	-	-0.025	-0.020	-0.075	-0.054	-	-	-0.086	-.033	-0.025
30		u_f (kg/cm²)	-0.400	-	-0.341	-0.304	-0.161	-0.497	-	-	-0.204	-.449	-0.399
31	F_s obtained using Rows 22, 23, 30		2.06	-	1.86** / 3.07	3.29** / 5.044#	1.20	3.23± / 2.91††	-	-	1.432Ψ	2.26 / 1.53§	3.46
32	F_s obtained using $(\sigma_1'/\sigma_3')_{max}$ criterion		2.09	-	2.86	3.905	1.14	3.60† / 3.25††	-	-	2.174	2.28 / 1.75§	3.29
33	Shear strength parameters from slow shear box tests	With dilatancy correction, Peak, c_{spc} (kg/cm²)	0.611	0.899Θ / 0.642✓	0.403 / 0.126+	0.373	0.101	0.318	0.568	0.390	-	-	-
34		With dilatancy correction, Peak, ϕ_{spc} (deg)	31.2	36.2Θ / 42.1✓	30.0 / 30.1+	41.3	29.0	25.9	29.7	31.4	-	-	-
35		With dilatancy correction, Quasi-residual, c_{src} (kg/cm²)	0.126	0.132Θ / 0.263✓	0.087 / 0.173+	0.214	0.140	0.163	-	-	-	-	-
36		With dilatancy correction, Quasi-residual, ϕ_{src} (deg)	18.0	29.1Θ / 24.8✓	30.9 / 19.3+	16.4	18.2	20.2	-	-	-	-	-
37		Without dilatancy correction, Peak, c_{sp} (kg/cm²)	0.748	1.028Θ / 0.777✓	0.483 / 0.000+	0.563	0.137	0.429	0.558	0.419	-	-	-
38		Without dilatancy correction, Peak, ϕ_{sp} (deg)	29.2	31.2Θ / 37.0✓	29.8 / 29.6+	39.7	26.0	22.5	26.5	28.1	-	-	-
39		Without dilatancy correction, Quasi-residual, c_{sr} (kg/cm²)	0.236	0.275Θ / 0.296✓	0.158 / 0.212+	0.257	0.160	0.205	-	-	-	-	-
40		Without dilatancy correction, Quasi-residual, ϕ_{sr} (deg)	15.6	28.4Θ / 25.0✓	29.1 / 18.5+	15.8	18.1	19.7	-	-	-	-	-
41	F_s obtained from slow shear box tests using u_f values in Row 30	With dilatancy correction, Peak	3.50	4.82Θ / 4.23✓	2.55 / 1.55+	3.75	1.90	4.63	6.91§§	-	-	-	-
42		With dilatancy correction, Quasi-resl.	1.14	1.65Θ / 1.93✓	1.45 / 1.29+	1.70	1.73	2.92	-	-	-	-	-
43		Without dilatancy correction, Peak	3.91	5.05Θ / 4.42✓	2.84 / 1.08+	4.59	2.03	5.14	6.51§§	-	-	-	-
44		Without dilatancy correction, Quasi-resl.	1.45	2.14Θ / 2.06✓	1.62 / 1.40+	1.89	1.88	3.19	-	-	-	-	-
45	F_s by residual strength from iswests		0.86	-	-	0.95	-	0.89	0.93	-	0.85	0.58	-
46	Average K_o		1.57	-	-	1.64	1.38	-	-	-	-	1.42	1.40

* Using iswest series B/10° results
† From the results of seven tests
@ From field measurements
Θ Shear plane horizontal
✓ Shear plane inclined to horizontal between 25° and 45°
\+ Specimen flooded with water after application of normal load
** Obtained from hand-fitted envelopes
†† From the results of eight tests
# By Janbu's (1973) GPS
§ From tests on 102 mm dia. specimens

‡

Assumption	ΔV = 0	ΔV=0; ε_D=0
F_s	4.987	4.992

Ψ

Assumption	ΔV = 0	φ = 0	$\Delta\varepsilon_{so}+\Delta\varepsilon_s$=0	B.&H.'s membrane corrections valid	All these combined
F_s	1.432	1.695	1.427	2.572	2.559

§§ Using u_f values (Row 30) from triaxial tests for location C/1

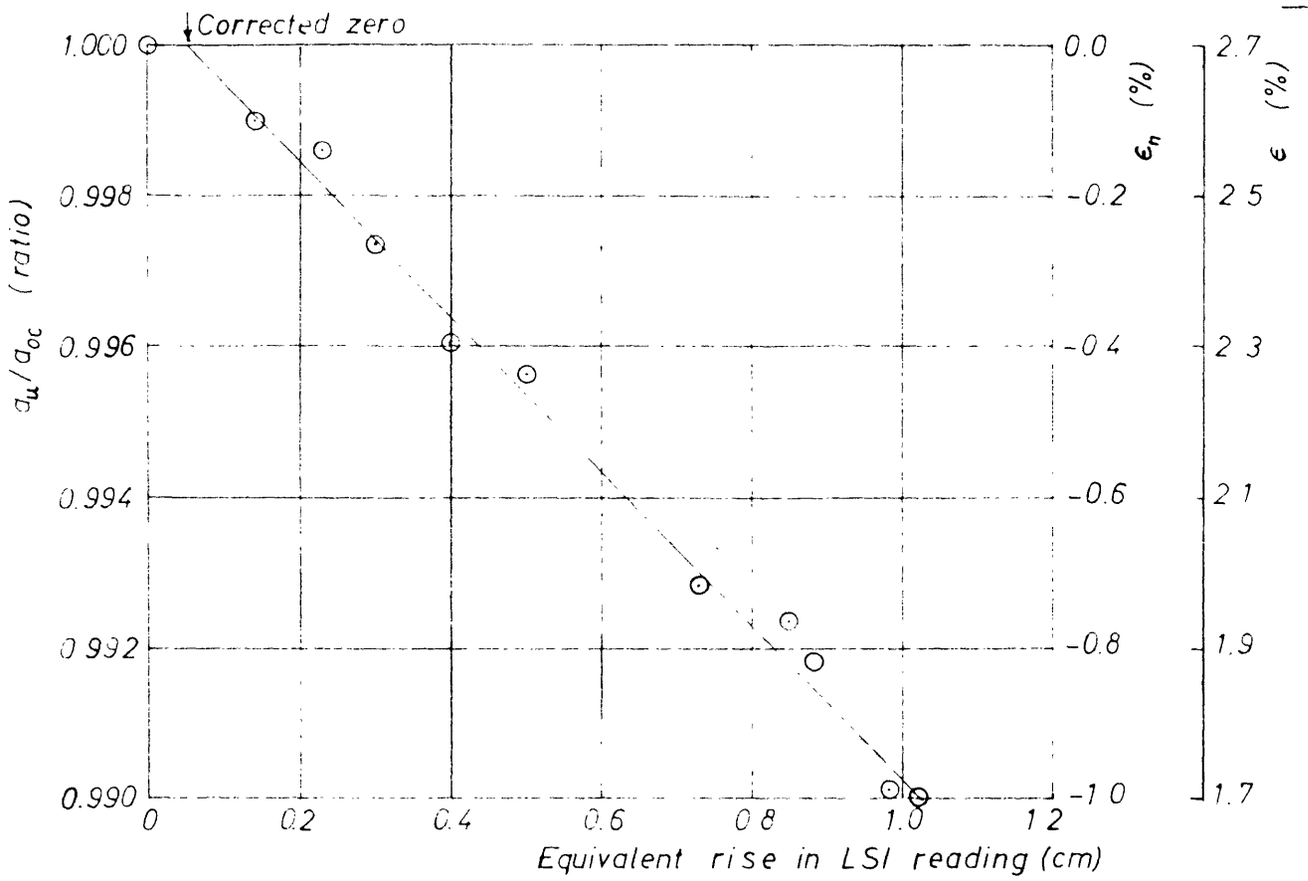

Fig. 6.1. Typical plot of a_u/a_{oc} versus equivalent rise in LSI reading (Test 2/8, Table 6.4)

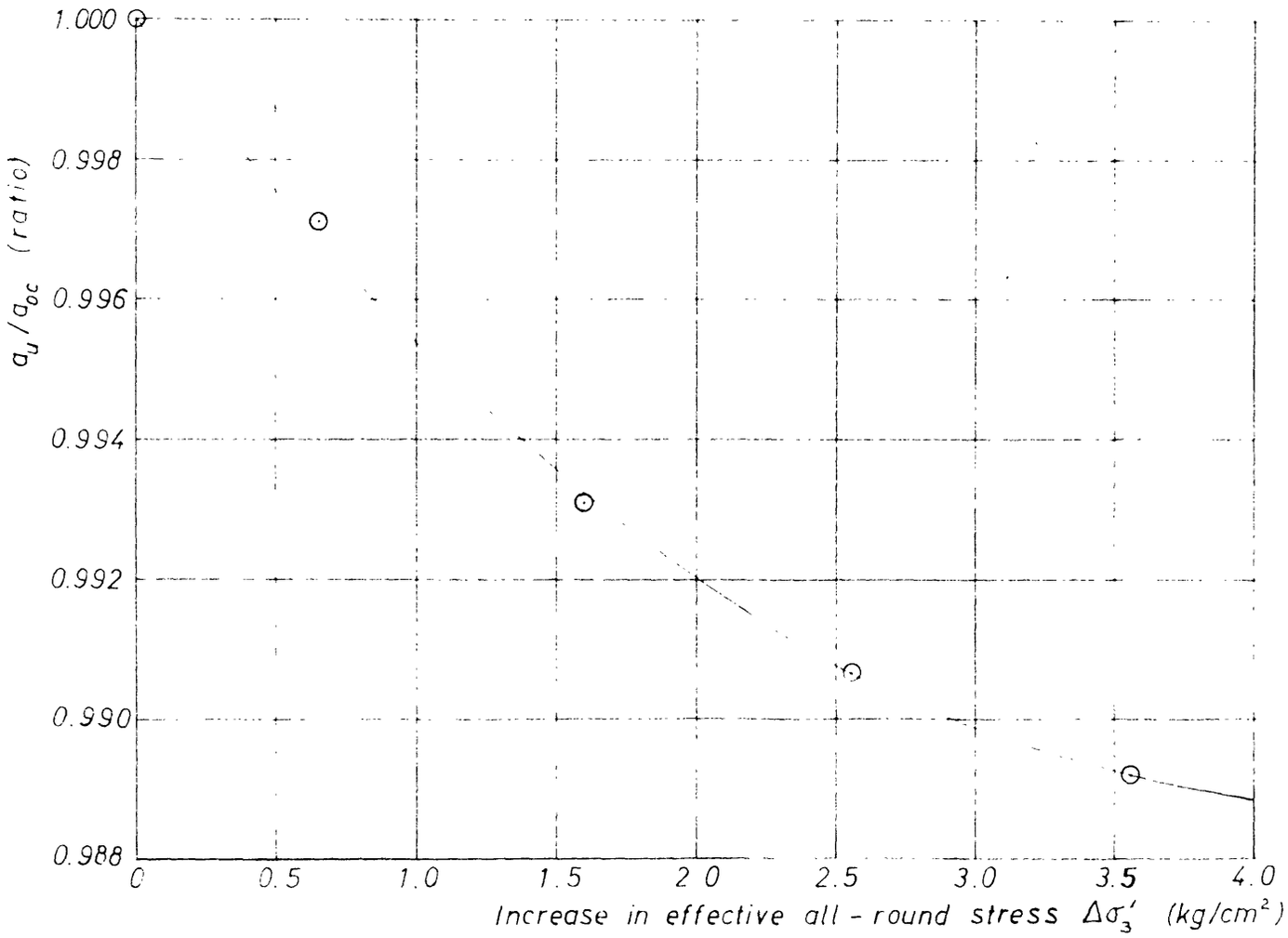

Fig. 6.2. Typical plot of a_u/a_{oc} versus increase in effective all-round stress (Test 2/8, Table 6.4)

(a) Mode 1 : by bulging
(Test 1/9,
Tables 6.1 - 6.3)

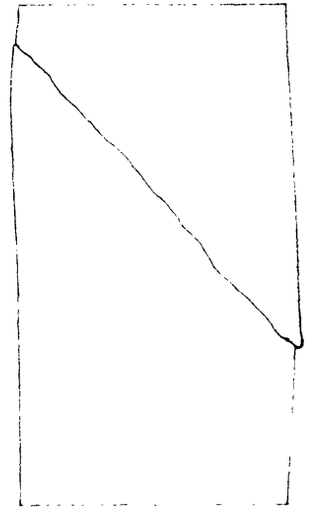

(b) Mode 2 : bulging followed by
shear along a single plane
(Test 1/5, Tables 6.1 - 6.3)

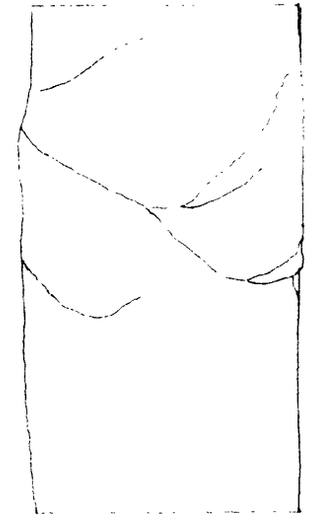

Front view

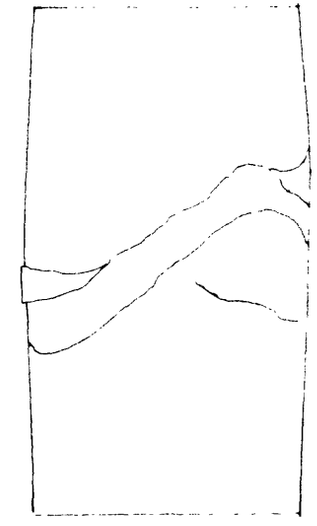

Rear view

(c) Mode 3 : bulging followed by splitting along
a number of planes
(Test 1/1, Tables 6.1 - 6.3)

Fig. 6.3 . Examples of main modes of failure in triaxial shear tests (Table 6.3, Column 2)

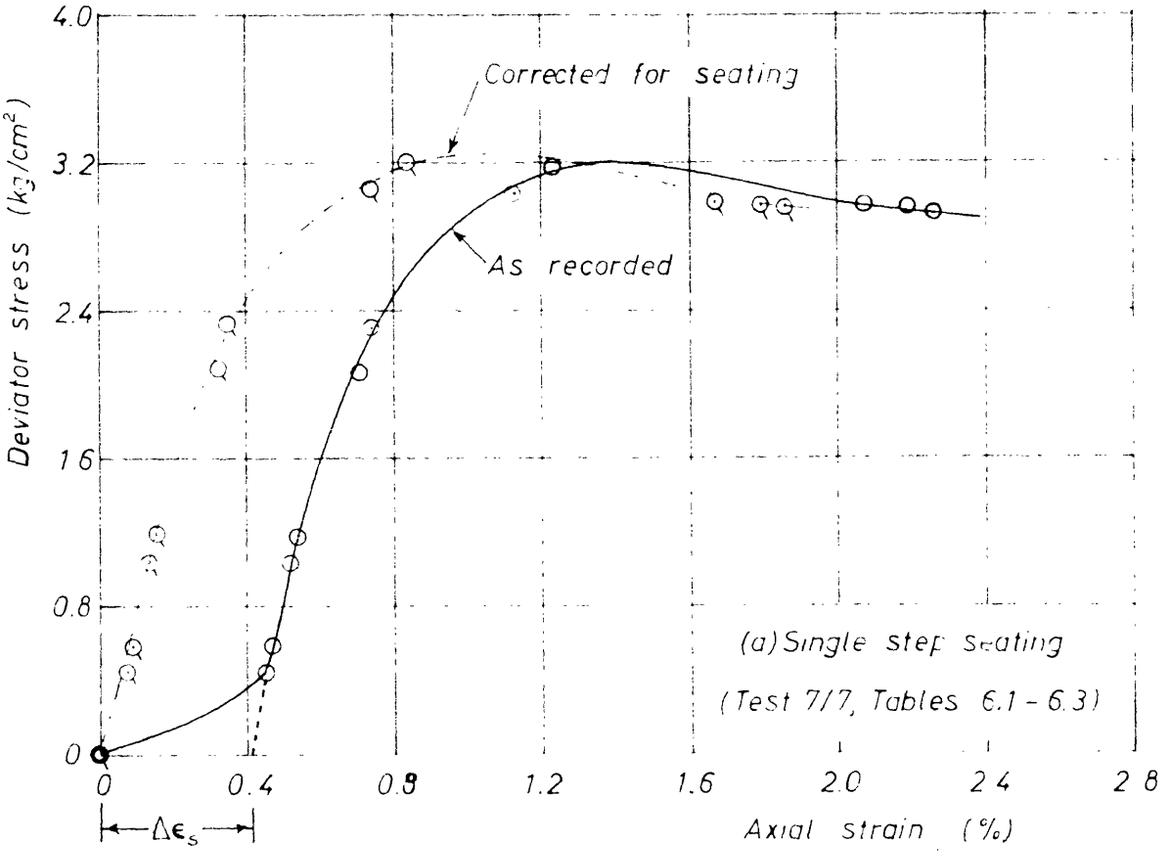

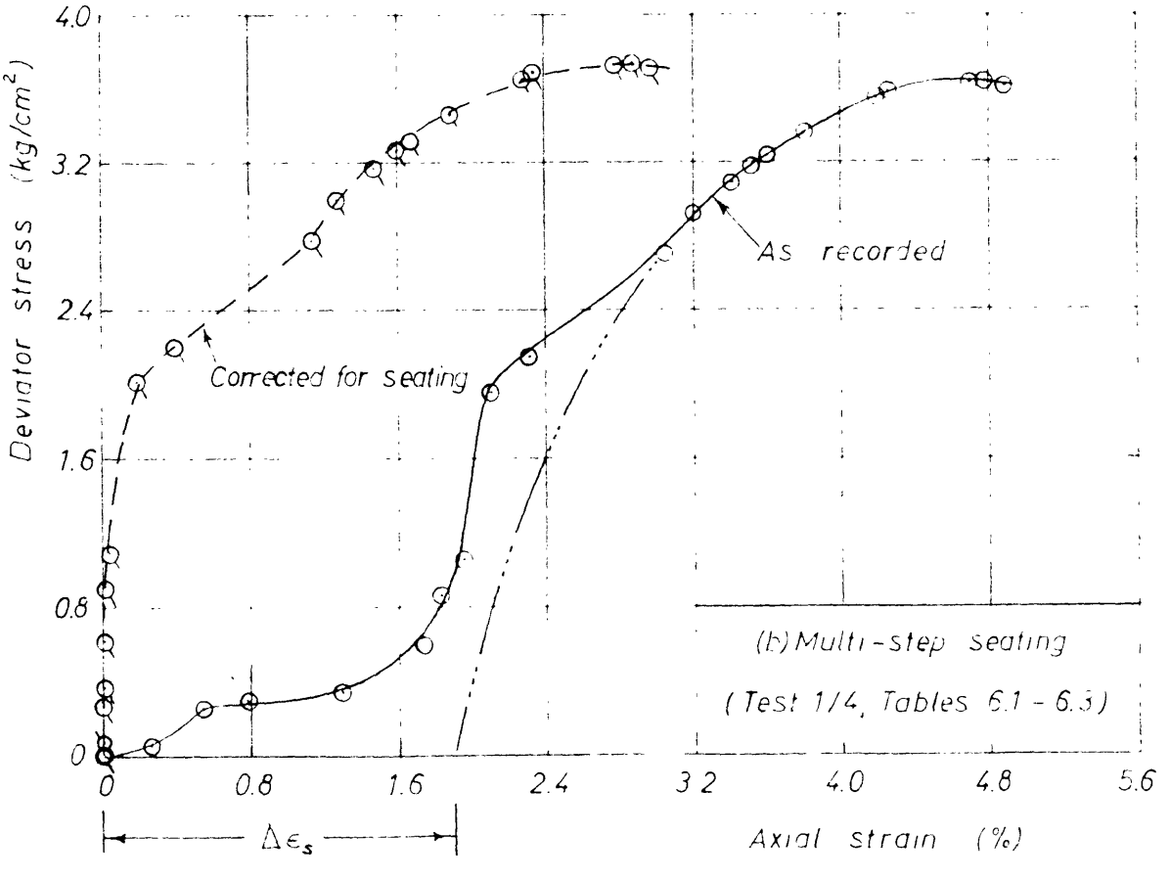

Fig 6.4 Typical curves of deviator stress vs. axial strain in triaxial tests

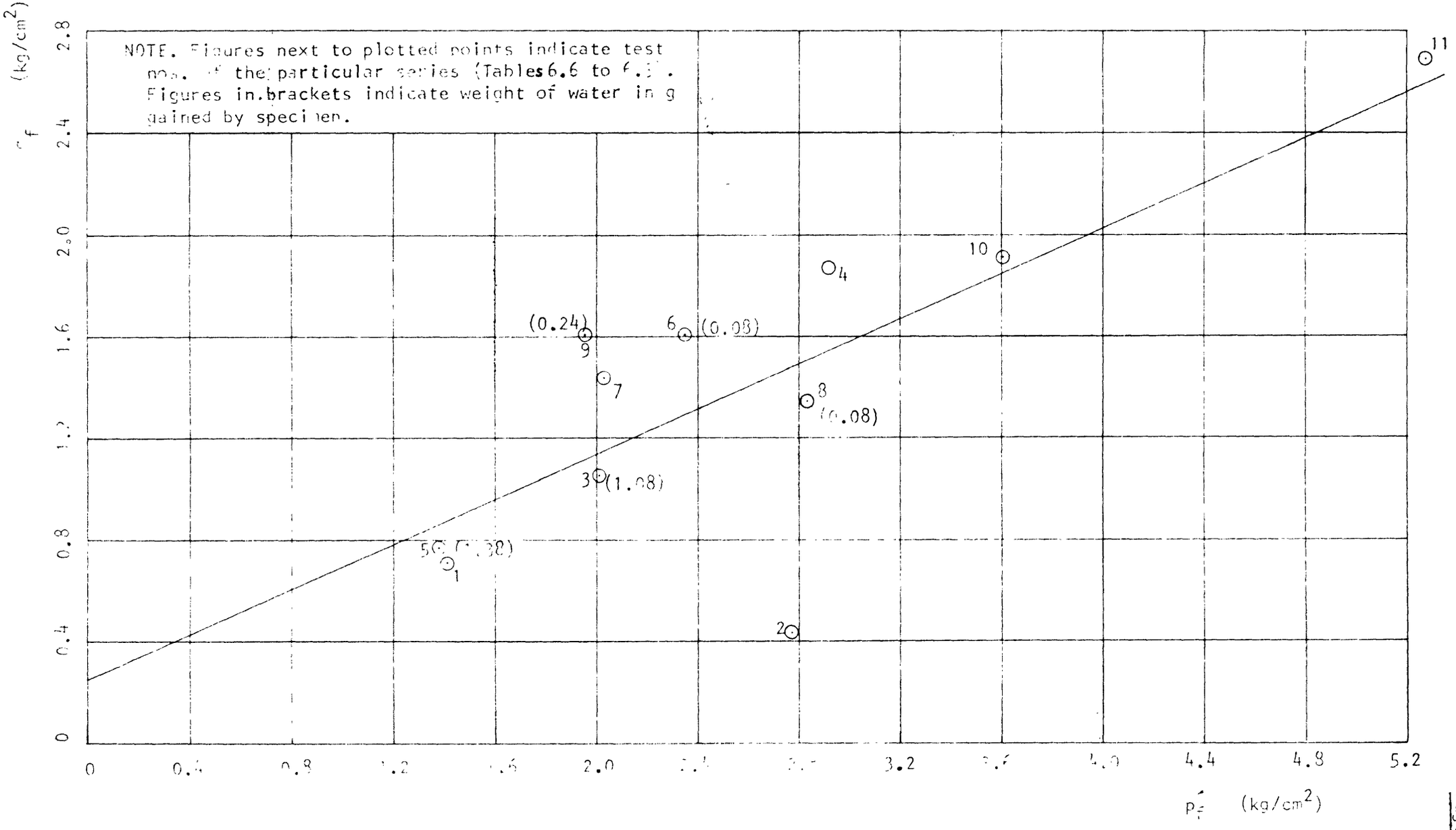

Fig. 6.[illegible] Plot of p_f' versus σ_f for triaxial test series 1

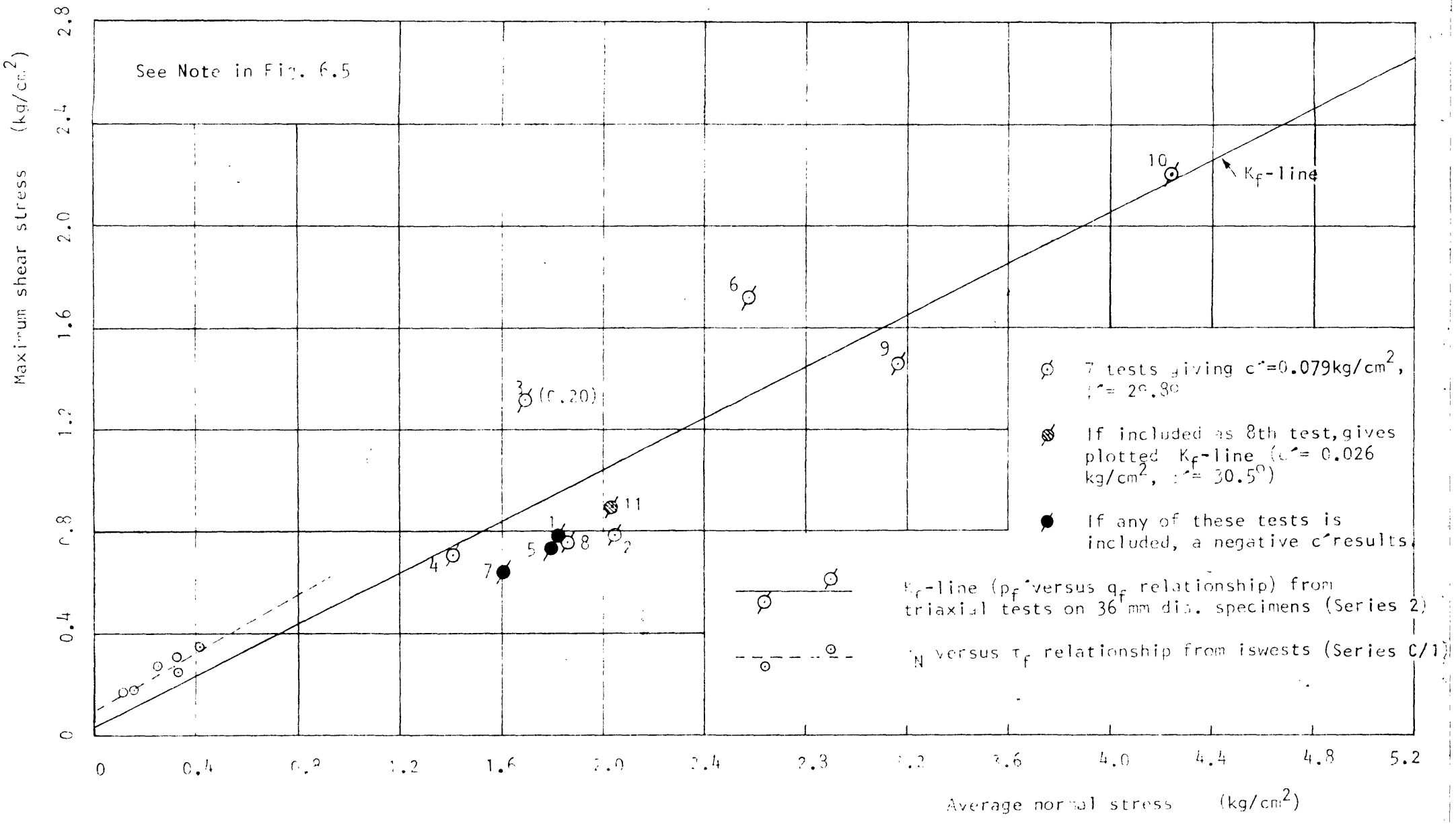

Fig. 6.6. Comparison of relative scatter obtained in iswests and in triaxial tests on small laboratory specimens (Location C/1).

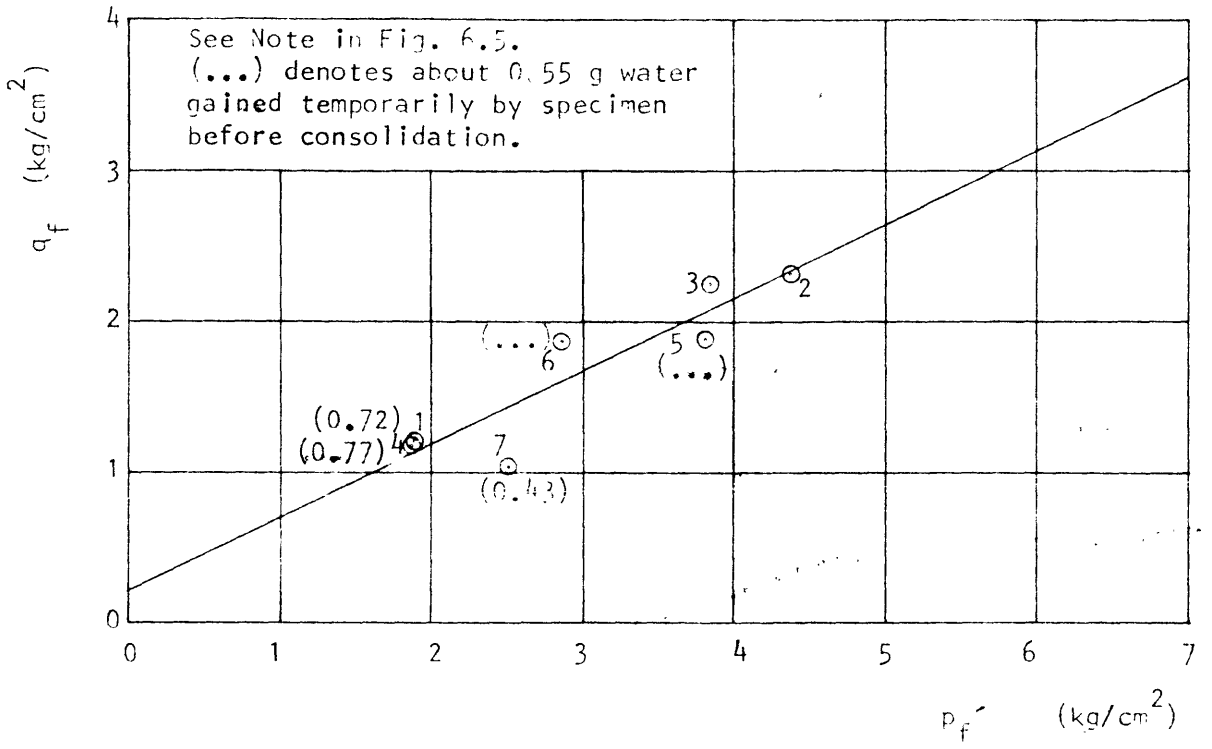

Fig. 6.7. Plot of p_f' versus q_f for triaxial test series 3

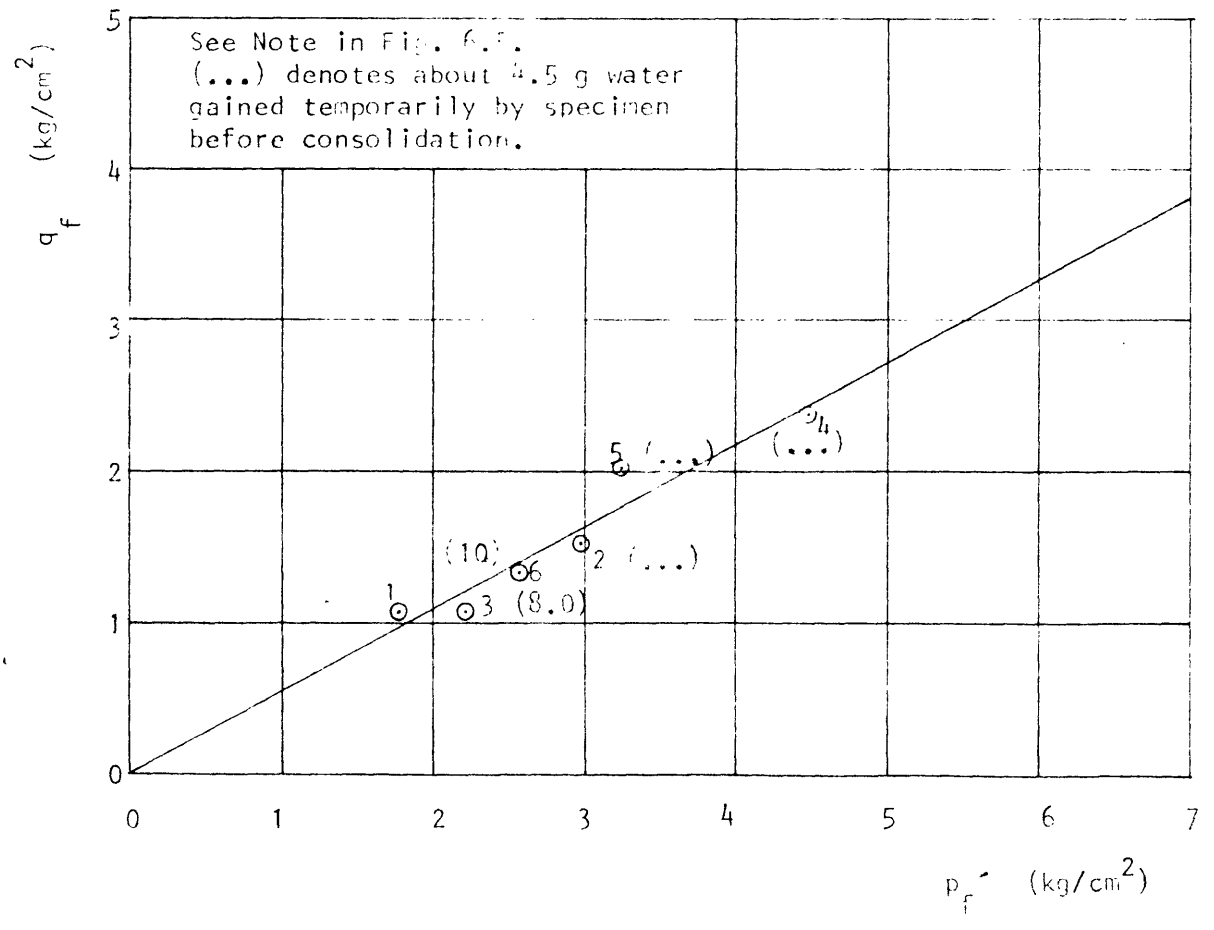

Fig. 6.8. Plot of p_f' versus q_f for triaxial test series 4

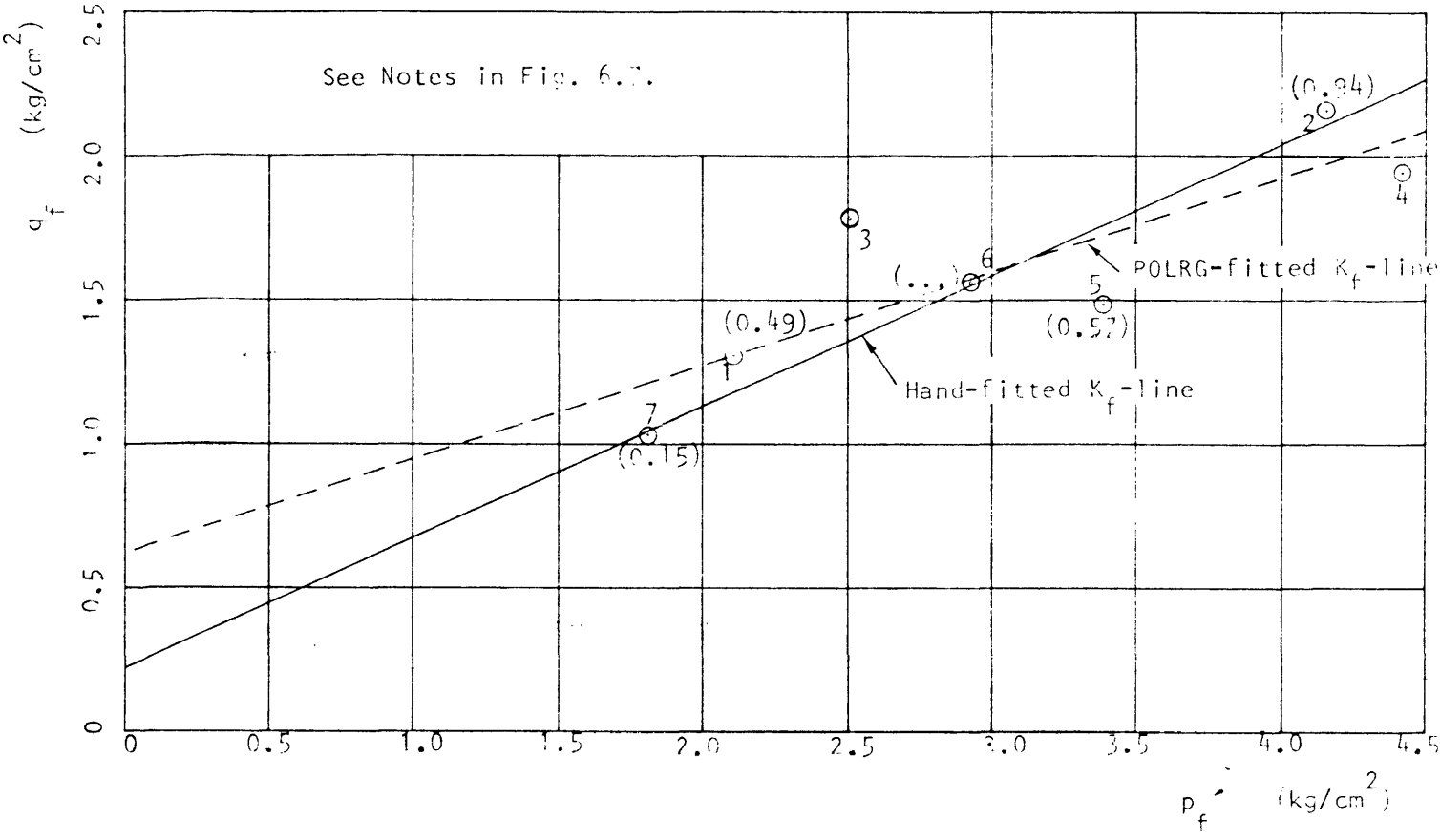

Fig. 6.9. Plot of p_f' versus q_f for triaxial test series 5

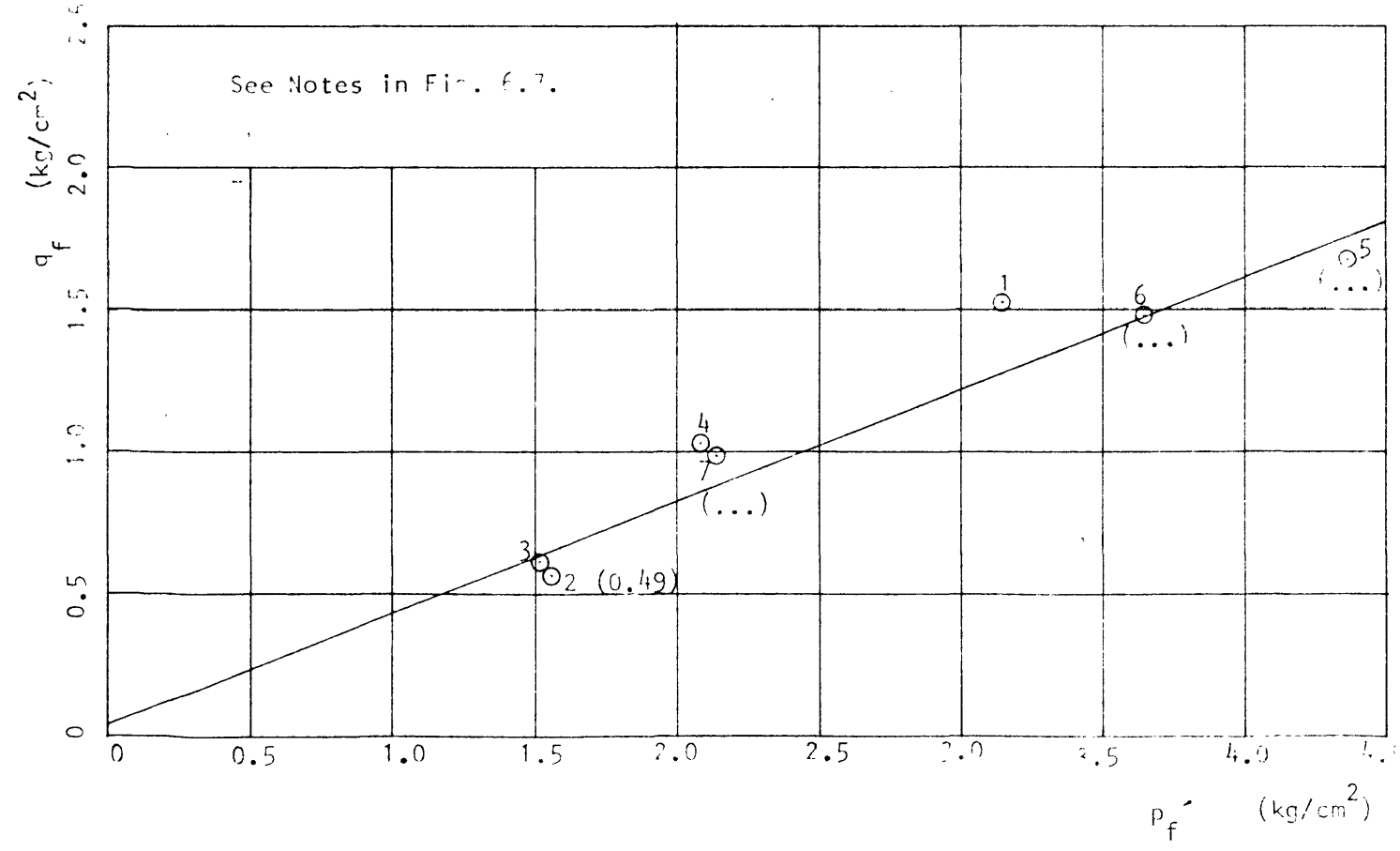

Fig. 6.10. Plot of p_f' versus q_f for triaxial test series 6

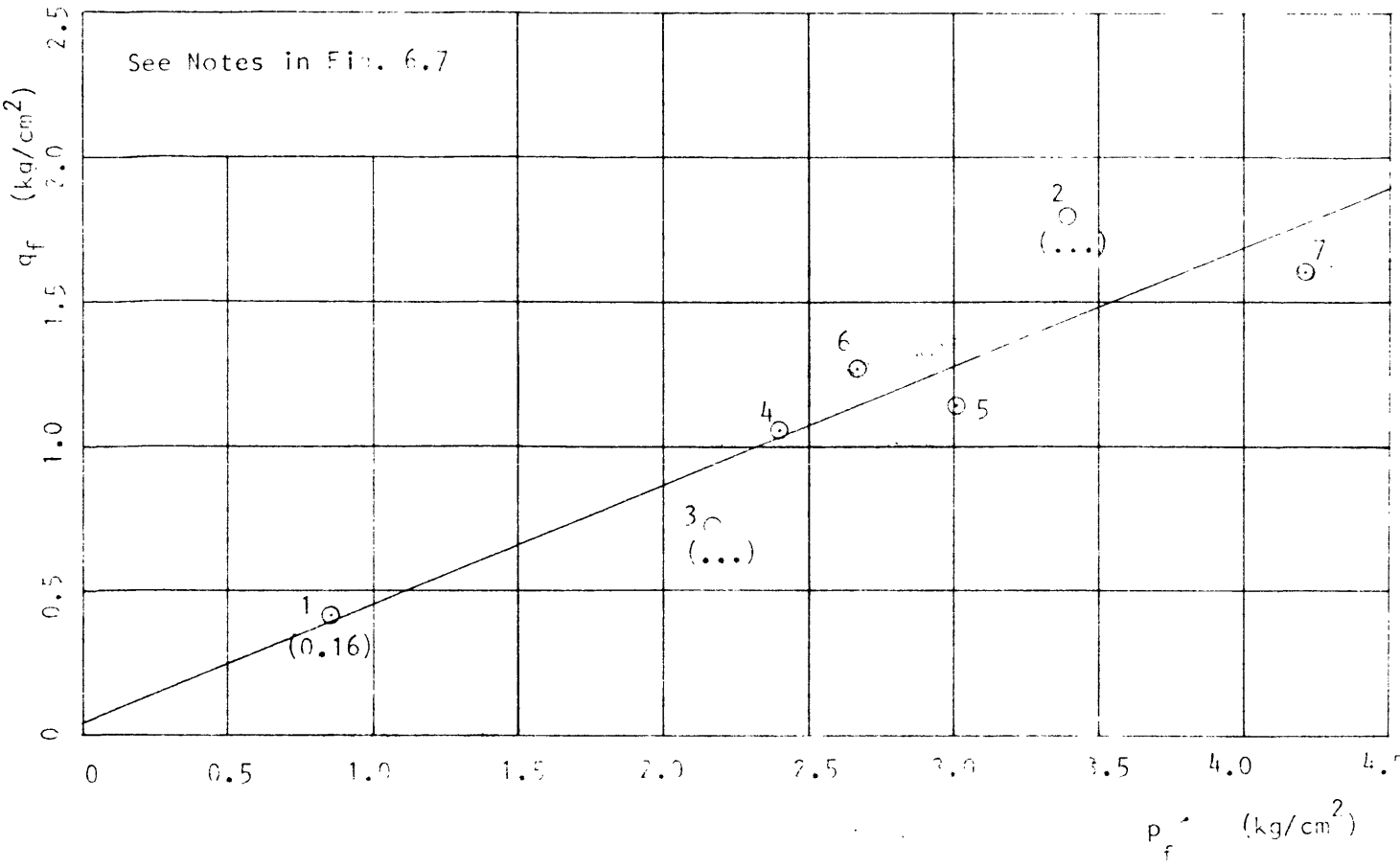

Fig. 6.11. Plot of p_f' versus q_f for triaxial test series 7

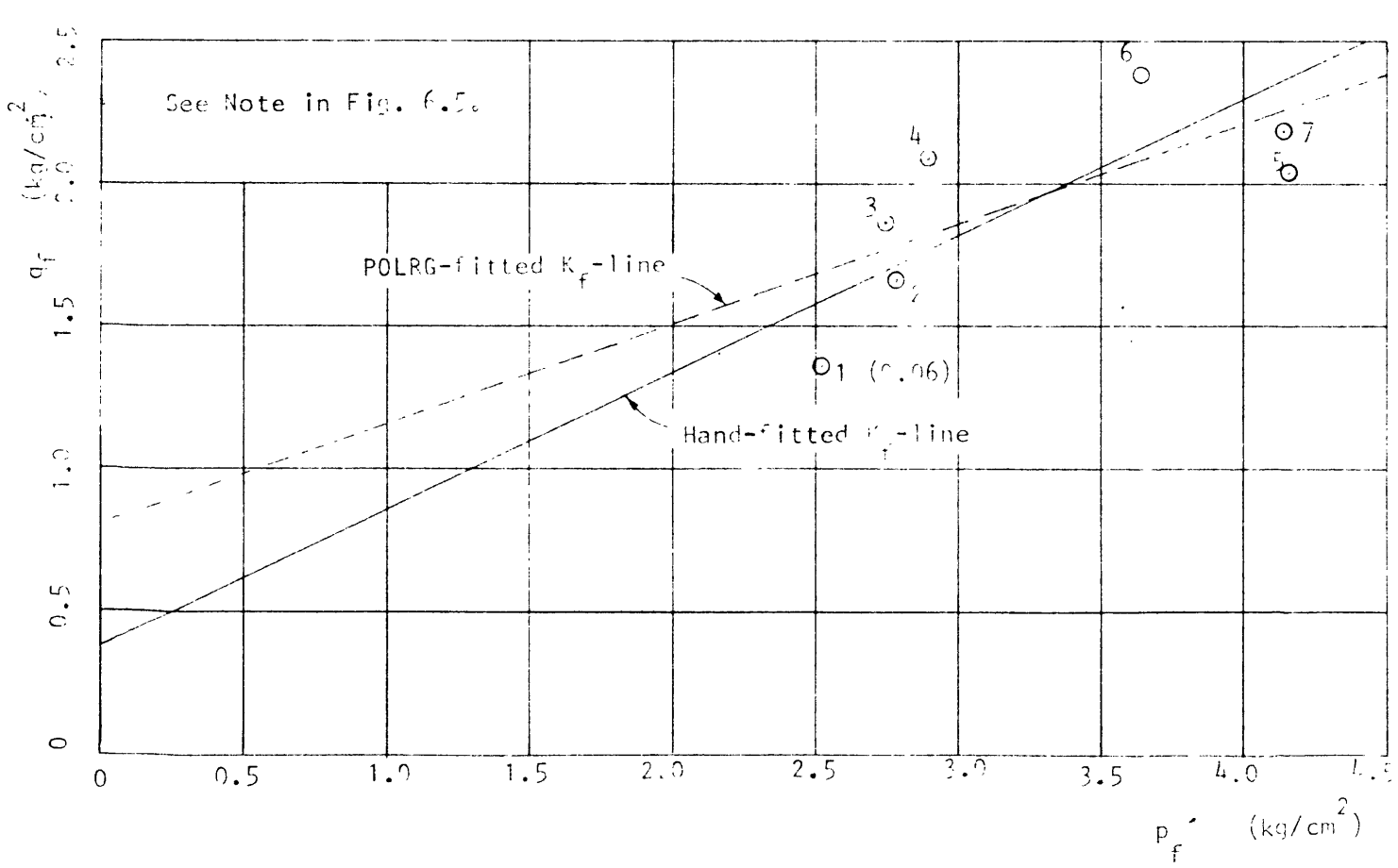

Fig. 6.12. Plot of p_f' versus q_f for triaxial test series 8

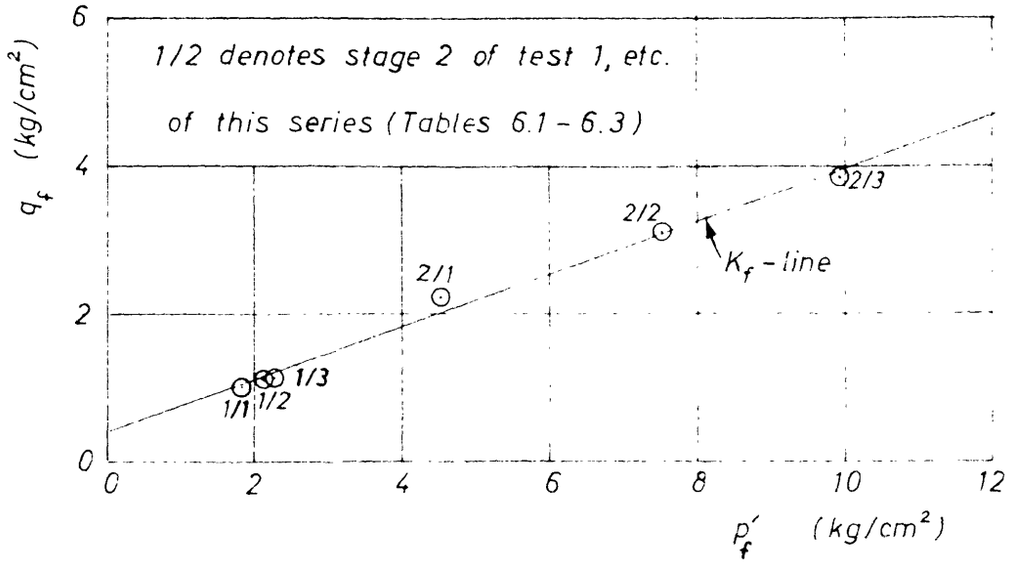

Fig. 6.13 Plot of p_f' versus q_f for triaxial test series 9 (multi-stage)

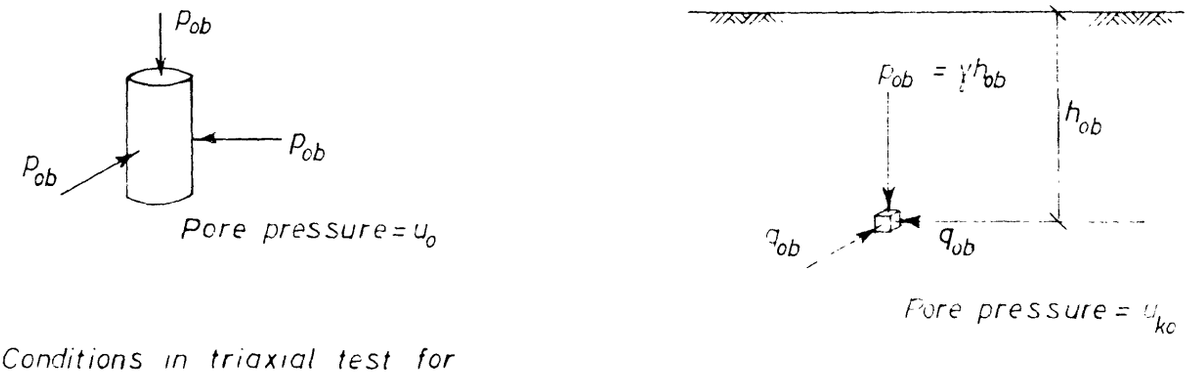

(a) Conditions in triaxial test for measurement of u_o

(b) Geostatic condition

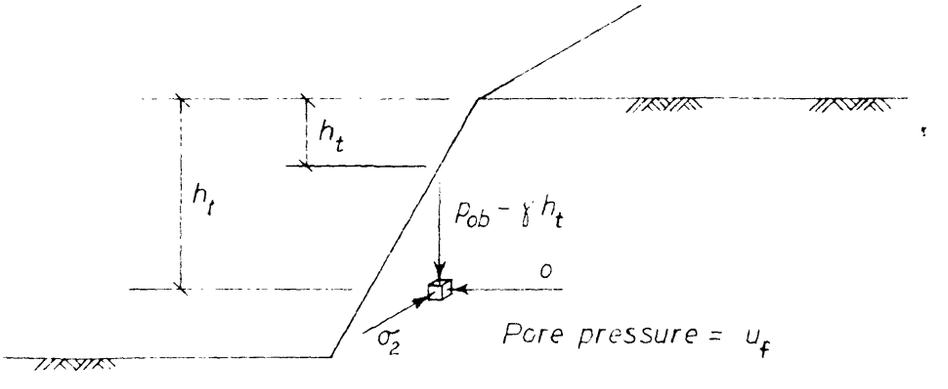

(c) Assumed conditions after excavation

Fig. 6.14. Steps in estimating pore pressures in cut slopes from results of triaxial tests

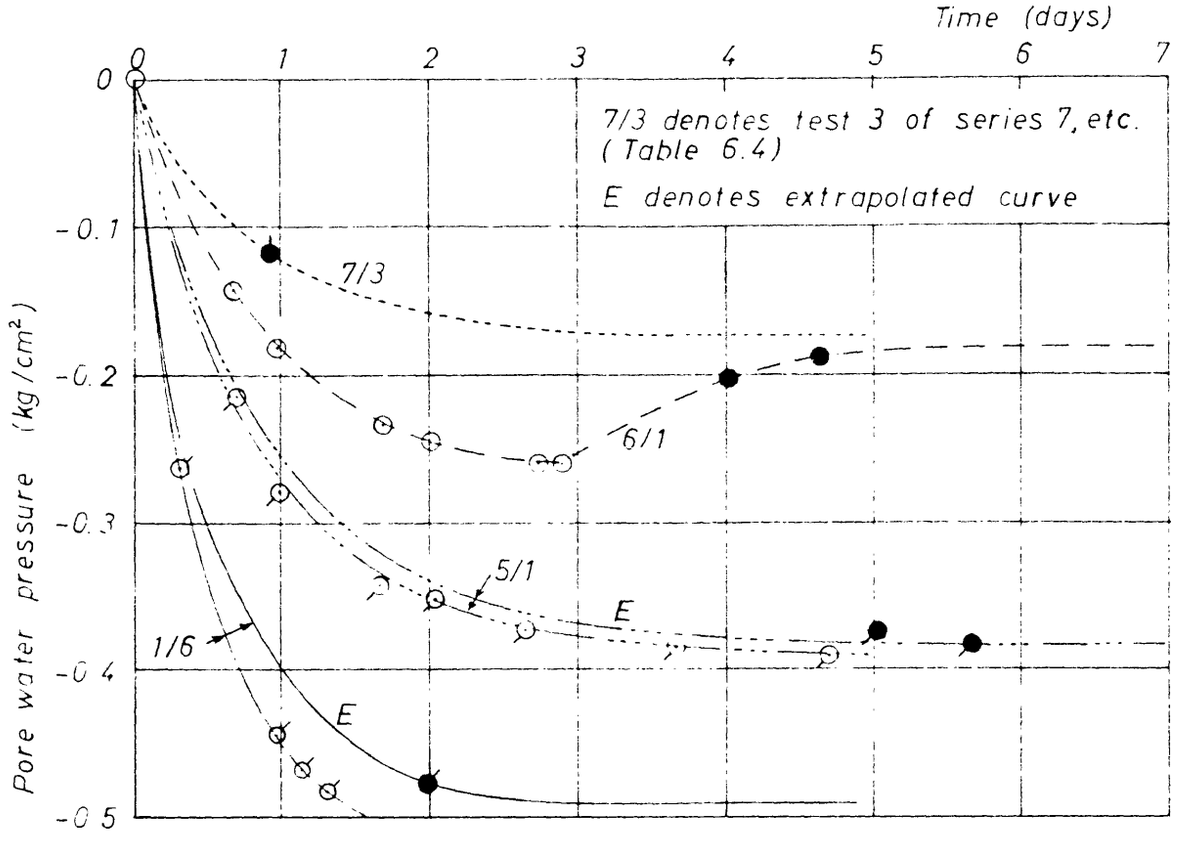

Fig. 6.15 Typical results of tests for estimating pore pressure u_o

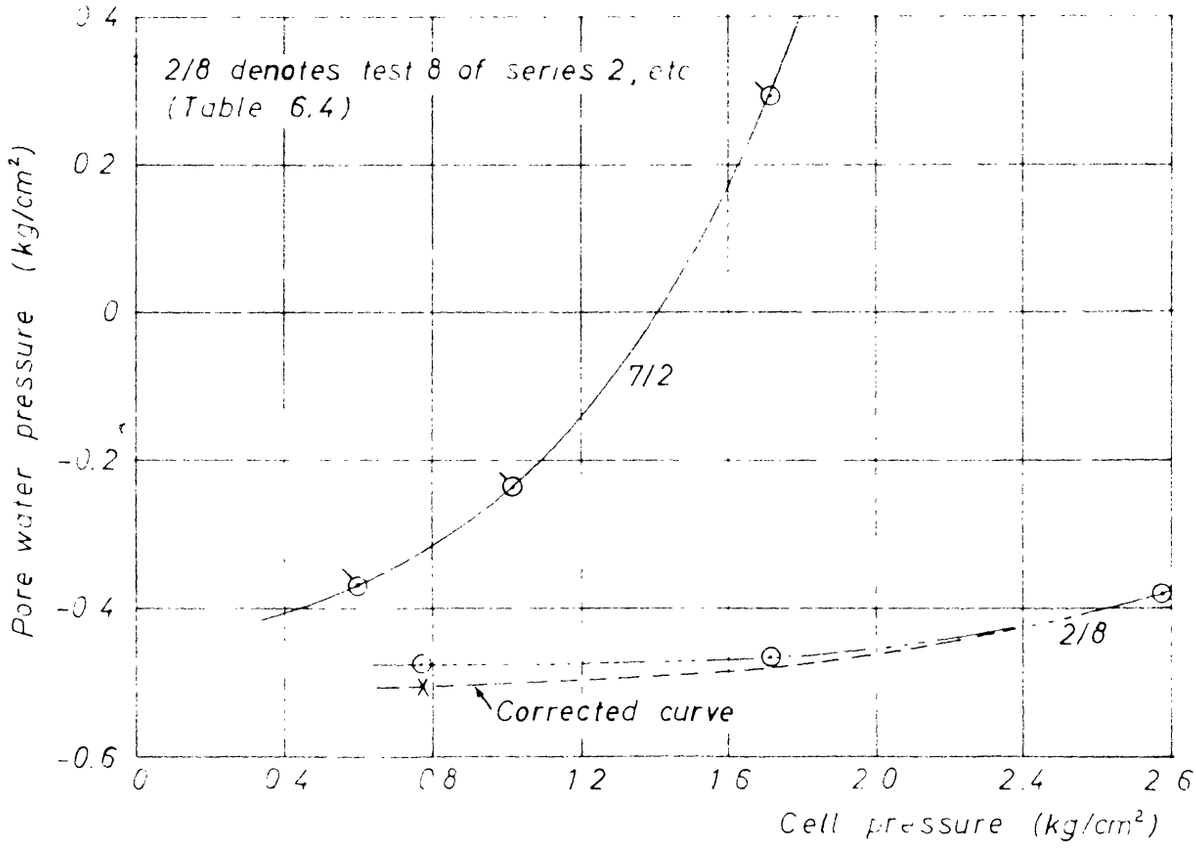

Fig. 6.16. Typical results of tests for determination of pore pressure coefficient B_o

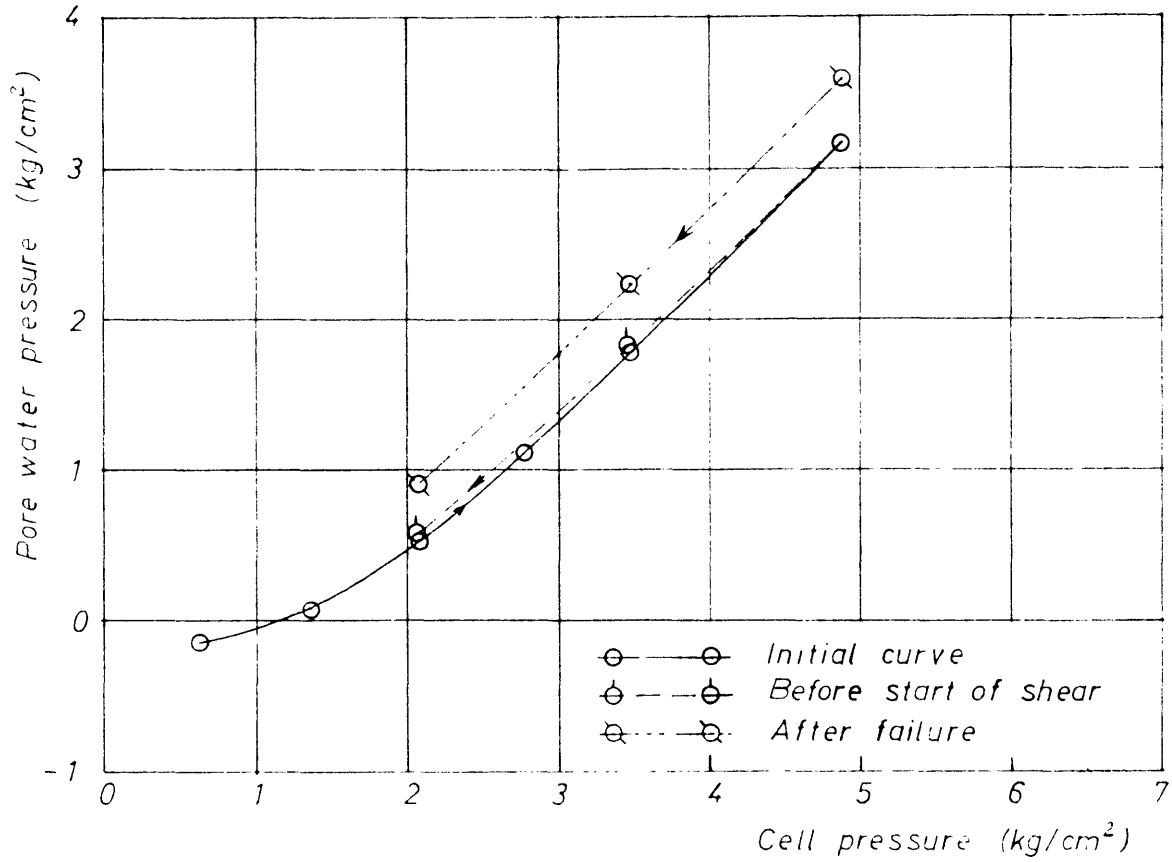

Fig. 6.17. Typical pore pressure vs. cell pressure curves under different conditions (test 6/2, Table 6.4)

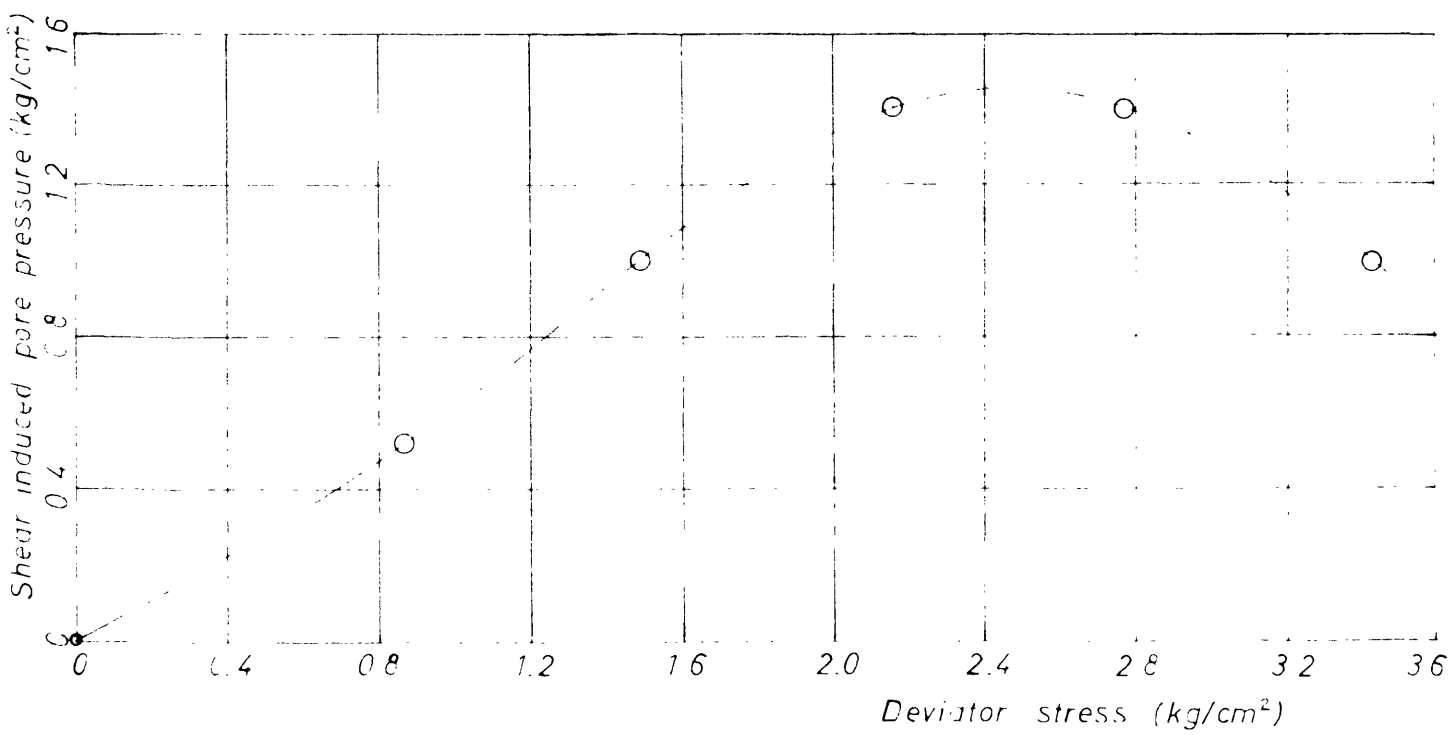

Fig. 6.18. Typical variation of shear induced pore pressure with deviator stress (test 1/5, Table 6.4)

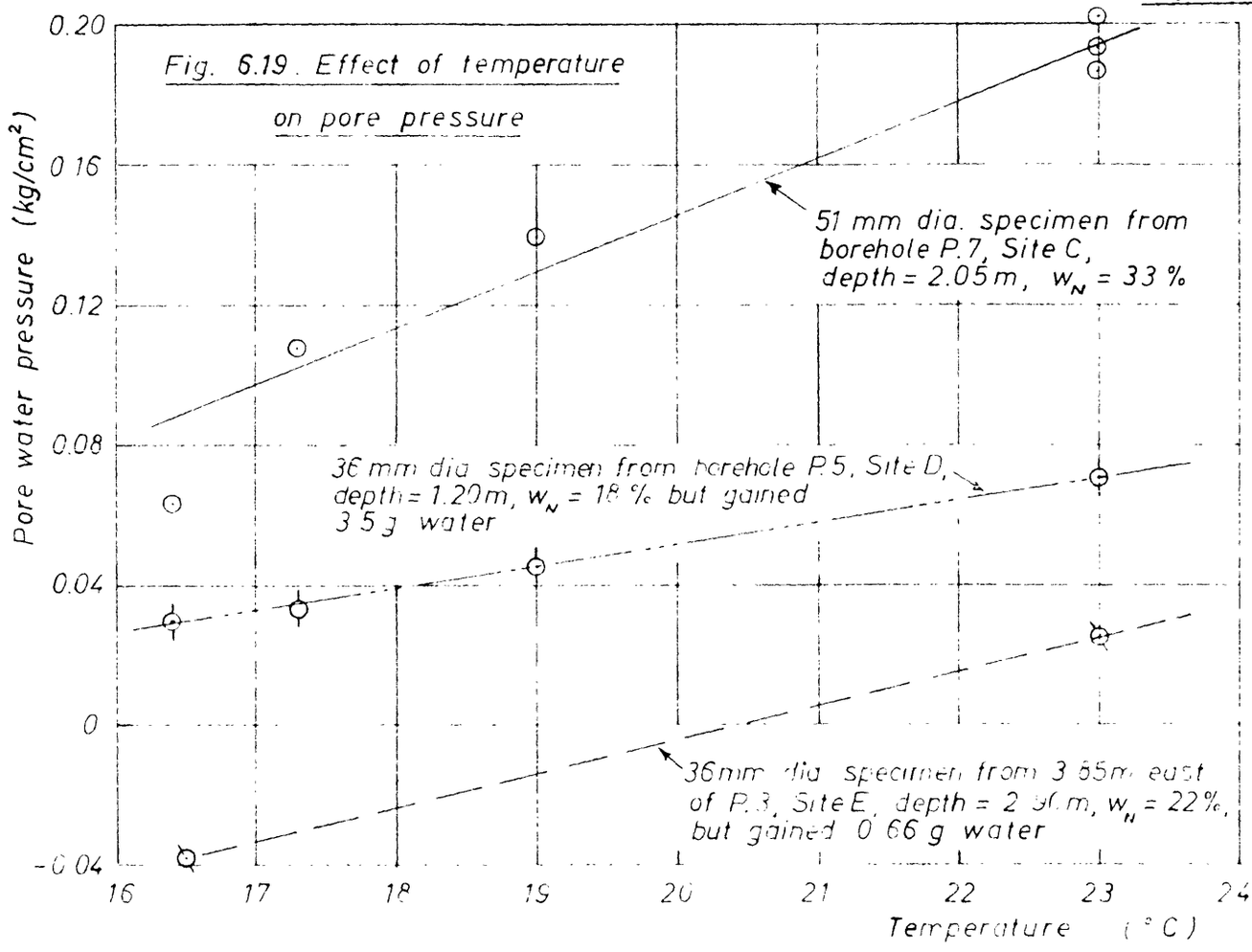

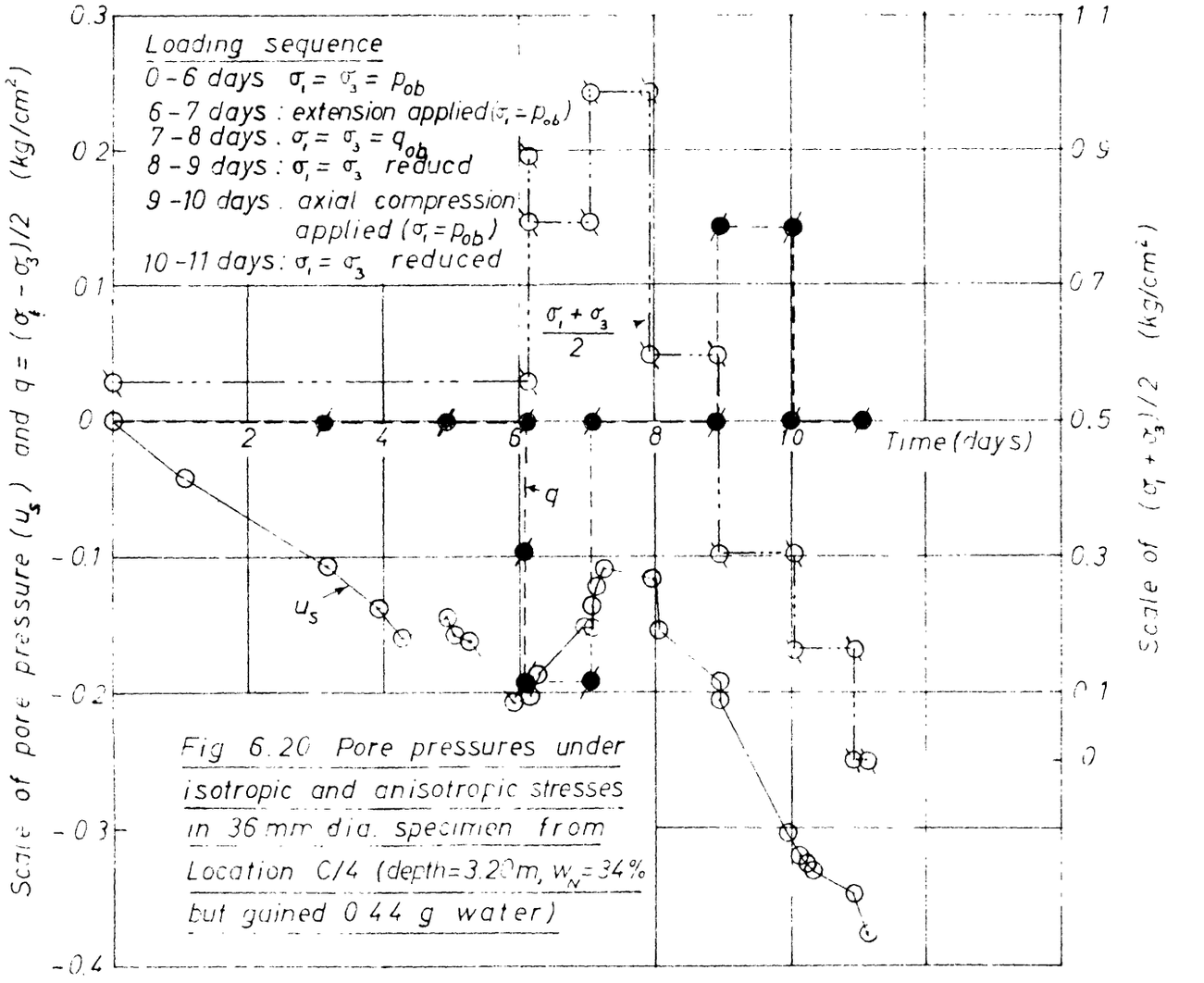

Fig. 6.20 Pore pressures under isotropic and anisotropic stresses in 36 mm dia. specimen from Location C/4 (depth=3.20m, w_N=34% but gained 0.44 g water)

All dimensions in mm

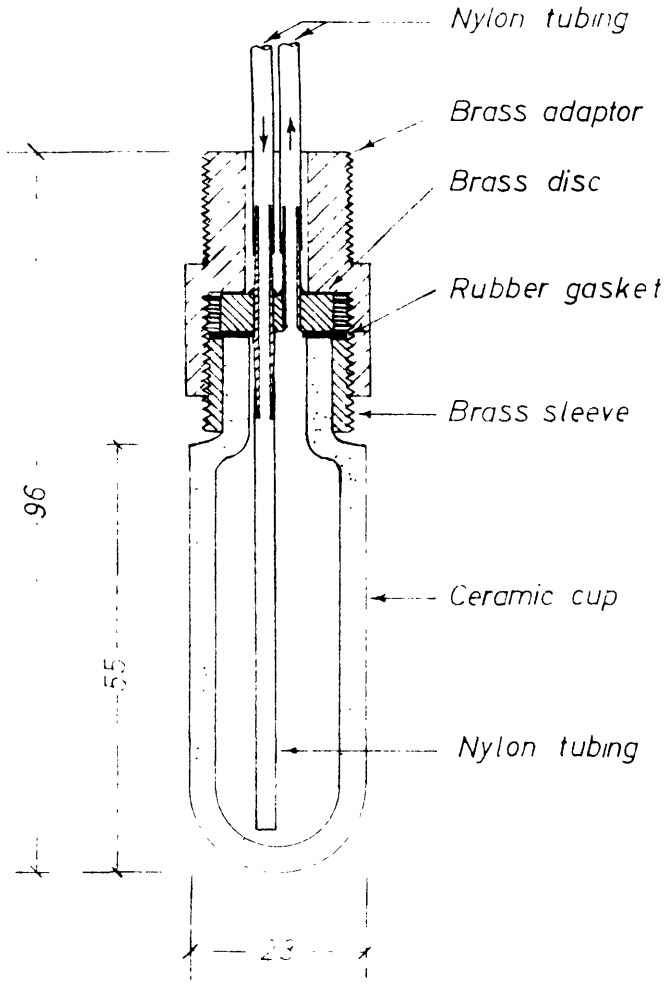

(a) Piezometer tip

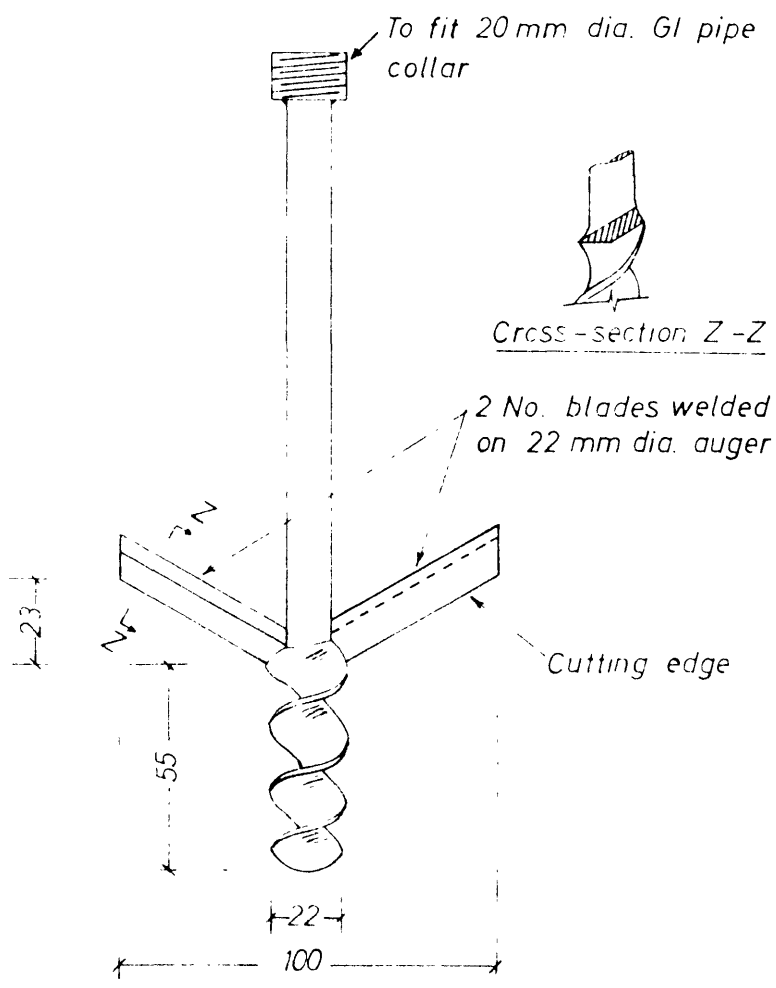

(b) Tool for shaping bottom of borehole

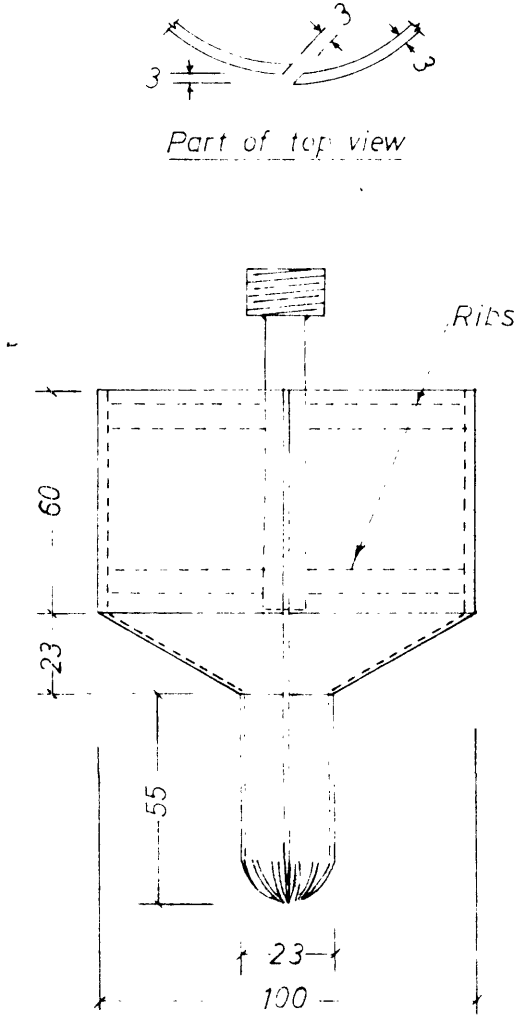

(c) Tool for cleaning shaped bottom of borehole

Fig. 6.21. Equipment devised for in situ pore pressure measurements

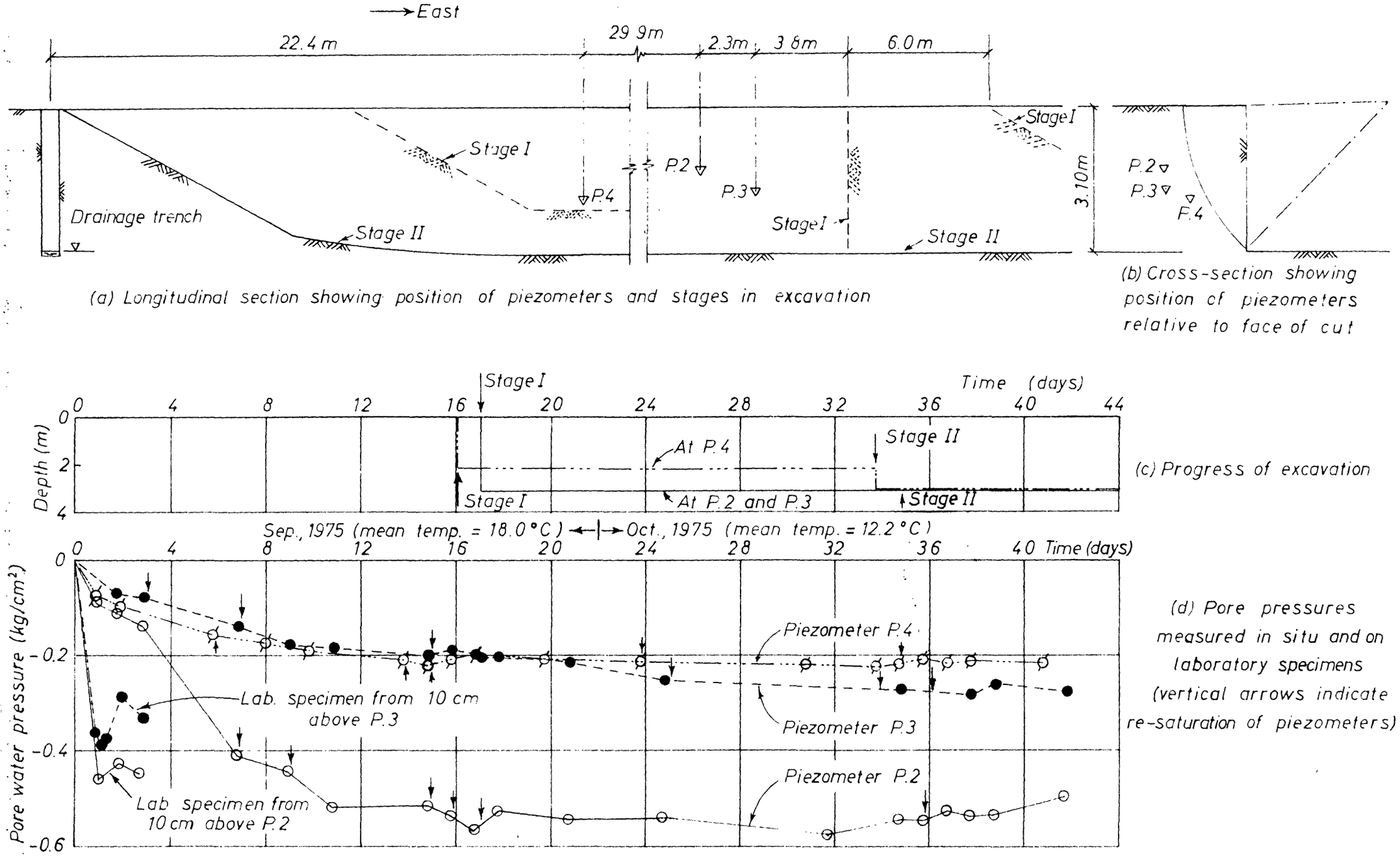

Fig 6.22. Effect of excavation on pore pressures in the slope at Site E

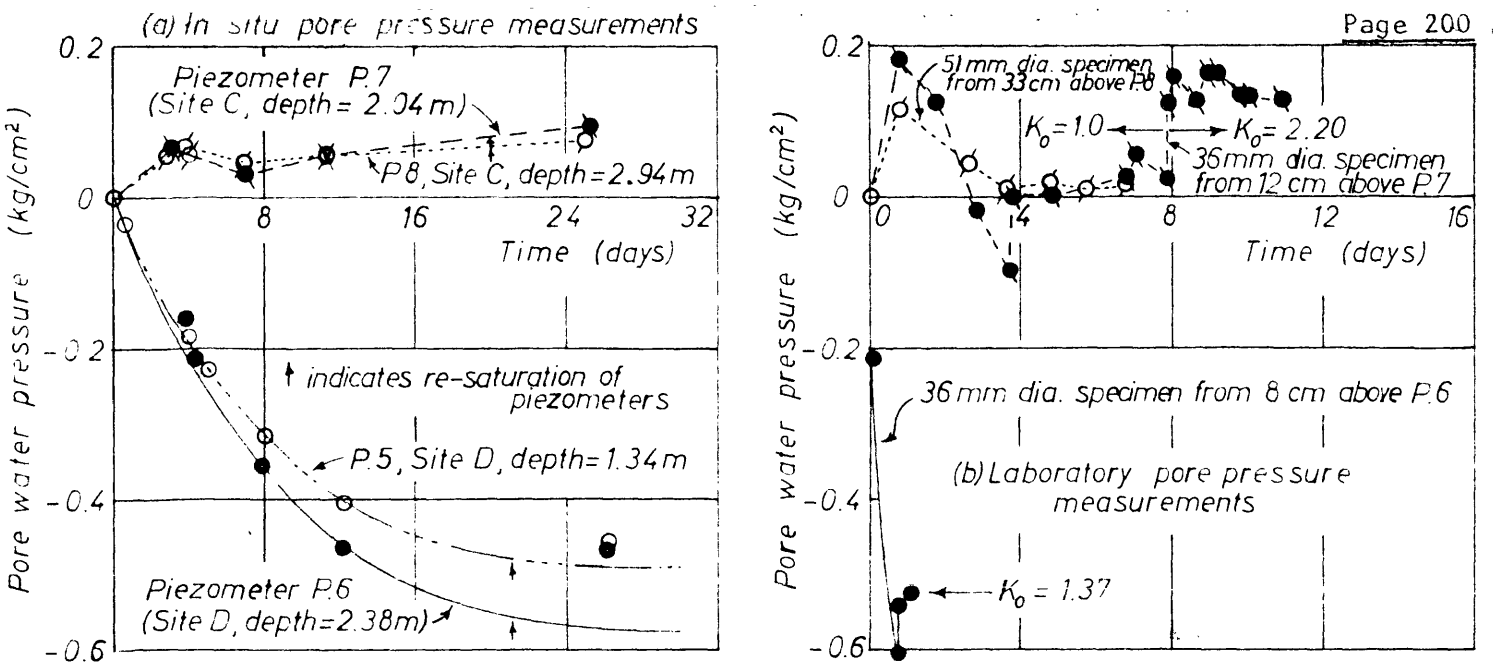

Fig. 6.23. Comparison of in situ and laboratory measurements of pore pressure at Sites C and D

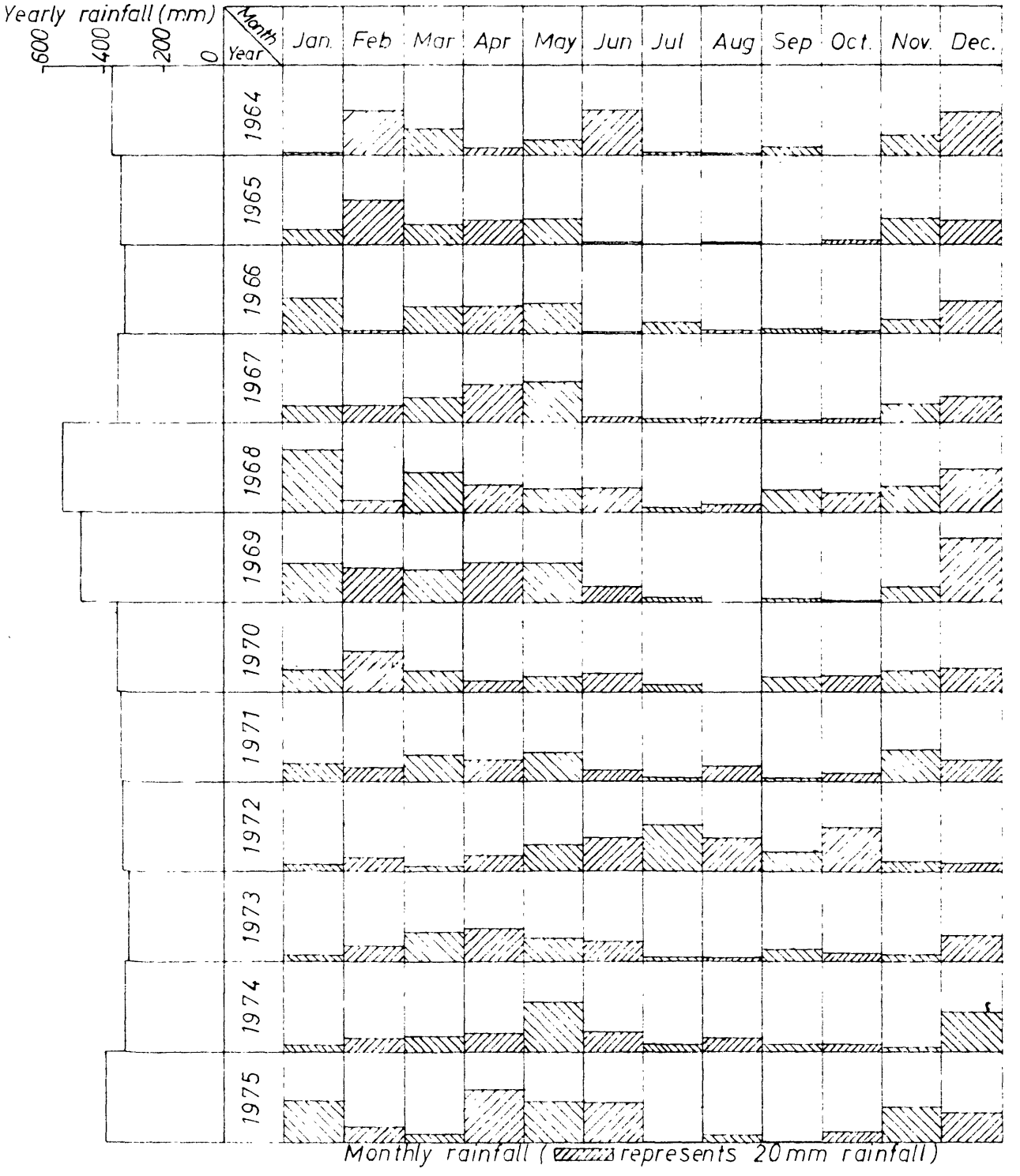

Fig. 6.24. Monthly and yearly rainfall at M.E.T.U. (Sites C, D, E)
(Plotted from records made available by courtesy of the staff of the General Directorate of Turkish State Meteorological Office)

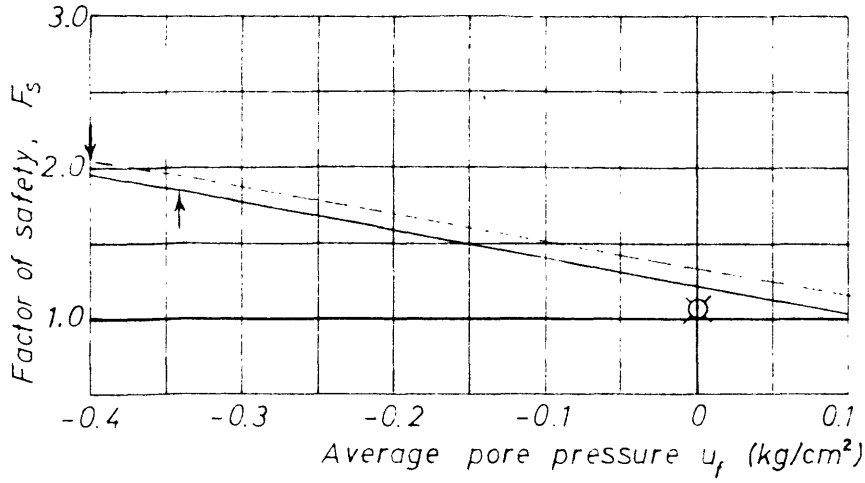

(a) Slip 1 at Site B

Location	Representation	
	Triaxial tests	Iswests
B/Sl.1	– – – – – –	
B/10°	———	⊠

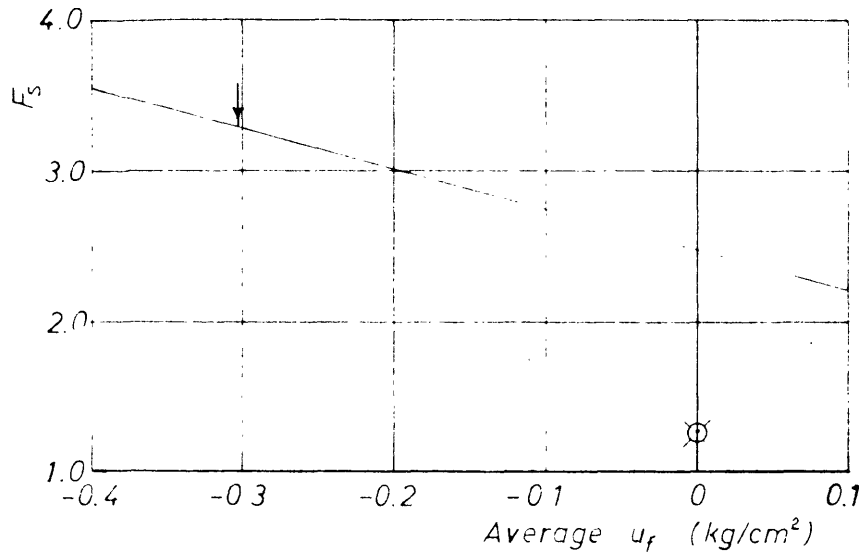

(b) Slip 2 at Site B

Location	Representation	
	Tiaxial tests	Iswests
B/Sl.2	———	
B/10°		⊠

NOTE. (1) Tension cracks given in Table 6.6 Row 7 assumed.
(2) Vertical arrows denote pore pressures estimated as in Section 6.3.

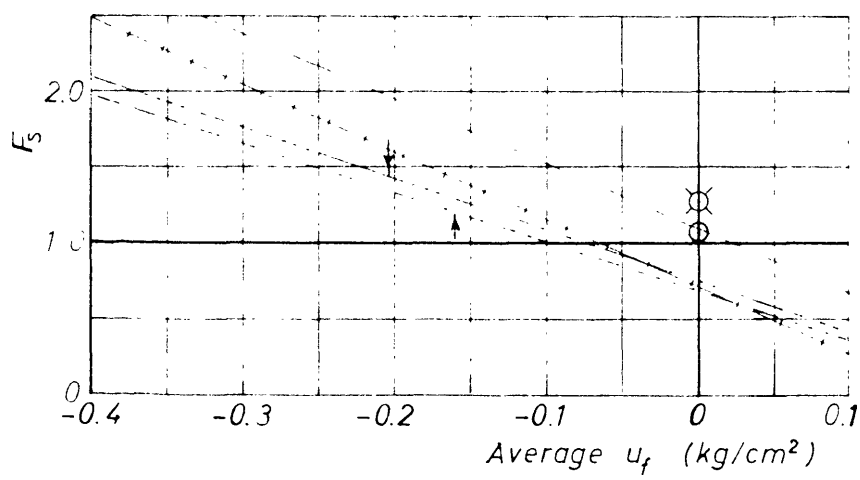

(c) Slip C

Location	Representation	
	Triaxial tests	Iswests
C/Sl.	– – – – – –	
C/1	7 tests ——— 8 tests – · – · –	⊠
C/4	——— · ——— · ———	⊙

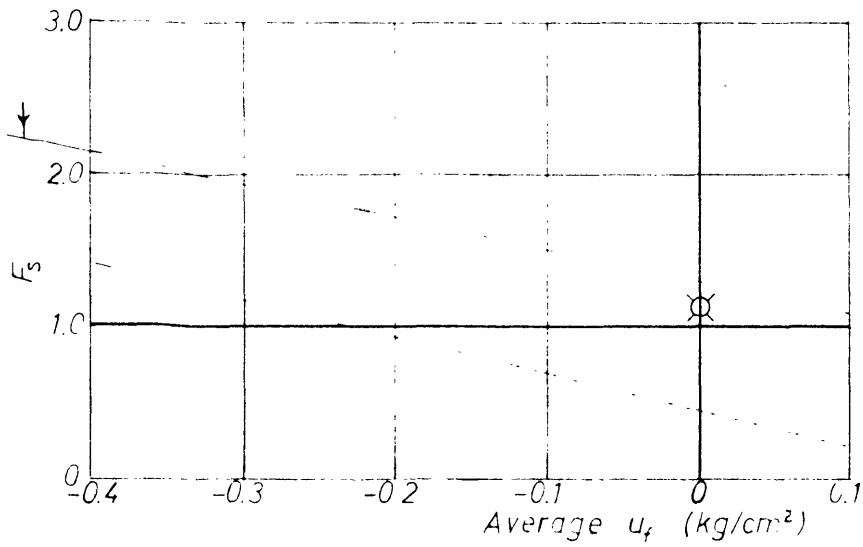

(d) Slip D

Location	Representation	
	Triaxial tests	Iswests
D	102mm – – – –	⊠
D	36 mm ·····	⊠

Fig. 6.25. Variation of factor of safety obtained from triaxial tests with assumed average pore pressure

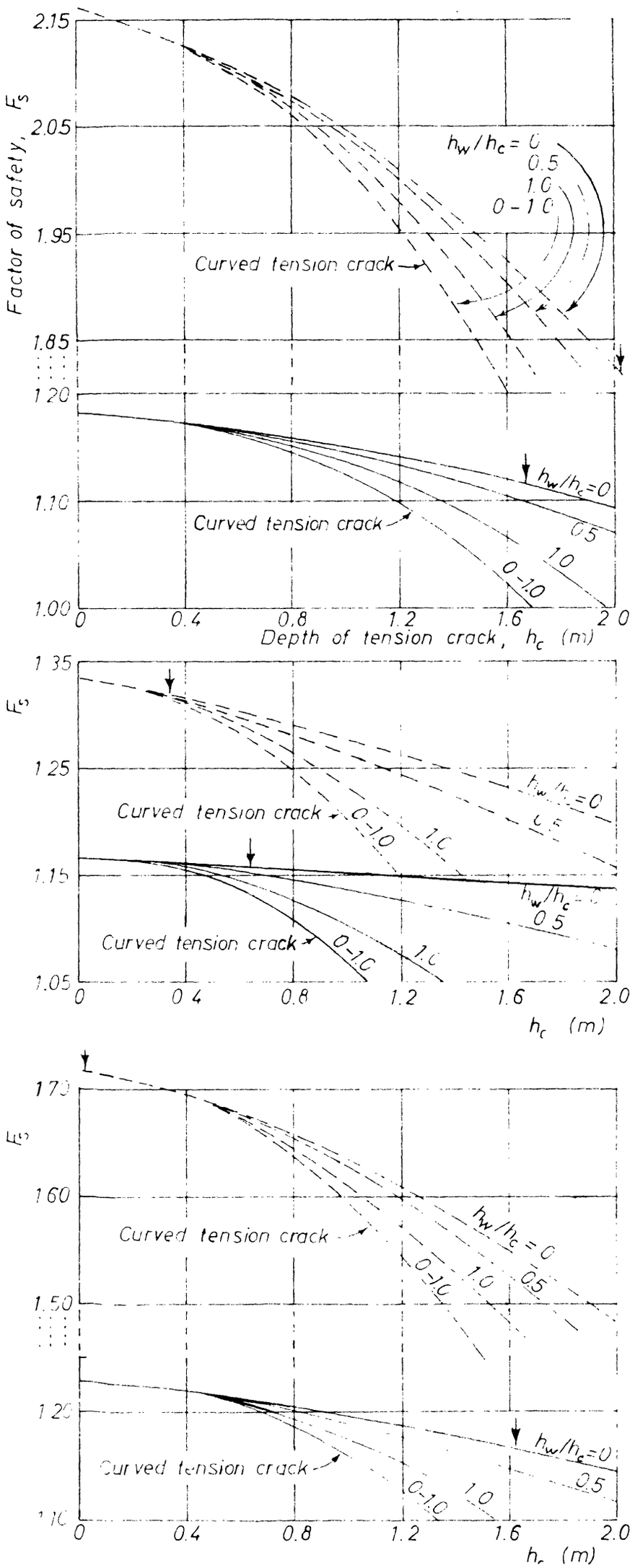

(a) Slip 1 at Site B

– – – – Triaxial test series 5 (Location B/10° ; hand-fitted envelope)

——— Iswest series B/10°

NOTES (1) ↓ indicates half the theoretical depth of tension cracks, based on the results of the particular test series.

(2) These curves are based on values given in Table 6.6, Rows 22, 23, 30, 18, and 19.

(b) Slip C

– – – Triaxial test series 6 (location C/Slip)

——— Iswest series C/4

(c) Slip D

– – – – Triaxial test series 4 (102 mm dia specimens)

——— Iswest series D

Fig. 6.26. Variation of factor of safety with depth of tension crack and the depth of water in such crack

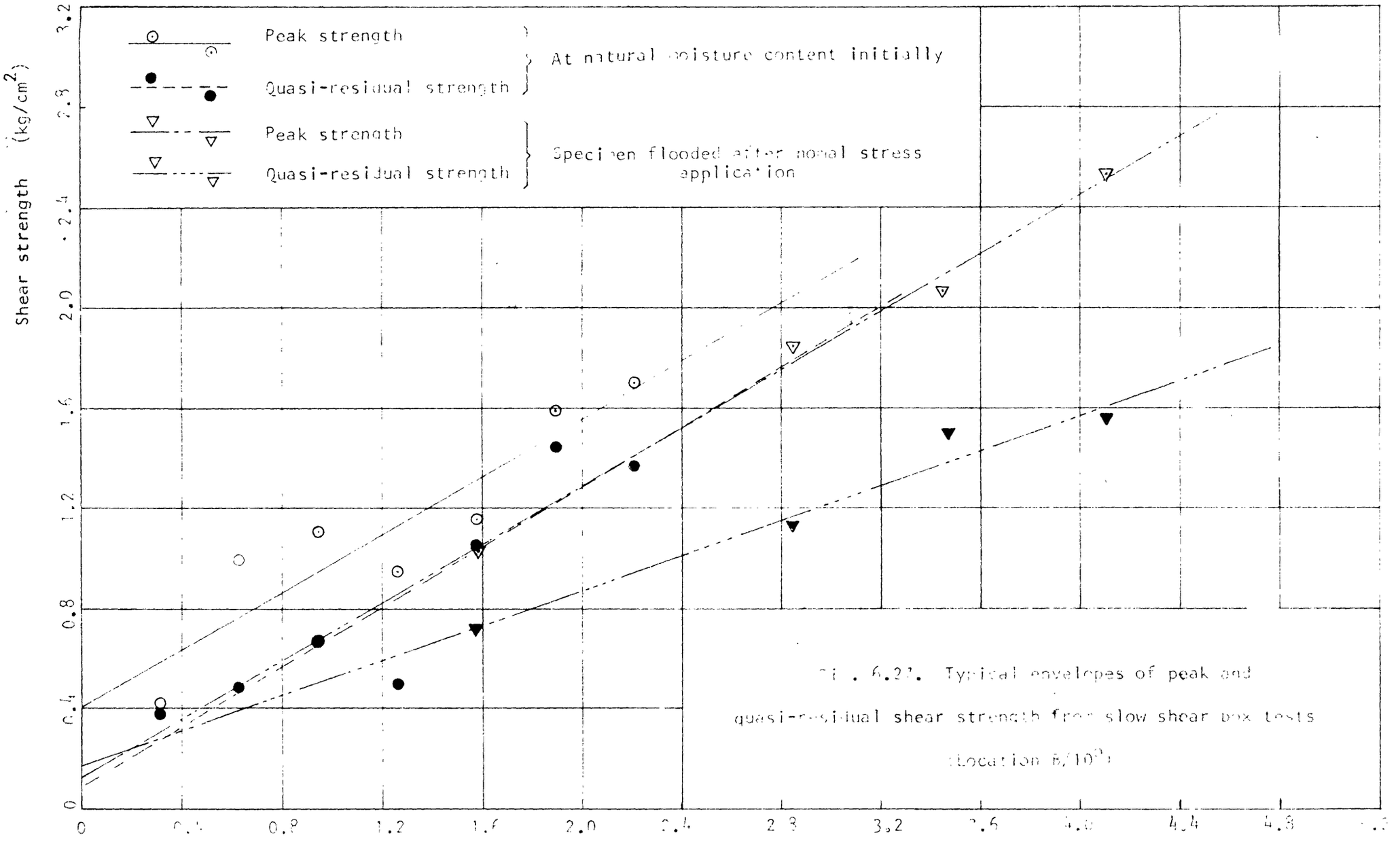

Fig. 6.27. Typical envelopes of peak and quasi-residual shear strength from slow shear box tests (Location B/10)

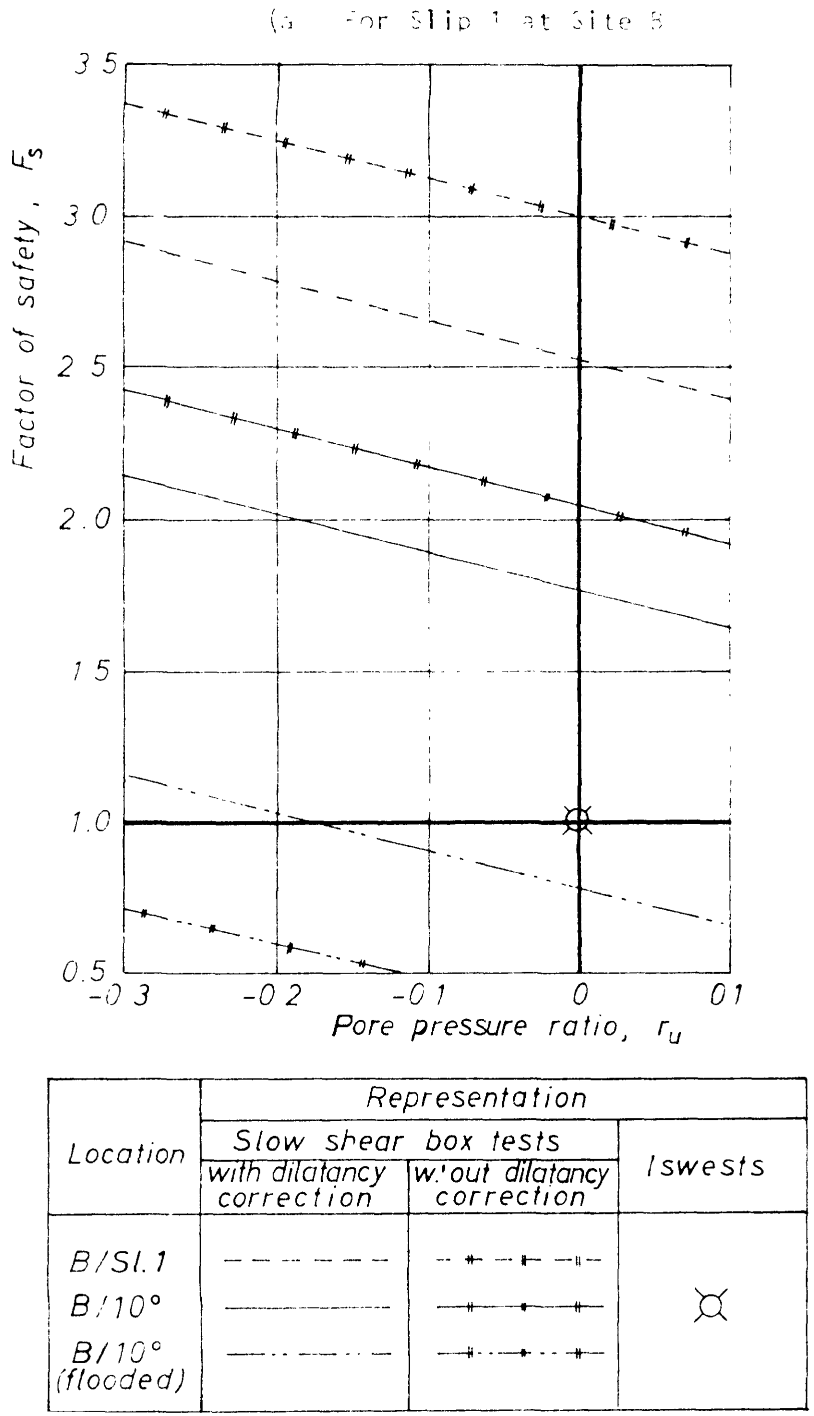

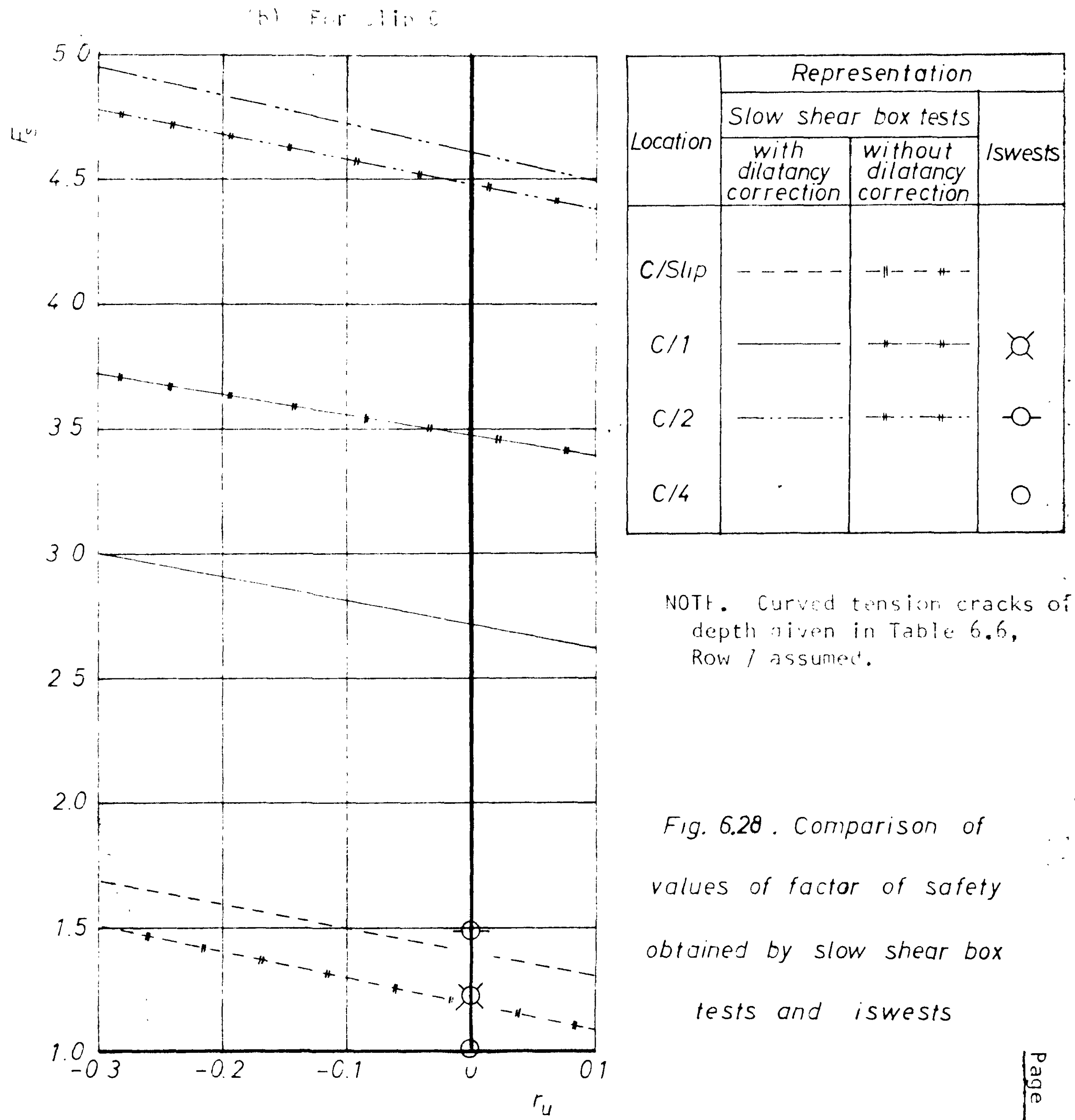

NOTE. Curved tension cracks of depth given in Table 6.6, Row 7 assumed.

Fig. 6.28. Comparison of values of factor of safety obtained by slow shear box tests and iswests

CHAPTER 7

DISCUSSION OF RESULTS

7.1 Iswest results

7.1.1 Effects of different factors on test results

7.1.1.1 Non-uniformity of normal stress

In Table 5.1, Columns 11 and 15 are given the values of the percentage difference $\delta\sigma_N / \sigma_N$ between the normal stress at the trailing end of the soil wedge and the average normal stress, at the peak strength and at the residual strength respectively.

Some idea about the effect of non-uniformity of normal stress on the measured strength may be gained by comparing the F_s values obtained through tests for which the values of $\delta\sigma_N / \sigma_N$ were rather different. Table 5.1, Column 11 shows that the average value of $\delta\sigma_N / \sigma_N$ for iswest series B/10^0 is 31.2 %, but had β been taken into account would probably be around 50 % (Section 7.1.1.3); whereas the corresponding figure for the absolute values of $\delta\sigma_N / \sigma_N$ in iswest series C/4 is 20.0 %. In spite of this, Table 6.6, Row 20 shows that these two series have given the F_s value of the corresponding slopes with equal proximity. Although other factors might have influenced the F_s values, the discussions in the subsequent sub-sections show that such influences could not be large, and so this comparison can be taken as sufficient evidence that the effect of

non-uniformity of normal stress on the measured peak strength could not be large either. In any case, it is relieving to note that by careful application of the procedure given in Section 4.3.3.2, it is possible to keep $\delta\sigma_N / \sigma_N$ to within about $\pm$ 10 %.

7.1.1.2 Orientation of principal stresses and stress path

Iswests D/7; C/2/4 and 8; and C/4/2, 5, 7, 8 and 10 (Table 5.1) have been performed using the mode of loading shown in Fig. 4.11(a). The orientation of principal stresses in these tests are therefore quite different from that in the remainder of the iswests in these three series for which the mode of loading shown in Fig. 4.11(b) has been used. The points representing the results of these tests, however, do not show an unusual deviation from their corresponding shear strength envelopes (Figs 5.12, 5.13 and 5.20), nor do they all fall on the same side of these envelopes. The orientation of principal stresses therefore does not seem to have significantly affected the measured strength in the case of the Ankara Clay. A more convincing proof of this is the proximity of the two envelopes (dashed and chain-dotted lines in Fig. 5.20), each obtained from five tests using a different mode of loading, and the fact that the undrained shear strength parameters obtained from these enveleopes have given the factor of safety of slip C as 1.077 and 1.084 (respectively), the corresponding value from all ten tests being 1.075.

The effect of the orientation of principal stresses on

the measured strength being so insignificant may be explained by the low respose of pore pressures to stress changes (Table 6.6, Rows 28, 29). This property of the soil probably also minimized the effect of the difference between the stress path followed in the iswest and that followed by an element of soil in the actual slope stability problem (Fig. 7.1) .

7.1.1.3 Rotation of test mould

Fig. 5.15(a) shows that the slight rotation β of the test mould during the iswest does not affect the measured shear strength at all. It does, however, have a small effect on the measured displacements of the test mould (Fig. 5.15(b)), and a marked effect on the calculated moments acting on the shear plane as reflected by the plot of $\delta\sigma_N / \sigma_N$ in Fig. 5.15(c). Fig. 5.15(c) together with the last twenty-seven rows in Table 5.1, Columns 11 and 15, suggest that seldom a quantity greater than 30 % might have had to be added to the values of $\delta\sigma_N / \sigma_N$ had β been taken into account for all previous tests. This would affect the shear strength parameters obtained, if the addition of these quantities were to increase the value of $\delta\sigma_N / \sigma_N$ to 100 % or more, because this would entail the use of equations 4.14 to 4.16 instead of 4.6, 4.12 and 4.13; but there seems to be very few such cases, and these are mostly amongst the values of $\delta\sigma_N / \sigma_N$ at residual strength. So it is unlikely that particularly the peak shear strength parameters quoted here would be in serious error due to the neglect of β in the earlier computations.

The slight rotation of the mould in a plane normal to the direction of loading (Section 5.2.5) is believed to have no significant effect on the test results, but points out the advisability of recording δ_y close to the plane of symmetry of the test mould (Section 4.4 (9)).

7.1.1.4 Area of shear and sample disturbance

Iswests D/3 and C/2/3 have been performed using a 30 degree test mould with a length of shearing plane 1.5 times larger than that of the rest of the test moulds, but with the same width. The area of shear being larger, these tests would normally be expected to reflect the effect of fissures more representatively, and hence to yield a lower strength than a 30 degree mould with the smaller area of shear. Comparison of the peak strength obtained for iswests D/3 and C/2/3 (Figs 5.12 and 5.13) respectively with the peak strength obtained for iswests D/2 and C/2/2, which were performed at the same level using the smaller 30 degree mould, indicates that the strength given by the larger mould is in fact higher. This can be explained by the fact that in these particular instances, the failure plane in iswests D/2 and C/2/2 coincided with more fissures. More such comparative tests are needed to ascertain how close the strength measured by the normal, 900 cm^2 moulds is to the operational strength (Lo, 1970) of the material tested, but these two tests indicate that it cannot be far from the latter.

In none of the forty-nine iswests performed so far did a soil wedge break due to fissures during preparation,

whereas quite a high percentage of the laboratory specimens were lost in this way. This is an indication of the low degree of disturbance caused to the soil during the preparation of the test wedge. It also means that every test performed adds to the truly representative area of the soil tested. Thus for testing a larger area, increasing the number of tests may be used as a convenient substitute for using a test mould that has a larger shear plane area but is more difficult to handle.

Finally it may be noted that particles as large as 38 mm are tolerated in the 305 mm x 305 mm shear box (Akroyd, 1957) which also has an area of about 900 cm^2.

7.1.1.5 Differences in location and time of slips and iswests

There is an average distance of 20 m between Slip 1 at Site B and the location of iswest series $B/10^{\circ}$ (Fig. 5.1). Also there is a time lag of several years between the slips at Sites C and D, and the corresponding iswests. These factors could have resulted in differences in the soil properties.

Comparing the results of triaxial and slow shear box tests (Table 6.6, Rows 22 to 44) for the locations B/Sl .1 and $B/10^{\circ}$ shows that had iswests been performed at the location of Slip 1, a higher factor of safety F_s would have resulted. But comparing the values of F_s given by iswests and by slow shear box tests (Rows 20 and 43) for the locations C/Slip, C/1, C/2 and C/4 (very close to C/Slip) shows that the

F_s values given by iswests are not affected in the same proportion as those obtained from small laboratory specimens. So the increase in the F_s value, had iswest series $B/10^o$ been performed at the location of Slip 1, is not likely to be significant.

For Site C, it is possible to compare the soil conditions, at the time of the slip and during the iswests, through comparisons of the laboratory test results on specimens, taken soon after the slip and at the time of the iswests. Such comparisons show that the conditions during iswest series C/4 were very close to those at the time of the slip (cf. curves for triaxial test series 6 and 7, Fig. 6.25(c)).

For Site D, an extrapolation regarding the soil conditions at the time of the slip has been made through in situ pore pressure measurements and the comparison of the rainfall in the months preceding the slip, the iswests, and these measurements (Section 6.2.5.7.2), and the error due to the time lag between the slip and the iswests is believed to be small.

7.1.1.6 Range of normal stresses

In all the three slips analysed by iswests, the average normal stress along the actual slip surface, estimated by neglecting the inter-slice forces, was just under a half of the average normal stress at peak strength in the corresponding iswests (cf. Table 6.6, Row 5 with Figs 5.9, 5.13, and 5.20). Probably the most important feature of the iswest making it

appear so promising is that it automatically measures the strength of the soil over a range of normal stresses of the order of those existing in a critical slope of the material being tested. The stronger is the material, the higher is the load that has to be applied in the iswest to bring the soil wedge to failure (Fig. 4.13), and the higher is the normal stress; but the critical slope of a given inclination in such a material is also higher, and so are the normal stresses along the potential slip surface. Thus the difficulty of Ø in terms of total stresses decreasing, as the degree of saturation increases in an unsaturated soil under increasing pressure, is overcome.

It may be rightly argued that if iswests are used to estimate the factor of safety of a slope which is far from critical, the results obtained will no longer be as close to the true factor of safety, as in the case of the critical slope. But in such a case the error involved will be on the safe side and more of academic interest than of practical significance; no engineer will be worried about a slope whose factor of safety is obtained as 3.5, say, and is known to be in fact somewhat greater.

7.1.1.7 Orientation of shear plane

With the method of selecting the inclination of the shear plane and the mould angle in iswest series C/1, D, C/2, and C/4 (Section 5.2.3), the undrained shear strength parameters obtained reflect not only the change in strength with normal stress but also the strength changes caused by

the change in the orientation of the shear plane. Thus the high angle of frictional resistance $\emptyset_{is}$ measured in iswest series D (Table 6.6, Row 19) can be explained by the fact that in iswests D/1 and D/2 (Table 5.1), failure took place completely along fissures and joints, reflecting the predominance of joints in sub-vertical planes at this site. That the effect of shear plane orientation is included in the measured shear strength parameters must have contributed to the success with which the factor of safety of the slips is predicted though the iswests, particularly in the case of the slip at Site D.

Although much more work is required to establish the degree of anisotropy of the shear strength of the Ankara Clay, it may be noted that a slight decrease in strength on moving from the horizontal to inclined planes is also indicated by the results of two series of slow shear box tests at the location B/H (Table 6.6, Rows 43, 44), one series performed on specimens with the failure planes horizontal, the second on specimens with the failure planes inclined at between 30° and 45° to the horizontal.

7.1.2 Reliability of the peak shear strength parameters in predicting short-term slope stability

From Table 6.6, Row 20 it is seen that, with a reasonable depth of a water-filled vertical tension crack (Row 7), and the use of the peak shear strength parameters (c_{is}, $\emptyset_{is}$) measured in iswests the factor of safety F_s of the Slip 1 at Site B and the slips at Sites C and D are given with a

maximum overestimate of 13 %. The use of Janbu's (1973) GPS for the calculation of F_s for Slip 2 at Site B (using iswest series B/10° results) and for Slip C shows that the simplifying assumptions regarding the inter-slice forces in BISIM, used for all the rest of the F_s calculations, tend to overestimate F_s by about 4 %. On the other hand, the study by Baligh and Azzouz (1975) indicates that had a three dimensional analysis, taking end effects in the slips into account, been performed, the F_s values would be slightly higher than given by BISIM, which assumes plane strain conditions. So these are minor and probably counterbalancing effects, and the estimates of F_s using c_{is}, $\emptyset_{is}$ can be regarded as very satisfactory. The tendency of the iswests to slightly overestimate F_s may be explained partly by the variable shear displacement at failure (Table 5.1, Column 9), which, as pointed out e.g. by Duncan and Seed (1966(b)), leads to a mobilized strength lower than the peak along part of the slip surface; and partly by the fact that the strength measured in the iswests is probably slightly higher than the operational strength of this material (Lo, 1970).

Table 6.6, Row 21 shows that if the depth of the tension cracks is assumed to be the same as in Row 7, but the crack is assumed to be curved, following the slip surface in cross-section, more favourable values of F_s are obtained. Although this assumption may be criticized in view of the more common assumption of verticality of such cracks, it does not appear totally impossible when the measured shape of the actual slip surfaces is considered (Figs 5.2 and 5.6).

The continuous curves in Fig. 6.26 show that even with the most unfavourable assumption regarding tension cracks, the maximum overestimate in F_s obtained by iswests does not exceed 23 %.

7.1.3 Reliability of the residual strength parameters

There are reasons to believe that iswest series B/10° and C/1 have been terminated somewhat before the residual strength was fully reached (cf. curve for iswest C/1/6 with the other curves in Fig. 5.14). So the correct residual strength envelopes for these series should lie slightly below those shown in Figs 5.9 and 5.11.

Figs 5.9, 5.11, 5.12, 5.13, 5.16, and 5.20 show that the residual value ϕ_{isr} of ϕ is generally greater than the peak value ϕ_{is}. If Bishop's (1971) view that "the establishment of a negative pore pressure across a rupture surface is unlikely" is correct, this may explain the higher values of ϕ_{isr} than ϕ_{is}, as a higher initial negative pore pressure and hence a larger drop in undrained strength at large strains would occur under the lower normal stresses.

In Table 6.6, Row 45 are given the values of F_s calculated by using the residual strength parameters (c_{isr}, ϕ_{isr}) measured in the iswests. These appear to underestimate the true factor of safety by about as much as the peak strength parameters overestimate it, except for Slip D where the F_s value given by the former parameters is as low as 0.58.

7.2 Triaxial test results

7.2.1 Effect of different factors on test results

7.2.1.1 Drying of specimens

In Table 6.1, Column 12 are given the changes in moisture content between sampling and specimen preparation, and in Table 6.2, Column 17 the changes in moisture content between specimen preparation and the end of UU tests, each expressed as a percentage of the moisture content under the former condition. Both positive and negative values exist amongst these changes, showing that they are probably due to local differences in moisture content. So no significant drying of the specimens during preparation and/or storage seems to have occurred.

7.2.1.2 Wetting of specimens

In Table 6.2, Column 21 are given the changes in the weight of the specimen before and after the test. The negative values are either due to the test being PCU, or due to small fragments of the specimen sticking on to the pedestal of the triaxial cell. Positive values however indicate either a previously undetected hole in the rubber membrane, or the FPSD used being over-wet (Section 6.2.4.1.4). There are, however, very few such cases, and these have not been excluded from the determination of the shear strength parameters, firstly because, as the results are expressed in terms of effective stresses, the effect of wetting on pore pressures would not affect the measured strength, and secondly

because it was felt that the effect, on the final results, of any reduction in the strength parameters themselves due to the wetting of any one specimen would be smaller than neglecting the results of the test on that specimen altogether. The weight of water gained by the specimens have been indicated in brackets on the p'_f versus q_f plots in Figs 6.5 to 6.13. The PCU tests in which the specimen temporarily gained some water from the over-wet FPSD have also been indicated. It is seen from these plots that any reduction in measured strength, which may have resulted due to a temporary or permanent wetting of the specimen, has caused a decrease in the factor of safety of the slips relative to what would otherwise have been obtained. The use of pore pressures estimated from such specimens (Table 6.4, Column 20) has had a similar effect.

The values of F_s given in Table 6.6, Row 31 as 2.06, 3.07, 1.20, 2.26, and 1.53 are altered respectively to 1.68, 3.33, 1.80, 4.98, and 2.17 if the results of UU tests on specimens that have gained more than 0.20 g of water are neglected in the calculation of the shear strength parameters. This verifies both the view that the wetted specimens have tended to reduce the F_s values, and the earlier feeling that in some cases the neglect of the results of the wetted specimens may have a larger effect on the final results than the reduction in F_s due to wetting (cf. the first figures in the series quoted).

7.2.1.3 Volume changes during shear

Table 6.3, Column 8 shows that, with a few exceptions,

the volumetric strain due to shear is well below ± 1.0 % at failure. Neglecting this volume change altogether in the calculations resulted in a drop in the factor of safety F_s obtained for Slip 2 at Site B (Table 6.6) from 5.044 to 4.987 using triaxial test series 8, and had no effect on F_s for Slip C as given by triaxial test series 7. It can therefore be concluded that particularly in routine studies of the short-term stability of slopes in the Ankara Clay, using the type of triaxial tests described here, the volume changes during shear can be neglected without any significant effect on the results, thus simplifying the testing procedure and the computations.

7.2.1.4 Membrane, bedding and seating corrections

Table 6.3, Column 18 shows that the use of Bishop and Henkel's (1962) simpler expression for the restraint of the rubber membrane would have resulted in an underestimate of the membrane correction applied to the measured deviator stress by as much as 90.8 %, and the result of this on F_s for Slip C as given by triaxial test series 7, for example, would have been to increase this value from 1.432 to 2.572. This is mainly because Bishop and Henkel's expression neglects the effect of volume change of the specimen, giving increasingly higher underestimates as the volume change during the consolidation stage of PCU tests increases.

For specimens failing along a single slip plane (mode 2 in Table 6.3, Column 2), Pachakis' (1976) membrane corrections, with the modification of taking the undrained Ø value for the

soil into account, has been used. As seen from Table 6.3, Columns 4, 11, 13, and 15, the net effect of using this correction on the test results has been to accept that the specimen has reached its peak strength before the appearance of a slip plane, in 18 of the 20 tests in which such a plane developed. The effect, for test series 7, of applying Pachakis' correction without the proposed modification would have been to increase F_s for Slip C from 1.432 to 1.695.

The effect on the same value of F_s of neglecting the seating correction applied here (Section 6.2.2.3) would have been to decrease this from 1.432 to 1.427. The effect of neglecting the bedding strain (Section 6.2.2.1.3) would have been to alter F_s obtained for Slip 2 at Site B, by assuming zero volume change during shear, from 4.987 to 4.992. It is thus seen that both these corrections are more of academic interest than of practical significance.

7.2.1.5 <u>End restraint</u>

In Table 6.2, Column 19 are given the values of the difference in moisture content between the middle and the two ends of the specimen, expressed as a percentage of the average value at the ends. These differences being mostly positive verifies the findings by other investigators, quoted in Section 3.3, that for this type of soil, end restraint results in higher pore pressures at the ends than at the centre of the specimen, causing a migration of pore water towards the centre. The values of this difference for test series 4 all being negative can be explained by the possibility of cavitation having taken

place in the pore pressure lines on reduction of the cell pressure at the end of the test, the specimen thus absorbing water from these lines. In fact in test 4/6, the pore pressure lines were opened to atmosphere to prevent such cavitation thus encouraging more water to be absorbed by the specimen.

If, as quoted in Section 3.3, end restraint affects mostly the value of the pore pressure coefficient A_f, because of the low values of B_o (Table 6.6, Row 25), it is unlikely that the error in A_f could have affected the calculated changes Δu_e in pore pressure (Table 6.6, Row 29), and hence the F_s values obtained, to any significant extent.

7.2.1.6 Temperature

The mean soil temperatures during the iswests (Table 6.6, Row 17) indicate that the soil temperature at the time of the slips were probably lower than the average laboratory temperature of 23°C by some 7°C. Fig. 6.19 shows that such a drop in temperature results in a decrease of about 0.08 kg/cm^2 in the estimated pore pressures, and Fig. 6.25 implies that an underestimate of about 0.20 units exists in the values of F_s calculated through the triaxial tests. This neglects the slight increase in the shear strength parameters themselves with a decrease in temperature, which appears likely judging by the work by Noble and Demirel (1969) on another clay (w_L = 89 %, w_P = 30 %, C = 80 %, mineralogical composition:

calcium montmorillonite)*. A more definite conclusion regarding the effect of temperature on the measured strength of the Ankara Clay requires further research.

7.2.1.7 Failure criterion

Comparing Rows 31 and 32 in Table 6.6 shows that the use of the maximum principal effective stress criterion results in values of F_s mostly very close to those given by the maximum deviator stress criterion. So it appears immaterial which criterion is used in deciding the point of failure in triaxial tests on the Ankara Clay.

7.2.1.8 Scatter of test results

Examination of Figs 6.5 to 6.12 shows that the scatter of test results is considerable, and this inevitably must have influenced the F_s values obtained; that is, another seven samples from the same location could give quite a different F_s value for any one slope. This possibility must always be kept in mind in studying the stability of slopes through triaxial tests, or the number of tests must be increased to such a level that a further test does no longer significantly affect the F_s value obtained.

*X-ray analyses by Söylemez (1972) have yielded the following estimate for the relative abundance of predominant clay minerals at the sites of the slips studied here.

Site (Figs 2.1, 2.2)	Percentage of illite	kaolinite	montmorillonite	vermiculite
B	56	30	14	-
C	46	36	9	9
D	50	22	13	15

In the case of tests series 5 and 8 (Figs 6.9 and 6.12), the K_f-lines fitted by POLRG (IBM, 1969) have appeared so unreasonable that hand-fitted K_f-lines have been tried. The F_s values obtained by both envelopes are given in Table 6.6, Row 31.

Fig. 6.6, where the τ_f versus σ_N relationship for the corresponding iswests has been plotted to the same scale as the triaxial test results, rules out the possibility of performing undrained triaxial tests over the same range of normal stresses as in the iswest , and analysing the stability in terms of total stresses; the scatter of points obtained from triaxial tests is relatively so large that, even when the order of magnitude of the effective normal stresses applied is about ten times that of the total normal stresses in the iswests , the K_f-line is difficult to define accurately.

7.2.1.9 Difficulties encountered in testing 102 mm diameter specimens

The relatively large weight of the 102 mm dia. specimens (around 3000 g as compared to the 130 g of 36 mm dia. specimens) resulted in a good contact being established between the base of the specimen and the ceramic disc, and hence a very rapid rise in the suction in the pore pressure lines. As the disproportionately small inlet for cell water prevented the cell being filled fast enough, cavitation is suspected to have taken place in the pore pressure lines in most of the tests of series 4 (Tables 6.1 to 6.3). Precautions to prevent this,

either by momentarily opening and closing the pore pressure lines to atmosphere, as done by Gibbs (1963), or the placement of a ring of thin wire between the top edge of the pedestal and the specimen, this ring being embedded in the soil on application of cell pressure and not affecting subsequent pore pressure readings, a procedure apparently practised at the Imperial College (Ergun, 1974), unfortunately came a bit too late to the Author's attention. However, it is believed that any cavitation that may have occurred affected mainly the pore pressures in the initial stages of cell pressure application, and not the effective stress shear strength parameters measured in such tests.

7.2.2 Reliability of triaxial tests in predicting short-term slope stability

Table 6.6, Row 31 shows that triaxial tests on 36 mm dia. specimens have resulted in an overestimate of F_s for the four slips by an amount ranging from 20 % to 229 %. Tests on 102 mm dia. specimens have overestimated F_s for Slip D by 53 %. The discussion in Sections 7.2.1.2 and 7.2.1.6 shows that with no unintentional wetting of some of the specimens, and with tests performed at temperatures closer to the in situ soil temperatures, these overestimates would have been even higher.

One reason for the overestimate of F_s by triaxial tests is the inadequate representation of fissures by small specimens. Another possible reason is the tendency, pointed out by Terzaghi (quoted by Skempton and LaRochelle, 1965),

of fissures to open up because of the stress release upon excavation, thus allowing water to percolate into the ground, increasing the average pore pressure, acting along the slip surface, above the highly negative values measured on laboratory specimens.

Fig. 6.25 shows that assuming the average pore pressure along the slip surface as zero may be used as an empirical means of obtaining a more realistic value of F_s from triaxial tests on small specimens. For tests on 102 mm dia. specimens, taking the average of the F_s value obtained by the predicted pore pressures and that obtained by assuming pore pressures as zero appears to yield a satisfactory value.

7.3 Reliability of strength parameters from slow shear box tests in predicting short-term slope stability

Table 6.6, Row 43 shows that the use of the peak shear strength parameters measured in the slow shear box tests, together with the pore pressures estimated by triaxial tests, results in an overestimate of F_s by between 103 % and 359 %. This is partly due to the inadequacy of the small shear box specimens in reflecting the effect of fissures, and partly becasue the effect of undissipated negative pore pressures are intrinsic in the shear strength parameters. Fig. 6.28 shows that even assuming pore pressures as zero is, in this case, of not much avail in improving the estimate of F_s. Table 6.6, Row 44 shows that the use of the quasi-residual shear strength parameters instead of the peak values reduces the overestimate in F_s to between 45 % and 89 %. Another

possible empirical way of obtaining a better estimate of F_s may be the use of peak strength parameters obtained by flooding the specimen after applying the normal load (Table 6.6, Row 43, Location B/10°), although this remains to be verified for other sites.

7.4 Comparison of factors of safety obtained by different methods

Figs 6.25, 6.26, and 6.28 provide a visual means of comparing the values of F_s obtained by iswests , triaxial tests, and slow shear box tests. These show that by far the best estimate of F_s is obtained through iswests , the triaxial tests giving the next better estimate, and the slow shear box tests being the least reliable in this respect.

It may be argued that, once half the theoretical depth of tension cracks is assumed to occur in practice (Section 5.3), the depth h_c of the cracks, as given by the test results being considered, should be used in the stability analysis. Such values of h_c have been indicated by vertical arrows in Fig. 6.26, and show that for some of the triaxial tests this procedure would have resulted in a higher value of F_s, and for some in a slightly lower value than given in Table 6.6, Row 30. In any case, this would not change the general conclusion in the previous paragraph regarding triaxial tests. In the case of slow shear box tests, the values of h_c calculated in this way would in some cases exceed the height of the slope, and would generally be unrealistic.

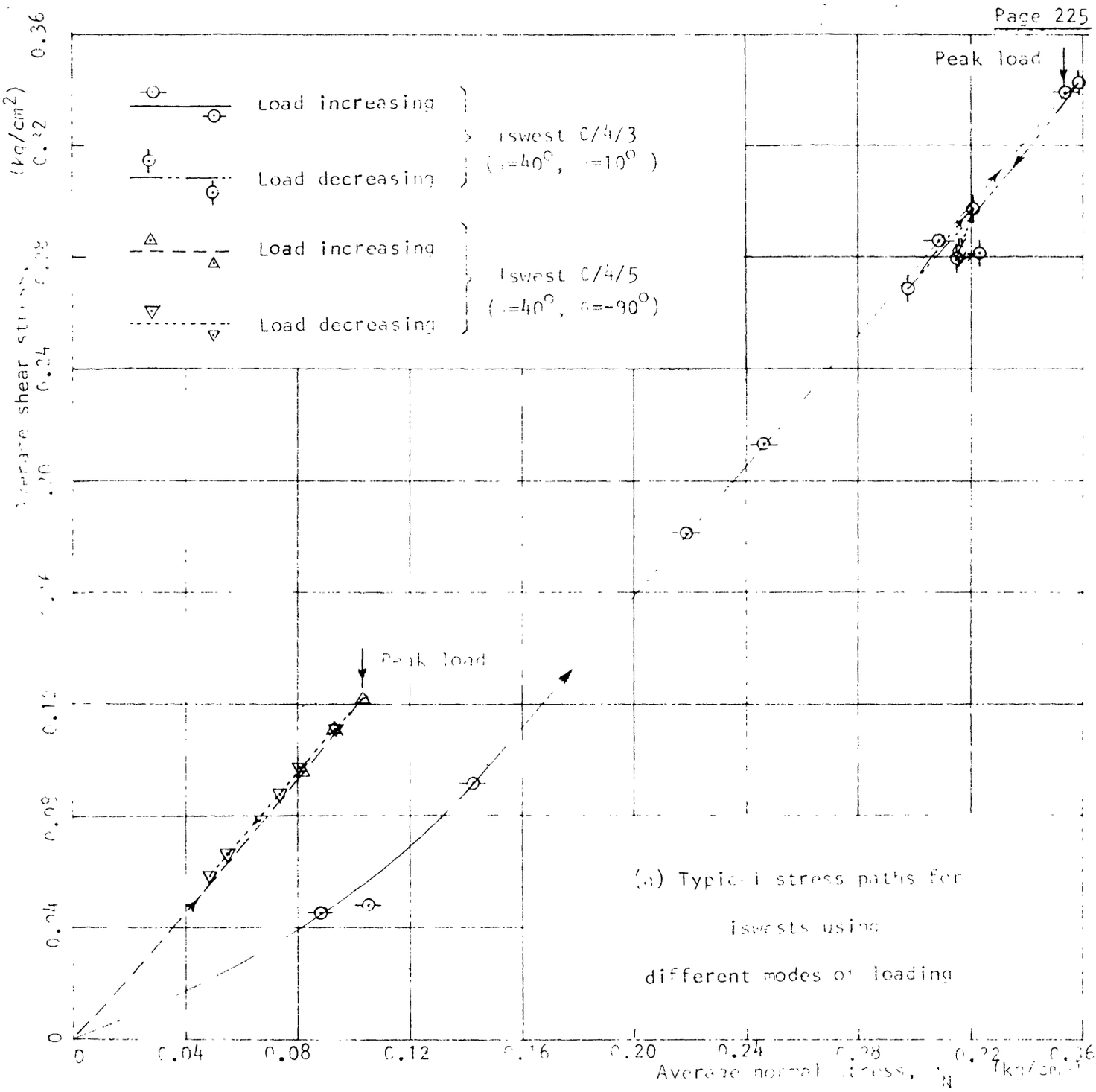

(a) Typical stress paths for iswests using different modes of loading

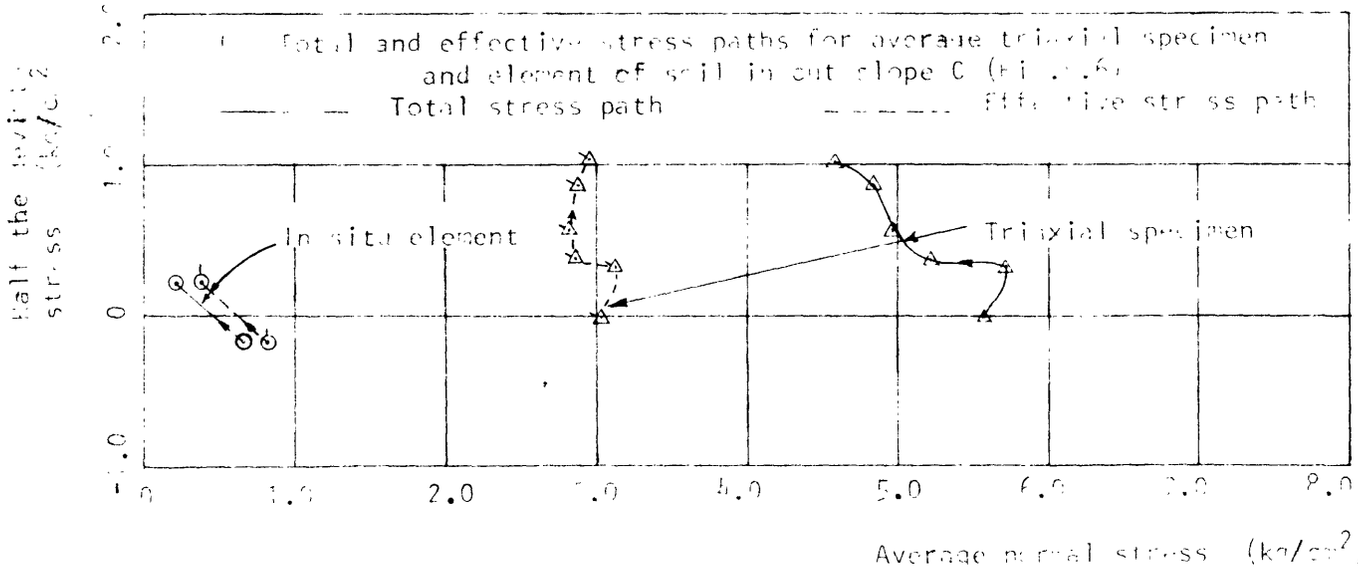

Fig. 7.7. Typical stress paths for iswest, triaxial test, and element of soil in slope

CHAPTER 8

SUMMARY OF CONCLUSIONS

A new testing technique has been developed whereby a single hydraulic jack and a set of simple devices are used to shear a wedge of the soil in situ. The test has been demonstrated to measure the undrained shear strength parameters of the unsaturated Ankara Clay, with a minimum of disturbance, and over approximately the same range of normal stresses as encountered in a critical slope of the soil being tested. Enabling the strength over an area of 900 cm^2, along a plane of any desired orientation, to be measured quite easily, thus allowing the effect of fissures and of anisotropy to be represented adequately in the measured strength, the test yields very promising results in the estimation of the short-term stability of slopes in the Ankara Clay.

Triaxial tests on 36 mm dia. specimens, performed by keeping the axial stress fairly constant and reducing the lateral stress, have generally overestimated the factor of safety of the slips studied by an average amount of about 100 %. The corresponding figure for tests on 106 mm dia. specimens at one site was 53 %. These assume negative pore pressures, estimated through triaxial tests and verified by a number of in situ pore pressure measurements, to exist in the slope. If it is empirically assumed that such pore pressures are zero, better estimates of the factor of safety result.

Shear strength parameters measured in slow shear box

tests on 63 mm dia. specimens together with pore pressures estimated by triaxial tests have overestimated the factor of safety of the slips by an average amount of about 240 %. To obtain a more realistic estimate of factor of safety by such tests, empirical use must be made of the residual strength parameters instead of the peak, or of the peak strength parameters measured in tests where the specimen is flooded after the application of normal stress, thus artificially increasing the moisture content and decreasing the strength of the soil. Clearly such empirical estimates are bound to be rough at best.

Admittedly the comfort of an air conditioned laboratory does not exist in a test pit, but if a truly reliable prediction of the short-term stability of slopes in the Ankara Clay is desired, the use of the in situ test developed appears to be well worth the additional manual effort required.

ACKNOWLEDGEMENTS

This work has been done at the Middle East Technical University, and has been partially supported by the Scientific and Technical Research Council of Turkey. The special devices described in Chapter 4 have been made in the General Workshops and in the workshops of the Departments of Civil and Mechanical Engineering.

The Author is indebted to his former lectures, Professor N.R. Morgenstern and Dr. P.R. Vaughan, the former for encouraging the Author to start on research on the Ankara Clay, and providing valuable advice at different stages of the work; the latter for his stimulating criticisms and suggestions on the two earlier versions of the paper eventually published in Géotechnique (Mirata, 1974). Thanks are also due to ProfessorsJ.M. Duncan and P. LaRochelle for answering a number of queries regarding their work.

The Author is grateful also to the following: the technical staff of the Soil Mechanics Laboratory, in particular Mr. O. Bal for valuable help with the field tests and in the sampling and preparation of specimens, Mr. İ. Özdoğan for help in the field and laboratory testing, Mr. H. Dallı for help in the laboratory testing and for performing the wet sieving analyses on which the values given in Table 6.1, Columns 18 and 19 are based, and Mr. C. Kaya for help in making some of the equipment and for typing the manuscript; all his colleagues who have helped in different ways, particularly those, who have held administrative positions during the past

nine years, for their speedy approval for the making and the purchase of the necessary equipment, and for provision of funds to enable the Author to attend the oral examination; Dr. M. Öner for help with the earlier computer programs, and for making his GPS program available; Mr. H. Başoğlu for help with the computer programming; the lady staff of the Central Computing Laboratory for punching some 9000 data and some 1600 program cards; all the technicians who have had a share in the making of the equipment or have helped in different ways, in particular Messrs B. Avcı, N. Meriç, C. Özgün, L. Sarptır, H. İnver, A. Yalçın, and F. Yörük; Messrs Y. Baykal and B. Avcı for help with the photography; Mrs. C. İskender for typing Tables 6.1 to 6.6, and Mrs. Ç. Birkan for checking the typed tables; Mr. F. Bakkal, Resident Engineer at Site B, for his kind permission for the tests at this site; and last but not least, the staff of the Documentation Centre of the Scientific and Technical Research Council of Turkey for the valuable scanning of available literature.

APPENDIX A

Derivation of equations 4.17 to 4.23

Referring to Fig. 4.4, if, having undergone the average displacements $\bar{u}$ and $\bar{v}$, the test mould rotates by a small angle β, the deflections δ_y and δ_x of independently supported dial gauges (originally at distances d_1 and d_2 respectively from the outer right corner of the test mould; now at distances $(d_1 - \delta_x)$ and $(d_2 + \delta_y)$ respectively) will be given by the following equations.

$$\delta_y = \bar{u} \sin\alpha + \bar{v} \cos\alpha - \overline{O_3F} \cdot \beta \cdot \cos\psi_1 \quad \ldots\ldots\ldots \quad (A.1)$$

$$\delta_x = \bar{u} \cos\alpha - \bar{v} \sin\alpha - \overline{O_3E} \cdot \beta \cdot \sin\psi_2 \quad \ldots\ldots\ldots \quad (A.2)$$

Eliminating $\bar{v}$ and $\bar{u}$ in turn from equations A.1 and A.2 the following equations are obtained.

$$\bar{u} = (\delta_y \cdot \sin\alpha + \delta_x \cdot \cos\alpha) + \left\{ \overline{O_3E} \cdot \cos\psi_1 \cdot \sin\alpha + \overline{O_3F} \cdot \sin\psi_2 \cdot \cos\alpha \right\} \beta \quad \ldots\ldots\ldots \quad (A.3)$$

$$\bar{v} = (\delta_y \cdot \cos\alpha - \delta_x \cdot \sin\alpha) + \left\{ \overline{O_3E} \cdot \cos\psi_1 \cdot \cos\alpha - \overline{O_3F} \cdot \sin\psi_2 \cdot \sin\alpha \right\} \beta \quad \ldots\ldots\ldots \quad (A.4)$$

If the values of u and v from equations 4.7 and 4.8 are substituted in equations A.3 and A.4 respectively, equations 4.17 and 4.18 are obtained.

Expressing the distances $\overline{O_3G}$, $\overline{GE}$, $\overline{O_3H}$, $\overline{HF}$ in terms of d, d_1, d_2, $\bar{u}$, $\bar{v}$, t and α, the following equations can be obtained.

$$\psi_1 = \arctan \left\{ \frac{\frac{1}{2}\cdot(d+\bar{u}) \sin\alpha + t}{d\cdot\cos\alpha + t - d_1 + (\bar{u}\cdot\cos\alpha - \bar{v}\sin\alpha) - \frac{1}{2}(d+\bar{u})\cos\alpha} \right\} \quad \ldots\ldots\ldots (A.5)$$

$$\psi_2 = \arctan \left\{ \frac{d\cdot\sin\alpha + t - d_2 - (\bar{u}\sin\alpha + \bar{v}\cdot\cos\alpha) - \frac{1}{2}(d-\bar{u})\sin\alpha}{\frac{1}{2}(d-\bar{u})\cos\alpha + t} \right\} \quad \ldots\ldots\ldots (A.6)$$

$$\overline{O_3E} = \left(\frac{d+\bar{u}}{2} \sin\alpha + t \right) / \sin\psi_1 \quad \ldots\ldots\ldots\ldots (A.7)$$

$$\overline{O_3F} = \left(\frac{d-\bar{u}}{2} \cos\alpha + t \right) / \cos\psi_2 \quad \ldots\ldots\ldots\ldots (A.8)$$

Hence equations 4.17 and 4.18 should strictly be solved by successive approximations. However, it has been found in practice that replacing $\bar{u}$ and $\bar{v}$ by u and v in equations A.5 to A.8 yields values of $\bar{u}$ and $\bar{v}$ (through equations 4.17 and 4.18) that are within $\pm$ 0.1 mm of the final values. So for practical purposes further iteration is unnecessary, and equations A.5 to A.8 can therefore be simplified into equations 4.19 to 4.22.

The derivation of equation 4.23 can best be obtained if, after raising the loading equipment by Δy_p relative to the test mould, the test mould is assumed to rotate by $+\beta$ about the single ball together with the loading equipment, with no relative movement between the test mould and the hydraulic jack. The deflection $(\delta_y)_i$ that would be recorded by the dial gauge for measuring δ_y due to this rotation is given by

$$(\delta_y)_i = (D + d_1 + n - t)\beta \quad \ldots\ldots\ldots\ldots\ldots\ldots (A.9)$$

If then the test mould is allowed to move parallel and perpendicular to the hydraulic jack until it reaches its final position, the former movement will not affect the reading $(\delta_y)_i$; the latter will reduce this value by the amount of downward movement of the test mould relative to the jack, $-(\Delta y_{MP} + \Delta y_P)$ by definition. Hence the actual reading δ_y will be given by

$$\delta_y = (\delta_y)_i + \Delta y_{MP} + \Delta y_P \quad \ldots\ldots\ldots\ldots\ldots\ldots \quad (A.10)$$

If equation A.9 is substituted in equation A.10, and β made the subject, equation 4.23 results.

In these derivations, second order of small quantities, such as terms in β^2, have been neglected.

APPENDIX B

Derivation of the curves in Figs 4.13 and 4.14

By combining equations 4.1 to 4.5 with the Mohr-Coulomb failure criterion in terms of total stresses, and neglecting the change in area during the test, the following equation is obtained. The curves in Fig. 4.13 have been plotted using this equation.

$$P_f = \frac{A_s \cdot c + K_1 \left(W + W_{BC} + W_{LP} \right) \sin \theta + K_2 \left(W + \frac{M_B}{D} \right) \cos \theta}{K_1 - \mu K_2} \quad \ldots(B.1)$$

where A_s = area of shearing plane of test mould

$K_1 = \cos \alpha - \tan \phi \cdot \sin \alpha$ .....(B.2)

$K_2 = \sin \alpha + \tan \phi \cdot \cos \alpha$ .....(B.3)

P_f = theoretical value of P required to cause failure along the plane ABDE (Fig. 4.1(b))

c, ϕ = shear strength parameters in terms of total stresses.

From equation (B.1) it can be seen that if the friction terms is neglected, P_f goes to infinity for $\alpha = 90 - \phi$. The effect of friction is to reduce this theoretical upper limit for α for any given ϕ by about 0.5 degree. The upper limit for α is in practice determined by the three-dimensional passive resistance of the soil at the critical end of the loading pit.

Equation B.1 neglects the possibility of shear failure taking place along a plane inclined at an angle λ to the

direction of loading, where $\lambda > \alpha$. This is likely to occur particularly for low values of α and ϕ.

In order to determine the inclination of the plane along which failure will take place, using the same equations as for equation B.1 and neglecting side friction, an expression has been derived for the ratio τ / τ_f of applied shear stress to the shear strength of the soil along a plane inclined at λ to the direction of loading, and its derivative equated to zero to give the value of λ for which the value of τ / τ_f will be a maximum and therefore greater than that along the plane of inclination α, for the hypothetical value of P_f required to cause failure along the latter plane. The expression obtained is

$$\lambda = \frac{1}{2} \arctan \left(\frac{-b_1 + \sqrt{b_1^2 - 4 a e}}{2 a} \right) \quad \ldots\ldots\ldots \text{(B.4)}$$

where

$$a = D_1^2 \cdot \tan^2 \phi - E^2 Y^2 \quad \ldots\ldots\ldots\ldots\ldots\ldots \text{(B.5)}$$

$$b_1 = 2 E Y (E X + D_1 \cdot \tan \phi) \quad \ldots\ldots\ldots\ldots\ldots \text{(B.6)}$$

$$e = D_1^2 \tan^2 \phi - (E X + D_1 \cdot \tan \phi)^2 \quad \ldots\ldots\ldots \text{(B.7)}$$

where

$$D_1 = X^2 + Y^2 \quad \ldots\ldots\ldots\ldots\ldots\ldots\ldots\ldots\ldots\ldots \text{(B.8)}$$

$$E = 2 \cdot c \cdot A_{LF} \quad \ldots\ldots\ldots\ldots\ldots\ldots\ldots\ldots\ldots \text{(B.9)}$$

where

$$A_{LF} = A_s \cdot \sin \alpha \quad \ldots\ldots\ldots\ldots\ldots\ldots\ldots\ldots\ldots \text{(B.10)}$$

where α = the fixed angle between the shearing plane and the direction of loading for any one mould.

Equation B.4 shows that λ is a function of X which is

dependent on P_f (Equation 4.1). It is thus necessary to obtain the correct value λ iteratively. For this, A_s in equation B.1 is replaced by $A_{LF} / \sin \lambda$ and this equation then used to re-calculate P_f by substituting λ for α. The new value of P_f so found is then used to re-calculate λ which will generally be within $\pm 0.1^{o}$ of the correct solution, at this second iteration.

This method has been used to calculate λ for different values of c, ϕ and θ for each test mould. For each set of θ and c, the values of ϕ were then plotted against λ. A series of straight lines resulted whose intersection with the line $\lambda = \alpha$ for the particular mould gave the minimum value of ϕ for failure to take place along the prescribed plane (ABDE in Fig. 4.1(b)). These values of ϕ were then plotted against the corresponding α in Fig. 4.14.

REFERENCES

1. Ağaoğlu, S. (1974). Anisotropy in compressibility of M.E.T.U. campus clay. M.S. thesis, M.E.T.U., Ankara

2. Akroyd, T.N.W. (1957). Laboratory testing in soil engineering, pp. 1-233. London: Soil Mechanics Ltd.

3. Amar, S., Baguelin, F., Jezequel, J.F. and Lemasson, H. (1975). Some problems on the in-situ measurement of the shearing resistance in fine soils. Istanbul Conf. Soil Mech. Fdn Engng 2, 165 - 182.

4. Arda, Ş. (1966). Preconsolidation of Ankara Clay. M.S. thesis, M.E.T.U., Ankara.

5. Baligh, M.M. and Azzouz, A.S. (1975). End effects on stability of cohesive slopes. Jnl Geot. Engng Div. Am. Soc. Civ. Engrs 101, No. GT 11, 1105 - 1117.

6. Barden, L. (1963). Discussion. Symp. Lab. Shear Testing of Soils, Ottawa, ASTM STP No. 361, 184.

7. Baykam, Z. (1974). Effect of size of sample on engineering behaviour of M.E.T.U. Campus Clay. M.S. thesis, M.E.T.U., Ankara.

8. Bell, J.M. (1968). General slope stability analysis. Jnl Soil Mech. Fdn Div. Am. Soc. Civ. Engrs 94, SM 6, 1253 - 1270.

9. Biarez, J. (1968). Feldgerät zum gleichzeitigen Messen des Reibungswinkels und der Kohäsion. VDI Zeitschrift 110, No. 12, 484.

10. Birand, A. (1963). Swelling properties of Ankara Clay. M.S. Thesis, M.E.T.U, Ankara

11. Bishop, A.W. (1950). Discussion. Géotechnique 2, No. 2, 113 - 116.

12. Bishop, A.W. (1955). The use of the slip circle in the stability analysis of slopes. Géotechnique 5, No. 1, 7 - 17.

13. Bishop, A.W. (1966). The strength of soils as engineering materials. Géotechnique 16, No. 2, 91 - 130.

14. Bishop, A.W. (1971). Shear strength parameters for undisturbed and remoulded soil specimens. Proc. Roscoe Memorial Symposium, Cambridge, 3 - 58. Henley-on-Thames: Foulis.

15. Bishop, A.W. and Blight, G.E. (1963). Some aspects of effective stress in saturated and partly saturated soils. Géotechnique 13, 117 - 197.

16. Bishop, A.W. and Eldin, A.K.G. (1950). Undrained triaxial tests on saturated sands and their significance in the general theory of shear strength. Géotechnique 2, No.1, 13 - 32.

17. Bishop, A.W. and Green, G.E. (1965). The influence of end restraint on the compression strength of a cohesionless soil. Géotechnique 15, No. 3, 243 - 266.

18. Bishop, A.W., Green, G.E., Garga, V.K., Andersen, A. and Brown, J.D. (1971). A new ring shear apparatus and its application to the measurement of residual strength. Géotechnique 21, No.4, 273 - 328.

19. Bishop, A.W. and Henkel, D.J. (1962). The measurement of soil properties in the triaxial test, pp. 1 - 228. London: Edward Arnold.

20. Bjerrum, L.(1967). Progressive failure in overconsolidated plastic clay and clay shales. Jnl Soil Mech. Fdn Div. Am. Soc. Civ. Engrs 93, SM5, 3 - 49.

21. Blight, G.E. (1961). Strength and consolidation characteristics of compacted soils. Ph.D. thesis, University of London.

22. Blight, G.E. (1963(a)). The effect of nonuniform pore pressures on laboratory measurements of the shear strength of soils. Symp. Lab. Shear Testing of Soils, Ottawa, ASTM STP No. 361, 173 - 184.

23. Blight, G.E. (1963(b)). Discussion. Symp. Lab. Shear Testing of Soils, Ottawa, ASTM STP No.361, 199 - 204.

24. Blight, G.E. (1967). Effective stress evaluation for unsaturated soils. Jnl Soil Mech. Fdn Div. Am. Soc. Civ. Engrs 93, SM 2, 125 - 148.

25. BS 1377 (1967). Methods of testing soils for civil engineering purposes, pp. 1-234. British Standards Institution.

26. Bundred, J. (1975). Assessment of strength parameters in fissured clay. Proc. Istanbul Conf. Soil Mech. Fdn Engng 1, 112 - 119.

27. Chen, W.F. and Giger, M.W. (1971). Limit analysis of stability of slopes. Jnl Soil Mech. Fdn Div. Am. Soc. Civ. Engrs 97, SM 1, 19 - 26.

28. Crawford, C.B. (1963). Discussion. Symp. Lab. Shear Testing of Soils, Ottawa, ASTM STP No. 361, 279.

29. Cullen, R.M. and Donald, I.B. (1971). Residual strength determinations in direct shear test. Proc. 1st Australia-New Zealand Conf. on Geomechanics 1, 1 - 10.

30. Çolpan, M. (1969). Correlation between laboratory and field vane shear strength. M.S. thesis, M.E.T.U., Ankara.

31. Dinç, D.(1965). Considerations on methods of slope stability analysis. M.S. thesis, M.E.T.U., Ankara.

32. Doruk, M.(1968). Swelling properties of clays on the M.E.T.U. campus. M.S. thesis, M.E.T.U., Ankara.

33. Duncan, J.M. and Seed, H.B. (1965). Errors in strength tests and recommended corrections. Report No. TE 65-4, Department of Civil Eng., Univ. of California, Berkeley, Calif.

34. Duncan, J.M. and Seed, H.B. (1966(a)). Anisotropy and stress reorientation in clay. Jnl Soil Mech. Fdn Div. Am. Soc. Civ. Engrs 92, SM 5, 21 - 50.

35. Duncan, J.M. and Seed, H.B. (1966(b)). Strength variation along failure surfaces in clay. Jnl Soil Mech. Fdn Div. Am. Soc. Civ. Engrs 92, SM 6, 81 - 104.

36. Duncan, J.M. and Seed, H.B. (1967). Corrections for strength test data. Jnl Soil Mech. Fdn Div. Am. Soc. Civ. Engrs 93, SM 5, 121 - 137.

37. Dunlop, P. and Duncan, J.M. (1970). Development of failure around excavated slopes. Jnl Soil Mech. Fdn Div. Am. Soc. Civ. Engrs 96, SM 2, 417 - 493.

38. Dunlop, P., Duncan, J.M. and Seed, H.B. (1968). Finite Element Analyses of Slopes in Soil. Report No. TE-68-3, Soil Mech. Lab., Univ. of California, Berkeley.

39. Ekmekçioğlu, O. (1975). A treatise on the strength behaviour of two clay formations from the general Ankara region. M.S. thesis, M.E.T.U., Ankara.

40. Elias, M. (1967). An investigation of mositure movement in soils and the concept of equilibrium moisture distribution with its bearing on pavement performance. M.S. thesis, M.E.T.U., Ankara.

41. El-Ruwayih, A.A.(1976). Design manufacture and performance of a lateral strain device. Géotechnique 26, No.1, 215 - 216.

42. Ergun, U. (1974). Private Communication.

43. Erol, O. (1962). Ankara Kili hakkında jeolojik not. University of Ankara. Unpublished work.

44. Erol, O. (1964). Geological map and sections of greater Ankara. Prepared for the Water Authority of Ankara Municipality.

45. Erol, O. (1966). Geomorphological map of Ankara Region. Unpublished.

46. Erol, O. (1974). Private communication.

47. Fagnoul, A. and Bonnechère, F. (1970). Cisaillement in situ d'un massif de sol hétérogène. Géotechnique 20, No. 4, 373 - 386.

48. Gibbs, H.J. (1963). Pore pressure control and evaluation for triaxial compression. Symp. Lab. Shear Testing of Soils, Ottawa, ASTM STP No. 361, 212 - 221.

49. Gibbs, H.J. and Coffey, C.T. (1969). Techniques for pore pressure measurements and shear testing of soil. Proc. 7th Int. Conf. Soil Mech., Mexico 1, 151 - 157.

50. Gibson, R.E. (1963). D.I.C. lecture notes on earth pressure.

51. Günece, T. (1968). Stability of unsupported vertical cuts in Ankara Clay. M.S. thesis, M.E.T.U., Ankara.

52. Gürkök, A. (1970). Long term consolidation tests. M.S. thesis, M.E.T.U., Ankara.

53. Hambly, E.C. (1969). A new true triaxial apparatus. Géotechnique 19, No. 2, 307 - 309.

54. Hambly, E.C. and Roscoe, K.H. (1969). Observations and predictions of stresses and strains during plane strain of wet clay. Proc. 7th Int. Conf. Soil Mech., Mexico 1, 173 - 181.

55. Handy, R.L. and Fox, N.S. (1967). A soil bore-hole direct-shear test device. Highw. Res. Bd. News 27, 42 - 51.

56. Holubec, I. and Finn, P.J. (1969). A lateral deformation transducer for triaxial testing. Canad. Geotech. Jnl 6, 353 - 356.

57. IBM (1969). System /360 scientific subroutine package, 4 th ed., pp. 1 - 454. Form H20-0205-3, IBM Corporation, Technical Publications Department, New York.

58. Ildız, Ö. (1974). Effect of side friction on the preconsolidation characteristics of the M.E.T.U. campus clay. M.S. thesis, M.E.T.U., Ankara.

59. İnal, T. (1967). A study of the shear strength characteristics of Ankara Çay in terms of effective stresses. M.S. thesis, M.E.T.U., Ankara.

60. James, P.M. (1971). The role of progressive failure in clay slopes. Proc. 1st Australia-New Zealand Conf. Geomech. 1, 344 - 348.

61. Janbu, N. (1973). Slope stability computations. pp. 47-86 of Embankment-Dam Engineering (Casagrande Volume). New York: Wiley.

62. Jones, G.K. (1963). Chemistry and flow properties of bentonite grouts. Symposium on Grouts and Drilling Muds in Engineering Practice, London, 22 - 28. Butterworths.

63. Kaya, T. (1965). Rapid consolidation test on Ankara Clay. M.S. thesis, M.E.T.U., Ankara.

64. Khera, R.P. and Krizek, R.J. (1967). Measurement and control of radial deformation in the triaxial test of soils. Materials Research and Standards 7, No.9, 392-396.

65. Kirkpatrick, W.M. and Belshaw, D.J.(1968). On the interpretation of the triaxial test. Géotechnique 18, No.3, 336 - 350.

66. Kirkpatrick, W.M., Seals, R.K. and Newman, F.B. (1974). Stress distribution in triaxial compression samples. Jnl Geot. Engng Div. Am. Soc. Civ. Engrs 100, GT2, 190-196.

67. Kocabayoğlu, E. (1971). Contribution of desiccation to the preconsolidation of Ankara Clay. M.S. thesis, M.E.T.U, Ankara.

68. Kogan, B.I. and Lupashko, A.A. (1970). Stability analysis of slopes. Soil Mech. Fdn Engng, No. 3, 153 - 157 (translated from Russian).

69. Ko, H.Y. and Scott, R.F. (1967). A new soil testing apparatus. Géotechnique 17, No. 1, 40 - 57.

70. Lambe, T.W. and Whitman, R.V. (1969). Soil Mechanics, pp. 1 - 553. New York: Wiley.

71. LaRochelle, P. (1967). Membrane, drain and area correction in triaxial test on soil samples failing along a single shear plane. 3rd Pan-Am. Conf. Soil Mech., Venezuela 1, 273 - 293.

72. LaRochelle, P. (1970). Private communication.

73. Lee, I.K. and Ingles, O.G. (1972). Strength and deformation of soils and rocks. Ch. 4. Soil Mechanics-Selected Topics. New York: Am. Elsevier Publ. Co.

74. Lee, K.L. and Shubeck, R.J. (1971). Plane-strain undrained strength of compacted clay. Jnl Soil Mech. Fdn Div. Am. Soc. Civ. Engrs 97, SM 1, 219 - 234.

75. Lo, K.Y. (1970). The operational strength of fissured clays. Géotechnique 20, No. 1, 57 - 74.

76. Lo, K.Y., Adams, J.I. and Seychuk, J.L. (1969). The shear behaviour of stiff fissured clay. Proc. 7th Int. Conf. Soil Mech., Mexico 1, 249 - 255.

77. Lo, K.Y. and Lee, C.F. (1973). Analysis of progressive failure. Proc. 8th Int. Conf. Soil Mech., Moscow 1.1, 251 - 258.

78. Lohnes, R.A. (1974). The engineering properties of the Ankara Clay: a geological perspective. M.E.T.U., Ankara. Unpublished work.

79. Marsland, A. (1971). The use of in-situ tests in a study of the effects of fissures on the properties of stiff clays. Proc. 1st Australia- New Zealand Conf. on Geomechanics 1, 180 - 189.

80. Mineiro, A.J.C. (1969). Pore water pressure prediction under plane strain. Proc. 7th Int. Conf. Soil Mech., Mexico 1, 275 - 279.

81. Mirata, T.(1970). A critical review of existing literature on geotechnical properties of Ankara Clay. Unpublished work.

82. Mirata, T.(1972). The in situ wedge shear test: a new technique in soil testing. Unpublished work.

83. Mirata, T. (1973(a)). The in situ wedge shear test: a new technique in soil testing. Unpublished work.

84. Mirata, T.(1973(b)) Ankara Kilinde üç şev kaymasının yeni bir teknikle incelenmesi. IV. Bilim Kongresi, Ankara.

85. Mirata, T.(1974). The in situ wedge shear test — a new technique in soil testing. Géotechnique 24, No.3, 311 - 332 (Corrigenda: Géotechnique 24, No.4, 698 and 25, No.1,157 - 158).

86. Mirata, T. (1975(a)). Yerinde kama kesme deneyi : Yeni bir zemin deney tekniği. Proje No. MAG-277, Scientific and Technical Research Council of Turkey.

87. Mirata, T.(1975(b)). Expansible segments for support of test pit walls. Proc. Istanbul Conf. Soil Mech. Fdn Engng 1, 291 - 297.

88. Mirata, T.(1975(c)). Discussion on Session 1. Proc. Istanbul Conf. Soil Mech. Fdn Engng 3, 63.

89. Mirata, T.(1975(d)). Discussion on Session 2. Proc. Istanbul Conf. Soil Mech. Fdn Engng 3, 117 - 118.

90. Mitchell, R.J. (1973). An apparatus for plane strain and true triaxial testing of undisturbed soil samples. Canad. Geotech. Jnl 10, No. 3, 520 - 527.

91. Morgenstern, N.R. and Price, V.E. (1965). The analysis of the stability of general slip surfaces. Géotechnique 15, No. 1, 79 - 93.

92. Noble, C.A. and Demirel, T.(1969). Effect of temperature on strength behaviour of cohesive soil. Proc. Int. Conf. on Effects of Temp. and Heat on Engng Behaviour of Soils, Washington D.C., 204-219. Highway Res. Bd., Spec. Rep. No. 103.

93. Nonveiller, E. (1965). The stability analysis of slopes with a slip surface of general shape. Proc. 6th Int. Conf. Soil Mech., Montreal 2, 522 - 525.

94. Olson, R.E. and Campbell, L.M. (1967). Bushing friction in triaxial shear testing. Jnl Materials Res. and Standards 7, No. 2, 45 - 52.

95. Oral, C.(1964). Stabilization of Ankara Clay. M.S. thesis, M.E.T.U., Ankara.

96. Ordemir, İ. and Alyanak, I. (1964-65). Reports of soil studies of Stad Hotel, Kocatepe Mosque, Ziraat Bankası and Emlak Kredi Bankası, Ankara. Unpublished work.

97. Ordemir, İ., Alyanak, I. and Birand, A. (1965). Report on Ankara Clay. Publ. No. 12, Eng. Faculty, M.E.T.U., Ankara.

98. Öner, M.(1974). Program GPS : slope stability analysis by Janbu's generalized procedure of slices. Norwegian Inst. of Technology, Trondheim.

99. Özkan, O.Ö.(1965). The effect of strain rate on the shear strength of cohesive soils. M.S. thesis, M.E.T.U., Ankara.

100. Pachakis, M.D. (1976). The influence of the membrane restraint on the measured strength of a soil sample failing along a single shear plane in the triaxial test. Géotechnique 26, No. 1, 226 - 230.

101. Pearce, J.A. (1971). A new true triaxial apparatus. Proc. Roscoe Memorial Symposium, Cambridge, 330 - 339. Henley-on-Thames: Foulis.

102. Plum, R.L. and Esrig, M.I.(1969). Some temperature effects on soil compressibility and pore water pressure. Proc. Int. Conf. on Effects of Temp. and Heat on Engng Behaviour of Soils, Washington D.C., 231 - 242. Highway Res. Bd., Spec. Rep. No. 103.

103. Robertson, A.M.G.(1971). Accounting for cracks in slope stability analysis. Proc. 5th Reg. Conf. for Africa on Soil Mech. Fdn Engng, Luanda, Angola 1, 4.3 - 4.10.

104. Rowe, P.W. and Barden, L.(1964). Importance of free ends in triaxial testing. Jnl Soil Mech. Fdn Div. Am. Soc. Civ. Engrs 90, SM 1, 1 - 27.

105. Sarma, S.K. (1972). A note on the stability analysis of earth dams. Géotechnique 22, No. 1, 164 - 166.

106. Schmertmann, J.H. (1955). The undisturbed consolidation behaviour of clay. Trans. Am. Soc. Civ. Engrs 20, 1201 - 1227.

107. Schmertmann, J.H. (1975). The measurement of insitu shear strength. Specialty Conf. on Insitu Measurement of Soil Prop. Am. Soc. Civ. Engrs, SOA paper on Session 3.

108. Skempton, A.W.(1954). The pore pressure coefficients A and B. Géotechnique 4, No. 4, 143 - 147.

109. Skempton, A.W.(1961). Horizontal stresses in an over - consolidated Eocene clay. Proc. 5th Int. Conf. Soil Mech., Paris 1, 351 - 357.

110. Skempton, A.W. (1964). Long-term stability of clay slopes. Fourth Rankine Lecture. Géotechnique 14, No.2, 77 - 102.

111. Skempton, A.W. and LaRochelle, P.(1965). The Bradwell slip: a short-term failure in London Clay. Géotechnique 15, No. 3, 221 - 242.

112. Saylemez, N. (1972). Minerological analysis of Ankara Clay by X-ray powder diffraction method. M.S. thesis, M.E.T.U., Ankara.

113. Spencer, E. (1967). A method of analysis of the stability of embankments assuming parallel inter-slice forces. Géotechnique 17, No. 1, 11 - 26.

114. Spencer, E. (1973). The thrust line criterion in embankment stability analysis. Géotechnique 23, No.1 85 - 100.

115. Şener, C. (1966). Correlation between some mechanical properties of clays. M.S. thesis, M.E.T.U., Ankara.

116. Taylor, D.W. (1948). Fundamentals of soil mechanics. pp. 1 - 700. New York : Wiley.

117. Terzaghi, K. (1943). Theoretical soil mechanics, pp. 1 - 510. New York : Wiley.

118. Terzaghi, K. and Peck, R.B. (1948). Soil mechanics in engineering practice. pp. 1 - 566. New York : Wiley.

119. Thorley, A., Broise, Y., Calhoon, M.L., Zeman, Z.P. and Watt, W.G. (1969). Borehole instruments for economical strength and deformation in-situ testing. Proc. Conf. on in situ investigations in soils and rocks, Inst. Civ. Engrs, London, pp. 155 - 165.

120. Tice, J.A. and Sams, C.E. (1974). Experiences with landslide instrumentation in the southeast. Transp. Res. Rec. No. 482, 18 - 29.

121. Topkara, E. (1974). Strength characteristics of M.E.T.U. campus clay with emphasis on residual behaviour. M.S. thesis, M.E.T.U., Ankara.

122. Tosun, T. (1966). Vertical and horizontal permeabilities of Ankara Clay. M.S. thesis, M.E.T.U., Ankara.

123. Tuncer, E.R. (1972). The sensitivity of cohesive soils. M.S. thesis, M.E.T.U., Ankara.

124. Tümerdem, Ö.F. (1973). Comparison of observed and calculated settlements of two buildings on the Ankara Clay. M.S. thesis, M.E.T.U., Ankara.

125. Uçkan, S. (1966). An investigation of the shear strength of Ankara Clay. M.S. thesis, M.E.T.U., Ankara.

126. U.S.B.R. (1960). Earth manual. pp. 1 - 751. US Dept. of Interior, Bureau of Reclamation.

127. Vaughan, P.R. and Walbancke, H.J. (1973). Pore pressure changes and the delayed failure of cutting slopes in overconsolidated clay. Géotechnique 23, No. 4, 531 - 539.

128. Wade, N.H. (1968). Discussion on Corrections for strength test data. Jnl Soil Mech. Fdn Div. Am. Soc. Civ. Engrs 94, No. SM3, 800 - 805.

129. Ward, W.H., Samuels, S.G. and Butler, M.E. (1959). Further studies on the properties of London Clay. Géotechnique 9, No. 2, 33 - 58.

130. Whitman, R.V. and Bailey, W.A. (1967). Use of computers for slope stability analysis. Jnl Soil Mech. Fdn Div. Am. Soc. Civ. Engrs 93, SM 4, 475 - 498.

131. Wright, S.G., Kulhawy, F.H. and Duncan, J.M.(1973). Accuracy of equilibrium slope stability analysis. Jnl Soil Mech. Fdn Div. Am. Soc. Civ. Engrs 99, SM 10, 783 - 791.

132. Wroth, C.P. and Hughes, J.M.O. (1973). An instrument for the in-situ measurement of the properties of soft clay. Proc. 8th Int. Conf. Soil Mech., Moscow 1.2, 487 - 494.

ABBREVIATIONS

Abbreviation	Meaning	Abbreviation	Meaning
addl.	additional	LSI	lateral strain indicator
aver.	average	m/c	moisture content
bet.	between	M.E.T.U.	Middle East Technical University
B. & H.	Bishop and Henkel (1962)		
BISIM	Bishop's (1955) simplified method	MSL	Mean sea level
		max.	maximum
ch.	change	mech^{l}	mechanical
consdn.	consolidation	membr.	membrane
corr.	correction	mid.	middle
deg	degree (angular unit)	p.	pressure
degr.	degree	para.	parameter
det'd	determined	PCU	partly consolidated-undrained
dia.	diameter		
diff^{ce}	difference	POLRG	polynomial regression
ht.	height	p.p.	pore pressure
iswest	in situ wedge shear test (plural:iswests)	press.	pressure
		reln.	relation
FPSD	filter paper side drains	satn.	saturation
GI	galvanized iron	spec.	specimen
GPS	generalized procedure of slices	temp.	temperature
		UU	unconsolidated - undrained
G.S.	ground surface		

INDEX TO DEFINITION OF SYMBOLS

(Continues ...

INDEX TO DEFINITION OF SYMBOLS (CONTINUED)

INDEX TO EQUATIONS, TABLES, AND FIGURES

(a) EQUATIONS

(b) TABLES

(c) FIGURES

APPLIED SCHEDULE OF WORK

In a pamphlet published by the University of London, Advisory Service for External Students, for the guidance of Ph. D. candidates, it is advised that the candidate should start writing up as soon as he has accumulated a reasonable amount of material. Reference is also made to the number of years taken by past Ph.D. students to complete a satisfactory thesis. This record, originally kept for the Author's own use, is presented with the hope that it might be of interest particularly to prospective Ph. D. candidates.

The Author has followed the advice quoted above, and believes that otherwise it would have been much more difficult to condense the work of some 9600 hours spread over nearly nine years, from which a 45 cm high pile of notes, data and calculation sheets, and an equally high pile of computer outputs emerged.

Item 14 in the appended schedule is concerned mainly with the assembly of triaxial testing equipment. The earlier years have been spent mainly on the development of the in situ test described in the thesis, on laboratory shear box tests, and on index property tests. When the formal writing up of the thesis began in April 1975, most of Chapters 4 and 5 and part of Chapter 7 had already been written up in some form.

Distribution of the hours of effort spent on different items over the years

Scale: an area ═══ represents 100 hours throughout

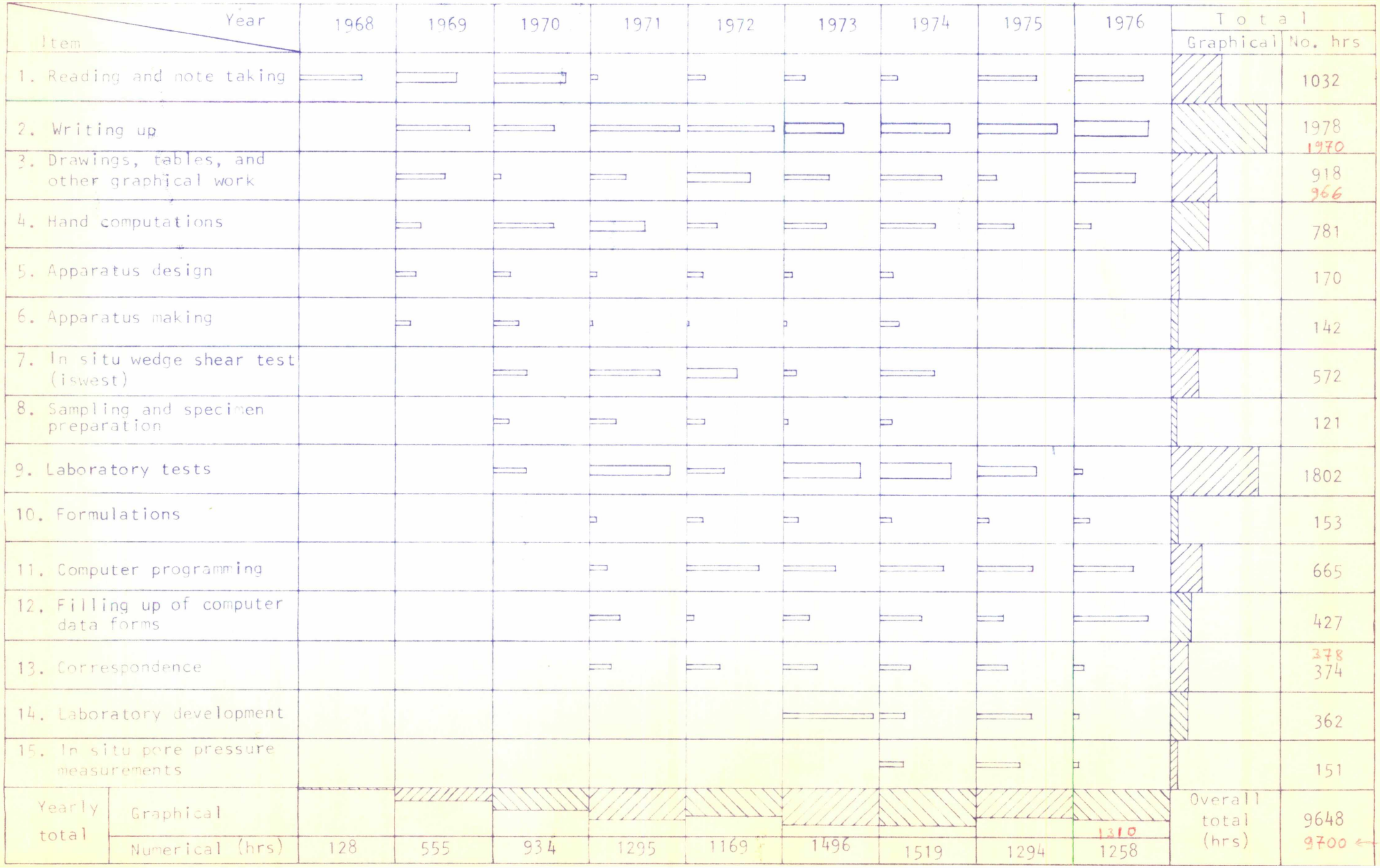

Item \ Year	1968	1969	1970	1971	1972	1973	1974	1975	1976	Total Graphical	Total No. hrs
1. Reading and note taking											1032
2. Writing up											1978 1970
3. Drawings, tables, and other graphical work											918 966
4. Hand computations											781
5. Apparatus design											170
6. Apparatus making											142
7. In situ wedge shear test (iswest)											572
8. Sampling and specimen preparation											121
9. Laboratory tests											1802
10. Formulations											153
11. Computer programming											665
12. Filling up of computer data forms											427
13. Correspondence											378 374
14. Laboratory development											362
15. In situ pore pressure measurements											151
Yearly total — Graphical										Overall total (hrs)	9648 9700 ← *p to Postlay
Yearly total — Numerical (hrs)	128	555	934	1295	1169	1496	1519	1294	1310 1258		

Mirata, T. (1976). Ph.D. Thesis, Univ. of London

CORREGENDA/1 (Feb., 1981)

p.24, Fig.2.5. "$I_p = w_L - 20$" should read "$I_p = 0.73(w_L - 20)$".

p.44, Eq 4.23. This equation should be replaced by the following:

$$\beta = (\delta_{yo} - \Delta y_{MP} - \Delta y_p) \;/\; (d_3 + \delta_{xo}) \qquad \text{(radians)}.....4.23$$

where $\delta_{xo} = \bar{u} \cdot \cos\alpha - \bar{v} \cdot \sin\alpha$

$\delta_{yo} = \bar{u} \cdot \sin\alpha + \bar{v} \cdot \cos\alpha$

and d_3= perpendicular distance from the single ball to the grooved face of LP.2.

p.44, pa.1, l.17. "D, n, Δy_p have ..." should read "Δy_p has the same meaning as in equation 4.9. Equations 4.17 to 4.23 have to be solved by iteration, two iterations being sufficient for practical purposes."

p.89, Table 5.1. Columns 8 to 15 should be modified as follows for iswests C/3/4-7 and C/4/1, 3-10 for when β is considered.

1	2	8	9	10	11	12	13	14	15
C/3	4	- 1.28	9.2	- 0.4	36.4	- 1.60	41.5	3.8	93.8
	5	- 1.29	10.5	- 0.6	14.0	- 1.60	40.6	2.3	53.4
	6	- 1.22	2.5	- 0.9	37.7	- 1.69	37.1	4.2	100
	7	- 0.36	22.8	- 0.8	11.1	- 2.44	95.8	0.6	- 6.9
C/4	1	1.07	27.0	- 2.1	50.5	3.41	81.8	- 4.0	31.2
	3	0.79	14.2	- 5.5	0.9	4.75	89.7	- 2.0	- 53.6
	4	- 0.24	9.9	- 2.1	- 2.3	1.03	136.3	- 5.4	14.6
	5	- 0.27	1.9	0.2	- 13.8	- 1.40	30.4	2.1	- 84.4
	6	- 1.42	3.6	- 1.4	25.6	- 0.14	71.8	- 0.8	28.2
	7	0.09	7.1	- 1.0	2.4	- 2.29	57.4	3.2	- 55.8
	8	- 0.16	5.6	1.3	4.6	- 2.75	24.9	5.5	- 24.1
	9	- 3.66	3.1	- 3.5	31.4	- 6.52	100.5	- 8.1*	82.3
	10	0.66	6.3	0.5	- 21.6	- 2.35	85.9	15.3	- 45.5

* The previous value should have been - 6.4 and not 6.4.

p.203, Fig.6.27. The triangles in front of "Quasi - residual ...." should be solid.

p.231. The last paragraph and the first 10 lines on p.232 should be replaced by the following:

"In Fig.4.4, if the test mould moved to the dotted position (without any rotation), by definition, Δy_{MP} would be $(\delta_{yo} - \Delta y_p)$. Any further change in Δy_{MP} would be due to the rotation β of the test mould resulting in a change $-\beta(d_3 + \delta_{xo})$ in Δy_{MP}. The difference between the measured value of Δy_{MP} and what would have been measured if no rotation took place is thus given by:

$$\Delta y_{Mp} - (\delta_{yo} - \Delta y_p) = -\beta(d_3 + \delta_{xo}) \quad \ldots\ldots\ldots\ldots\ldots\ldots \quad (A.9)$$

from which equation 4.23 results".

p.250. Add d_3, δ_{xo}, δ_{yo} (all now defined on p.44, corrected as above) to the Index to the Definition of Symbols.

p.251. α_p is defined on p.136 and not 134.

p.252. Delete equation A.10 from the Index to Equations.

Addendum and Corrigendum (Published in Géotechnique 24, No. 4, 698)

Page 316, equation (14) should read

$$d_c = 3 \left\{ \left(\frac{d - u}{2} \right) - M/(X \sin \alpha + Y \cos \alpha) \right\} \quad \ldots\ldots \quad (14)$$

Expressions used in equations (17) and (13) are defined as follows

$$\overline{O_3E} = \left\{ (d + u) \frac{\sin \alpha}{2} + t \right\} / \sin \psi_1$$

$$\overline{O_3F} = \left\{ (d - u) \frac{\cos \alpha}{2} + t \right\} / \cos \psi_2$$

Corrigendum (Published in Géotechnique 25, No. 1, 157-158)

On p. 322, Table 2, Column 4, the second figure should read 20(N), and in Column 5, the units should be kg/cm^2.

The Author supplies the following information.

A punching error has been detected in the program used for the evaluation of the last eleven 'iswests' reported in the paper. As a result the particulars of 'iswest' 6/7 given in Table 3 should read as follows.

1	2	3	4	5	6	7	8	9	10	11	12	13	14
6/7	1.0	0.0	45	15	0†	-	23.6	-1.0	3.9	-	100.7	0.5	-72.5
						-0.26	23.1	-0.9	10.9	-1.68	97.3	0.5	-8.5

The same error and the fact that one other point has been overlooked, have led to erroneous values of factor of safety quoted in the Addendum, pp. 331-332. This point is that, σ_N not being constant during the 'iswest', the values of τ/σ_N are not necessarily indicative of the peak or residual strength. Particularly when loading is in sub-vertical directions (Fig. 8(a), p. 319), τ/σ_N can continue rising after the peak load has been reached. Taking the peak load as the criterion of failure, the corrected values of factor of safety quoted on p. 332 have been found as 1.031, 1.022 and 1.022 respectively. These results were evaluated by the use of a computer program by Öner (1971) and the shear strength parameters obtained from computer-fitted strength

envelopes: (c_{is} = 0.0637, 0.0519, 0.0608 kg/cm^2 and ϕ_{is} = 34.52°, 38.11° and 35.13° respectively).

The largest three maximum negative values of β observed so far have been -1.68, -1.78 and -3.88 degrees. Positive values of β have been recorded in two tests, the maximum values being 2.29 and 3.08 degrees.

The test mould has also been observed to rotate in the transverse direction by about $\pm$ 1.0 degree. The effect of this on the test results is believed to be insignificant, but it is advisable to record δ_y near the central axis of the mould.

REFERENCE

Öner, M. (1971). Computer application of slope stability analysis. M.S. Thesis, Middle East Technical University, Ankara.

Corrigendum (sent on 22 June, 1976 for publication in Géotechnique)

On page 317, δ_x in the denominator of equation (21) should be deleted.

On page 322, Table 2, the heading for column 14 should read c_{is}; in column 16, the value 0.97 should read 1.02.